Optimum Design Method and Performance Analysis of Unified Power Quality Conditioner with Distributed Generation

THESIS

Submitted in partial fulfilment of the requirements for the degree of

DOCTOR OF PHILOSOPHY

by

SISIR KUMAR YADAV
(2019PHXF0030P)

Under the Supervision of

PROF. HITESH DATT MATHUR

And Under the Co-supervision of

PROF. ASHISH PATEL

BIRLA INSTITUTE OF TECHNOLOGY & SCIENCE,
PILANI

2024

BIRLA INSTITUTE OF TECHNOLOGY & SCIENCE, PILANI (RAJASTHAN)

CERTIFICATE

This is to certify that the thesis titled **"Optimum Design Method and Performance Analysis of Unified Power Quality Conditioner with Distributed Generation"** submitted by **Mr. Sisir Kumar Yadav**, ID No. **2019PHXF0030P** for award of Ph.D. degree of the institute embodies original work done by him under our supervision.

Signature of the Supervisor	Signature of the Co-supervisor
Name: **PROF. HITESH DATT MATHUR**	Name: **PROF. ASHISH PATEL**
Designation: **Professor**	Designation: **Assistant Professor**

Date: **18 November 2024**

Acknowledgements

I am very thankful for the successful completion of this challenging academic journey, and I wish to convey my deepest appreciation to the persons and organizations that have played crucial parts in this remarkable achievement.

First and foremost, I extend my heartfelt gratitude to the almighty for granting me strength, wisdom, and resilience throughout this challenging endeavour. His divine guidance has been my unwavering source of inspiration and solace.

First and foremost, I express my profound appreciation to the Almighty for providing me with strength, knowledge, and resilience during this difficult journey. His spiritual direction has been my constant source of inspiration and comfort.

I am very grateful to my supervisor, Prof. Hitesh Datt Mathur, and Prof. Ashish Patel, my co-supervisor, for their essential knowledge, support, and patience. Their mentorship not only directed my research in the right direction, but also motivated me to pursue excellence.

I would like to express my gratitude to my colleague, Dr. Dhananjay Mishra, Dr. Heema Dave, Dr. Akhilesh Kumar Mishra, Dr. Pavitra Sharma, Ms. Preeti Sharma, Mr. Somesh Thanvi and Mr. Shubham Tiwary and Mr. Shubham Priyadarshi for your companionship and collaborative attitude, which have greatly enhanced my academic experience. The interchange of ideas, productive discussions, and collaborative obstacles have enhanced the satisfaction of this voyage. Furthermore, I extend my sincere appreciation to Birla Institute of Technology and Science, Pilani, including Prof. V. Ramgopal Rao (Vice Chancellor), Prof. Sudhirkumar Barai (Director), Prof. Shamik Chakraborty (Associate Dean of AGSRD), and Col. Soumyabrata Chakraborty (Registrar) for providing the conducive academic environment and resources necessary for the successful completion of my research. Special thanks to Prof. Navneet Gupta, the HOD of the EEE department, and dedicated staff members, Mr. Ravinder Yadav and Mr. Ashok Saini, for their continuous support. The institute's commitment to excellence has been a guiding force throughout my doctoral studies.

I am honored to express my sincere appreciation to my esteemed Doctoral Advisory Committee members, Prof. Dheerendra Singh and Prof. Aditya R. Gautam, for their invaluable guidance and insights that have added tremendous value to my

research work. I am equally grateful to Prof. Puneet Mishra, the convener of the Doctoral Research Committee, for his unwavering support and constructive feedback.

I am indebted to the Central Power Research Institute (CPRI), Bangalore, for providing the necessary resources for my PhD research. I want to express my sincere gratitude to CPRI for believing in the significance of my work and their commitment to advancing scientific knowledge. Their support has enhanced the quality of my research and broadened my academic horizons, for which I am truly thankful. Additionally, the funding support from Department of Science & Technology- Science and Engineering Research Board (DST-SERB) for my travel to the IEEE ETFG 2023 conference that was held at the University of Wollongong, Wollongong, Australia, has been a crucial catalyst in facilitating my participation.

Last but not least, special thanks to my family: my father, Mr. Ravi Shankar Yadav (Rtd. Chief Manager & Consultant/Electrical, PGCIL); my mother, Smt. Saroj Yadav, my brother, Mr. Hemant Kumar, and my younger sibling, Mr. Kshitij Kumar. I owe them an immeasurable debt of gratitude. Their unwavering support has been a pillar of strength for me.

In conclusion, I express my deepest gratitude to all those who have contributed to my academic and personal growth. This achievement would not have been possible without the collective support, encouragement, and inspiration from these exceptional individuals and institutions.

Place: BITS Pilani
Date: 18/11/2024

Sisir Kumar Yadav
(Department of Electrical & Electronics Engineering)

Abstract

The desire to meet energy needs with clean, green resources is sharply rising in the age of modern power distribution networks. As a result, there has been an increase in the use of power electronics conversion devices, which has caused the power distribution network's power quality to decline. In recent decades, a number of compensating custom devices have been developed, including unified power quality conditioners (UPQC), dynamic voltage restorers (DVRs), distributed static compensators (DSTATCOMs), etc. Combining a DSTATCOM and DVR in a back-to-back configuration with a shared DC link, a unified power quality conditioner is a multi-functional device capable of mitigating various power quality issues such as voltage sags, swells, harmonics, and unbalance. The stabilization of the DC link is necessary for the proper functioning of UPQC and the seamless integration of distributed generation into the power grid.

The proportional-integral (PI) controller, which is frequently used to control the DC link, does not perform well under various dynamic conditions, resulting in degraded performance. As the load or power source changes, the conventional controller may no longer be effective, causing the system to react poorly to disturbances. Traditional PI controllers often use linear approximations, which might not work well in nonlinear conditions because power systems are made up of different parts that don't behave linearly, like transformers, loads, and power sources. As a part of the thesis, a work on an innovative approach for real-time tuning of PI controllers in UPQC-DG systems using particle swarm optimization (PSO) have been presented. The goal is to improve the DC link voltage performance and stability under a range of different operating condition by dynamically optimizing the PI controller's settings. By making use of real-time data and PSO algorithms, the UPQC's performance have been enhanced across a range of operational scenarios.

The literatures available worldwide, has suggested various control strategies to improve the compensatory capabilities of UPQC, which includes reducing its size and cost. Inductors and RC filters are consistently used in UPQC to mitigate undesirable elements such as switching ripples. However, designing these passive filters optimally is a challenging task owing to their strong interdependence on UPQC. So, PSO algorithms has been utilized to design the passive elements in a way to maximize performance in terms of technological feasibilities such as reduced THD, higher

power factor, and better voltage regulation. The optimized parameters also aid in cost and size reduction.

Existing literatures also provides enormous details on the various merits and demerits of different control strategies of UPQC. These strategies impact its ability to mitigate power quality issues, and power losses are a critical factor in any power quality solution. A detailed study on the power losses associated with such control strategies needs careful attention. So, the performance of UPQC have been analysed by conducting a comprehensive comparison of power losses between UPQC-P, UPQC-Q, and UPQC-S across a variety of operating scenarios. In real-world applications, the work performed may estimates which one controller is superior to UPQC. In addition to the control algorithm, a thorough comparison of the power losses of UPQC and UPQC-DG/IDG are carried out in a real-time simulator using Opal-RT. This analysis validates the practical feasibility of the most efficient UPQC configuration.

Finally, this research makes a contribution to the existing body of information about the enhancement of power quality in smart distribution networks by providing additional capabilities to UPQC-DG. In addition to compensation of reactive power for loads, the work includes the UPQC-DG to export reactive power to the grid in a controllable way. The proposed UPQC-DG system is validated using comprehensive real time simulations in Opal-RT, which evaluate both steady-state and dynamic performance.

Contents

List of Figures

List of Tables

List of Abbreviations

ANN	Artificial Neural Network
ANFIS	Adaptive Neuro Fuzzy Inference System
APF	Active Power Filter
CCM	Continous Conduction Mode
CHIL	Controller Hardware In Loop
CSI	Current Source Inverter
CSD	Current Synchronous Detection Method
DFIG	Doubly Fed Induction Generator
DFT	Discrete Fourier Transform
DG	Distributed Generation
DSTATCOM	Distribution Static Synchronous Compensator
DVR	Dynamic Voltage Restorer
EPPL	Enhanced Phase Locked Loop
FFT	Fast Fourier Transform
FST	Fourier Series Theory
FLC	Fuzzy Logic Controller
IRPT	Instantaneous Reactive Power Theory
ISCT	Instantaneous Symmetrical Component Theory
LPF	Low Pass Filter
MPC	Model Predictive Control
MPPT	Maximum Power Point Tracking
MRAS	Model Reference Adaptive System
P_S	Source Power (W)
P_L	Load Power (W)
P_UPQC_Loss	Total UPQC Losses (W))
P & O	Perturb and Observe
PAC	Power Angle Control

PBT	Power Balance Theory
PCC	Point of Common Coupling
PQ	Power Quality
PSO	Particle Swarm Optimization
PV	Solar Photovoltaic
PI	Proportional Intergral
PLL	Phase Locked Loop
PWM	Pulse Width Modulation
SPPT	Single Phase PQ Theory
SRFT	Synchronous Reference Frame Theory
SFIG	Singly Fed Induction Generator
SAPF	Series Active Power Filter
SHAPF	Shunt Active Power Filter
STT	Stockwell Transformation Theory
SS-FL	Steady State at Full Load
SS-PL	Steady State at Partial Load
THD	Total Harmonic Distortion
UPQC	Unified Power Quality Conditioner
UPQC-DG	Unified Power Quality Conditioner with Distributed Generation
UVTG	Unit Vector Template Generation
VA	Volt-Ampere rating
VSI	Voltage Source Inverter

List of Symbols

V_S	Source voltage
V_L	Load voltage
V_{PV}	Voltage of PV array
V_{LL}	Line to line voltage
C_{DC}	Capacitance of DC link
V_{Sr}	Injected voltage by series APF
I_S	Source current
I_L	Load current
L_S	Source inductance
R_{DC}	Load resistance of rectifier
I_{Sh}	Injected current by shunt APF
I_{cr}	Ripple current
L_B	Inductance of boost converter
Q_{sr}	Reactive power of series parameter
P_L	Load active power
L_{sh}	Shunt APF inductance
V_{sw}	Voltage across switch
I_{sw}	Switch current
V_{DC}	DC link voltage
f	Frequency of source voltage
f_s	Switching frequency
m	Modulation index
V_{VSC}	Voltage rating of VSI
VSI	Voltage source inverter
P_L	Load power
I_{Sr}	Current rating of shunt APF
S_{Sr}	Apparent power ratio of series APF

a	Overloading factor
n_T	Turns ratio of series injection transformer
P, Q, S	Real power, reactive power, and complex power respectively

Greeks letters

ϕ	Load phase angle
ω	Angular frequency of grid voltage
δ	Power angle
δ_C	Calculated value of power angle in every time step
δ_{max}	Maximum permissible value of power angle
λ	Ratio of reactive power shared by series APF to total reactive power of load
α	Angular frequency of load voltage

Subscripts

a, b, c	For phase A, B, C (or R-Y-B) of quantities in a three phase system
cr, pp	Peak to peak ripple current of compensator
DC	DC link/side quantities
dc	DC link/side quantities
L	Parameters relating load
S	Source quantities
Sh	Shunt APF parameters
Sr	Series APF parameters
T	Parameters of transformer
PV	PV array parameters
VSC	Voltage source converter

Chapter 1

Introduction

1.1 Background

When discussing electrical power quality, one must consider how it relates to the gadgets and equipment used by the customer. The matter concerns the dependability and uniformity of the voltage applied to electrical equipment. Systems and associated devices may experience faults, disturbances, or damage as a result of low power quality.

Power quality is the combinations of many essential factors that define the characteristics of electrical power and determine its suitability for different applications. An essential factor to consider is voltage quality, which refers to maintaining a consistent and reliable source of power. Variations, imbalances, and voltage sags can negatively impact the longevity and functionality of interconnected equipment. Ensuring the power supply remains within standard frequencies, such as 50 Hz or 60 Hz, is an important factor in supporting time-dependent technology. Unwanted frequency components called harmonics and inter-harmonics can introduce distortions that might affect sensitive electronic devices [1], highlighting the need of maintaining high-quality voltage waveforms. Disruptions may arise due to transients, which are brief fluctuations in voltage caused by switching or lightning.

Furthermore, voltage flicker, defined as rapid changes in voltage, and power factor, defined as the effectiveness of power use, are important factors in assessing overall power quality. Power quality needs to be monitored and maintained in industrial, commercial, and residential homes since poor power quality can lead to equipment damage, operational problems, data corruption, energy inefficiency, and downtime [2]. Adherence to set standards, the application of corrective devices, and

continual improvements in power quality management techniques are necessary to address these important factors.

Poor power quality can have detrimental effects on equipment and operating efficiency in a number of different areas [2, 3]. The possibility of equipment damage is one important outcome. Voltage sags, surges, and oscillations may cause rapid failure of linked equipment, leading to higher maintenance expenses and increased downtime. Operational problems also occur because low-quality electricity can cause sensitive electronic devices, such as computers and industrial machinery, to malfunction or operate improperly. Another serious issue is data corruption, which is particularly problematic in situations where accurate data processing is essential. Electronic systems can be interfered with by harmonics and transients, which may result in data loss or corruption. Another effect is energy inefficiency, especially when low power factor is involved. Subpar usage of electrical power and increased energy expenses are the results of this inefficiency. Low power quality can lead to severe financial losses and decreased productivity in industrial environment where continuous operation is crucial. A complete strategy is needed to address these effects, including consistent power quality monitoring, adherence to set guidelines, and the installation of corrective equipment such voltage regulators and power factor correction units. These units are supposed to maintain balanced sinusoidal voltages of constant magnitude and frequency. Consumers are expected to draw sinusoidal balanced currents at the unity power factor for sensitive loads such as hospitals and industries.

In industrial plants, harmonics caused by non-linear loads are the main problem that power conditioners attempt to solve. Active Power Filters (APFs) have become essential components in modern power distribution systems, serving a vital function in reducing power quality concerns and improving system dependability. In light of the increasing need for reliable electrical power, APFs provide advanced remedies to mitigate a wide range of issues, including voltage drops, surges, harmonics, and reactive power fluctuations. APFs are designed to actively inject counteracting harmonic currents to ensure a cleaner power supply and decrease distortions that can put sensitive equipment at risk [1, 4–6]. Dynamic voltage restorers, often known as DVRs, are an essential component in the process of ensuring that voltage sags/swell do not disrupt the operation of essential loads. In order to safeguard equipment against voltage-related issues, DVRs are able to detect fluctuations in the voltage and dynamically inject compensatory voltage in order to guarantee a consistent supply of power. Distribution static synchronous compensators (DSTATCOM) are primarily

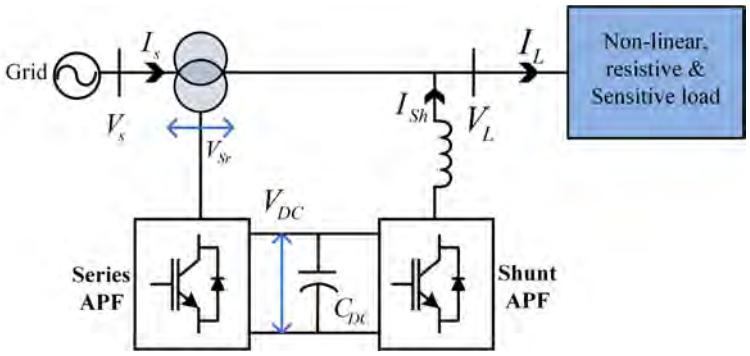

Figure 1.1: Conventional UPQC

designed to achieve reactive power compensation and voltage management as their primary objectives. In distribution networks, they achieve the correction of power factor imbalances and the stabilisation of voltage levels. They are especially helpful in circumstances in which fluctuations in voltage may be the result of varied load demands.

Unified Power Quality Conditioners (UPQC) combine shunt and series active power filters (DSTATCOM & DVR) to address a variety of power quality problems in a comprehensive manner [1, 7–11]. In contexts where numerous power quality constraints coexist, UPQCs provide complete support by simultaneously addressing voltage and current-related issues. Their wide range of applications, which includes both residential and commercial spaces, greatly enhances the dependability and effectiveness of power systems. When combined, these advanced devices demonstrate the diverse strategy needed to guarantee a high level of power quality in present electrical networks. The UPQC tackles various power quality problems by integrating the features of shunt and series active power filters. By injecting compensatory voltage in series with the load, the UPQC functions as a dynamic voltage restorer in the series arrangement, reducing voltage sags and swells. In addition, by injecting equal and opposite compensating currents, the shunt portion of the UPQC acts as a DSTATCOM, reducing reactive power imbalance and other current-related problems. The UPQC is able to deliver a solution that is both versatile and effective because to its integrated approach, which allows it to address multiple power quality issues simultaneously. The single-line diagram in Fig. 1.1 illustrates the layout of a UPQC, which also shows the connections between its series and shunt components in the power system.

1.2 Motivation and Problem Description

Power quality in electrical distribution networks has been greatly enhanced by unified power quality conditioners (UPQCs), yet there are still issues and knowledge gaps that need to be filled. UPQCs rely heavily on their control algorithms [12–15], which are critical to their overall effectiveness and performance. The difficulty is finding a middle ground between minimising system losses and attaining efficient power quality mitigation along with minimizing cost. A crucial area of research is the comparison of losses in various control algorithms for UPQCs. It is important to estimate power losses of UPQC and UPQC-DG for various reasons. Firstly, precise estimation enables engineers to assess system efficiency, helping them identify areas for improvement and optimise the design for enhanced performance. With a deep understanding of power loss and system optimisation, designers can implement strategies to minimise inefficiencies and improve overall energy efficiency. In addition, accurately calculating power losses is crucial for economic factors to be taken into account. Greater losses result in higher operating expenses as a result of energy being wasted. Through the analysis of these losses, decision-makers can assess the financial viability of various design alternatives and choose the most cost-effective solution. Although there is literature available on the advantages and disadvantages of different control systems [1, 8], a thorough comparative study is required, taking into account variables including operational costs, steady-state performance, and dynamic performance reaction.

For UPQCs, choosing a control method requires balancing computational complexity, real-time responsive, and simplicity. The complex dynamics in modern power networks necessitate the development of a sophisticated UPQC controller. DC link stability is essential in UPQC-DG systems because it directly influences the performance and reliability of the entire power conditioning system. The DC link serves as the energy storage component, balancing power between the series and shunt active filters. If the DC link voltage is unstable, it can lead to inadequate power compensation, causing voltage sags, swells, increased harmonics distortion, and other power quality issues. Stable DC link voltage ensures that the UPQC can effectively mitigate these disturbances, thereby maintaining optimal power quality and protecting sensitive electrical equipment. The integration of renewable energy sources, variable load profiles, and the increasing frequency of grid failures need the use of a sophisticated controller to dynamically alter UPQC operation in order to maintain power

quality requirements across these fluctuations. A significant research gap in this field is the development of robust, adaptive control methods that can dynamically tune the PI controllers in real-time to handle varying operational conditions. Traditional methods, such as the Ziegler-Nichols (ZN) approach, often fail to provide optimal performance under dynamic and unpredictable load conditions. These conventional tuning methods are typically static and do not adapt to changes in the system, leading to suboptimal performance and potential stability issues in the DC link voltage. To sustain optimal performance amid changing load demands and grid conditions, this adaptive control is essential. Particle Swarm Optimization (PSO) presents a superior approach for tuning the PI controller for the DC link due to its ability to dynamically optimize parameters in real-time. PSO is a population-based stochastic optimization technique [16] inspired by the social behavior of birds flocking or fish schooling. It excels in finding optimal solutions in complex, multi-dimensional spaces with its iterative improvement process. By employing PSO, the PI controller parameters can be continuously adjusted to respond to changing load conditions and disturbances, ensuring optimal performance and stability of the DC link voltage. This adaptability and real-time optimization capability make PSO a better choice for maintaining the stability and reliability of UPQC-DG systems compared to traditional tuning methods. In addition, the use of advanced control algorithms, such as the power angle control [17] approach, results in increased efficiency, reduced energy losses, and optimised UPQC operation with respect to particular goals like harmonic reduction and voltage regulation. Furthermore, enhanced controllers enable UPQC to participate in ancillary services and grid support activities via smooth connection with the grid. Enhancing understanding of the losses caused by different control mechanisms would significantly contribute to the development of UPQC systems that are more efficient and adaptable.

The ideal size of UPQCs has a significant impact on both their overall performance and cost-effectiveness. In order to do this, the proper rating and capacity of UPQCs must be determined in accordance with the load profiles, power system characteristics, and particular power quality concerns that need to be resolved. Dynamic fluctuations in load circumstances are common in power systems, and it can be challenging to figure out the ideal size of UPQCs given different load profiles. Developing methods and algorithms to dynamically modify UPQC sizes in response to shifting load situations, making sure they stay at the ideal size for effective power quality enhancement. Implementing optimisation frameworks that take additional

performance measures into account in addition to cost-effectiveness. These frameworks can help designers make well-informed decisions and achieve a balance between competing objectives. When evaluating UPQC integrated with distributed generation (UPQC-DG), it is important to take into account the extra complexity that distributed generation brings together with the performance of the system in terms of reducing power quality problems. Variations that affect power losses differently are introduced by the existence of distributed generation in UPQC-DG. The integration of distributed generation sources, such as wind turbines or solar panels, brings new elements and operational considerations with UPQC-DG. In addition to losses in the distributed generation system, such energy storage losses and inverter conversion losses, the losses in UPQC-DG also include losses related to the UPQC itself.

UPQC combined with distributed generation [18–21] can also export reactive power to the grid in a controlled and regulated way in addition to load reactive power compensation. Complex control procedures are needed when exporting reactive power to the grid via UPQC-DG. Complex control algorithms are required due to the dynamic characteristics of reactive power and the unpredictable behaviour of distributed generation. The interactions between power systems and the grid are governed by grid rules and regulations. These restrictions apply to reactive power export, and strict monitoring is required to ensure compliance.

1.3 Objectives of Proposed Research

Proposed research work has been divided into the following objectives:

1. To develop improved control strategies for enhanced power sharing using an advanced controller for a UPQC integrated with renewable energy under various operating conditions of the load, grid & DGs.

2. To develop an optimal UPQC design technique for sizing passive filtering elements with increased performance based on modified SRF-PAC.

3. To evaluate losses associated with UPQC and UPQC-DG using different control strategies under different operating conditions.

4. Enhancing utilization of UPQC integrated with renewable energy in smart grids by providing reactive power support to the grid.

1.4 Thesis Organization

The organization of the thesis is as follows:

Chapter-1 outlines the background, motivation, and aims of the research conducted in the thesis.

Chapter-2 describes the literature surveys and various existing control techniques of UPQC-DG and identifies research gaps for further improvement.

Chapter-3 explains the design and development of Unified Power Quality Conditioner (UPQC) and UPQC-DG (Distributed Generation) in MATLAB simulation and evaluate its performance using Synchronous Reference Frame (SRF) and Unit Vector Template Generation (UVTG) management techniques.

Chapter-4 proposes a method to improve the tuning of PI control for enhanced DC link voltage stabilization. This study also incorporates power angle control (PAC), which distributes the reactive power burden among APFs to optimize the size of UPQC-DG. The PAC control approach includes VA limits to ensure that converters operate within design ratings. The proposed technique demonstrates superior performance compared to conventional ZN methods in managing DC voltage stabilization. This study is validated through real-time simulation using the Opal-RT OP4512.

Chapter-5 suggests control and design strategies to improve UPQC's compensation while minimizing size and expense. It proposes optimizing passive filters using Particle Swarm Optimization (PSO) to improve key performance indexes such as optimizing THD, power factor, losses, and voltage control. This proposed method surpasses traditional techniques in terms of improving the system's efficiency.

Chapter-6 examines the comparative power loss in UPQC-P, UPQC-Q, and UPQC-S. It uses MATLAB simulations to determine the power consumption losses of three-phase UPQC control techniques (P, Q, and S) under different grid and load disturbances.

Chapter-7 compares the power losses caused by non-linear loads under different operating conditions using UPQC and UPQC-DG/IDG. It demonstrates that the UPQC-DG system is more effective and practical for real-world applications.

Chapter-8 proposes enhancements to the UPQC-DG system to provide controllable reactive power support to the grid. Utilizing Synchronous Reference Frame (SRF) and Unit Vector Template Generation (UVTG) theories, the control method incorporates an additional PI controller to regulate reactive power flow.

Chapter-9 presents the hardware result validation of the shunt APF, UPQC-DG for different operating conditions and proposed PSO-based PI controller on PV-fed shunt APF.

Chapter-10 concludes the thesis by providing an overview to research accomplishments and the future research prospects.

Bibliography

[1] B. Singh, A. Chandra, and K. Al-Haddad, *Power quality: problems and mitigation techniques*. John Wiley & Sons, 2014.

[2] N. G. Hingorani and L. Gyugyi, *Understanding FACTS: concepts and technology of flexible AC transmission systems*. Wiley-IEEE Press, 2000.

[3] A. Ghosh and G. Ledwich, *Power quality enhancement using custom power devices*. Springer science & business media, 2012.

[4] H. Akagi, "Trends in active power line conditioners," *IEEE transactions on power electronics*, vol. 9, no. 3, pp. 263–268, 1994.

[5] B. Singh, K. Al-Haddad, and A. Chandra, "A review of active filters for power quality improvement," *IEEE transactions on industrial electronics*, vol. 46, no. 5, pp. 960–971, 1999.

[6] D. Li, T. Wang, W. Pan, X. Ding, and J. Gong, "A comprehensive review of improving power quality using active power filters," *Electric Power Systems Research*, vol. 199, p. 107389, 2021.

[7] H. Fujita and H. Akagi, "The unified power quality conditioner: The integration of series and shunt-active filters," *IEEE Transactions on Power Electronics*, vol. 13, no. 2, pp. 315–322, 1998.

[8] V. Khadkikar, "Enhancing electric power quality using UPQC: A comprehensive overview," *IEEE Transactions on Power Electronics*, vol. 27, no. 5, pp. 2284–2297, 2012.

[9] W. C. Lee, D. M. Lee, and T. K. Lee, "New control scheme for a unified power-quality compensator-Q with minimum active power injection," *IEEE Transactions on Power Delivery*, vol. 25, no. 2, pp. 1068–1076, 2009.

[10] H. Akagi, Y. Kanazawa, and A. Nabae, "Instantaneous reactive power compensators comprising switching devices without energy storage components," *IEEE Transactions on industry applications*, no. 3, pp. 625–630, 1984.

[11] S. Bhattacharya and D. Divan, "Synchronous frame based controller implementation for a hybrid series active filter system," in *IAS'95. Conference Record of the 1995 IEEE Industry Applications Conference Thirtieth IAS Annual Meeting*, vol. 3. IEEE, 1995, pp. 2531–2540.

[12] N. Patnaik and A. K. Panda, "Performance analysis of a 3 phase 4 wire UPQC system based on PAC based SRF controller with real time digital simulation," *International Journal of Electrical Power & Energy Systems*, vol. 74, pp. 212–221, 2016.

[13] Y. Lu, G. Xiao, X. Wang, F. Blaabjerg, and D. Lu, "Control strategy for single-phase transformerless three-leg unified power quality conditioner based on space vector modulation," *IEEE Transactions on Power Electronics*, vol. 31, no. 4, pp. 2840–2849, 2016.

[14] A. Q. Ansari, B. Singh, and M. Hasan, "Algorithm for power angle control to improve power quality in distribution system using unified power quality conditioner," *IET Generation, Transmission & Distribution*, vol. 9, no. 12, pp. 1439–1447, 2015.

[15] V. Khadkikar, "Fixed and variable power angle control methods for unified power quality conditioner: operation, control and impact assessment on shunt and series inverter kVA loadings," *IET Power Electronics*, vol. 6, no. 7, pp. 1299–1307, 2013.

[16] J. Kennedy and R. Eberhart, "Particle swarm optimization," in *Proceedings of ICNN'95 - International Conference on Neural Networks*, vol. 4, 1995, pp. 1942–1948 vol.4.

[17] A. Patel, S. K. Yadav, H. D. Mathur, S. Bhanot, and R. C. Bansal, "Optimum sizing of PV based UPQC-DG with improved power angle control," *Electric Power Systems Research*, vol. 182, p. 106259, 2020.

[18] A. R. Reisi, M. H. Moradi, and H. Showkati, "Combined photovoltaic and unified power quality controller to improve power quality," *Solar Energy*, vol. 88, pp. 154–162, 2013.

[19] V. Madhaiyan and V. Subramaniam, "Extended reference signal generation scheme for integration of unified power quality conditioner in grid-connected photovoltaic system," *Electric Power Components and Systems*, vol. 43, no. 8-10, pp. 914–927, 2015.

[20] S. Devassy and B. Singh, "Enhancement of power quality using solar PV integrated UPQC," in *2015 39th National Systems Conference (NSC)*. IEEE, 2015, pp. 1–6.

[21] S. Devassy and B. Singh, "Design and performance analysis of three-phase solar PV integrated UPQC," *IEEE Transactions on Industry Applications*, vol. 54, no. 1, pp. 73–81, 2017.

Chapter 2

Literature Review

2.1 Preamble

A Unified Power Quality Conditioner (UPQC) is a special type of electrical device used to improve the quality of power in a distribution system. It is a complete solution made to reduce different types of disruptions in distribution networks and improve power quality. To solve voltage and current-related problems at the same time, they [1] successfully integrate the features of a Distribution Static Compensator (DSTATCOM) and a Dynamic Voltage Restorer (DVR) into a single device. Together, these two filters have the ability to significantly reduce a variety of power quality issues, improving the dependability and effectiveness of the power supply for delicate equipment.

In section 2.2, this chapter covers the topologies and controls of UPQC and provides a brief overview of recent advances. A brief introduction of power angle control (PAC) is explained in section 2.3. Enhanced power quality and energy efficiency using UPQC-DG are described in section 2.4. A summary of the literature review is offered in the form of research gaps at the conclusion of the study (section 2.5).

2.2 Topologies and Control Techniques of UPQC

2.2.1 Topologies

A number of topologies have been developed in recent decades to address different power quality issues. The UPQC topologies are determined by the types of converters [2, 3] utilised, the supply system, the topology configuration, and the control

algorithms that impact the overall system rating. The two primary categories into which the UPQC is divided are 1) physical structure and 2) control mechanism. The complete hierarchy of the classification is shown in the Fig. 2.1.

UPQC can be categorised based on the physical structure to address power quality issues. Variations in the physical configuration of its components can influence the performance, control system design, implementation complexity, and overall implementation costs. These structural changes play a critical role in determining the efficiency and effectiveness of the UPQC in mitigating power quality problems. The first category is based on the converter types [2, 3], UPQCs can be modelled using voltage source inverters (VSI) [4–9], current source inverters (CSI) [2, 3] and multilevel converter [10–12]. Compared to UPQC-VSI, UPQC-CSI exhibits better current control ability and reliability. This is due to its faster response to changes in load current, ability to inject reactive power to regulate output voltage during voltage interruptions, and the need for fewer switching operations to control output current. But unlike UPQC-VSI, which is significantly smaller and less costly, UPQC-CSI uses larger DC side filters and lacks the proper switching devices which makes it costly and causes power losses.

UPQC can be supplied either by for single phase supply $(1-\phi)$ and three phase supply $(3-\phi)$. A single-phase UPQC (two wire) [13, 14] is specifically designed for use in environments with single-phase power systems, commonly found in residential or small commercial applications. It addresses power quality issues specific to single-phase loads, incorporating a series compensator to handle voltage-related problems and a shunt compensator to manage current-related issues in this context. On the other hand, a three-phase UPQC (three wire and four wire) [15, 16] is engineered to cater to larger and more complex three-phase power systems, prevalent in industrial and commercial applications. It provides a comprehensive solution for correcting power quality issues in three-phase environments, including voltage imbalances, harmonic distortions, and power factor irregularities. A three-phase UPQC ensures the overall stability and quality of the three-phase power supply by configuring both series (DVR) and shunt (DSTATCOM) compensators to simultaneously handle the complexity of multiple phases. Three-phase, three-wire UPQC is the most widely researched design. While the DVR is linked in series with the grid system via an injection transformer, the DSTATCOM is connected in parallel with the load. The DVR's VSC and the DSTATCOM's VSC are both connected to the same DC connection. The purpose of controlling these two VSCs is to increase the load currents

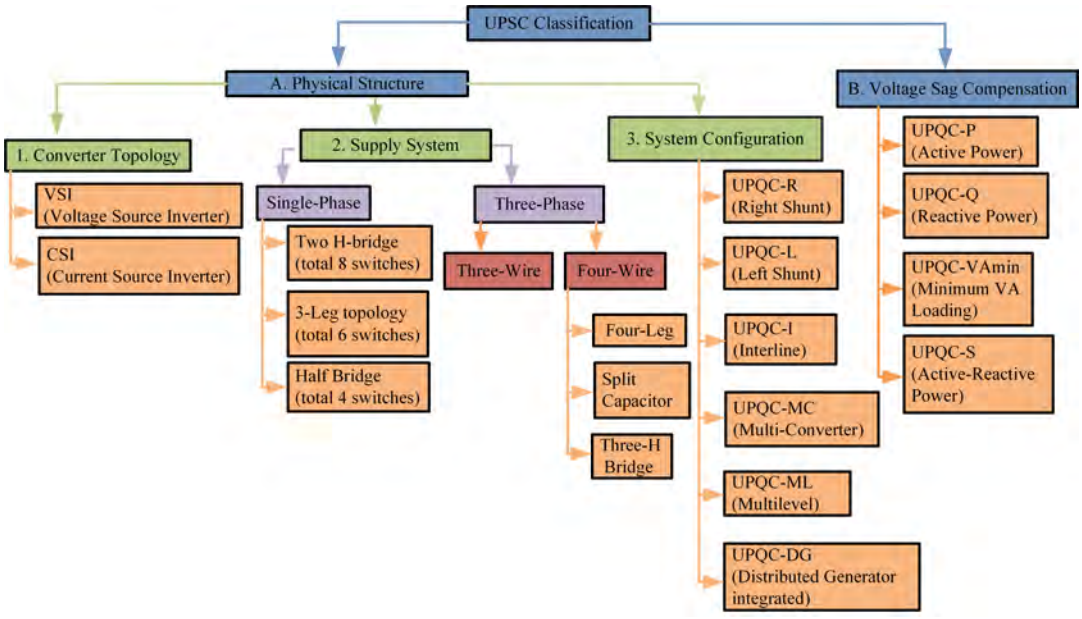

Figure 2.1: Classification of UPQC topologies

and PCC voltage as well as the power quality. Nonetheless, a fourth wire known as a neutral conductor referred to as a 3-phase 4 wire UPQC is necessary to reduce the high neutral current and has been developed in a variety of configurations such as UPQC with Four leg inverter, UPQC with split capacitor, and UPQC with three H-bridge inverter.

Another way to categorise UPQC is by topology or configuration, such as left shunt compensator (UPQC-L) [17] and right shunt compensator (UPQC-R) [18]. The DSTATCOM is attached to the right side of the load in UPQC-R to handle load current problems and enhance the overall power factor by injecting or absorbing reactive power as required. The DVR reduces sag and swell to manage the terminal voltage at the load. For important and sensitive loads, current-based compensation is provided when the shunt compensator is connected to the left side of the UPQC-R load. It has higher control complexity and is more expensive than UPQC-R. When compared to UPQC-L, structurally, UPQC-R provides a greater overall UPQC performance [3]. Because the current flow through a series transformer in a UPQC-R arrangement is primarily sinusoidal, UPQC-R is frequently employed. The UPQC-L is rarely employed to mitigate interference between passive filters and shunt inverters.

There are instances where the UPQC is connected to two feeders supplying loads from different substations, with the first feeder equipped with a series compensator

and the second feeder with a shunt compensator. When dealing with sensitive loads, the industrial sector often uses a configuration known as I-UPQC (interline) [19]. The voltage of feeder 1 (line) can be regulated while maintaining the power flow across feeder 2 (line) with UPQC connected between them. The purpose of interline UPQC is to enhance the power quality of multi-connected feeders.

Multilevel UPQC is another configuration that is developed by swapping out the two-level inverter of series and shunt compensator with the multilevel inverter. The number of semiconductor switches may be increased for specific levels, such as the 3 level, 5 level, and so on, to achieve high power. This increases the control complexity of the system and makes it even bulkier.

As an alternative to conventional centralised power plants, distributed generation (DG) is an evolution in the generation and distribution of energy. In addition to increasing the electricity grid's resilience and dependability, this strategy lowers transmission losses and lessens the effect of single-point failures. It generates electricity locally using smaller sources, such as wind turbines or solar panels. This reduces the possibility of issues impacting a wide region, which contributes to the reliability of energy. DG's frequent usage of greener energy sources makes it advantageous for the environment as well. To increase the potential of DG to reduce power losses and enhance the power quality of distribution networks, it can be combined with custom power devices. These devices are termed as UPQC-DG [2, 20–23]. The DG is connected to the DC link of the UPQC in order to provide the grid with controlled and regulated active power. A battery can be added to the UPQC-DG at the DC link, which is useful for storing excess produced power and serving as a backup in the event of an islanding mode (or interconnected mode).

Based on the control mechanism (or sag compensation) the UPQC can be further classified into four types: UPQC-P, UPQC-Q, UPQC-VA_{min} and UPQC-S. The disruption in the rms value line voltage carried on by a temporary reduction in the real voltage between 0.1 and 0.9 p.u. is known as voltage sag. It may affect devices and systems that are linked to the electrical grid in a number of ways, including failures in delicate electronic devices and inefficient performance of variable-frequency motors. It is known as UPQC-P (active power) [24, 25] when voltage sag is corrected by injecting active power via UPQC. In this approach, in-phase voltage is injected in series with the source voltage via an injection transformer by a series APF, while the shunt APF compensates for reactive power. The subtracted amplitude of the load voltage from the desired voltage equals the amount of voltage that is injected. Both

voltage swell and voltage sag compensation can accomplished with this technique. By using a series inverter in UPQC, voltage sag can also be compensated by injecting reactive power. When this occurs, it is referred to as UPQC-Q compensation [7], with Q representing reactive power. The reactive power is injected perpendicularly to the source voltage without any active power injection using a series inverter. The voltage at the load is the resultant of the vector addition of the injected voltage and the source voltage. Nevertheless, active power injection is unnecessary as a result of this approach. A shunt inverter is used to maintain a unity power factor at the load side. However, in some literature, rather of injecting the in-phase/quadrature component directly into the line, it is injected at a certain optimal angle to limit the VA loading of the UPQC. The term often used to refer to this kind of compensation is UPQC-VA_{min} [5].However, when the series APF delivers both active and reactive power at a predetermined angle with VA limits to fully utilize the VA rating of the inverters, this type of UPQC is known as UPQC-S [6], where S is denoted for apparent power. This unique concept solves both the sag and swell compensation problems. The compensation burden is shared between series APF and shunt APF.

2.2.2 Control Techniques

Operating a UPQC requires using a range of advanced control strategies to achieve best performance in addressing power quality problems. Several control algorithms have been devised to regulate the DSTATCOM and DVR. The control algorithm identifies the reference signals for current and voltage and adjusts the fraction of voltage and current to be injected in order to achieve the desired performance of UPQCs. These control strategies/ algorithms/ techniques fall into two categories: time domain and frequency domain (Table 2.1). The time domain group includes the Synchronous Reference Frame Theory (SRFT) (D-Q Theory) [26–30], the Instantaneous Reactive Power Theory (IRPT) (p-q Theory) [1, 31–33], the Instantaneous Symmetrical Component Theory (ISCT), the Enhanced Phase Locked Loop Theory (EPPL), and Unit Vector Template Generation (UVTG) (also known as PI controller-based). Discrete Fourier Transform (DFT), Fast Fourier Transform (FFT), Wavelet Transformation Theory [34], Kalman Filter Theory [35] etc. belong to the category of frequency domain techniques. The time domain techniques are faster than the frequency domain techniques and better suited for real-time control of UPQC [3]. Frequency domain methods are mostly used for power quality monitoring, such as in

power analyzers, PQ instruments, and so on, while some have been used for control of UPQC but are slow and require heavy computational calculation.

SRFT and IRPT are the most widely used time domain control techniques. Both methods transform the voltage and current signals in the ABC form to a stationary reference form (p-q theory) or a synchronously rotating frame (d-q theory). The p-q theory uses the Clark transformation of current and voltage to determine zero-sequence power, real power, and imaginary power. IRPT [6, 22, 36] is used to separate the fundamental positive and negative sequence components of instantaneous currents. This transformation technique has also been used for the power angle control (PAC) of UPQC [6, 37, 38]. The P-Q theory shows limitations when the supply voltages are distorted or unbalanced, whereas the D-Q theory is able to get a pure sinusoidal current waveform even in the presence of distorted voltages. In UTVG, the three-phase reference signals are extracted using a PLL (phase-locked loop) to get a pure sinusoidal signal at the fundamental frequency. The ISCT does not need a phase-locked loop to determine the current references. It extracts the fundamental positive sequence component when the supply voltage is unbalanced. In order to optimise the utilisation of the DSTATCOM and DVR, a technique known as power angle control is devised [36–40]. This method distributes the reactive power demand appropriately between both inverters while ensuring that the overall UPQC rating remains unaffected.

Enhanced power quality is the result of implementing a hysteresis controller

Table 2.1: Algorithms for UPQC control

S.No.	Time domain algorithms	Frequency domain algorithms
1.	Synchronous reference frame theory	Fourier series theory
2.	Instantaneous reactive power theory	Discrete Fourier transform theory
3.	Unit vector Template Generation	Fast Fourier transform theory
4.	Instantaneous symmetrical components theory	Kalman filter based control
5.	Power balance theory	Wavelet transform theory
6.	Neural Network Theory	Stockwell transformation theory
7.	PI controller based algorithm	
8.	Current synchronous detection (CSD) method	
9.	Single phase PQ theory	
10.	Enhanced phase locked loop based control	
11.	Conductance based control algorithm	

based on ANFIS [41]. This methodology controls the output voltage and current of the series active power filter (APF) and the shunt APF, respectively, via neural network back propagation. In UPQC the regulation of DC link voltage enhances the compensation capability of UPQC. To regular the DC link, online self tuning of PI is used in article [42] is achieved using Model Reference Adaptive System (MRAS) technique is used. On the basis of the state-space model, the MPC control algorithm is implemented in UPQC in some publications [43, 44]. The objective of the control strategy is to maintain the load voltage and source current at the specified levels.

2.3 Power Angle Control - A brief description

The introduction of the power angle control algorithm in UPQC systems represents a notable progress in contrast to traditional methods. Traditional methods for load-reactive power adjustment mostly depend on the use of shunt inverters, while series inverters are largely used to handle voltage-related concerns. By using the power angle control approach, the shunt and series APFs work together to distribute the load-reactive power demand [37]. This novel method not only decreases the shunt APF rating but also enhances the utilisation of the series inverter, resulting in cost reductions and enhanced device efficiency. The power angle control approach guarantees that the series APF may effectively assist in correcting for load-reactive power demand without adding extra active power load on the source during steady-state operation. Moreover, this sophisticated control method improves the efficiency of UPQC in different operational scenarios, enabling rapid adjustment to fluctuations in active and reactive power, as well as load properties. In summary, the power angle control algorithm used in UPQC systems provides a more advanced and synchronised control method that enhances the distribution of reactive power between shunt and series inverters. This leads to enhanced performance, efficiency, and cost-effectiveness when compared to traditional techniques.

In article [40], the proposed SRF-based PAC technique improves power quality and regulates the distribution of reactive power in UPQC. This is achieved by using a novel control algorithm that guarantees equal sharing of reactive power between the shunt and series inverters, even when the source voltage is imbalanced. This technique use synchronous reference frame (SRF) control to calculate the power angle for sharing reactive power, even when there is voltage imbalance. The method successfully coordinates the inverters to share reactive power by using decoupled load

current parameters. This coordination remains efficient even when there are fluctuations in the source voltage, such as sag, swell, or unbalancing. This method facilitates the consistent and balanced allocation of reactive power between the shunt and series inverters, resulting in enhanced power quality and optimal functioning of the UPQC system.

However, relying on the source voltage as the reference signal restricts the system's ability to adapt to changes in load conditions. This limitation can result in less efficient power transfer and reduced overall system performance. In situations where the load voltage deviates significantly from the source voltage, using the source voltage as a reference signal may lead to increased power losses due to inefficient power transfer and reactive power compensation. This constraint may lead to decreased power transmission efficiency and diminished overall system performance. When the load voltage differs much from the source voltage, utilising the source voltage as a reference signal might result in higher power losses owing to inefficient power transfer and reactive power adjustment.

Utilising the source voltage as the reference signal may lead to instability in the system, particularly when there are significant power angle disparities between the source and load voltages. This instability has the potential to impact the overall dependability and functioning of the system. A rectification is necessary to enhance power angle support for improved control of reactive power, in addition to adjusting the VA rating of converters. In order the address the issue, the load voltage is used as reference signal in [45] for larger power angle. That means, the controller can effectively manage the larger reactive power compensation provided by the series and shunt compensators, optimizing their utilization and ensuring efficient operation under varying load conditions.

2.4 UPQC-DG for Enhanced Power Quality and Energy Efficiency

Renewable energy sources, namely solar and wind energy, are essential foundations in the shift towards a sustainable and eco-friendly energy framework. Solar energy uses photovoltaic cells to capture and convert sunlight into electrical energy. The accessibility of this technology has been steadily improving, as seen by the widespread use of solar panels on roofs and the establishment of large solar farms that harness

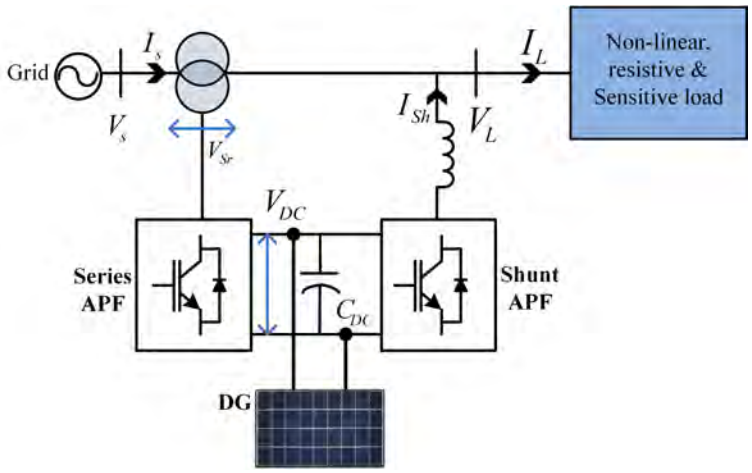

Figure 2.2: Unified Power Quality Conditioner with Distributed Generation (UPQC-DG)

sunlight to produce environmentally friendly electricity. Conversely, wind energy harnesses the kinetic energy of the wind to rotate turbines and generate electricity. Wind farms, often located in expansive regions or offshore sites, provide a substantial contribution to the worldwide capacity of renewable energy. Solar and wind [46] energy both have many benefits, such as unlimited availability, less greenhouse gas emissions, and the possibility of decentralised power generation.

The incorporation of renewable energy into the UPQC system has significantly accelerated in recent years. The system configuration is referred to as UPQC-DG (Fig. 2.2). The UPQC-DG is a sophisticated electrical device that aims to improve power quality in distribution networks by integrating distributed generating technology. This system integrates the features of a unified power quality conditioner (UPQC) with the capacity to capture electricity from renewable energy resources such as solar panels or wind turbines. The UPQC component actively handles voltage and current-related disturbances, such as sags, swells, harmonics, and power factor concerns, guaranteeing a clean and steady power supply. Concurrently, the distributed generating component enables the incorporation of renewable energy into the system, fostering sustainability. The UPQC-DG not only addresses power quality concerns but also helps to minimise the environmental footprint by using clean and sustainable energy sources. This comprehensive method offers a complete solution for contemporary power distribution systems, in line with the objectives of dependability, effectiveness, and environmental awareness in the changing field of electrical power production and distribution.

The DG is connected to the UPQC using a DC link capacitor that is linked to

both the DSTATCOM and DVR. If there is a disruption in the power supply, the distributed generation (DG) system will provide power to the load by using the shunt active power filter (APF) of the UPQC-DG. It has extra functionality in addition to its existing power quality adjustment capabilities. In the article, the wind generator is linked to the DC link via the rectifier [47–49]. The turbine's mechanical energy is transformed into electrical energy through the utilization of a generator. The wind energy system supplies power through two modes: interconnected mode and islanding mode. During the first mode, wind generators supply power to both the source and load. In the second mode, wind generators only supply power to the load when there is a voltage interruption. The UPQC system comprises three components: a wind turbine, an induction generator, and a rectifier. Most two type of indiuction generator are used DFIG and SFIG. SFIG has negative impact on the stability as fails to remain connected to the grid in the event of grid voltage dip or line fault due to excessive reactive power requirement. Due to new grid code, SFIG is phased out and replaced with DFIG as it remained connected even in the presence of the disturbance. In order to improve the low voltage ride through capability of the DFIG [50], suppress voltage oscillations under unbalanced faults and regulate DFIG output power during fluctuated wind speed conditions (ESD-UPQC) [51] is proposed.

Solar PV is integrated to DC link of the UPQC-DG through a DC-DC converter [52]. It provides additional active power to the load and regulated DC voltage during availability of solar energy. Generally a DDC boost converter is used to boost the voltage of the Solar panel. However in some case solar panel is directly connected to the solar PV is integrated into the DC link of the UPQC-DG through a DC-DC converter (Fig. 2.2). It provides additional active power to the load and regulates DC voltage during the availability of solar energy. Generally, a DC-DC boost converter is used to boost the voltage from the solar PV. However, in some cases, the solar panel is directly connected to the DC link via a reverse blocking diode to reduce the cost of the overall system. The hybrid Wind-PV UPQC is implemented in the literature to gain the advantage of both distributed generations. Since this method is based on a dual compensation scheme, the parallel converter works as a sinusoidal voltage source, while the series converter works as a sinusoidal current source.

2.5 Research Gaps

Based on an exhaustive literature survey, the following research gaps have been identified in a study of UPQC. These are then taken up in this work, as described in the subsequent chapters.

- The SRF-PAC technique is used to enhance the efficiency of UPQC-based compensation, which depends on the stability of the DC link. However, a comprehensive online implementation of controlling DC link voltage, including DG, has not been documented in the available literature.
- The appropriate size of a passive filter in a UPQC is an important topic that requires attention. In modern power systems, it is crucial to carefully choose an RC filter and interface inductors that can effectively minimize losses and improve the performance of the Unified Power Quality Conditioner.
- Many studies tend to only generalize losses by doing a specific examination, which complicates a thorough understanding. To bridge this gap, a detailed investigation that integrates simulation and real-world situations is required to provide precise insights into power loss variances across UPQC control schemes.
- Furthermore, the power losses analysis in the UPQC and UPQC-DG lacks a thorough examinations that considers different grid circumstances, load types, and degrees of DG integration, which hinders the appropriate implementation and evaluation of performance in real-world situations.
- Although conventional UPQC has used reactive power support to strengthen its role as an ancillary service provider within smart grid distribution systems, UPQC-DG has not yet integrated with this provision into its operations.

Bibliography

[1] H. Fujita and H. Akagi, "The unified power quality conditioner: The integration of series and shunt-active filters," *IEEE Transactions on Power Electronics*, vol. 13, no. 2, pp. 315–322, 1998.

[2] V. Khadkikar, "Enhancing electric power quality using UPQC: A comprehensive overview," *IEEE Transactions on Power Electronics*, vol. 27, no. 5, pp. 2284–2297, 2012.

[3] B. Singh, A. Chandra, and K. Al-Haddad, *Power quality: problems and mitigation techniques*. John Wiley & Sons, 2014.

[4] G. S. Kumar, P. H. Vardhana, B. K. Kumar, and M. K. Mishra, "Minimization of VA loading of unified power quality conditioner (UPQC)," in *2009 International Conference on Power Engineering, Energy and Electrical Drives*. IEEE, 2009, pp. 552–557.

[5] W. C. Lee, D. M. Lee, and T. K. Lee, "New control scheme for a unified power-quality compensator-Q with minimum active power injection," *IEEE Transactions on Power Delivery*, vol. 25, no. 2, pp. 1068–1076, 2010.

[6] V. Khadkikar and A. Chandra, "UPQC-S: A novel concept of simultaneous voltage sag/swell and load reactive power compensations utilizing series inverter of UPQC," *IEEE Transactions on Power Electronics*, vol. 26, pp. 2414–2425, 2011.

[7] V. Khadkikar and A. Chandra, "A novel control approach for unified power quality conditioner Q without active power injection for voltage sag compensation," in *2006 IEEE International Conference on Industrial Technology*. IEEE, 2006, pp. 779–784.

[8] V. Khadkikar, A. Chandra, A. Barry, and T. Nguyen, "Power quality enhancement utilising single-phase unified power quality conditioner: digital signal processor-based experimental validation," *IET Power Electronics*, vol. 4, no. 3, pp. 323–331, 2011.

[9] T. Zhili and Z. Dongjiao, "Design of DC voltage controller for UPQC by using its small signal model," in *2010 International Conference on Electrical and Control Engineering*, 2010, pp. 3572–3575.

[10] J. A. Muñoz, J. R. Espinoza, C. R. Baier, L. A. Moran, E. E. Espinosa, P. E. Melin, and D. G. Sbarbaro, "Design of a discrete-time linear control strategy for a multicell UPQC," *IEEE Transactions on Industrial Electronics*, vol. 59, no. 10, pp. 3797–3807, 2012.

[11] X. Xiao, J. Lu, C. Yuan, and Y. Yang, "A 10kV 4MVA unified power quality conditioner based on modular multilevel inverter," in *Proc. IEEE International Electric Machines & Drives Conference*. IEEE, 2013, pp. 1352–1357.

[12] S. A. González and M. I. Valla, "UPQC implemented with cascade asymmetric multilevel converters," *Electric Power Systems Research*, vol. 124, pp. 144–151, 2015.

[13] J. Correa, S. Chakraborty, M. Simoes, and F. Farret, "A single phase high frequency AC microgrid with an unified power quality conditioner," in *38th IAS Annual Meeting on Conference Record of the Industry Applications Conference, 2003.*, vol. 2. IEEE, 2003, pp. 956–962.

[14] J. Correa, F. Farret, and M. Simoes, "Application of a modified single-phase PQ theory in the control of shunt and series active filters in a 400 Hz microgrid," in *2005 IEEE 36th Power Electronics Specialists Conference*. IEEE, 2005, pp. 2585–2591.

[15] V. Khadkikar and A. Chandra, "A novel structure for three-phase four-wire distribution system utilizing unified power quality conditioner (UPQC)," *IEEE Transactions on Industry Applications*, vol. 45, no. 5, pp. 1897–1902, 2009.

[16] B. Singh and P. Venkateswarlu, "A simplified control algorithm for three-phase, four-wire unified power quality conditioner," *Journal of Power Electronics*, vol. 10, no. 1, pp. 91–96, 2010.

[17] N. Patnaik and A. K. Panda, "Extensive application of UPQC-L for a dual point of common coupling system with multiple loads under unbalanced source condition," *Electric Power Components and Systems*, vol. 45, no. 15, pp. 1653–1666, 2017.

[18] B. Mohammed, K. R. Rao, R. Ibrahim, and N. Perumal, "Performance evaluation of R-UPQC and L-UPQC based on a novel voltage detection algorithm," in *2012 IEEE Symposium on Industrial Electronics and Applications*. IEEE, 2012, pp. 167–172.

[19] A. K. Jindal, A. Ghosh, and A. Joshi, "Interline unified power quality conditioner," *IEEE Transactions on Power Delivery*, vol. 22, no. 1, pp. 364–372, 2006.

[20] S. Devassy and B. Singh, "Dynamic performance of solar PV integrated UPQC-P for critical loads," in *Proc. 12th IEEE India Council International Conference*, 2015, pp. 1–6.

[21] S. Devassy and B. Singh, "Enhancement of power quality using solar PV integrated UPQC," in *2015 39th National Systems Conference (NSC)*. IEEE, 2015, pp. 1–6.

[22] S. Devassy and B. Singh, "Modified pq-theory-based control of solar-PV-integrated UPQC-S," *IEEE Transactions on Industry Applications*, vol. 53, no. 5, pp. 5031–5040, 2017.

[23] S. Devassy and B. Singh, "Design and performance analysis of three-phase solar PV integrated UPQC," *IEEE Transactions on Industry Applications*, vol. 54, no. 1, pp. 73–81, 2017.

[24] V. Khadkikar, A. Chandra, A. Barry, and T. Nguyen, "Analysis of power flow in UPQC during voltage sag and swell conditions for selection of device ratings," in *2006 Canadian Conference on Electrical and Computer Engineering*. IEEE, 2006, pp. 867–872.

[25] V. Khadkikar, A. Chandra, A. O. Barry, and T. D. Nguyen, "Conceptual study of unified power quality conditioner UPQC," in *2006 IEEE International Symposium on Industrial Electronics*, vol. 2, 2006, pp. 1088–1093.

[26] S. Bhattacharya and D. Divan, "Synchronous frame based controller implementation for a hybrid series active filter system," in *IAS'95. Conference Record of the 1995 IEEE Industry Applications Conference Thirtieth IAS Annual Meeting*, vol. 3. IEEE, 1995, pp. 2531–2540.

[27] D. Graovac, V. Katic, and A. Rufer, "Power quality compensation using universal power quality conditioning system," *IEEE Power Engineering Review*, vol. 20, no. 12, pp. 58–60, 2000.

[28] A. Elnady and M. Salama, "New functionalities of an adaptive unified power quality conditioner," in *2001 Power Engineering Society Summer Meeting. Conference Proceedings (Cat. No. 01CH37262)*, vol. 1. IEEE, 2001, pp. 295–300.

[29] R. SudeepKumar and P. Ganesan, "250 kVA unified power quality controller," in *TENCON 2006-2006 IEEE Region 10 Conference*. IEEE, 2006, pp. 1–4.

[30] M. Kesler and E. Ozdemir, "Synchronous-reference-frame-based control method for UPQC under unbalanced and distorted load conditions," *IEEE Transactions on Industrial Electronics*, vol. 58, no. 9, pp. 3967–3975, 2011.

[31] H. Akagi, Y. Kanazawa, and A. Nabae, "Instantaneous reactive power compensators comprising switching devices without energy storage components," *IEEE Transactions on industry applications*, no. 3, pp. 625–630, 1984.

[32] M. Aredes, K. Heumann, and E. H. Watanabe, "An universal active power line conditioner," *IEEE Transactions on Power Delivery*, vol. 13, no. 2, pp. 545–551, 1998.

[33] A. Moghadasi, S. Torabi, and M. Salehifar, "Performance evaluation of unified power quality conditioner with SMES," in *2010 First Power Quality Conferance*. IEEE, 2010, pp. 1–6.

[34] M. Forghani and S. Afsharnia, "Online wavelet transform-based control strategy for UPQC control system," *IEEE Transactions on Power Delivery*, vol. 22, no. 1, pp. 481–491, 2007.

[35] K. H. Kwan, P. L. So, and Y. C. Chu, "An output regulation-based unified power quality conditioner with kalman filters," *IEEE Transactions on Industrial Electronics*, vol. 59, no. 11, pp. 4248–4262, 2012.

[36] A. Q. Ansari, B. Singh, and M. Hasan, "Algorithm for power angle control to improve power quality in distribution system using unified power quality conditioner," *IET Generation, Transmission & Distribution*, vol. 9, no. 12, pp. 1439–1447, 2015.

[37] V. Khadkikar and A. Chandra, "A new control philosophy for a unified power quality conditioner (UPQC) to coordinate load-reactive power demand between shunt and series inverters," *IEEE Transactions on Power Delivery*, vol. 23, no. 4, pp. 2522–2534, 2008.

[38] V. Khadkikar, "Fixed and variable power angle control methods for unified power quality conditioner: operation, control and impact assessment on shunt

and series inverter kVA loadings," *IET Power Electronics*, vol. 6, no. 7, pp. 1299–1307, 2013.

[39] N. Patnaik and A. K. Panda, "Performance analysis of a 3 phase 4 wire UPQC system based on PAC based SRF controller with real time digital simulation," *International Journal of Electrical Power & Energy Systems*, vol. 74, pp. 212–221, 2016.

[40] A. K. Panda and N. Patnaik, "Management of reactive power sharing and power quality improvement with SRF-PAC based UPQC under unbalanced source voltage condition," *International Journal of Electrical Power & Energy Systems*, vol. 84, pp. 182–194, 2017.

[41] A. S. Kumar, S. Rajasekar, and P. A.-D.-V. Raj, "Power quality profile enhancement of utility connected microgrid system using ANFIS-UPQC," *Procedia Technology*, vol. 21, pp. 112–119, 2015.

[42] A. Senthilkumar and P. A.-D.-V. Raj, "ANFIS and MRAS-PI controllers based adaptive-UPQC for power quality enhancement application," *Electric Power Systems Research*, vol. 126, pp. 1–11, 2015.

[43] G. Wang, Z. Wu, and Z. Liu, "Predictive direct control strategy of unified power quality conditioner based on power angle control," *International Journal of Electrical Power & Energy Systems*, vol. 156, p. 109718, 2024.

[44] J. Kotturu, S. Kothuru, and P. Agarwal, "Simplified predictive control of unified power quality conditioner," in *2018 9th IEEE International Symposium on Power Electronics for Distributed Generation Systems (PEDG)*, 2018, pp. 1–6.

[45] A. Patel, S. K. Yadav, H. D. Mathur, S. Bhanot, and R. C. Bansal, "Optimum sizing of PV based UPQC-DG with improved power angle control," *Electric Power Systems Research*, vol. 182, p. 106259, 2020.

[46] N. Jayanti, M. Basu, M. F. Conlon, and K. Gaughan, "Optimising the rating of the UPQC for applying to the fault ride through enhancement of wind generation," in *Proc. 41st IEEE UPEC*, 2006, pp. 123–127.

[47] M. S. K. Khadem, M. Basu, and M. Conlon, "Power quality in grid connected renewable energy systems: Role of custom power devices," *Renewable Energy and Power Quality Journal*, vol. 8, p. 505, 04 2010.

[48] M. Hosseinpour, A. Yazdian, M. Mohamadian, and J. Kazempour, "Design and simulation of UPQC to improve power quality and transfer wind energy to grid," *Journal of Applied Sciences*, vol. 8, pp. 3770–3782, 2008.

[49] D. I. Mahdi and G. Gorel, "Design and control of three-phase power system with wind power using unified power quality conditioner," *Energies*, vol. 15, no. 19, p. 7074, 2022.

[50] H. Fayek, I. Elamvazuthi, N. Perumal, and B. Venkatesh, "The impact of DFIG and SFIG wind farms on the small signal stability of a power system," in *2014 5th International Conference on Intelligent and Advanced Systems (ICIAS)*. IEEE, 2014, pp. 1–6.

[51] R. H. Yang and J. X. Jin, "Unified power quality conditioner with advanced dual control for performance improvement of DFIG-based wind farm," *IEEE Transactions on Sustainable Energy*, vol. 12, no. 1, pp. 116–126, 2020.

[52] A. R. Reisi, M. H. Moradi, and H. Showkati, "Combined photovoltaic and unified power quality controller to improve power quality," *Solar Energy*, vol. 88, pp. 154–162, 2013.

Chapter 3

Design and Simulation of UPQC

3.1 Preamble

When dealing with power quality problems, accuracy and economy are becoming more and more important in the field of power systems engineering. The "Design and Validation of Unified Power Quality Conditioners (UPQC)" is at the heart of this technology progress. This work goes into great detail about the complicated steps needed to plan, build, and almost certainly test UPQC systems, which are modern devices designed to rectify many different kinds of power quality problems. The introduction provides a comprehensive reviews of several aspects, starting with the first concepts on the system requirements, to the selection of UPQC configurations, and finally the development of an effective control strategy. The introduction talks about how important advanced simulation tools like MATLAB/Simulink are for carefully making UPQC models and how important mathematical modelling is. As this topic goes on, it covers the important steps of validating through modelling, which makes sure that the planned UPQC works well in a variety of operating situations. The introduction provides an overview of this work by demonstrating how theoretical planning, detailed models, and their practical results can improve the quality and effectiveness of power distribution systems.

The development of UPQCs [1] involves the use of two converters: shunt APF and series APF. The two APFs are connected in a back-to-back arrangement, with a common DC link connection linking them. The shunt APF, referred as DSTATCOM (Distribution Static Synchronous Compensator) [2, 3], offers reactive power compensation, load balancing, neutral compensation, and harmonic mitigation. It is connected to the parallel circuit of the load. The series APF, also known as DVR

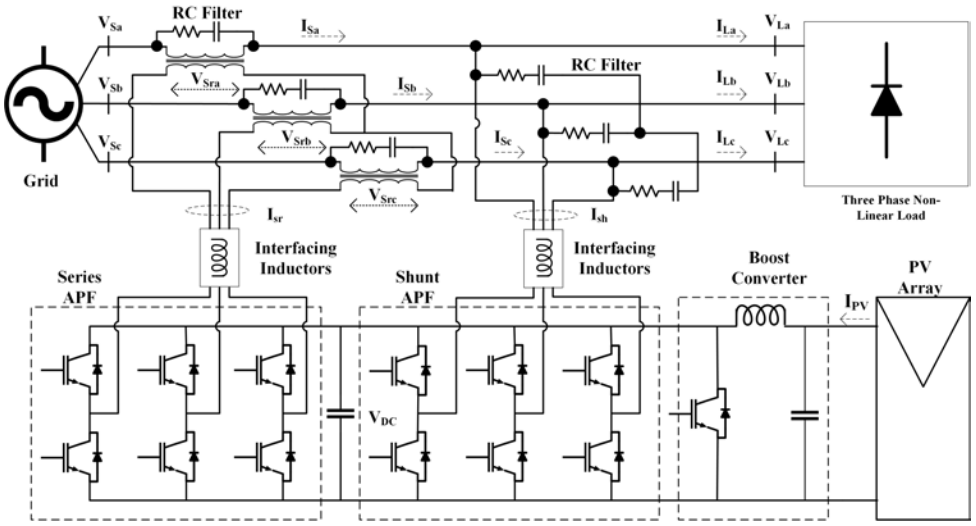

Figure 3.1: Configuration of UPQC-DG with solar PV connected to DC link via a boost converter

(Dynamic Voltage Restorer) [4], ensures that the load voltage remains unaffected by any disruptions in the supply voltage. The system is connected to the grid using an injection transformer, which introduces compensatory voltage between the voltage source and the consumer load. For UPQC-DG, PV is chosen as a DG source due to its economic viability and environmental friendliness. It is linked to the DC link connected between two active power filters (APFs) as shown in Fig. 3.1. The shunt APF delivers active power generated by the photovoltaic (PV) system, eliminating the need for an additional grid-tied tie converter.

Each output of APFs is connected to interface inductors. Utilizing them reduces the amount of ripple current that enters the grid. The output of each APF is equipped with a high-pass RC filter to eliminate high-frequency components generated during the switching of the inverters' IGBTs. To allow high-frequency components to get through, the time constant of the RC filter must be much less than the fundamental time period.

This chapter addresses the conventional approach for developing a Unified Power Quality Conditioner (UPQC) and UPQC with Distributed Generation (UPQC-DG) (in section 3.2). The configuration used for the investigation of Unified Power Quality Conditioner (UPQC) is a three-phase, three-wire system. This chapter presents the guidelines for choosing the appropriate DC capacitor (section 3.3.1), interface inductor (section 3.3.2 & 3.4.2) and ripple filter (section 3.3.3 & 3.4.3).

3.2 Design Procedure of UPQC

The design process for a UPQC is a methodical and interdisciplinary approach that aims to identify and correct power quality problems in electrical power distribution networks. Designers start by defining precise system requirements and then identify the individual power quality issues to be addressed, including voltage sags, swells, harmonics, and power factor correction. The selection of the UPQC configuration, whether it is series or shunt compensators, is a critical decision that relies on the problems that have been determined. The ratings and capacities of the UPQC components are determined to ensure they are suitable for the size of disturbance in the power system. Our first focus should be the design of the APF (see section 3.3), followed by the various equipment linked to the APF's output [1, 5, 6]. The rating of the APF depends on the compensation need and the severity of load imbalance. The voltage rating of the device is determined by the DC link voltage. The design techniques for selecting the equipment for the UPQC and UPQC-DG are provided in the following subsection:

3.3 Design of Shunt APF

3.3.1 Designing the DC Bus Voltage

The shunt active power filter requires a minimum DC link voltage that is more than twice the peak value of the output phase voltage. The DC link voltage may be determined using the following formula [1]:

$$V_{DC,min} = 2\sqrt{2}V_{LL}/\sqrt{3}m \tag{3.1}$$

Keeping as 415 V, and m as 1.0, the minimum value of DC link voltage is found to be 677.7 V and nominal (reference) DC link voltage is selected as 700 V. V_{LL} represents

Table 3.1: Parameters of system

3-phase supply	415 V, 50 Hz, R_S = 0.05 Ω, L_S = 0.25 mH
Load-1	3-phase rectifier (R_{DC} = 15.69 Ω, L_S = 0.1 mH, P_{DC} = 20 kW)
Load-2	3-phase R-L load (10 kW, 0.554 p.f. lagging)
Load-3	3-phase R-L load (10 kW, 0.554 p.f. lagging)

the line-to-line voltage, whereas m represents the modulation index. In the case of the 3-phase system, the line-to-line voltage (V_{LL}) is set at 415V, and the reference direct current (DC) link voltage is chosen at 700 V. By setting the value of m as 1, the V_{DC} gets calculated to be 677.69 V.

The DC capacitor, which is attached to the common DC bus connection, serves as a power storage and provides the necessary DC voltage for the proper functioning of both the DSTATCOM and DVR. A sufficient amount of immediate energy should be available inside the system in order to provide power to DSTATCOM and DVR during instances of transient occurrences. Utilising the theory of energy conservation yields

$$\frac{1}{2}C_{DC}(V_{DC}^2 - V_{dc,1}^2) = 3k_1aVIt \tag{3.2}$$

The variables used in above equation are as follows: C_{DC} represents the capacitance value, V_{DC} represents the nominal DC link voltage, $V_{dc,1}$ represents the minimum DC voltage of the DC link, k_1 denotes the per unit fluctuation in energy during transients, $'a'$ represents the overloading factor, I represents the phase current, and t is the time required for the DC bus voltage to be restored. Given $V_{DC} = 700$ V, $V_{dc1} = 677.69$ V, k_1 = 0.1, $V = 239.60$ V, $I = 32$ A, $t = 30$ ms, and $a = 1.2$, the calculated capacitance value, C_{dc}, is 5560 μF, which is rounded down to 5500 μF.

3.3.2 Designing the Interfacing Inductor

The inductor that is connected between the shunt APF and the grid line is determined by the DC link voltage (V_{DC}), current ripple ($I_{cr,pp}$), and switching frequency (fs). The equation (3.3) that describes this relationship is as follows [6];

$$L_{sh} = \sqrt{3}mV_{DC}/12af_sI_{cr,pp} \tag{3.3}$$

The modulation index, denoted as m, is defined as the ratio of the peak amplitude of the modulating signal to the peak amplitude of the carrier signal. The overloading factor, denoted as a, represents the extent to which a system is overloaded. Given the parameters $I_{cr,pp}$= 10% of 32 A, $f_s = 15$ kHz, and $V_{DC} = 700$ V, with $a = 1.2$ and $m = 1.0$. The value of L_{sh} is determined to be 1.75 mH, and the rounded value is chosen as 1.8 mH.

The shunt APF has a per-phase current rating of 32 A. The rated phase voltage of the APF is equal to the load voltage, and it is kept constant by the series APF. The shunt APF has a three-phase VA rating of 40 kVA.

3.3.3 Designing the RC Filter

The first-order RC high-pass filter is used to eliminate noise from the voltage at the PCC. The filter design requirement necessitates a much smaller time constant in comparison to the fundamental period. The filter's impedance should be high for the fundamental frequency, resulting in minimal current draw at the fundamental frequency [1]. The ripple filter parameters have been chosen as $R = 5\ \Omega$ and $C = 10\ \mu F$, resulting in a time constant of 50 μs. The impedance supplied at the switching frequency is 5.93 Ω, while at the fundamental frequency it is 318 Ω.

3.3.4 Designing the rating of switch

The voltage rating of the switches (V_{sw}) calculated under dynamic circumstances is provided as an estimate:

$$V_{sw} = V_{DC} + V_{d,peak} \tag{3.4}$$

where $V_{d,peak}$ is the maximum overshoot in the DC link

The current rating of the switches under dynamic situations is provided as an estimate.

$$I_{sw} = 1.25(I_{cr,pp} + I_{peak}) \tag{3.5}$$

The switches have a voltage rating of 770 V and a current rating of 60.56 A. The VSCs of DSTATCOM and DVR are equipped with IGBTs that have been carefully chosen to meet the safety requirements, with a voltage rating of 1200 V and a current rating of 300 A.

3.4 Design of Series APF

3.4.1 Selection of Injection Transformer

An injection transformer is used to connect the series APF to the grid. The output voltage of the transformer is determined by the injected voltage when sag compensation is applied. For 40% sag compensation, when taking into account a load with a power factor of 1, the estimated injected voltage (V_c) can be calculated as:

$$V_c = V_{LL} * 0.4 = 239.6 \times 0.4 = 95.8 \tag{3.6}$$

The equation provided below gives the maximum turn ratio of the injecting transformer:

$$n_{T,max} = V_{VSC}/V_{Sr} = 415/(95.8 \times \sqrt{3}) = 2.5 \tag{3.7}$$

The VA rating of the injection transformer is

$$S_{sr} = 3V_{sr}I_{sr} = 3 * 85.8 \times (40000/(3 \times (239.6 - 0.4 \times 239.6))) = 12kVA \tag{3.8}$$

During a sag event, the voltage provided by the source falls, causing the sources to increase their output in order to keep the load power at the same level. The magnitude of the current passing through the secondary winding of the injection transformer is governed by the magnitude of the source current during a sag in voltage. The computation is performed in the following manner:

$$I_{S,sag} = P_L/3(V_S - V_{Sr}) \tag{3.9}$$

With the total load specified in Table 3.1, the active power amounts to 40 kW. The nominal source voltage per phase (V_S) is 239.6V, while the series voltage drops to 95.84 V during a 40% sag. Using these values, the sag is measured at $92.75A$. Similarly, the series transformer has a VA rating of 12 kVA. Given that the power flowing through the injection transformer also passes through the APF, it is assumed that the rating of the series APF is the same as that of the injection transformer.

3.4.2 Selecting Interfacing Inductor

The actual magnitude of the load directly determines the current that passes through the secondary side of the injection transformer. To determine the design of the interface inductor for the series APF, it is necessary to compute the supply current I_S during a voltage swell event.

$$I_{S,swell} = P_L/3(V_S + V_{Sr}) \tag{3.10}$$

When taking into account the 5% fluctuation in the source current ($I_{cr,pp}$). The modulation index is set to 1, the direct current voltage (V_{dc}) is 700V, the injection transformer turn ratio (n_T) is 1.0, the overloading factor is 1.2, and the switching frequency (f_s) is 15 kHz. The value of the interfacing inductance L_{Sr} of the series APF is calculated (7 mH) as:

$$L_{Sr} = \sqrt{3}mV_{DC}n_T/12af_sI_{cr,pp} \tag{3.11}$$

3.4.3 Selecting RC filter

The design criteria for the RC filter in the DVR are similar to those for the shunt APF. However, for the series APF, the resistance is reduced, and the capacitance is intentionally increased. The resistive value, R, is 2 Ω, while the capacitive value, C, is 20 μF. The impedance at a frequency of 5 kHz is 2.6 Ω, whereas the impedance at the fundamental frequency is 159.2 Ω. The resultant time constant is 40 μs.

3.4.4 Selecting the rating of switch

The voltage rating of IGBT switches in series APF is equivalent to that of shunt APF because they both utilize a shared DC link. The current rating of the switch (39.75 A) for DVR is calculated as:

$$I_{sr} = I_{sr,sag}/N_{sr} = (40000/(3 \times (239.6 - 0.4 \times 239.6)))/N_{sr} \tag{3.12}$$

3.4.5 Design of Solar PV array

This research also covers the discussion on the integration of distributed energy in UPQC. Solar PV is widely recognised as a viable and sustainable energy option. For

the design of UPQC-DG, a suitable solar PV array is selected to provide power at the maximum power point. The SPR-305E-WHT-D PV module has been chosen for the construction of the PV array. Table 3.2 displays the manufacturing specifications. A string is formed by connecting ten PV modules in series, and a complete PV array is formed by connecting five such strings in parallel.

Table 3.2: Specifications of solar PV module

Maximum Power	305.2 W
Number of cells per module	96
Open circuit voltage	64.2 V
Short circuit current	5.96 A
Voltage at MPP	54.7 V
Current at MPP	5.58 A

The specifications of a solar PV array under standard test conditions ($1000\,W/m^2$, 25°) are displayed in the Table 3.3.

Table 3.3: Parameters of solar PV array

Maximum Power	15.3 kW
Open circuit voltage	642 V
Short circuit current	30.3 A
Voltage at MPP	547 V
Current at MPP	27.9 A

3.4.6 Design of DC-DC converter

The DC-DC converter is attached to the DC link of the UPQC-DG. It is utilised to increase the voltage at the DG terminal to match the DC-link voltage and efficiently harness the maximum power available from the DC source through MPPT control. The input rated input voltage is 545 V, which represents the maximum power point under standard environmental conditions. The converter is designed to be a boost converter, with a DC link output voltage of 700 V. The input voltage range is set at 500–575 V to accommodate any fluctuations in PV output. To achieve a stable CCM mode of operation, the inductance of the boost converter can be determined using Eq. 3.13 [7]:

$$L_B = V_{PV}(V_{DC} - V_{PV})/\Delta I_L f_S V_{DC} \tag{3.13}$$

In the given Eq. (3.13), the values of V_{PV}, V_{DC}, ΔI_L, and f_S are provided (545 V, 700 V, 2.0 A, 15 kHz), resulting in the calculation of L_B as 4.02 mH, which is rounded up to 5 mH. Based on the boost converter's maximum input current and voltage, the estimated VA rating is 16.1 kW. Unlike typical DC-DC converters, the UPQC-DC does not need an output capacitor filter since it already has a DC link capacitor.

3.5 Modeling and Simulation of UPQC

The process of modelling and simulating a Unified Power Quality Conditioner (UPQC) in MATLAB/Simulink systematically includes representing its fundamental components, control algorithms, and interactions to evaluate its effectiveness in addressing power quality problems. Each component of the system, such as the voltage source, nonlinear load, series APF, and shunt APF is modeled separately. The control algorithms guiding the both APFs are built to provide accurate correction for voltage and current distortions. The model incorporates power electronics components, including Voltage Source Converters (VSC) for the series APF and Current Source Inverters (CSI) for the shunt APF. The simulation model settings, such as the time period and the solver types, are configured in order to create an environment that closely resembles reality. The components of the UPQC are coupled to create a unified system, and a simulation is conducted to examine its behaviour under various operating conditions. An analysis of the UPQC's performance measures, such as power factor correction, compensation reaction time and waveforms analysis is conducted using simulation. In addition, response analysis is performed by altering key parameters (such as load and voltage) to withstand the system's resilience and flexibility. Engineers may use this technique to thoroughly evaluate the behaviour of the UPQC, optimise its design, and verify its efficiency prior to real-world implementation, guaranteeing dependable enhancement of power quality.

3.5.1 Modeling of UPQC-DG in MATLAB/Simulink

A detailed MATLAB model of a UPQC is created using the SimPowerSystems block set in the simulink library, as seen in Fig. 3.2. The UPQC model is created to tackle power quality problems in a three-phase power system. The model includes crucial

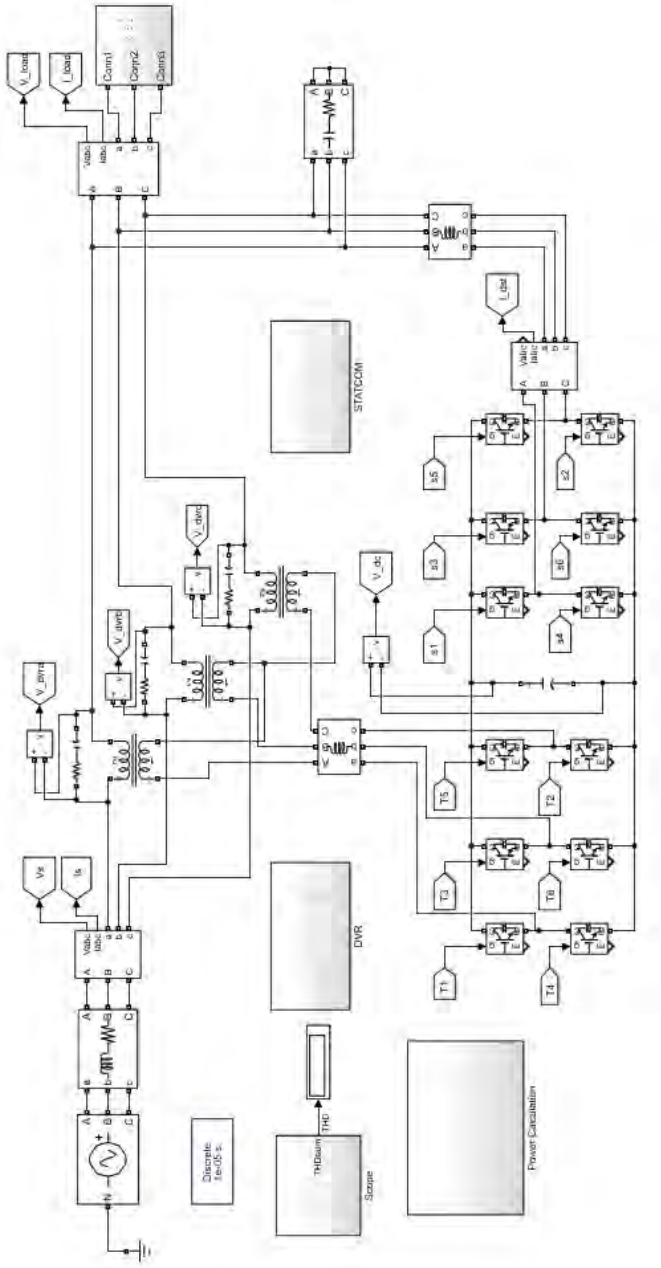

Figure 3.2: MATLAB/Simulink model of UPQC

elements such as a 3-phase programmable voltage source to represent the power grid, a nonlinear load to resembles real-world situations, and the UPQC itself to demonstrate its compensating powers. A programmable voltage source is used to generate voltage disturbances like sag, swell, and harmonics at different time intervals. Three kinds of loads, including two linear and one nonlinear loads, are included, as shown in Fig. 3.3. The simulation time step is set at 10 μs.

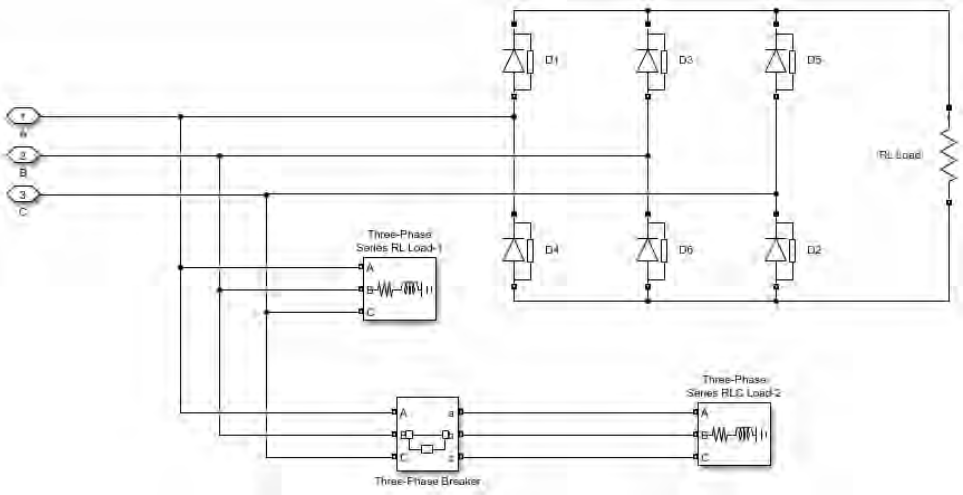

Figure 3.3: MATLAB Simulink model of three phase load

˘The various parameters of the UPQC simulink model are accurately designed with the techniques outlined in section 3.2. The specified parameters are shown in the Table 3.4. A three-phase power system is supplying a load of 40 kVA using a combination of linear and non-linear loads. The system operates at an AC line voltage of 415 V (rms) and 50 Hz, with a power factor of 0.554 lagging. The UPQC consists of a Distribution Static Synchronous Compensator (DSTATCOM) and a Dynamic Voltage Restorer (DVR) using two VSCs sharing a DC bus capacitor of 5500 μF. Its purpose is to correct the power factor of the load to unity at the main AC supply and to mitigate voltage fluctuations to prevent disruptions to the load. The source resistance is 0.5 Ω and the source inductance is 0.25 mH. The DSTATCOM has a rating of 40 kVA, whereas the DVR has a rating of 12 kVA. The simulink library has a linear transformer model with suitable losses, which is used for simulating the series injection transformer of the DVR. n_T represents the turn ratio and S_T represents the kVA rating of each series injection transformer. L_{Sh} and L_{Sr} are inductors used for AC interfacing to link the output of series and shunt APF to the grid lines.

The UPQC block is precisely set up with detailed control settings, reference voltages, and gains to replicate its dynamic behaviour in reducing common power quality issues such as voltage sags, swells, and harmonics. The simulation uses the simulink framework to model the dynamic interactions between components, offering a complete understanding of the UPQC's performance.

Table 3.4: Parameters of UPQC-DG

3 Phase supply	415 V, 50 Hz, R_S = .05 Ω, L_S = 0.25 mH
DC link	V_{DC} = 700 V, C_{DC} = 5500 μF
Shunt APF	40 kVA, L_{Sh} = 1.75 mH
Series APF	12 kVA, L_{Sr} = 7 mH, n_T = 1, S_T = 12 kVA
Series transformer	10 kVA (each phase), n_T = 1 (240/240 V)
Load-1	Thyristor bridge rectifier (R = 15.69 Ω)
Load-2	3-phase R-L load (10 kW, 0.554 p.f. lagging)
Load-3	3-phase R-L load (10 kW, 0.554 p.f. lagging)

3.5.2 Control of UPQC

The primary objective of active power filter is to significantly enhance the power quality of an electrical system. This is achieved by using a modern control approach that addresses every aspect of the electrical distribution network. The main objective of the shunt APF is to mitigate harmonic distortion, a common issue resulting from non-linear loads in the power system. It eliminates unwanted distortions by injecting controlled currents with equal and opposite harmonics, hence minimizing negative effects on equipment and network performance. Another crucial objective is to provide compensation for reactive power. The shunt APF adjusts the power factor dynamically to enhance system efficiency by decreasing reactive power use. In this way, the distribution grid becomes more efficient and energy is conserved as a consequence which leads to voltage stabilization. Controlling reactive power injection is essential for ensuring the reliability and longevity of electrical equipment by maintaining constant voltage levels.

The Synchronous Reference Frame (SRF) (Fig. 3.4) approach is used to control shunt APF. The SRF [8] approach includes converting the variables of a three-phase system, such as voltages and currents, from the time domain to a rotating synchronous reference frame. Referring to the control block diagram in Fig. 3.4 feedback signals for the shunt APF are obtained by sensing the load current (I_{load}) and DC voltage (V_{DC}). The load currents signals from three phases are transformed into $dq0$ using the Parks transformation (Eq. 3.14). This transformation transformation rotates the three-phase signals from the abc reference frame (where a, b, and c represent the three-phase voltages or currents) to the $d-q$ reference frame (where

d represents the direct-axis component and q represents the quadrature-axis component), making further control signals easier to handle. The d-axis in the SRF indicates is the fundamental component of load current, whereas the q-axis is reactive power, respectively. The terms $\sin(\omega t)$ & $\cos(\omega t)$ are the rotational components that map three-phase quantities into a rotating reference frame aligned with the rotating magnetic field in an AC system. These terms, along with other coefficients in the transformation matrix, are derived based on the frequency of the system and represent the synchronous rotating frame's angular velocity, (ω). The system frequency (f) of the AC signal is used to determine the angular frequency (ω), where $\omega = 2\pi f$. This angular frequency reflects the rate at which the reference frame rotates with respect to the stationary three-phase system. Whereas, $\sin(\omega t)$ & $\cos(\omega t)$ are functions of the angular velocity and time, representing the rotation angle at time t. These terms are essentially phase-shifted sinusoidal signals synchronized to the grid's frequency, where the angle (ωt) defines the position of the rotating reference frame. In the Park transformation matrix, these trigonometric terms are arranged based on the desired projection of the three-phase a,b,c components onto the rotating d,q frame. The matrix coefficients $\sin(\omega t - \frac{2\pi}{3})$, $\cos(\omega t - \frac{2\pi}{3})$,etc, correspond to the phase shifts for each of the three-phase components, aligning them with the d and q axes.

A three-phase Phase-Locked Loop (PLL) is used to synchronise these signals with the source voltage (V_s) signals. The direct axis current is filtered using a low-pass filter to isolate the DC component of the I_d. PI controllers adjust the DC voltage, and the resulting error signal is combined with the reference d-axis current. The q axis signal assumed to be (-)1 and zero axis assumed to be zero to obtain the source reference current indirectly using the inverse park transformation method. The later signal is subtracted from the measured load current to get the shunt APF reference current. This signal is compared with the actual shunt APF current in the hysteresis controller block to generate necessary compensating currents to inject into the system.

$$\begin{bmatrix} i_{Ld} \\ i_{Lq} \\ i_{L0} \end{bmatrix} = \frac{2}{3} \begin{bmatrix} sin\omega t & sin(\omega t - \frac{2\pi}{3}) & sin(\omega t + \frac{2\pi}{3}) \\ cos\omega t & cos(\omega t - \frac{2\pi}{3}) & cos(\omega t + \frac{2\pi}{3}) \\ 1/2 & 1/2 & 1/2 \end{bmatrix} \begin{bmatrix} i_{La} \\ i_{Lb} \\ i_{Lc} \end{bmatrix} \tag{3.14}$$

Applying vector-based control techniques (Unit Vector Template Generation) in DVRs [9] requires a structured method to address source voltage disturbances in

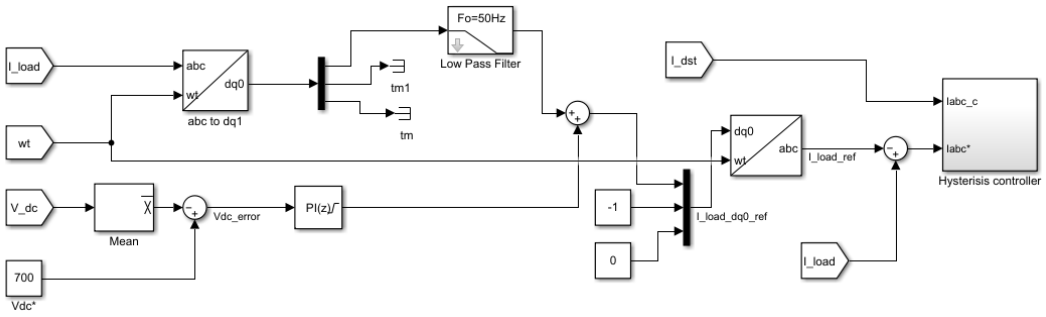

Figure 3.4: Control of shunt APF

power systems. As shown in the Fig. 3.5 voltage sensors initially monitor the system's disturbed voltage. Afterward, a reference vector (Eq. 3.15) is created using the actual voltage signal with the help of 3 phase PLL, which signifies the perfect voltage that the DVR aims to introduce into the system. Any phase shift in the input signal, due to noise, harmonics, or grid instability, will cause an incorrect estimation of $\sin(\omega t)$ and other values. This misalignment impacts the synchronization, leading to errors in active and reactive power control or in applications like power factor correction. Harmonic distortions in the AC waveform, often from nonlinear loads, can lead to inaccuracies in extracting the fundamental frequency. If these distortions are not effectively filtered, the UVTG may generate unit vectors that are not pure sinusoids, leading to control errors. So, the desired (reference) magnitude of load voltage is multiplied to these vectors to get reference load voltage signals. The control process involves calculating the error, which comes from the difference between the measured (disturbed) voltage vector (actual load Voltage) and the reference voltage vector. The resultant signal is fed to voltage PWM controller of series APF is get the desired pulse signal. Generating the compensating voltage signal is essential to determine the necessary corrective action for voltage restoration. When working with a DVR, the compensating voltage vector guides the inverters output which managed by pulse width modulation (PWM). Adjusting the pulse width in the inverter output simulates the necessary compensatory voltage, which helps in restoring the system voltage to its intended level.

$$\begin{bmatrix} U_a \\ U_b \\ U_c \end{bmatrix} = \begin{bmatrix} sin\omega t \\ sin(\omega t - 2\pi/3) \\ sin(\omega t + 2\pi/3) \end{bmatrix} \tag{3.15}$$

Firstly, it promotes the maximum use of renewable energy by harnessing solar

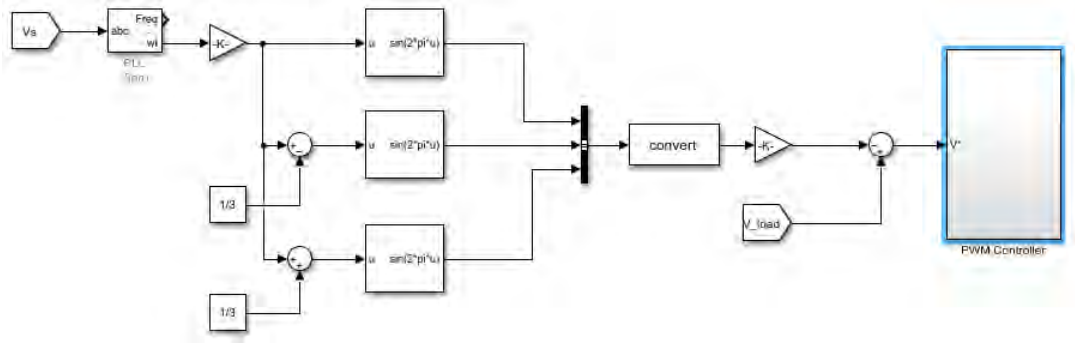

Figure 3.5: Control of series APF

power and transforming it into active power. The DC-DC boost converter is necessary to raise the voltage level of the generated active power to align it with the DC link voltage of the UPQC-DG system. This facilitates seamless integration into the distribution network. Furthermore, the MPPT controller ensures that the solar panel operates at its maximum power point, optimizing its power generation independent of variations in external parameters such as irradiation change and temperature. By constantly adjusting the system, the effectiveness of harnessing solar energy is maximized, leading to enhanced renewable energy system performance.

In addition, the UPQC-DG system can also offer support for reactive power to the grid (Chapter 9), in addition to generating active power, which improves grid stability and voltage regulation. Functionally, the solar panel harnesses the power of sunlight to generate DC current, which is then efficiently managed by the MPPT controller to maximise power output. The DC-DC boost converter increases the DC power voltage to match the DC link voltage of the UPQC-DG system. This integrated system efficiently integrates solar-generated power into the distribution network, offering active and reactive power support as needed.

3.5.3 UPQC Performance Analysis: Findings and Discussion

The developed model in MATALB/Simulink is used to simulate the performance of a three-phase, three-wire UPQC in different conditions, such as steady state, voltage sag, and voltage swell.

The graph in Fig. 3.6 depicting load voltage (V_{load}) demonstrates the ability of the UPQC to control and stabilise the voltage at the load terminals. When the load voltage remains stable, it shows that the UPQC is effectively compensating for disturbances. The waveform of source current (I_s) is sinusoidal and in phase with the

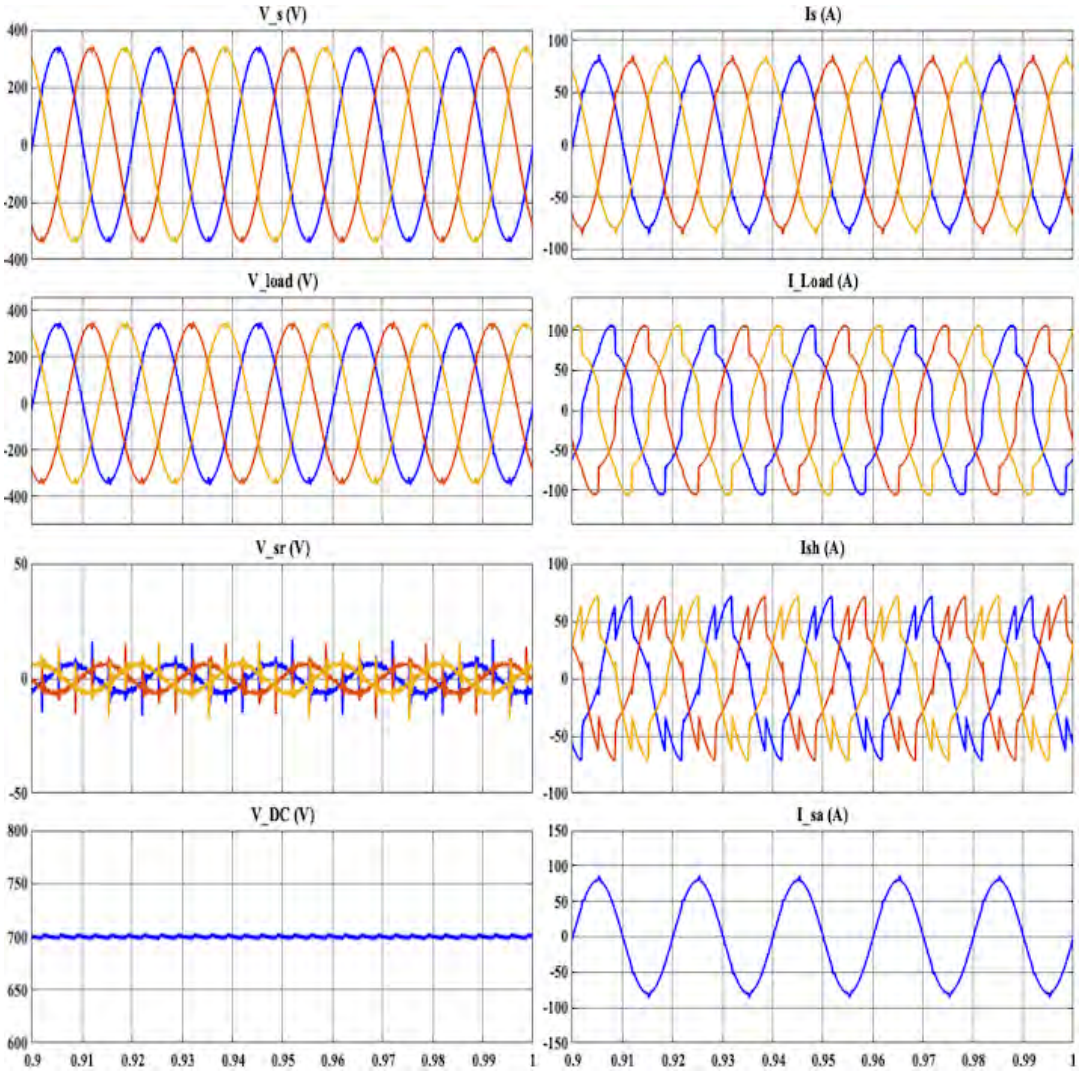

Figure 3.6: MATLAB Simulation results for steady state

source voltage (V_s) which illustrates the impact of the shunt APF compensation. The shunt APF improves the source current profile by compensating for reactive power and harmonics. Under stable operating circumstances, the series APF (V_{sr}) does not introduce any voltage injection. The DC connection voltage stays constant at the specified value of 700 V.

During voltage sag occurrence, the UPQC plays a crucial role in reducing negative impacts of voltage disturbance on the electrical system. The source voltage (V_s) waveform (in Fig. 3.7) experiences a sag with a decrease in amplitude (30%), leading to a quick reaction series APF (V_{sr}). The voltage compensator ensures stability and minimizes interruptions by promptly injecting active power to stabilize and regulate

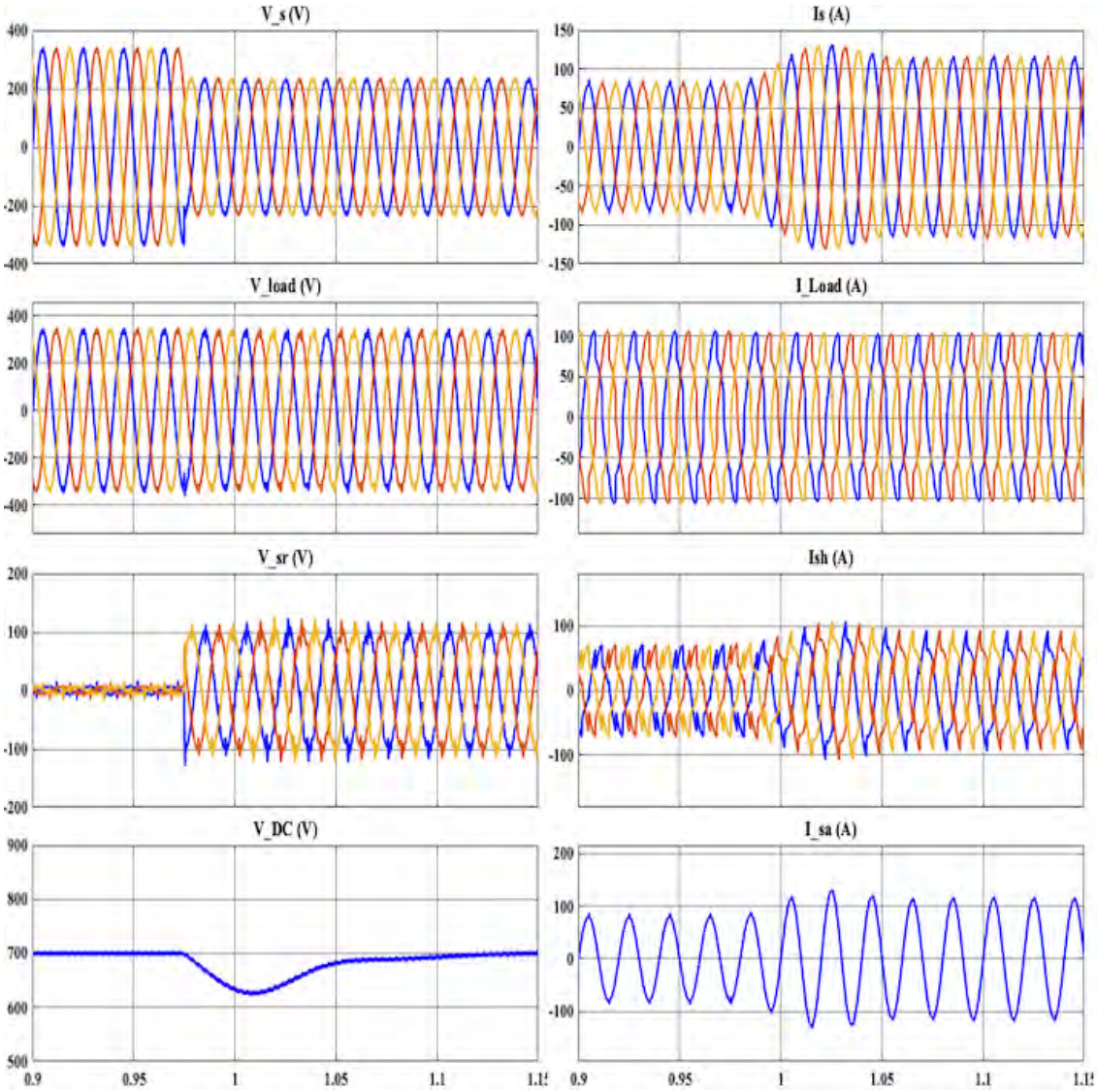

Figure 3.7: MATLAB Simulation results during voltage sag

the power supply in response to voltage sags as seen in waveform of load voltage (V_{load}). At the same time, the source current (I_s) waveform shows rise in amplitude and harmonics. The shunt APF in the UPQC injects compensatory current (I_{sh}) to improve power factor, minimize harmonics, and stabilize source current, therefore enhancing power quality. Voltage sags may cause undershoot in the DC link voltage (V_{DC}) of the UPQC, which might impact its stability. The UPQC utilizes control techniques (PI control) to reduce undershoot, maintaining steady DC link voltage and enabling continuous effective compensation.

Similarly UPQC is able react to a swell (Fig. 3.8) occurrence by detecting the

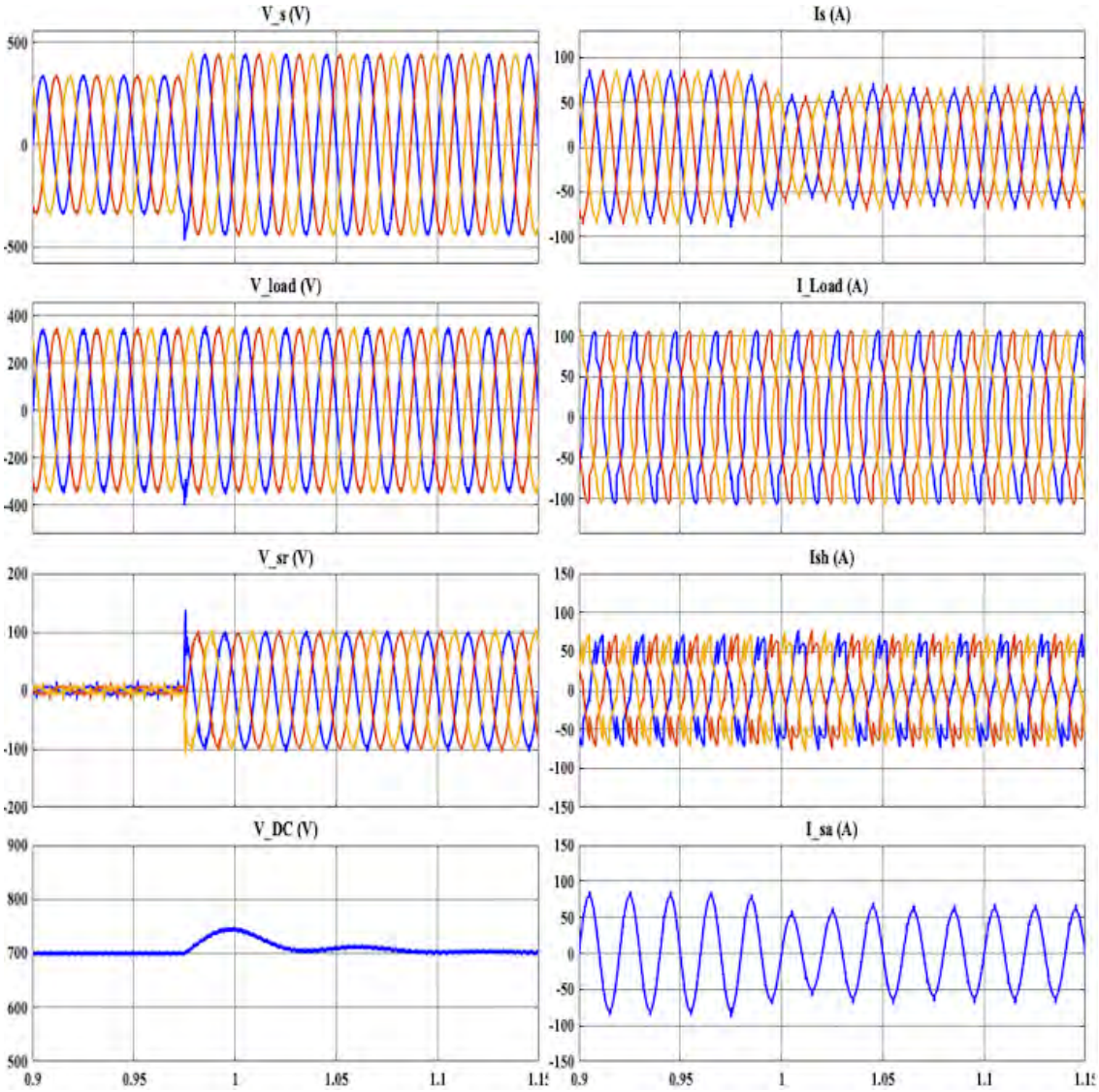

Figure 3.8: MATLAB Simulation results for voltage swell

disturbance and injecting compensatory voltages into the system (see waveform of V_{sr}). This phenomenon arises when the system experiences a temporary increase in the magnitude of the voltage (V_s). Voltage surges may alter source current waveforms, causing reactive power oscillations and reduction in amplitude. In reaction, shunt APF component injects compensatory current (I_{sh}) in order to reduce power factor distortions and to keep the source current (I_s) constant and sinusoidal. During voltage swell occurrences, the series APF operates to mitigate the excessive voltage. It injects a compensating voltage that is equal in magnitude but opposite in phase to the excess voltage caused by the swell which maintain the constant load voltage

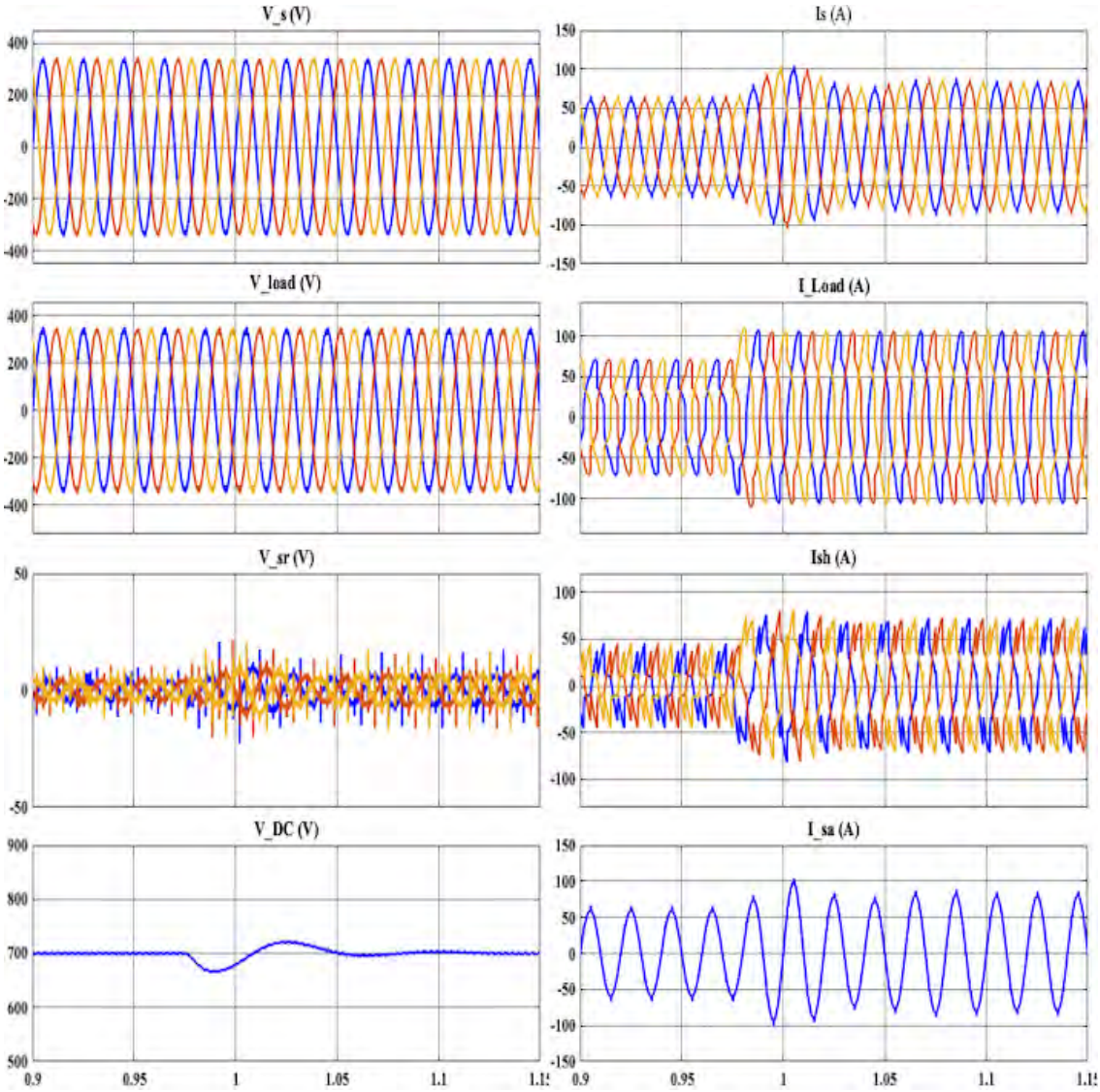

Figure 3.9: MATLAB Simulation results during change in load

(V_{load}). This voltage injection effectively eliminates the swell, ensuring that the load voltage remains at its designated value. This stability is important for the protection of sensitive equipment and the overall reliability of the power system.

During changes in load within the electrical distribution system, the shunt APF adapt the load fluctauation by modifying its compensator current (I_{sh}). In situations with increased load demand (as shown in Fig. 3.9), the shunt APF introduces compensatory currents (I_{sh}) to mitigate voltage dips and maintain voltage levels within acceptable thresholds. On the other hand, in the process of load reduction, it effectively absorbs surplus reactive power in order to maintain voltage levels and guarantee the

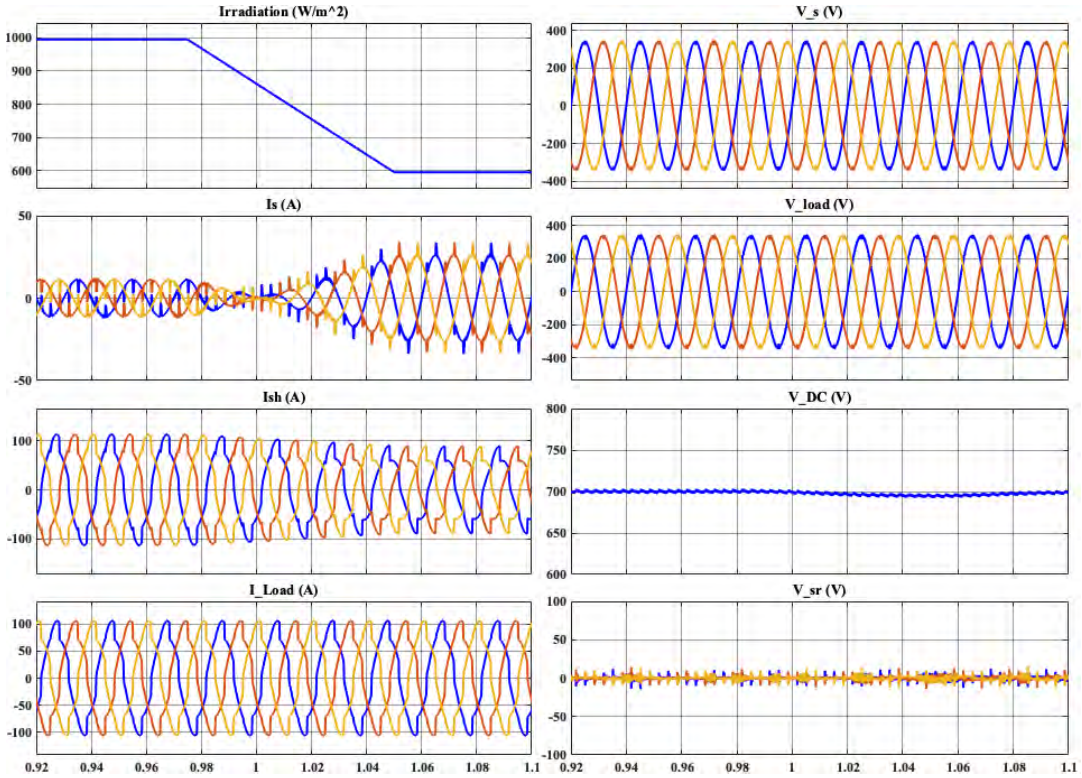

Figure 3.10: MATLAB Simulation results during change in solar irradiation

stability of the system. In the same way, the series APF adjusts its voltage injection in real-time to maintain the appropriate voltage profile at the PCC throughout variations in the load. During moments of increased load (as shown in Fig 3.9), the series APF introduces voltage (V_{sr}) to offset any decreases, ensuring reliable power supply to the load. In contrast, as the load decreases, the system modifies the voltage injection in order to mitigate voltage increases, so ensuring the maintenance of stable voltage levels.

During a transition in solar irradiation from 1000 W/m^2 to 600 W/m^2 (Fig. 3.10), the UPQC-DG experience changes to adapt to the new conditions. Initially, the source current (I_s) supplied by the source increases proportionately to the reduced irradiation, reflecting the decrease in solar power generation. The shunt APF current I_{sh} in the UPQC-DG system adjusts its operation to accommodate changes in load conditions, which may require making giving more reactive power support and reduce load current harmonics. At the same time, the voltage waveform of the DC link (V_{DC}) may experience fluctuations due to variations in solar irradiation. This requires the implementation of PI control mechanisms to maintain it within acceptable limits.

In general, the UPQC-DG system adjusts its operation to maintain optimal performance. It uses the controller (UVTG+SRF) to address issues such as reactive power compensation, voltage regulation, and harmonic mitigation. This helps to minimize the impact of solar irradiation fluctuations on power quality in the smart distribution network.

3.6 Summary

The simulation modeling and performance evaluation of the Unified Power Quality Conditioner (UPQC) illustrate its robust and effective capability to enhance power quality in various scenarios. The design of UPQC mainly concentrates on the selection of circuit characteristics and its reaction to voltage sag and voltage swell situations is analyzed using a detailed MATLAB/Simulink model with the SimPowerSystems block set. Both steady-state and transient performance simulations are conducted which shows the system's rapid and precise reaction while under various operating conditions. The controlled waveforms of source voltage (V_s), source current (I_s), and load voltage (V_{load}) demonstrated the compensating effects of the shunt and series APFs. The shunt APF effectively reduced current harmonics, resulting in a steady and sinusoidal load current waveform (I_{load}). The series APF effectively injected compensatory voltage (V_{sr}) i.e active power to compensate sag-induced variations, delivering a continuous and consistent power supply. The UPQC injected compensating voltages to properly control the load voltage and prevent it from exceeding permissible limits. The shunt APF effectively reduced power factor in the source current, resulting in a smooth and sinusoidal waveform. The control techniques used by the UPQC reduced overshoot and undershoot in the DC link voltage, assuring steady operation. The UPQC frequently shown rapid response, exact compensations, and overall improvement in power quality measures, proving to be a helpful in mitigating power quality.

Bibliography

[1] B. Singh, A. Chandra, and K. Al-Haddad, *Power quality: problems and mitigation techniques*. John Wiley & Sons, 2014.

[2] B. Singh and J. Solanki, "A comparison of control algorithms for DSTATCOM," *IEEE transactions on Industrial Electronics*, vol. 56, no. 7, pp. 2738–2745, 2009.

[3] B. Singh, P. Jayaprakash, D. P. Kothari, A. Chandra, and K. Al Haddad, "Comprehensive study of DSTATCOM configurations," *IEEE Transactions on Industrial Informatics*, vol. 10, no. 2, pp. 854–870, 2014.

[4] A. Moghassemi and S. Padmanaban, "Dynamic voltage restorer (DVR): a comprehensive review of topologies, power converters, control methods, and modified configurations," *Energies*, vol. 13, no. 16, p. 4152, 2020.

[5] J. Ye, H. B. Gooi, and F. Wu, "Optimization of the size of UPQC system based on data-driven control design," *IEEE Transactions on Smart Grid*, vol. 9, no. 4, pp. 2999–3008, 2018.

[6] S. Devassy and B. Singh, "Design and performance analysis of three-phase solar PV integrated UPQC," *IEEE Transactions on Industry Applications*, vol. 54, no. 1, pp. 73–81, 2017.

[7] S. Devassy and B. Singh, "Dynamic performance of solar PV integrated UPQC-P for critical loads," in *Proc. 12th IEEE India Council International Conference*, 2015, pp. 1–6.

[8] S. Bhattacharya and D. Divan, "Synchronous frame based controller implementation for a hybrid series active filter system," in *IAS'95. Conference Record of the 1995 IEEE Industry Applications Conference Thirtieth IAS Annual Meeting*, vol. 3. IEEE, 1995, pp. 2531–2540.

[9] V. Khadkikar, P. Agarwal, A. Chandra, A. Barry, and T. Nguyen, "A simple new control technique for unified power quality conditioner (UPQC)," in *Proc. 11th IEEE International Conference on Harmonics and Quality of Power*, 2004, pp. 289–293.

Chapter 4

Real-time PI controller tuning of the UPQC-DG using PSO

4.1 Preamble

Power quality has become a critical concern in modern electrical systems due to the increasing complexity and sensitivity of electronic devices and industrial equipment [1–3]. Disturbances such as voltage sags, swells, and harmonic distortions can severely impact the performance and reliability of these systems. The Unified Power Quality Conditioner (UPQC) [4–6] is a versatile device designed to address these issues by compensating for both voltage and current disturbances. By addressing these issues, industries can ensure that their electrical systems operate more efficiently, reduce energy waste, and extend the lifespan of their equipment. It combines the functionalities of a series compensator, which mitigates voltage-related problems, and a shunt compensator, which addresses current-related issues. Ensuring high power quality is imperative in modern electrical systems, especially with the increasing penetration of renewable energy sources such as photovoltaic (PV) systems and distributed generation (DG).

The integration of DG sources allows the UPQC to also contribute to power generation, improving overall system reliability and efficiency. In UPQC-DG systems, the DG sources are typically connected to the DC link of the VSIs used in the series and shunt APFs [7–9]. This allows seamless integration of the generated power into the compensating process, enhancing the overall performance of the UPQC system. DG sources provide additional power during supply interruptions or peak demand periods. Local generation reduces transmission losses and improves overall system efficiency. So, the integration of DG sources further enhances the system's

capabilities, making UPQC-DG a comprehensive solution for modern power quality management.

The effectiveness of a UPQC largely depends on the performance of its control system, particularly the Proportional-Integral (PI) controllers that regulate its operation. By maintaining a stable DC link voltage [10, 11], PI controllers help mitigate voltage sags, swells, and harmonics, ensuring consistent power quality output. Their real-time control capabilities enable the system to quickly react to power quality disturbances, minimizing their impact on the electrical network. They are relatively inexpensive to implement and maintain compared to advanced control strategies, making them a cost-effective solution for power quality management. The simplicity of PI controllers reduces overall system complexity, leading to lower design and operational costs. In terms of system reliability and safety, PI controllers offer predictable and stable control behaviour, enhancing the reliability of the UPQC-DG system. PI controllers are favoured for their simplicity and effectiveness in providing stable and robust control [12]. However, the tuning of PI controller parameters is a crucial task that significantly influences the UPQC's ability to mitigate power quality disturbances.

Traditional methods of tuning PI controllers, such as Ziegler-Nichols [13] or trial-and-error, often fall short in dynamic and nonlinear environments, leading to suboptimal performance. One of the main issues with the ZN method is its tendency to produce relatively high value for PI parameter settings which is generally aggressive in nature. This aggressiveness can cause the control system to react strongly to deviations from the set-point, leading to large oscillations before the system eventually settles. While this might provide a fast response, it can also result in overshoot and additional stress on the system components due to high correction measures. Additionally, the ZN method fails to consider system stability margins or the specific dynamics of the controlled system. This leads to sustained oscillations or even instability, especially in systems with non-linear characteristics or significant delays in the feedback loop. Traditional PI tuning methods often rely on mathematical modelling of the system, which can be complex and may not accurately capture the dynamic behaviour of the system under real operating conditions. Additionally, these methods frequently require relaxing the output limits of the PI controllers during the online tuning process, which can pose safety risks to the hardware.

In recent years, optimization techniques have emerged as powerful tools for tuning control parameters in complex systems. Among these, Particle Swarm Optimization (PSO) has gained popularity due to its simplicity, ease of implementation, and ability to find optimal solutions in high-dimensional spaces. PSO is inspired by the social behavior of birds flocking or fish schooling, where individuals, referred to as particles, iteratively adjust their positions based on their own experience and the experience of neighboring particles to find the best solution.

PI controllers are also compatible with optimization techniques [14–19]. They can be effectively tuned using optimization methods like PSO [20–22], enhancing their performance without the need for complex mathematical modelling. This integration allows for fine-tuning of the PI controller parameters to achieve optimal performance, improving the overall efficacy of the UPQC-DG system in managing power quality. Furthermore, PI controllers facilitate the seamless integration of renewable energy sources such as PV systems with the UPQC-DG, ensuring a stable and reliable power supply. By maintaining power quality, PI controllers support the grid in accommodating distributed generation sources, contributing to a more resilient and sustainable power system.

The offline PI tuning involves adjusting the controller parameters using pre-recorded data or simulation models before the controller is deployed in the actual system. This method typically relies on historical data or system models to determine the optimal PI parameters, as shown in Fig. 4.1a. When using the ZN method, the tuning process involves setting the PID parameters based on the system's response to a step input and using the ultimate gain and ultimate period obtained from the system's response to sustained oscillations. Basically, only a single disturbance using step is considered for tuning the ZN method. Considering multiple disturbances will disturb the response received from step-change, thus making this approach impossible. However, because this method does not consider the model complexities, non-linearities and damping required to avoid oscillations, the resulting PI parameters can lead to an oscillatory response under certain operating conditions.

Online PI tuning is simpler and can be performed without disrupting the operational system, but it has the drawback of not accounting for real-time variations and dynamic changes in the system. As a result, the tuned parameters might not be optimal under all operating conditions, leading to suboptimal performance when the system is subjected to unforeseen disturbances or changes in load conditions.

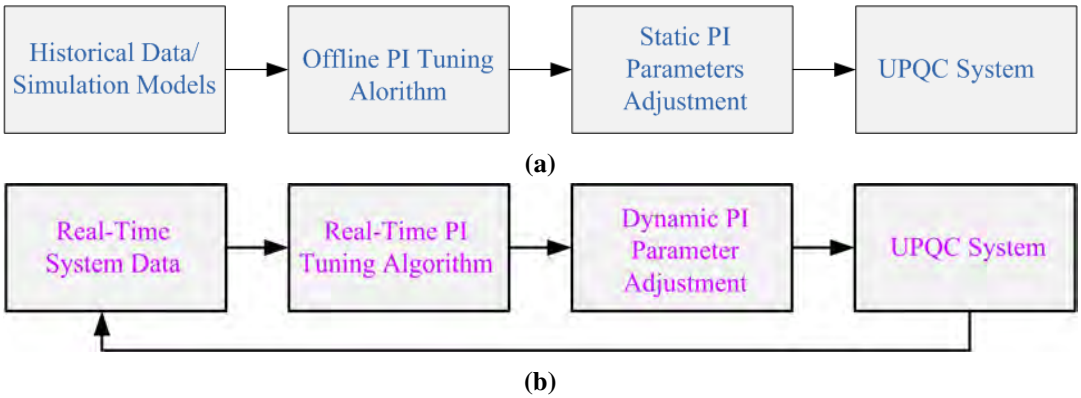

Figure 4.1: Approaches for tuning the proportional-integral (PI) controller (a) Traditional ZN method (b) Proposed tuning method.

Therefore, to address these challenges, this paper proposes an innovative PSO-based online PI tuning method for UPQC-DG systems. This method eliminates the need for mathematical modelling and continuously monitors the system's performance, and dynamically adjusts the PI parameters to adapt to changing conditions (see Fig. 4.1b). A basic version of the suggested PI tweaking was introduced in [23] with PV integrated shunt active power filter, and it is much improved with real-time implementation and details in this article with PV-integrated UPQC-DG. The proposed tuning method is more responsive and can handle variations in the system more effectively, ensuring that the controller maintains optimal performance even under fluctuating conditions. This approach can significantly enhance the system's robustness and stability, as it continuously fine-tunes the controller parameters based on real-time feedback.

The effectiveness of the proposed PI tuning method has been validated through real-time simulations of a PV-integrated UPQC-DG. The results demonstrate superior performance in regulating the DC link voltage of the integrated converter system across various operating conditions. This validation highlights the potential of the proposed method to enhance the robustness and efficiency of UPQC-DG systems in real-world applications.

The main contributions of this chapter include:

- The development of a novel online PSO-based PI tuning method that can be implemented in real-time without the need for mathematical modelling.
- Ensuring hardware safety by tuning the PI controller without relaxing its integral output limits.

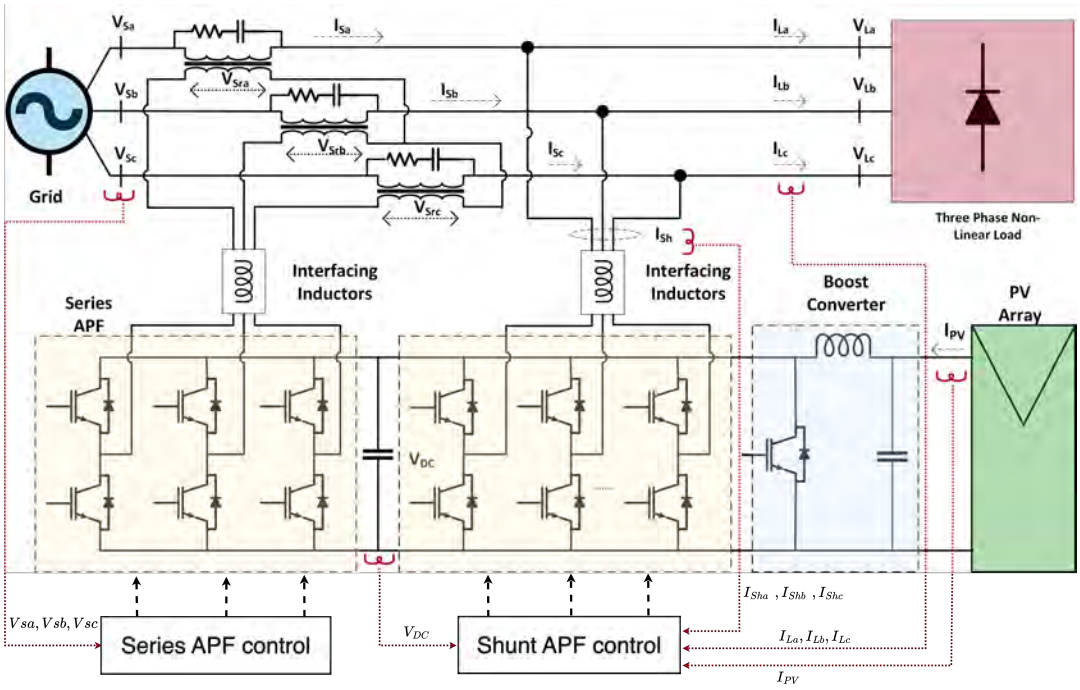

Figure 4.2: Power Circuit Diagram of UPQC-DG.

- Validation of the proposed method through real-time simulation of a PV-integrated UPQC-DG system.
- Demonstrating superior performance in regulating the DC link voltage under diverse operating conditions.

The chapter is organised into five distinct sections. In Section 4.2, the UPQC's structure and configuration are described, including the parameter design idea and controller technique for the shunt APF and series APF, following the introduction in Section 4.1. Section 4.3 provides a detailed discussion of PSO, including its enhanced versions and the method for implementing it in the UPQC model. Sections 4.4 and 4.5 include the experimental findings and conclusions, respectively.

4.2 Physical Configuration of UPQC-DG

UPQC-DG is an advanced power electronic device designed to enhance power quality in electrical systems (Fig. 4.2). It integrates the functionalities of a UPQC with the capabilities of Distributed Generation (DG) units, such as photovoltaic (PV) systems, wind turbines, or other renewable energy sources. The UPQC-DG system typically consists of two main components: a series compensator (Series Active Power Filter)

and a shunt compensator (Shunt Active Power Filter) connected to the distribution system. Additionally, the system includes the DG unit, typically integrated with the shunt compensator. The series compensator is connected in series with the distribution feeder. It consists of a voltage source inverter (VSI), a coupling transformer, and associated control circuits. The shunt compensator is connected in parallel with the load. It includes a VSI, a filter inductor or transformer, and control circuits.

The SPR-305E-WHT-D PV module has been selected for the PV array. Ten PV modules are connected in series to form a string, and five such strings are connected in parallel to develop a complete PV array of 15.3 kW with an output voltage of 547 V under standard irradiation and temperature conditions. The PV unit is connected to the DC link of the shunt compensator via the DC-DC boost converter to provide 38.25% of power to the total load (40 kW). With MPPT control, the boost converter effectively harnesses the maximum power from the PV source by raising the voltage at the PV terminal to match the DC-link voltage of 700 V. This allows the PV unit to supply power directly to the load or to the grid while also contributing to the DC link voltage regulation and overall power quality. The DC link voltage directly impacts the capability of the shunt APF to inject or absorb reactive power. PV active power & load reactive power demands together decide the kVA rating of the shunt inverter and the maximum current it feeds.

The UPQC-DG system is typically installed at strategic points in the distribution network, such as at the point of common coupling (PCC) between the utility and the consumer, to maximize its effectiveness in improving power quality and integrating distributed generation sources.

4.2.1 Series APF control

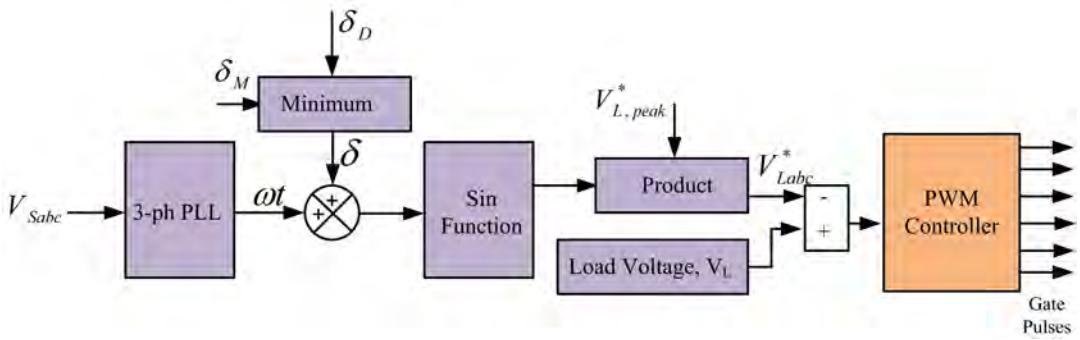

Figure 4.3: Series APF control.

The series active power filter (APF) in a UPQC-DG system is responsible for compensating voltage disturbances such as sags, swells, and harmonics [24]. The control strategy for the series APF often employs Unit Vector Template Generation (UVTG) to achieve accurate and effective voltage compensation. The series APF operates by generating a compensating voltage that is injected in series with the line voltage to ensure that the voltage supplied to the load remains stable and free from distortions. However, as a result of using the PAC approach [25], the series compensator provides a portion of reactive power by introducing voltage at a certain angle. Therefore, the responsibility of managing reactive power is divided between the two APFs. Equation (4.1) is used to determine the maximum power angle (δ_M), which ensures that the reactive power is shared in proportion to the VA rating of the converter. It represents the upper limit of the power angle that a system can handle safely. This estimation considers both the voltage and VA limits of the series converter. It includes the magnitude of the source voltage (V_S), the rated load voltage ($V_{L,rated}$), and the rated series APF voltage ($V_{Sr,rated}$).

$$\delta_M = \cos^{-1}\left[\frac{1+\left(\frac{V_S}{V_{L,rated}}\right)^2-\left(\frac{V_{Sr,rated}}{V_{L,rated}}\right)^2}{2\left(\frac{V_S}{V_{L,rated}}\right)}\right] \tag{4.1}$$

The desired power angle (δ_D) is the estimation of reactive power shared by series APF at which the system achieves the best power quality improvement, which is dependent on the magnitude of load reactive power (Q_L), load active power (P_L), and PV power (P_{PV}). Meanwhile, the λ is the ratio of series APF rating to the total sum of series and shunt APF rating as shown in Eq. (4.2).

$$\delta_D = \sin^{-1}\left(\frac{\lambda Q_L}{P_L - P_{PV}}\right) \tag{4.2}$$

The determination of the actual value of power angle, denoted by δ, is achieved by taking into account the minimum of δ_D and δ_M. This way, the system achieves balanced reactive power sharing within voltage and VA rating constraints. Figure 4.3 displays the complete series APF control block. The method is referred to as Unit Vector Template Generation [26]. For the purpose of generating a three-unit vector signal, the voltage source signal is processed using a three-phase phase-locked loop (PLL), and the extracted ωt is then added to the actual power angle (δ). As illustrated in the control figure, the basic signal is multiplied by the peak voltage signal ($V^*_{L,peak}$),

and then the resultant signal is subtracted from the load voltage signal (V_L). This process is repeated in order to provide the needed switching pulse generated by PWM controller.

4.2.2 Shunt APF control integrated with PV array

The shunt APF in a UPQC-DG is responsible for mitigating current-related issues such as harmonics, reactive power compensation, and load balancing. A sophisticated control strategy for the shunt APF involves using Synchronous Reference Frame - Power Angle Control (SRF-PAC) [25], which is especially effective in scenarios where photovoltaic (PV) generation is integrated into the DC link. This integration allows for the effective utilization of renewable energy sources while maintaining power quality.

From Fig. 4.4, the load currents (I_{La}, I_{Lb}, I_{Lc}) are transformed from the three-phase stationary frame (a-b-c) to the synchronous reference frame (d-q-0) using the Park transformation (in Eq. 5.3). To ensure that the transformation is in sync with the load voltage ramp signal, which is derived by combining the output of the three-phase phase-locked loop (PLL) with the power angle, the equation $\alpha t = \omega t + \delta$ is used. This transformation aligns the reference frame with the rotating reference frame of the fundamental frequency component.

$$\begin{bmatrix} I_{Ld} \\ I_{Lq} \\ I_{Lo} \end{bmatrix} = \frac{2}{3} \begin{bmatrix} sin\alpha t & sin(\alpha t - \frac{2\pi}{3}) & sin(\alpha t + \frac{2\pi}{3}) \\ cos\theta & cos(\alpha t - \frac{2\pi}{3}) & cos(\alpha t - \frac{2\pi}{3}) \\ \frac{1}{2} & \frac{1}{2} & \frac{1}{2} \end{bmatrix} \begin{bmatrix} I_{La} \\ I_{Lb} \\ I_{Lc} \end{bmatrix} \tag{4.3}$$

The power angle (δ) is calculated based on the active and reactive power components, as described in the previous subsection. The reference currents in the d-q frame (I_{Ld} & I_{Lq}) are generated to achieve the desired compensation. Typically, I_{Ld} is set to the average value of the fundamental active current to maintain the active power, and I_{Lq} is set to zero to achieve unity power factor operation. The DC link voltage (V_{DC}) is compared to the reference DC link voltage (V^*_{DC}), and the resulting error (E_{DC}) is analysed by a PI controller to provide the desired DC link current (I_{DC}). The average value of I_{Ld} is added to I_{DC} and subtracted from I_{pv} to create the reference d-axis current in the synchronous frame. The reference currents in the d-q frame are transformed back to the a-b-c frame using the inverse Park transformation to generate the compensating current references $(I^*_{sa}, I^*_{sb}, I^*_{sc})$. In order to generate the reference shunt

APF current $(I^*_{sha}, I^*_{shb}, I^*_{shc})$, the actual load current signal (I_{La}, I_{Lb}, I_{Lc}) is subtracted from the reference source current. A comparison is made between the acquired signal and the measured shunt APF current $(I_{Sha}, I_{Shb}, I_{Shc})$ in the hysteresis controller, which results in the required switching gate signal.

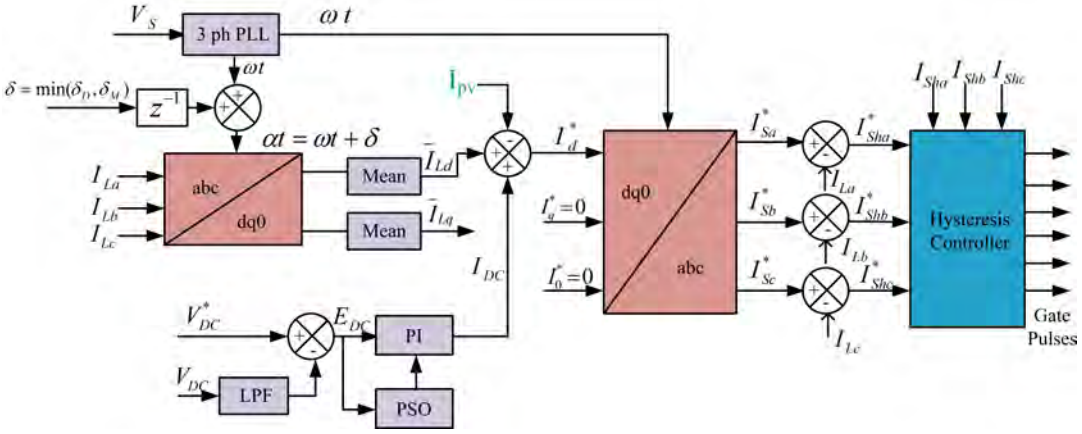

Figure 4.4: Shunt APF control.

The PV system is integrated into the DC link of the shunt APF. The generated PV power is fed into the DC link, stabilizing the DC voltage and providing the necessary energy for the APF operation. The PV system is connected to the DC link of the shunt APF through a boost converter, which is controlled by the Maximum Power Point Tracking (MPPT) technique using the Incremental Conductance method. The Incremental Conductance method tracks the MPP by comparing the incremental conductance $(\Delta I/\Delta V)$ to the instantaneous conductance (I/V). The key principle is that at the MPP, the derivative of power with respect to voltage is zero:

$$\delta_D = \frac{dI}{dV} = -\frac{I}{V} \tag{4.4}$$

The MPPT controller adjusts the duty cycle of the boost converter to drive the PV array to the MPP. This integration not only enhances the power quality but also maximizes the use of renewable energy, contributing to a more sustainable and efficient power system.

Table 4.1: Comparsion of different optimization algorithms

Optimization Technique	Convergence Speed	Computational Complexity	Ease of Implementation	Parameter Sensitivity	Global Search Ability	Addressing Nonlinear Constraints
Particle Swarm Optimzation	Fast	Low	Simple	Low	High	Good
Genetice Algorithms	Moderate	High	Moderate	High	High	Good
Simulated Annealing	Slow	Moderate	Simple	Moderate	Moderate	Poor
Ant colony Optimization	Moderate	High	Complex	High	High	Moderate
Differential Evolution	Moderate	Moderate	Simple	Moderate	High	Good
Artificial Bee Colony	Moderate	High	Complex	High	High	Moderate

4.3 Methodologies Involved in PSO-Based PI controller Tuning

Particle Swarm Optimisation (PSO) is an optimisation approach that is based on the collective behaviour of birds flocking or fish schooling [27]. PSO is well-known for its simple implementation, low computing cost, and fast convergence speed. When compared to other metaheuristic-based optimization approaches, which require more complex operations such as crossover and mutation [28, 29]. PSO involves straightforward mathematical operations with fewer parameters to adjust [30]. Its robustness and flexibility make it well-suited for dynamic environments for solving non-linear and non-continuous optimization problems where system parameters vary over time. As a result, various PSO-based algorithms have been developed to enhance control performances [31–34]. As shown in Table 4.1, the characteristics of PSO makes a robust and reliable choice for a wide range of optimization problems, surpassing other metaheuristic approaches in real-world scenarios [35, 36].

PSO optimises a problem by repeatedly enhancing a candidate solution based on a specified measure of quality. The algorithm employs a group of potential solutions known as particles, which navigate across the search space based on simple mathematical equations involving the particle's location and velocity. The movement of each particle is controlled by its own best-known position and is also directed towards the best-known places in the search space. These positions are updated when other particles find better positions. This method is iterated until an acceptable result is achieved. The first step is to initialize particles with the value of parameters obtained from the ZN method with random positions and velocities in a search space.

Each particle represents a potential solution to the optimization problem, which is a pair of k_p and k_i values. The velocity update Eq. (4.5) improves the velocities of the particles, leading them towards more optimal solutions. The fitness of each particle is evaluated using a predefined objective function. This function measures the quality of the solution represented by the particle. Each particle keeps track of its own best position (p_{Best}) and the best position found by the entire swarm (g_{Best}). The velocity and position of each particle are updated using the following equation:

$$V_i^{t+1} = w * V_i^t + c_1 r_1 * (p_{best,i} - X_i^t) + c_2 r_2 * (g_{best,i} - X_i^t) \tag{4.5}$$

$$X_i^{t+1} = X_t^i + V_i^{t+1} \tag{4.6}$$

where:

- V_i^t is the velocity of particle i (k_p or k_i) at the time t.
- X_i^t is the position of particle i at the time t.
- ω is the inertia weight.
- c_1 and c_2 are cognitive and social acceleration coefficients.
- r_1 and r_2 are random numbers between 0 and 1.

The new position update (Eq. 4.6) subsequently adjusts the current location of each particle according to its updated velocity, which represents the updated values of k_p and k_i for each particle.

In an online tuning, the real-time performance of the UPQC system is evaluated for each set of PI parameters. This involves running the UPQC system with the current PI parameters and measuring the resulting performance based on the objective function. Consequently, the Integral Time Absolute Error (ITAE) performance index provided in Eq. (4.7) is used as the objective function for the PSO-based PI tuning.

$$ITAE = \int_0^\infty t|e(t)|\,dt \tag{4.7}$$

In the above equation, t represents time and $e(t)$ is an error signal which represents a difference between the desired DC voltage and the actual DC voltage. ITAE is a performance index calculated for each particle's fitness (K_p & K_i). In order to achieve this goal, the simulation of UPQC-DG is carried out for a certain set of

Table 4.2: System Parameters

Source	Voltage, Frequency	415V, 50Hz
	Impedance	R_s = 0.05 Ω, L_s= 0.25mH
DC-link	Capacitor	C_{DC} = 5500μF
	DC-Link Voltage	700V
Shunt APF	Interfacing Inductor	2mH/ph
	Ripple Filter	$R = 5\Omega$/ph, $C = 50\mu F$/ph
Series APF	Interfacing Inductor	2mH/ph
	Ripple Filter	$R = 5\Omega$/ph, $C = 100\mu F$/ph
	Injection Transformer	10 kVA
Load 1	Rectifier Load	20 kW (15.69Ω, 0.1mH)
Load 2	3-ph R-L load	10 kW, 0.554 p.f. lagging
Load 3	3-ph R-L load	10 kW, 0.554 p.f. lagging
PV array	Maximum Power	P_{MPP} = 15.3 kW
	Voltage at MPP	V_{MPP} = 547 V

operational parameters. The personal best (p_{Best}) for each particle and the global best (g_{Best}) are continuously updated among all particles based on real-time performance evaluations. The velocities and positions of the particles are updated using the PSO equations to explore the search space for better PI parameters by minimizing the objective function. The process iterates, continuously refining the PI parameters until the performance of the DC link voltage stabilizes and the particles converge to optimal values.

The online PSO-based PI tuning methodology enables the UPQC-DG system to adapt dynamically to varying operating conditions, ensuring optimal power quality improvement and efficient integration of distributed generation resources.

4.4 Real-time Implementation & Result Validation

The real-time application of the proposed online PSO-based PI tuning method on a UPQC-DG system involves implementing and validating the method in FPGA-based Opal-RT. A three-phase, three-wire configuration of UPQC is used for the implementation. The system parameters taken are shown in the Table 4.2. Regarding load considerations, a 40 kW load includes three different types of load, specifically one non-linear load and two linear loads.

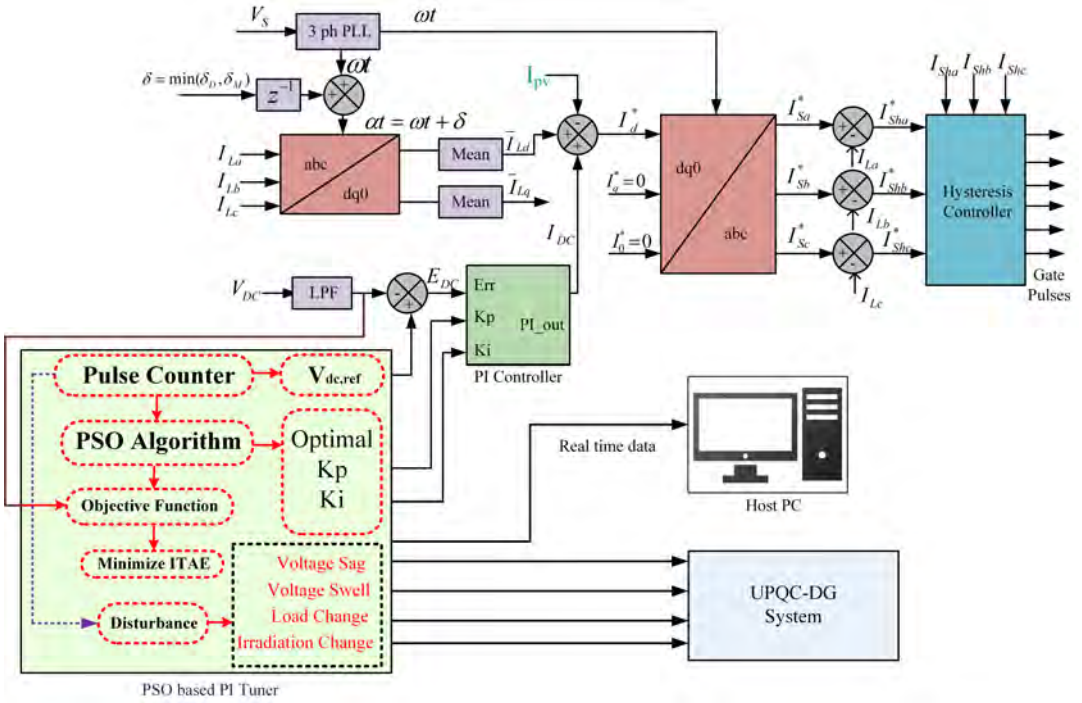

Figure 4.5: Proposed control block diagram of PSO-based PI tuner

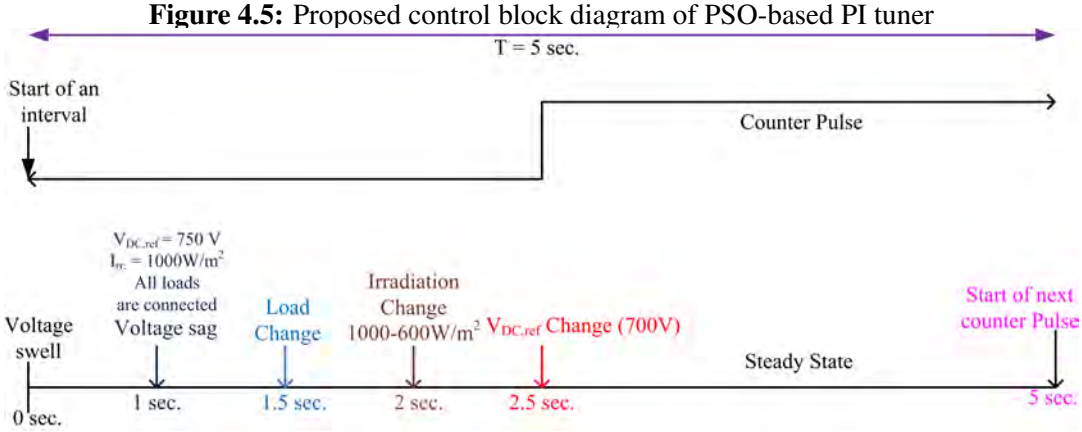

Figure 4.6: Chronology of disturbance introduced in the real-time simulation

4.4.1 Implementation in Real Time

In the online PSO-PI tuning, the system controller collects the data and dynamically adjusts the PI parameters based on the dynamic scenarios in real-time, as shown in Fig. 4.5. These scenarios are introduced based on the counter pulse and consist of multiple disturbances introduced to the system at certain intervals of time, as shown in Fig. 4.6. These disturbances are essential for assessing the dynamic response and robustness of the PI controller parameters in real-time. The system initially encounters a 30% voltage swell in the source voltage at $t = 0$. Subsequently, a step

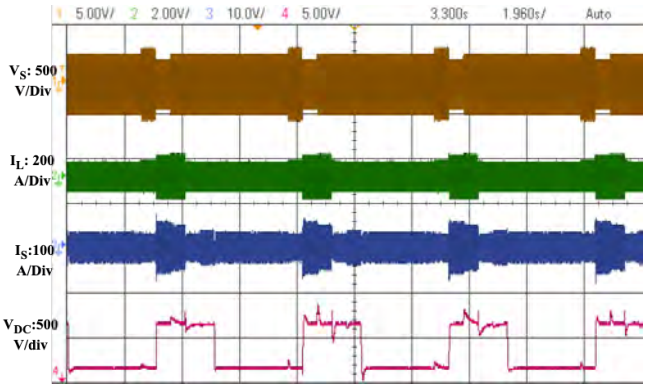

Figure 4.7: Sample waveform during the tuning of PI controller using online PSO tuner.

change in the DC voltage from 700V to 750V and a 20% voltage sag occur at $t = 1s$. The third disturbance involves a load change at $t = 1.5$, during which Load 2 is removed. Following this, the PSO tuner introduces an irradiation change from $1000Wm^2$ to $600Wm^2$ at $t = 2s$, followed by another step change in the DC voltage from 750V to 700V at $t = 2.5s$. Finally, the system remains in a steady state after the counter pulse reaches zero, from $t = 2.6s$ to $t = 5s$. The PSO controller computes ITAE at the end of each pulse counter and adjusts k_p and k_i parameters based on the system's performance in response to the disturbances. Based on this evaluation, the tuner modifies the local and global best placements of the particles. The primary objective of the tuning process is to minimize ITAE, which serves as the performance criterion. This objective function is particularly suitable for ensuring a quick and smooth response to disturbances in the system.

As the system operates, real-time performance data of error is continuously gathered and monitored in the host PC, as shown in the proposed control block Fig. 4.5. This error is used to compute the ITAE, reflecting how well the system maintains the DC link voltage under various conditions, including disturbances. The PSO algorithm then evaluates the fitness of each particle by calculating the ITAE for the corresponding PI parameters.

The updated PI parameters from the particle positions are applied to the UPQC-DG system in real-time. This real-time application allows the system to dynamically adjust to changing conditions, maintaining optimal control of the DC link voltage. The process iterates, with the PSO algorithm continuously refining the PI parameters based on ongoing performance evaluations. A sample waveform during the online tuning of the PI parameters is shown in Fig. 4.7. The iterative adjustment in the DC link voltage waveform ensures that the controller adapts effectively to disturbances,

minimizing the ITAE and enhancing overall system stability.

Through this method, the UPQC-DG system benefits from a robust and adaptive control mechanism that improves power quality by effectively managing the DC link voltage. The use of ITAE as the objective function ensures that the system not only responds swiftly to disturbances but also maintains long-term stability, reducing the duration and impact of errors. This dynamic and real-time tuning process, facilitated by the PSO algorithm, results in a significantly improved performance of the UPQC-DG system, making it highly effective in maintaining power quality in the presence of varying load conditions and disturbances.

4.4.2 Validation in Real-Time

The validation of the PSO-based online PI tuning method for the DC link of a UPQC-DG was conducted using the OPAL-RT 4512 real-time simulator (Fig. 4.8). The UPQC-DG model was simulated with a time step of 0.5 μs, ensuring high-fidelity and accurate real-time simulation. PSO algorithm employed with a population of 9 particles and 2 variable, iterating over 30 iterations to optimize the PI controller parameters dynamically. The performance of the PI controller was evaluated using ITAE as the objective function. Figure 4.9 illustrates the online variation of k_p, k_i, and ITAE with respect to iterations, considering the predefined set of disturbances outlined in Fig. 4.6. The figure depicts the adaptation process, where the k_p and k_i values initially adjust and then converge to steady states under these disturbances to achieve optimal operation. The proposed adaptive control mechanism dynamically updates the parameters k_p and k_i in real-time, ensuring the system maintains optimal performance by automatically adjusting to changes such as load variations, irradiation levels etc.

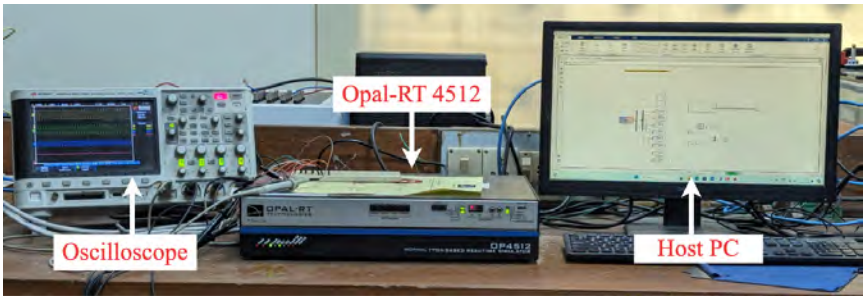

Figure 4.8: Setup for Real-Time Simulation.

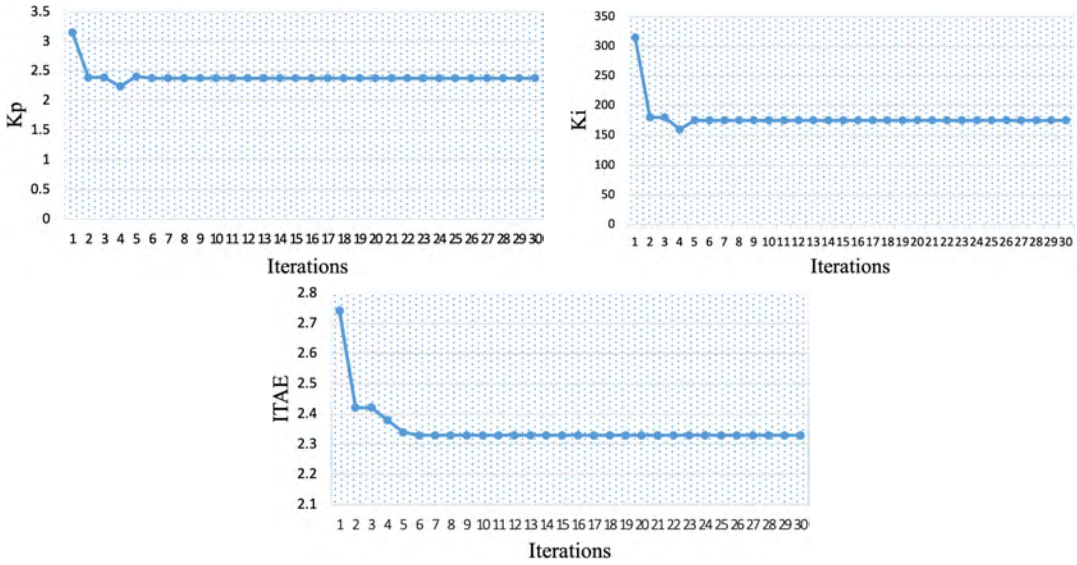

Figure 4.9: Online variation of k_p, k_i, *ITAE* with respect to iterations (considering different operating conditions)

Table 4.3: A comparison of real-time simulation outcomes of two approaches during

Method	Controller gains	ITAE (%)	Peak Overshoot
Z-N	k_p=3.15, k_i=350	4.82	190 V
PSO	k_p=2.376, k_i=175	2.38	40 V

If the magnitudes or patterns of these disturbances change, the proposed adaptive controller will update the k_p and k_i values accordingly to achieve optimal performance in the new scenarios.

To benchmark the performance of the PSO-based online PI tuning method, a comparison was made with the traditional Ziegler-Nichols (ZN) method, as shown in Table 4.3. By identifying the ultimate gain (K_u = 7) and ultimate period (P_u = 10.8ms) through controlled oscillation and applying the ZN tuning rules provides PI controller parameters of k_p = 3.15 and k_i = 350. In contrast, the PSO-based tuner optimized the PI parameters to k_p = 2.376 and k_i = 175.

The ITAE values for both methods (in Table 4.3) demonstrate the superior performance of the PSO-based approach. The ITAE for the ZN-tuned PI controller was 4.82%, whereas the PSO-based PI controller achieved a significantly lower ITAE of 2.38%. This reduction indicates that the PSO-based tuning method provides better control over the DC link voltage, resulting in less sustained error over time. This is clear from the DC link response of each pair of k_p and k_i from both approaches shown in Figs. 4.10 & 4.11.

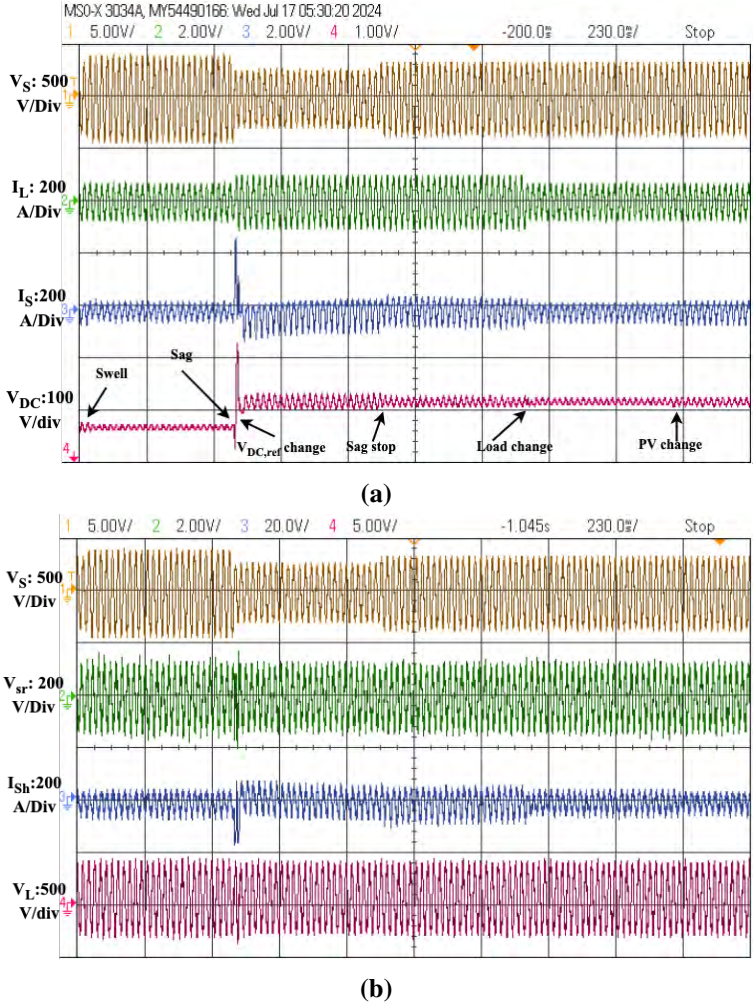

Figure 4.10: Output waveforms of ZN-tuned UPQC-DG (a & b).

The higher ITAE value indicates that the system experienced a more sustained error, reflected in the less smooth and more erratic voltage waveform (V_{DC}) as illustrated in Fig. 4.10a. In contrast, the DC link voltage response tuned by the PSO-based method showed significantly reduced oscillations and a faster settling time as shown in Fig. 4.11a. The lower ITAE value corresponds to a more stable and smoother voltage waveform, demonstrating the effectiveness of the PSO algorithm in dynamically optimizing the PI parameters. Fig. 4.12 provides a comparison between the DC response of both techniques, highlighting the disparity in peak overshoot and the controller's efficiency. The DC link voltage response tuned by the ZN method exhibited larger oscillations and a longer settling time.

The waveform under the ZN method tuning exhibited a higher peak overshoot ($190V$) during the change of $V_{DC,ref}$ (Fig. 4.12). This large overshoot indicates that

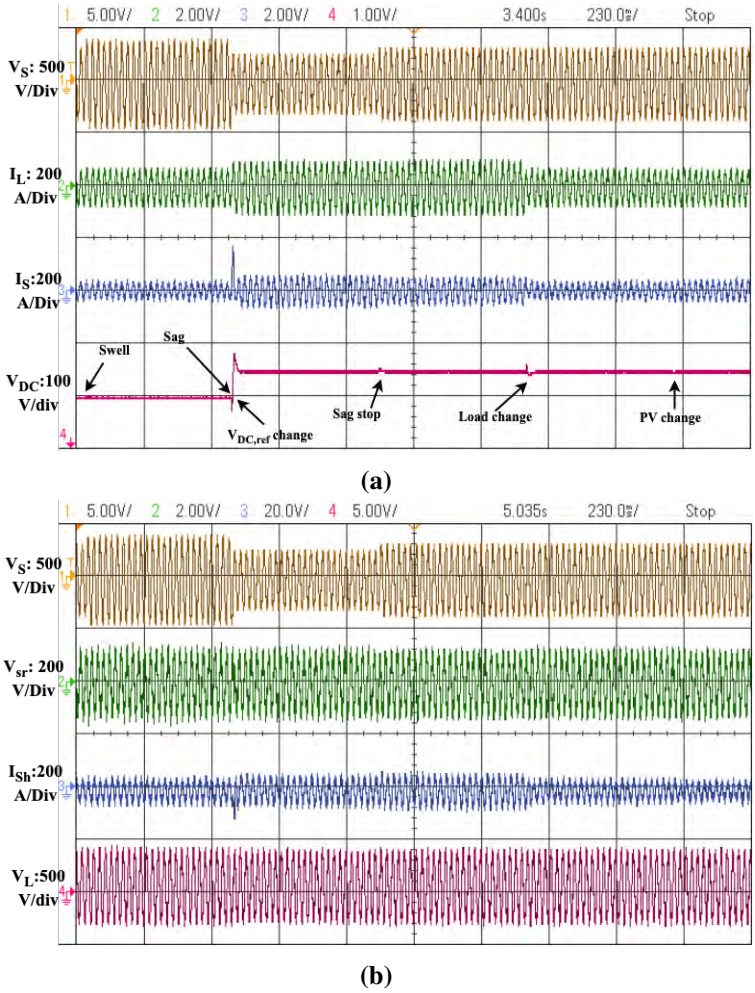

Figure 4.11: Output waveforms of PSO-tuned UPQC-DG (a & b).

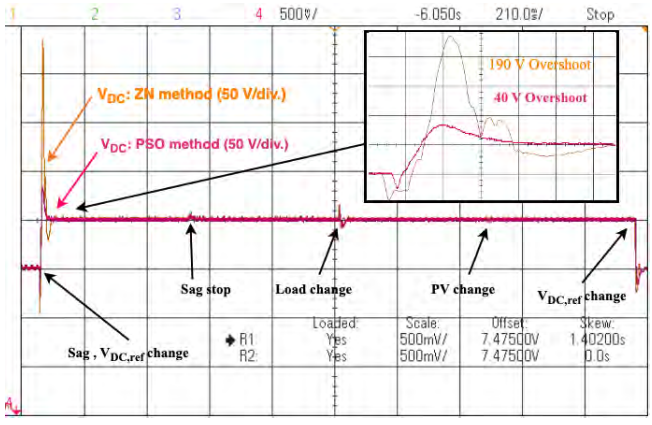

Figure 4.12: Comparison of the zoomed DC link response between ZN and PSO methods.

the ZN-tuned PI controller is less effective in maintaining a smooth and stable voltage response, leading to a more pronounced and potentially damaging transient response.

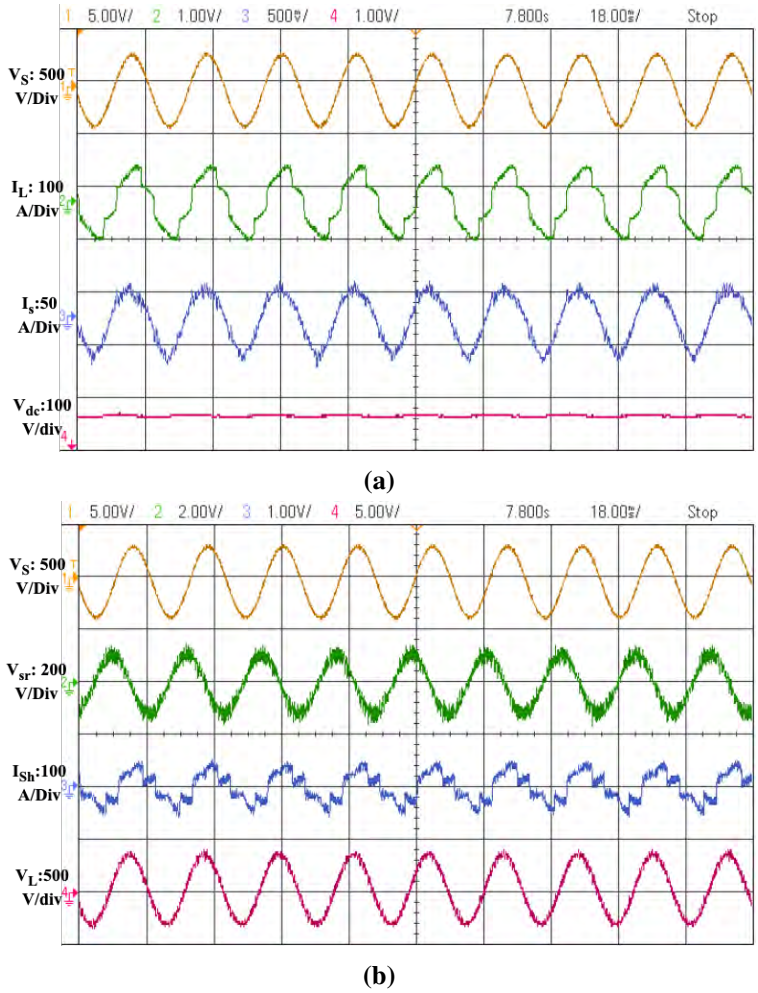

Figure 4.13: Zoomed waveforms of the ZN tuned UPQC-DG in steady state (a & b).

Similarly, during voltage sag, the DC link voltage experienced an undershoot of $50V$, and during load change, it experienced a $10V$ undershoot. The higher ITAE for the ZN method reflects these sustained oscillations and significant deviations.

Conversely, the DC link waveform under the PSO-based tuning demonstrated a much smoother transition with a minimal overshoot of $40V$. The minimized overshoot indicates a more controlled and stable response, reducing the risk of hardware stress and enhancing the reliability of the UPQC-DG system. In the case of voltage sag and load change, the DC link experienced an undershoot of $6V$ and $30V$, respectively, and settled to the desired voltage level more quickly, maintaining stability even in the presence of disturbances. The reduced ITAE value confirmed the effectiveness of the PSO approach in minimizing sustained errors and ensuring a robust control response. For voltage swell and PV change, both tuning approaches showed almost similar transient responses.

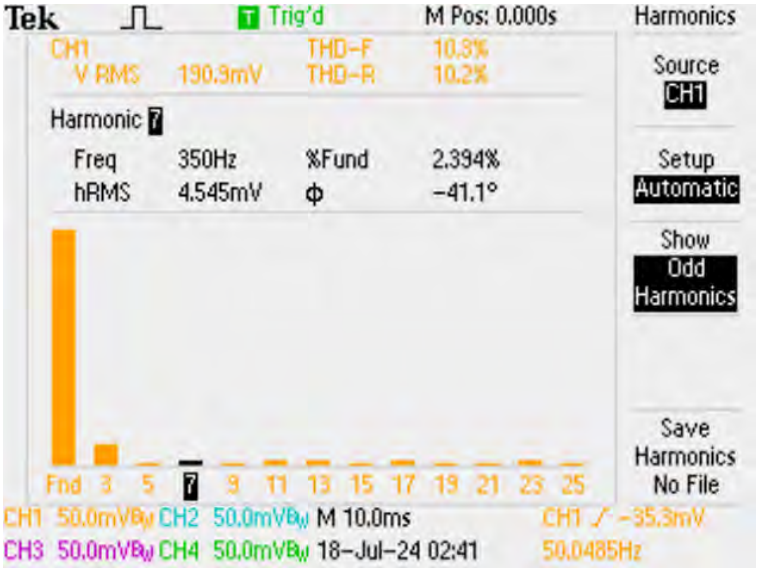

(a)

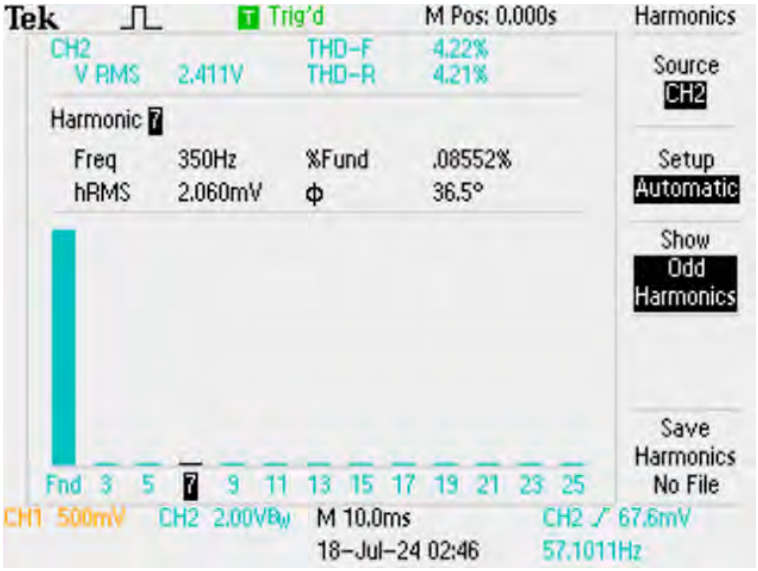

(b)

Figure 4.14: Harmonic spectrum of source current and load voltage of ZN tuned UPQC-DG in steady state (a & b).

The zoomed waveforms of the ZN-tuned UPQC-DG operating in a steady-state condition are shown in Figs. 4.13a & 4.13b. The DC link voltage waveform (V_{DC}) of a system can still display residual oscillations. However, these oscillations are less in amplitude compared to the initial transient response. The residual oscillations occur due to the fixed PI values, which may not be optimally suited for consistently maintaining a stable DC link voltage throughout all operating situations, resulting

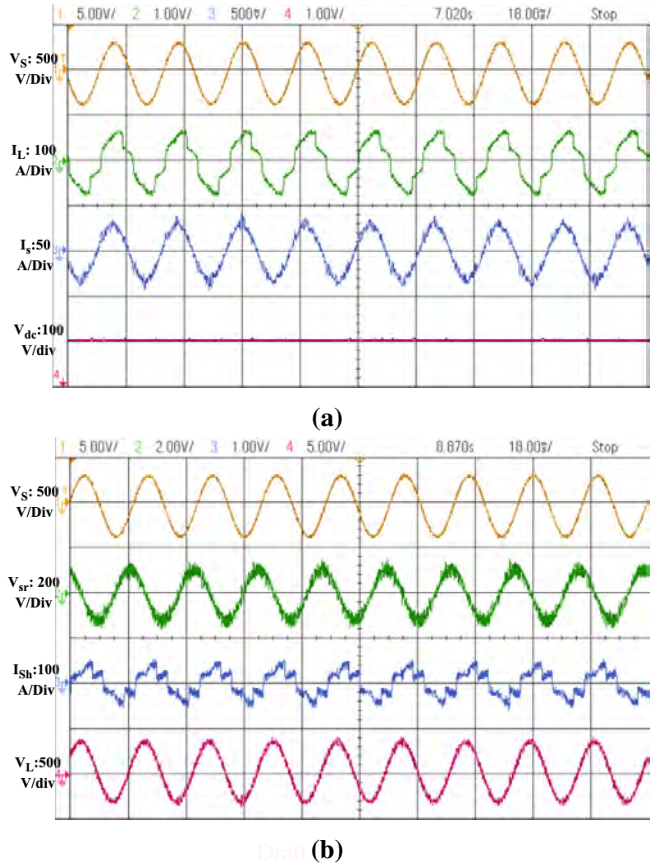

Figure 4.15: Zoomed waveforms of the PSO tuned UPQC-DG in steady state (a & b).

in less efficient suppression of oscillations. This causes the DC link voltage to exhibit a higher ripple voltage of 0.6898%. Figures 4.14a and 4.14 show the harmonic spectrum of the source current (10.30%) and load current (4.22%), respectively. The higher harmonic value indicates less effective compensation of harmonic distortions.

Fig. 4.15a & 4.15b illustrates the zoomed waveforms of the PSO-tuned UPQC-DG, operating in a steady-state condition. The source currents (I_s) exhibit a sinusoidal pattern and remain in phase with the source voltage (V_s). This phase alignment is achieved because the shunt APF effectively compensates for the non-linear and out-of-phase components of the load current. Additionally, the PV power contributes in-phase components to the shunt APF current, enhancing overall performance. The load voltage waveform (V_L), as depicted, remains stable and sinusoidal during steady-state operation. In a PSO-tuned UPQC-DG system, the DC link voltage ripple is significantly reduced to 0.5792%. The optimal PI parameters result in more effective suppression of voltage fluctuations. This stability is crucial as it indicates that the controller is successfully mitigating distortions and maintaining

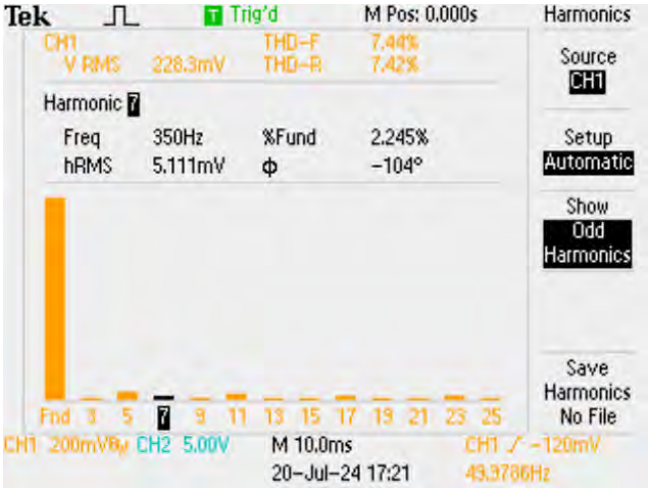

(a)

(b)

Figure 4.16: Harmonic spectrum of source current and load voltage of PSO tuned UPQC-DG in steady state (a & b).

the quality of the load voltage. The harmonic spectrum of source current and load voltage is shown in Fig. 4.16a and 4.16b which has a significantly lower harmonic content compared to the ZN-tuned system. The system has reduced the THD of the source current from 10.3% to 7.44%, and the THD of the load voltage from 4.22% to 3.21%.

In overall, the validation of the PSO-based online PI tuning method using the OPAL-RT 4512 real-time simulator showed significant improvements in the control performance of the DC link voltage in the UPQC-DG system compared to the Ziegler-Nichols method. The PSO-tuned PI controller not only achieved lower ITAE values but also provided a more stable and responsive DC link voltage control, as

evidenced by the smoother and quicker settling voltage waveforms. These results underscore the advantages of the PSO-based tuning approach in enhancing the performance and reliability of UPQC-DG systems in real-time applications.

4.5 Summary

The application of PSO-based online PI tuning in a UPQC-DG demonstrated significant enhancements in the control performance of the DC link voltage. Compared to the traditional Ziegler-Nichols (ZN) method, the PSO-tuned PI controller showed superior results, with lower ITAE values, reduced oscillations, and faster settling times. The PSO-based approach achieved PI parameters of k_p = 2.376 and k_i = 175, resulting in an ITAE of 2.38%, compared to the ZN-tuned parameters of k_p = 3.15 and k_i = 350, which resulted in an ITAE of 4.82%. The THD of the source current is 10.30%, while the load voltage has a THD of 4.22% when using the ZN approach. However, by using the online PSO method, the THD is decreased to 7.44% for the source current and 3.21% for the load voltage. The PSO-tuned system achieves lower harmonic content in both source current and load voltage, resulting in reduced THD and improved power quality. These findings underscore the efficacy of PSO in optimizing PI controller parameters dynamically, ensuring a more stable and responsive control system under varying operational conditions.

The PSO-based method not only reduces the overshoot voltage by a significant margin (from 190 V to 40 V) but also minimizes the oscillations in the DC link voltage response, which reduces the voltage ripple by 16.03%. These improvements result in a more stable and reliable power quality conditioner capable of maintaining optimal performance under varying operational conditions. By dynamically optimizing the PI parameters, the PSO algorithm enhances the stability and responsiveness of the UPQC-DG system, ensuring better power quality and reducing the risk of hardware stress due to excessive voltage overshoot and oscillations.

The implications of these findings are profound for the field of power quality management and control systems. The demonstrated ability of the PSO-based method to adaptively tune PI controllers in real-time implies that UPQC-DG systems can achieve higher reliability and efficiency. The PSO-based tuner eliminates the requirement to relax integral limits by dynamically optimizing the parameters of the PI controller, which prevents integrator windup and enhances the overall performance of control. This dynamic tuning capability is crucial for mitigating the impact

of disturbances and maintaining optimal performance, thereby enhancing the overall stability and quality of power delivery in distributed generation systems.

Furthermore, the reduced ITAE signifies improved long-term performance and resilience, which is vital for maintaining consistent power quality despite fluctuating loads and environmental conditions. Future research can further explore the integration of other advanced algorithms, such as Artificial Intelligence (AI) or Neural Network-based Algorithms (ANN), in future investigations to compare their performance with PSO and potentially develop hybrid approaches that combine the strengths of multiple techniques.

Bibliography

[1] S. Vijayalakshmi, R. Shenbagalakshmi, C. P. Kamalini, M. Marimuthu, and R. Venugopal, "Power quality issues in smart grid/microgrid," *Energy Systems in Electrical Engineering*, pp. 403–442, 2022.

[2] B. Singh, A. Chandra, and K. Al-Haddad, *Power quality: problems and mitigation techniques*. John Wiley & Sons, 2014.

[3] S. A. O. da Silva, L. B. G. Campanhol, G. M. Pelz, and V. de Souza, "Comparative performance analysis involving a three-phase UPQC operating with conventional and dual/inverted power-line conditioning strategies," *IEEE Transactions on Power Electronics*, vol. 35, no. 11, pp. 11 652–11 665, 2020.

[4] M. Madhavan and N. Anandan, "Unified power quality control based microgrid for power quality enhancement using various controlling techniques," *Indonesian Journal of Electrical Engineering and Computer Science*, vol. 29, no. 1, p. 75 – 84, 2023.

[5] V. Khadkikar, "Enhancing electric power quality using UPQC: A comprehensive overview," *IEEE Transactions on Power Electronics*, vol. 27, no. 5, pp. 2284–2297, 2012.

[6] A. Heenkenda, A. Elsanabary, M. Seyedmahmoudian, S. Mekhilef, A. Stojcevski, and N. F. A. Aziz, "Unified power quality conditioners based different structural arrangements: A comprehensive review," *IEEE Access*, vol. 11, pp. 43 435–43 457, 2023.

[7] S. Devassy and B. Singh, "Design and performance analysis of three-phase solar PV integrated UPQC," *IEEE Transactions on Industry Applications*, vol. 54, no. 1, pp. 73–81, 2018.

[8] S. C. Devi, B. Singh, and S. Devassy, "Modified generalised integrator based control strategy for solar PV fed UPQC enabling power quality improvement," *IET Generation, Transmission and Distribution*, vol. 14, no. 16, p. 3127 – 3138, 2020.

[9] B. Han, B. Bae, H. Kim, and S. Baek, "Combined operation of unified power-quality conditioner with distributed generation," *IEEE Transactions on Power Delivery*, vol. 21, no. 1, pp. 330–338, 2006.

[10] S. A. O. D. Silva, R. A. Modesto, L. P. Sampaio, and L. B. G. Campanhol, "Dynamic improvement of a UPQC system operating under grid voltage sag/swell disturbances," *IEEE Transactions on Circuits and Systems II: Express Briefs*, vol. 71, no. 5, pp. 2844–2848, 2024.

[11] M. Lu, M. Qin, J. Kacetl, E. Suresh, T. Long, and S. M. Goetz, "A novel direct-injection universal power flow and quality control circuit," *IEEE Journal of Emerging and Selected Topics in Power Electronics*, vol. 11, no. 6, pp. 6028–6041, 2023.

[12] S. A. Mohamed, "Enhancement of power quality for load compensation using three different FACTS devices based on optimized technique," *International Transactions on Electrical Energy Systems*, vol. 30, no. 3, p. e12196, 2020.

[13] H. Wu, W. Su, and Z. Liu, "PID controllers: Design and tuning methods," in *2014 9th IEEE Conference on Industrial Electronics and Applications*, 2014, pp. 808–813.

[14] S. J. Alam and S. R. Arya, "Volterra LMS/F based control algorithm for UPQC with multi-objective optimized PI controller gains," *IEEE Journal of Emerging and Selected Topics in Power Electronics*, vol. 11, no. 4, pp. 4368–4376, 2023.

[15] T. Arulkumar and N. Chandrasekaran, "Development of improved sparrow search-based PI controller for power quality enhancement using UPQC integrated with medical devices," *Engineering Applications of Artificial Intelligence*, vol. 116, p. 105444, 2022.

[16] S. K. Yadav and K. B. Yadav, "Firefly algorithm in FOPI controller for improving power quality of three-phase HES system integrated UPQC," in *2022 IEEE 3rd Global Conference for Advancement in Technology (GCAT)*, 2022, pp. 1–6.

[17] N. Zanib, M. Batool, S. Riaz, and F. Nawaz, "Performance analysis of renewable energy based distributed generation system using ANN tuned UPQC," *IEEE Access*, vol. 10, pp. 110 034–110 049, 2022.

[18] B. S. Goud, B. L. Rao, A. Flah, M. Bajaj, N. K. Sharma, and C. R. Reddy, "Biogeography-based optimization for power quality improvement in HRES system," in *Power Electronics and High Voltage in Smart Grid*. Springer Nature Singapore, 2022, pp. 309–316.

[19] B. S. Goud and B. L. Rao, "Power quality enhancement in grid-connected PV/wind/battery using UPQC: Atom search optimization," *Journal of Electrical Engineering & Technology*, vol. 16, no. 2, pp. 821–835, 2021.

[20] M. Nicola, D. SACERDOȚIANU, C.-I. Nicola, S. Ivanov, M. Ciontu, and M.-C. NIȚU, "Improved control strategy of unified power quality conditioner using fractional order controller and particle swarm optimization," in *2021 International Conference on Applied and Theoretical Electricity (ICATE)*, 2021, pp. 1–6.

[21] N. Khosravi, S. Echalih, Z. Hekss, R. Baghbanzadeh, M. Messaoudi, and M. Shahideipour, "A new approach to enhance the operation of M-UPQC proportional-integral multiresonant controller based on the optimization methods for a stand-alone AC microgrid," *IEEE Transactions on Power Electronics*, vol. 38, no. 3, pp. 3765–3774, 2023.

[22] G. S. Kumar, B. K. Kumar, and M. K. Mishra, "Mitigation of voltage sags with phase jumps by UPQC with PSO-based ANFIS," *IEEE Transactions on Power Delivery*, vol. 26, no. 4, pp. 2761–2773, 2011.

[23] A. Patel, S. K. Yadav, and H. Datt Mathur, "Particle swarm optimization based tuning method of PI regulator for PV fed shunt active power filter," in *2022 IEEE IAS Global Conference on Emerging Technologies (GlobConET)*, 2022, pp. 822–827.

[24] V. Remya, P. Parthiban, V. Ansal, and B. Chitti Babu, "Dynamic voltage restorer (DVR) – a review," *Journal of Green Engineering*, vol. 8, no. 4, p. 519 – 572, 2018.

[25] A. Patel, S. K. Yadav, and H. D. Mathur, "Utilizing UPQC-DG to export reactive power to grid with power angle control method," *Electric Power Systems Research*, vol. 209, p. 107944, 2022.

[26] V. Khadkikar, P. Agarwal, A. Chandra, A. Barry, and T. Nguyen, "A simple new control technique for unified power quality conditioner (UPQC)," in *Proc. 11th IEEE International Conference on Harmonics and Quality of Power*, 2004, pp. 289–293.

[27] M. Clerc, *Particle Swarm Optimization*. John Wiley and Sons, Ltd, 2006.

[28] P. A. Diaz-Gomez and D. F. Hougen, "Initial population for genetic algorithms: A metric approach." in *International Conference on Genetic and Evolutionary Methods, Las Vegas, Nevada*, 2007, pp. 43–49.

[29] Z.-L. Gaing, "A particle swarm optimization approach for optimum design of PID controller in AVR system," *IEEE Transactions on Energy Conversion*, vol. 19, no. 2, pp. 384–391, 2004.

[30] S. E. De León-Aldaco, H. Calleja, and J. Aguayo Alquicira, "Metaheuristic optimization methods applied to power converters: A review," *IEEE Transactions on Power Electronics*, vol. 30, no. 12, pp. 6791–6803, 2015.

[31] Z.-L. Gaing, "A particle swarm optimization approach for optimum design of PID controller in AVR system," *IEEE Transactions on Energy Conversion*, vol. 19, no. 2, pp. 384–391, 2004.

[32] W. Qiao, G. Venayagamoorthy, and R. Harley, "Design of optimal PI controllers for doubly fed induction generators driven by wind turbines using particle swarm optimization," in *The 2006 IEEE International Joint Conference on Neural Network Proceedings*, 2006, pp. 1982–1987.

[33] I.-Y. Chung, W. Liu, D. A. Cartes, and K. Schoder, "Control parameter optimization for a microgrid system using particle swarm optimization," in *2008 IEEE International Conference on Sustainable Energy Technologies*, 2008, pp. 837–842.

[34] W. Al-Saedi, S. W. Lachowicz, and D. Habibi, "An optimal current control strategy for a three-phase grid-connected photovoltaic system using particle swarm optimization," in *2011 IEEE Power Engineering and Automation Conference*, vol. 1, 2011, pp. 286–290.

[35] S. Gupta, P. K. Biswas, S. Debnath, A. Ghosh, T. S. Babu, H. M. Zawbaa, and S. Kamel, "Metaheuristic optimization techniques used in controlling of an active magnetic bearing system for high-speed machining application," *IEEE Access*, vol. 11, pp. 12 100–12 118, 2023.

[36] S. Sunaina, B. D. Shivahare, V. Kumar, S. K. Gupta, P. Singh, and M. Diwakar, "Metaheuristic optimization algorithms and recent applications: A comprehensive survey," in *2023 International Conference on Computational Intelligence, Communication Technology and Networking (CICTN)*, 2023, pp. 506–511.

Chapter 5

PSO based Optimum Design of Passive Filter Elements of UPQC

5.1 Preamble

Delivering uninterrupted and quality power is a core necessity of modern power industry. Any PQ problems such as voltage variation, flicker, and harmonics lead to the equipment failure causing loss for industrial and domestic loads. Critical equipment requires an interruption-proof and distortion-less power supply to obtain the desired performance. Such quality of power can be achieved through active power filters like UPQC [1–3]. Existing literature has shown the advantage of UPQC with its dynamical and behavioural performance.

Generally, UPQC consists of two voltage-source inverter connected back-to-back configurations sharing a common DC link capacitor. These inverters are connected in series and shunt configurations with the distribution grid. The series VSI resolves the voltage-related problem at point of common coupling (PCC) such as sag and swell, while the shunt VSI eliminates the harmonic components injected by the load current. Many control algorithms are reported in the literature for the simultaneous control of series and shunt VSIs such as Power Angle Control [4, 5], modified Synchronous Reference Frame Theory (SRF) based PAC [6]. In most of these works, control techniques are aimed at improving the simultaneous compensation of current and voltage by UPQC.

Designing UPQC-DG properly is essential for minimising costs, ensuring efficient operation, and complying with strict grid codes. When designing the UPQC-DG, it involves determining the appropriate sizes for the series and shunt converters

as well as the series injection transformers. When the shunt converter of UPQC-DG draws power from DG and provides reactive power to the load, its kVA rating increases significantly. Developed is the power angle control (PAC) method to distribute the reactive power load between a shunt converter and a series converter [7,8]. Utilising power angle control has proven to be beneficial in optimising the performance of series and shunt converters in conventional UPQC systems (without DG). In the context of UPQC-DG, this becomes even more crucial as the shunt converter of UPQC-DG experiences an extra VA burden due to the DG power passing through it.

As the technology advanced, attempts to reduce the size and cost of UPQC power converters have been reported in the literature [6, 9, 10]. Most of these attempts are mainly focused on optimising the VA rating of UPQC. Researchers have used the PSO algorithm in UPQC research for optimization. In the article [11], the authors have applied the technique of PSO to calculate the optimum angle for the series APF to inject in such a way to minimize the VA loading of UPQC and have used THD of source current and load voltage as the objective function. The assorted optimization algorithms used so far in UPQC are able to improve its compensation performance, VA utilization of its inverters and reduce the ratings of UPQC in comparison to conventional design approach, but not much attention has been given to the optimal design of passive filters of UPQC. Since the UPQC system consists of two VSIs which inject the unwanted current or voltage harmonics along with desirable components (compensating voltages and currents). The injection of these harmonics into the grid which creates a serious problem. These filters play a crucial role in enhancing the performance of UPQC in terms of harmonics mitigation, voltage drop, power factor and power losses which are difficult to be optimized using conventional design approach.

Therefore, in this work, a comprehensive approach to optimally design the passive filtering elements of UPQC is proposed. In our proposed design, the objective function comprises of four key indices namely THD, power factor, voltage regulation and power loss, which widens the possibility of obtaining better performance of UPQC. The proposed objective functions of the filter design takes care of the core function of UPQC:

- The THD component of objective function makes sure that the source current and load voltage THDs are minimum.

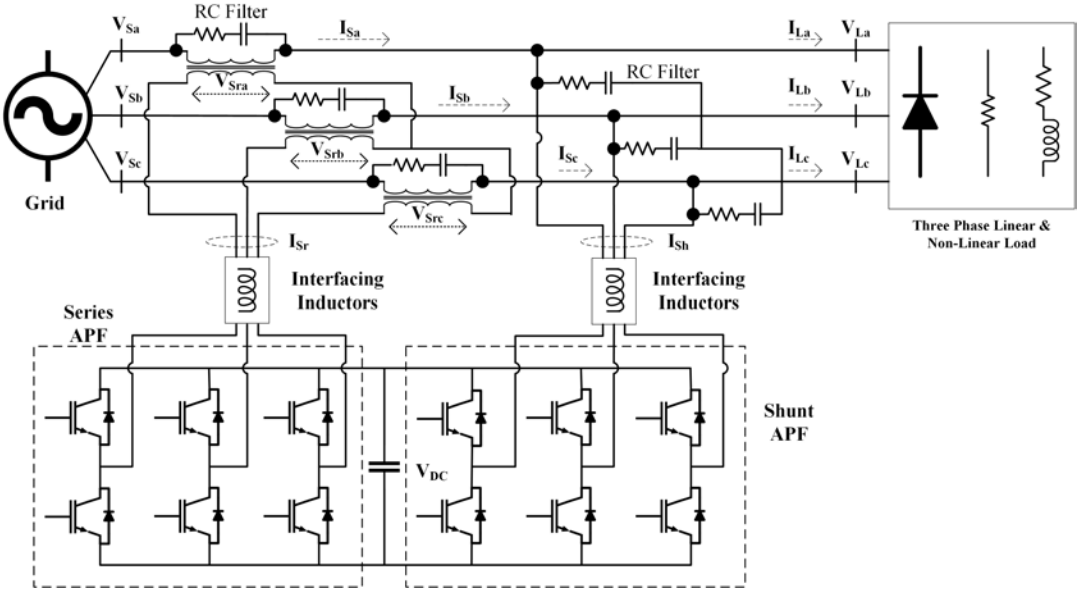

Figure 5.1: Power Circuit Diagram of UPQC

- The power factor component takes care of maintaining unity power factor at grid end.
- The voltage regulation component ensures load voltage to be held at desired level.
- Power loss component of objective function keeps the power losses in UPQC to minimum.

This chapter is organized into four sections. After the section 5.1 of preamble, the structure of UPQC is explained in section 5.2 with parameter design concept and controller strategy for shunt APF and series APF. Section 5.3.1 covers the explanation of PSO and the approach to implement in the UPQC model. Finally, the experiment result and conclusion are described in section 5.4.

5.2 Structure of UPQC

UPQC is a union of shunt inverter and series inverter with a DC link capacitor facilitated between them. These inverters act as active power filters to filter out the harmonics. Interfacing inductors are used to connect the APFs to the distribution grid.

The power circuit of UPQC is shown in Fig. 5.1. The left side inverter of the circuit is known as series active power filter, it injects compensating voltage during

occurrence of unbalanced & distorted terminal voltage. So, that the load terminal voltage is sinusoidal of constant magnitude irrespective of the disturbance in the grid voltage. The right side inverter of the circuit is called shunt active power filter, which acts as a current source and compensates for load current based power quality issues, such as load reactive power, current harmonics, unbalance, etc. In case of power angle control, the series APF injects voltage in steady state as well for supplying a part of load reactive power.

5.2.1 Existing Work Related to Filter Parameter Design

This section describes the conventional method of designing of passive interfacing elements of UPQC. The interfacing elements are of two types: the interfacing inductors and RC filters (ripple filters). The series RC filter (R_{sr}, C_{sr}) is connected across the secondary winding of a star-star transformer, whereas the series interfacing inductor (L_{sr}) is connected at the primary winding. At the output of shunt APF, the shunt RC filter (R_{sh}, C_{sh}) and shunt interfacing inductor (L_{sh}) are connected in star connection formation (Fig. 5.2). The purpose of RC filters is to block the high frequency switching components entering into the supply system. Using the formulae given in [12], the frequency can be calculated as

$$f_r = \frac{1}{2\pi R_f C_f} = \frac{f_s}{2} \tag{5.1}$$

where C_f is ripple filter capacitance and its resistance (R_f).f_s represents the switching frequency. Based on Eq. (5.1), the high pass RC filter is tuned at half of the switching frequency and it has high impedance at a fundamental frequency so that it draws very negligible fundamental current.

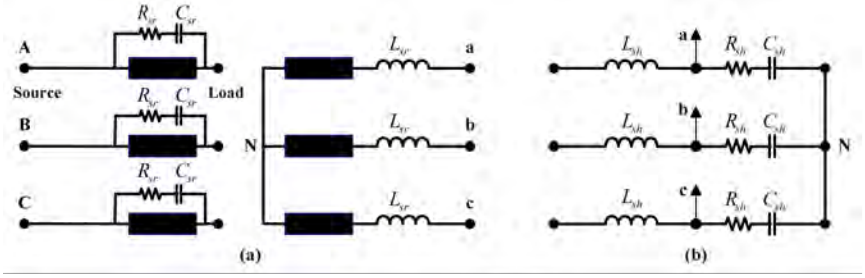

Figure 5.2: Schematics of the passive filters (a) Passive filters for series converter (b) Passive filter for shunt converter

Interfacing inductors play a crucial role in reducing ripple current & harmonics. They form an interfacing medium between APF and the grid lines. They are mainly used for suppressing current harmonics. The value of the inductor of shunt APF depends on the current ripple ($I_{cr,pp}$), switching frequency (f_s) and the DC voltage bus (V_{DC}), modulation index (m), the overloading factor (a) and can be calculated using Eq. 5.2 [12]

$$L_{r,sh} = \frac{\sqrt{3}mV_{DC}}{12af_sI_{cr,pp}} \tag{5.2}$$

Similarly, the interfacing inductor of series APF can be designed based on the source current ripple (δI_s), switching frequency (f_S) and the DC voltage bus (V_{DC}), modulation index (m), the overloading factor (a), the percent of voltage variation to be compensated (x), and series transformer turns ratio (n) can be expressed [12] as

$$L_{r,sr} = \frac{\left(\frac{\sqrt{3}}{2}\right)nxmV_{DC}}{6af_s\delta I_s} \tag{5.3}$$

Eqs. 5.1 to 5.3 are approximated formulas, which yield good enough results when values of unknown parameters such as overloading factor, current ripple and varying configuration etc. are carefully chosen, but it is difficult to arrive at optimum values using this approach due to which performance of UPQC and cost of its passive filters is not up to mark.

5.2.2 Controller Configuration

The control algorithm of UPQC used in this work is based on the power angle control (PAC) method because of its advantages [6]. The concept of PAC method enables the full utilization of shunt and series APFs by sharing of reactive power demand between the two APFs according to their rated VA capacities. The detailed phasor diagram of UPQC under PAC approach is shown in Fig. 5.3.

In Fig. 5.3, V_s is the rated source voltage having magnitude equal to k. δ (power angle) is the phase difference between load voltage (V_L) and source voltage (V_s). So, in steady state condition $V_s = V_L = k$. During sag condition, series voltage V'_{Sr} is injected by series APF to maintain load voltage constant. The magnitude of the

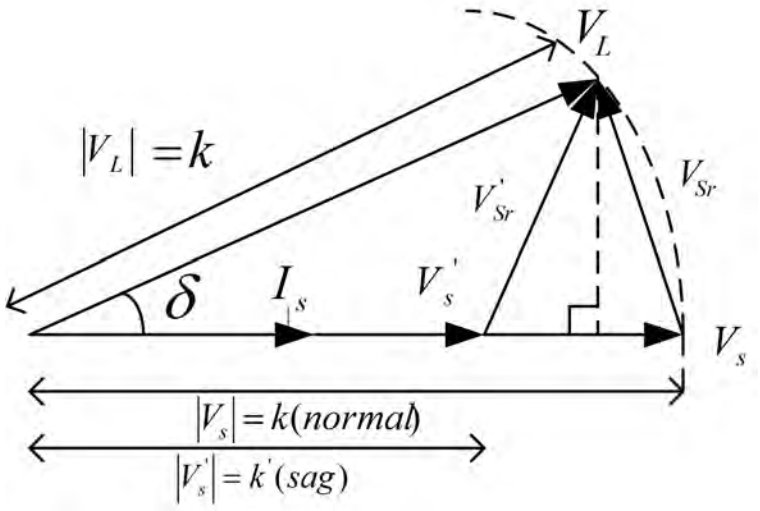

Figure 5.3: Phasor diagram of UPQC using PAC

injected series voltage can be computed as

$$V'_{Sr} = \sqrt{k^2 + K'^2 + 2kK'cos\delta} \tag{5.4}$$

The maximum value of injected series voltage by series APF is dependent on its VA rating. The maximum power angle (δ_M) changes in accordance with the variation in source voltage. So from Eq. (5.4) we can derive an equation for maximum power angle in terms of VA rating of series APF.

$$\delta_M = cos^{-1}[\frac{1 + K_s^2 - (S_{sr,rated}/3I_s k^2)}{2k_s}] \tag{5.5}$$

Where, k_s is the ratio of $|V'_s|/|V_s|$ and the desired power angle with VA limit can be calculated obtained below

$$\delta_D = sin^{-1}(\frac{\lambda Q_{sr}}{P_L}) \tag{5.6}$$

where, λ is the ratio of VA rating of the series inverter and sum of VA rating of series & shunt inverter. Q_{sr} is reactive power compensated by series APF and P_L is load active power. In the end, the minimum of δ_M and δ_D is acknowledged as actual power angle. Depending on the power angle, the series voltage is injected by series APF, which is described in next subsection.

5.2.3 Series APF control

Generally, the purpose of series APF is to act as voltage controlled source which maintains rated sinusoidal load terminal voltage. In conventional (non-PAC) control, the series APF works only during source voltage disturbances and shunt APF provides total reactive power of the load in steady state. However, in PAC method, the series compensator supplies a part of reactive power by injecting voltage at a certain angle. So, the burden of reactive power gets shared between the two APFs. The complete series APF control block is shown in Fig. 5.4. The technique is called Unit Vector Template Generation (UVTG) [13]. The power angle at each instant is determined by Eq. (5.6), which can be reframed in terms of $dq0$ quantities:

$$\delta_D = sin^{-1}(\frac{\lambda I_{Lq}}{I_{Ld}}) \tag{5.7}$$

where the value of I_{Lq} and I_{Ld} are obtained from Park's transformation as shown in shunt APF control block in Fig. 5.5. The rms value of source current I_s is equal to $(I_d^*)/\sqrt{2}$ where I_d^* is d-axis supply current taken from control block of shunt APF (Fig. 5.5). Hence, the maximum power angle meeting both VA rating limit and voltage limit is expressed as

$$\delta_M = cos^{-1}[\frac{1+K_s^2-(S_{sr,rated}/3I_d^*k)^2}{2k_s}] \tag{5.8}$$

So, actual value of power angle, δ is determined by considering the minimum of δ_D and δ_M. The voltage source signal is processed in 3-phase PLL and extracted ωt is summed with actual power angle (δ) to generate three-unit vector signal. The fundamental signal is multiplied with peak voltage signal and then is subtracted from load voltage signal to produce the required switching pulse as shown in Fig. 5.4.

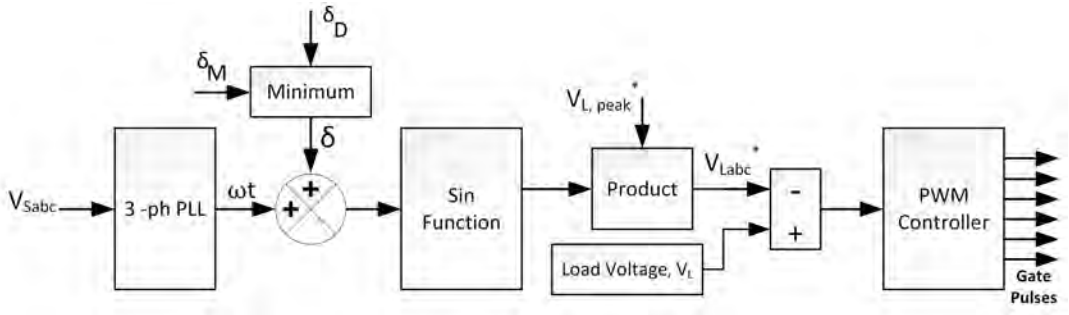

Figure 5.4: Series APF control

5.2.4 Shunt APF Control

In this chapter, modified SRF based PAC [6] technique is used to generate reference current signal for shunt APF. Figure 5.5 shows the controller block diagram of shunt active power filter control.

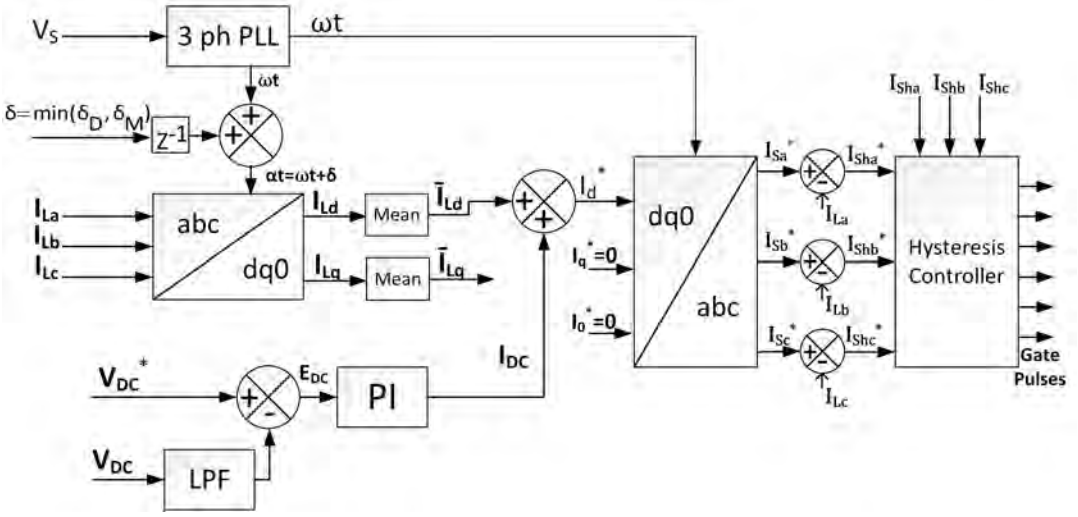

Figure 5.5: Shunt APF control

The controller injects suitable compensating current to mitigate power quality issues present in load current. The measured three-phase load current signals are converted from *abc* signal to $dq0$ frame (Eq. 5.9). The transformation is synchronized with the load voltage ramp signal which is obtained by adding the output of 3-phase PLL and power angle [i.e. $\alpha t = \omega t + \delta$]. The power angle estimation is already described in the previous subsection.

$$\begin{bmatrix} I_{Ld} \\ I_{Lq} \\ I_{Lo} \end{bmatrix} = \frac{2}{3} \begin{bmatrix} sin\alpha t & sin(\alpha t - \frac{2\pi}{3}) & sin(\alpha t + \frac{2\pi}{3}) \\ cos\theta & cos(\alpha t - \frac{2\pi}{3}) & cos(\alpha t - \frac{2\pi}{3}) \\ \frac{1}{2} & \frac{1}{2} & \frac{1}{2} \end{bmatrix} \begin{bmatrix} I_{La} \\ I_{Lb} \\ I_{Lc} \end{bmatrix} \tag{5.9}$$

$$I_{Ld} = \bar{I}_{Ld} + \tilde{I}_{Ld} \tag{5.10}$$

$$I_{Lq} = \bar{I}_{Lq} + \tilde{I}_{Lq} \tag{5.11}$$

The resultant $dq0$ signal consists of I_{Ld} (active power) and I_{Lq} (reactive power) components $\bar{I}_{Ld}$ and $\bar{I}_{Lq}$ are fundamental active and reactive components of the load current. $\bar{I}_{Ld}$ is obtained by passing I_{Ld} through a moving average block. DC link voltage is compared with reference DC link voltage and resultant error (E_{DC}) is processed

by PI controller to get required DC link current (I_{DC}). The mean $\bar{I}_{Ld}$ is summed with I_{DC} to form reference d-axis current in synchronous frame. The reference d-axis supply current transformed back to 3-phase reference source currents $(I^*_{sa}, I^*_{sb}, I^*_{sc})$ (Eq. 5.12) using Clark transformation. The actual load current signal (I_{La}, I_{Lb}, I_{Lc}) is subtracted from reference source current to produce reference shunt APF current $(I^*_{sha}, I^*_{shb}, I^*_{shc})$ (Eq. 5.13). The obtained signal is compared with measured shunt APF current $(I_{Sha}, I_{Shb}, I_{Shc})$ in hysteresis controller giving desired switching gate signal.

$$\begin{bmatrix} I^*_{sa} \\ I^*_{sb} \\ I^*_{sc} \end{bmatrix} = \begin{bmatrix} sin\omega t & cos\omega & 1 \\ sin(\omega t - \frac{2\pi}{3}) & cos(\omega t - \frac{2\pi}{3}) & 1 \\ sin(\omega t + \frac{2\pi}{3}) & cos(\omega t + \frac{2\pi}{3}) & 1 \end{bmatrix} \begin{bmatrix} I^*_d \\ I^*_q \\ I^*_0 \end{bmatrix} \tag{5.12}$$

$$\begin{bmatrix} I^*_{sha} \\ I^*_{shb} \\ I^*_{shc} \end{bmatrix} = \begin{bmatrix} I^*_{sa} \\ I^*_{sb} \\ I^*_{sc} \end{bmatrix} - \begin{bmatrix} I_{La} \\ I_{Lb} \\ I_{Lc} \end{bmatrix} \tag{5.13}$$

5.3 Concept of Applied method

5.3.1 Concept of Particle Swarm Optimisation

It is a population-based method where each particle called as solution updates its position based on past experience and neighbour's best experience to search for optimal solution. These particles communicate directly or indirectly with each other by search direction or gradient method. Each particle has its position vector and velocity vector which are calculated at every t^{th} iteration in the search space. Every particle has its local best position obtained by evaluating its fitness function which is updated continuously as better position is searched by the other particles. The best position among all particles is known as the global best position. This process continues until the best solution is obtained. The procedure for implementation of PSO algorithm for optimizing passive filters of UPQC is shown as follows:

- Initial swarm of particles (candidate solutions or positions) is generated within the bounds of variables. Each particle is composed of six variables for six parameters: series interfacing inductor (L_{sr}), resistance of series RC filter (R_{sr}), capacitance of series RC filter (C_{sr}), shunt interfacing inductor (L_{sh}), resistance of shunt RC filter (R_{sr}) and capacitance of shunt RC filter (C_{sh}).

- UPQC system model is simulated for prescribed set of operating conditions (including steady state and transient situation such as sag/swell). Based on the simulation output, the objective function is evaluated for all the particles of initial population.
- The local best position and global best position are computed for the first iteration. The position as well as velocity of particle (solution) get updated using equations described in next subsection.
- Again, the UPQC model is simulated for same set of operating conditions and simulation output is used to re-evaluate the objective function for updated particles. The local best and global best positions are found, and position and velocity are updated. The process of searching for best solution is repeated until the convergence criteria meets.

5.3.2 Problem Formulation and Implementation

The optimization problem is formulated to design the optimal passive filters of UPQC in various loading conditions. In minimization problem of the objective function consists of 6 variables with lower and upper bounds. The mathematical formulation of optimization problem is expressed as:

$$min.F_1 = w_1 THD + w_2 PowerLoss + w_3 VR + w_4 Obj2 \tag{5.14}$$

Subjected to

$$L_{sr,min} \leq L_{sr} \leq L_{sr,max} \tag{5.15}$$

$$R_{sr,min} \leq R_{sr} \leq R_{sr,max} \tag{5.16}$$

$$C_{sr,min} \leq C_{sr} \leq C_{sr,max} \tag{5.17}$$

$$L_{sh,min} \leq L_{sh} \leq L_{sh,max} \tag{5.18}$$

$$R_{sh,min} \leq R_{sh} \leq R_{sr,max} \tag{5.19}$$

$$C_{sh,min} \leq C_{sh} \leq C_{sh,max} \tag{5.20}$$

where, THD is averaged sum of per unit THDs of source current and load voltage; PowerLoss is per unit average power loss of UPQC; VR is per unit average voltage

regulation of load voltage. Since the objective function is modelled for minimization, the power factor is considered as a new variable represented as:

$$Obj2 = 1 - PF \tag{5.21}$$

where PF is the average power factor. While endeavoring to improve THDs, power losses tend to increase, so the objective function is cautiously coordinated in such a way that it will yield an optimum balance between these indexes. Weights w_1, w_2, w_3, w_4 can be selected based on the requirement of a specific application, for example, if a requirement of THD minimization is high, then w_1 assumes a higher value. Upper and lower bounds on controlled variables are selected based on the designer's experience with the system.

The above mentioned PSO algorithm is coded on MATLAB script platform to find the most suitable solution for passive filters of the UPQC. The initial population of candidate solutions (or particles) are found around a guess value obtained from the design method described in [12]. Next step is to initialize the velocity of the particle within the domain of decision variable. These particles evolve and inspect possible solutions in the feasible region and remember the best position they have located. The optimal solution is obtained with the help of particle population as each particle of the population move continuously throughout search space and find the optimal solution by sharing movement experience. To make sure, the new position does not cross feasible region, an upper and lower bound are applied to the variable. Then the local best position (p_{best}) of each particle has been evaluated based on best fitness value of decision variable and is stored as "p_{best}". The term "g_{best}" is used for the entire population whereas "p_{best}" is used for every individual particle member.

In the process of evaluating the objective function, global best position is selected from the local best positions on the basis of the best fitness value and stored as "g_{best}". The updated particle velocity can be determined as:

$$V_i^{t+1} = w * V_i^t + c_1 r_1 * (p_{best,i} - X_i^t) + c_2 r_2 * (g_{best,i} - X_i^t) \tag{5.22}$$

where, w is inertia weight. It is used to balance the local and global search during the optimization process. The inertia weight 'w' should be between 0.4 and 0.9. The parameters r_1 and r_2 are random numbers, whose values should be between 0 and 1. The newly updated velocity is then added to the particle's previous position to

determine the particle's freshly updated position as follows:

$$X_i^{t+1} = X_t^i + V_i^{t+1} \tag{5.23}$$

After the current position is updated, the objective function is evaluated which updates the fitness function (f_i). The personal best position of every particle updates based on the following condition:

$$\left.\begin{array}{l} p_{best,i} = X_i \\ f_{pbest,i} = f_i \end{array}\right\} \quad \text{if } f_i < f_{Pbest,i} \tag{5.24}$$

In addition to that, the global best position of the particles is also updated as per the following condition:

$$\left.\begin{array}{l} g_{best} = P_{best,i} \\ f_{gbest} = f_{pbest,i} \end{array}\right\} \quad \text{if } f_i < f_{gbest,i} \tag{5.25}$$

The PSO algorithm converges to the best solution after performing a certain number of iterations, irrespective of the initial assumption.

5.4 Result and Discussion

The optimum design of UPQC passive filter is obtained using the proposed PSO algorithm in MATLAB/Simulink environment. Along with it, the passive filter parameters of series APF and shunt APF are designed using conventional approach for

Table 5.1: System Parameters

Source	Voltage, Frequency	415V, 50Hz
	Impedance	R_s = 0.05 Ω, L_s= 0.5mH
DC-link	Capacitor	C_{DC} = 5500uF
	Ref. DC-Link	700V
Shunt APF	Interfacing Inductor	2mH/ph
	Ripple Filter	$R = 5\Omega$/ph, $C = 50uF$/ph
Series APF	Interfacing Inductor	2mH/ph
	Ripple Filter	$R = 5\Omega$/ph, $C = 50uF$/ph
	Injection Transformer	4.5 kVA
Load 1	15.69Ω	(Linear Load)
Load 2	18 kVA	(Non-Linear Load)
Load 3	18 kVA	(Non-Linear Load)

Table 5.2: Result of best parameter values obtained from PSO algorithm

Sr. No.	$L_{sr}(mH)$	R_{sr} (Ω)	C_{sr} (μF)	L_{sh} (mH)	R_{sh} (Ω)	C_{sh} (μF)	Obj. Func.
Base	2	5	50	2	5	50	-
Opt.1	9.96	7.84	17	1.65	4.2	5	2.5
Opt.2	5.86	7.49	85.4	1.69	6.6	40	2.10
Opt.3	4.52	0.5	170.5	1.63	6.53	5	2.17
Opt.4	**3.45**	**6.22**	**76.8**	**2.24**	**7.13**	**20.5**	**1.9**
Opt.5	4.84	2.79	72	1.22	5.07	27	2.19

Table 5.3: Result of power losses, voltage regulation, power factor and THD

Parameter	Mean P-Loss	Mean VR	Mean PF	THD
Base	0.0347	0.0167	0.9859	0.0921
Opt.4	0.0154	0.0226	0.9863	0.0858

comparison. Various iterations of PSO with different variants resulted in slightly different optimized unique values, which were then validated and compared with conventional design parameters. The specifications of the case study system are listed in Table 5.1. Three phase source voltage of 415 V, 50 Hz with a source resistance of 0.05 Ω and source inductance of 0.05 mH is considered. The reference value for the DC link is 700 V. Three different types of load (linear and non-linear) are applied to the system. Load 1 consists of a three-phase uncontrolled rectifier with resistive load whereas, Load 2 and Load 3 are different combinations of resistive and inductive AC loads. All of these loads are introduced to the system at separate times.

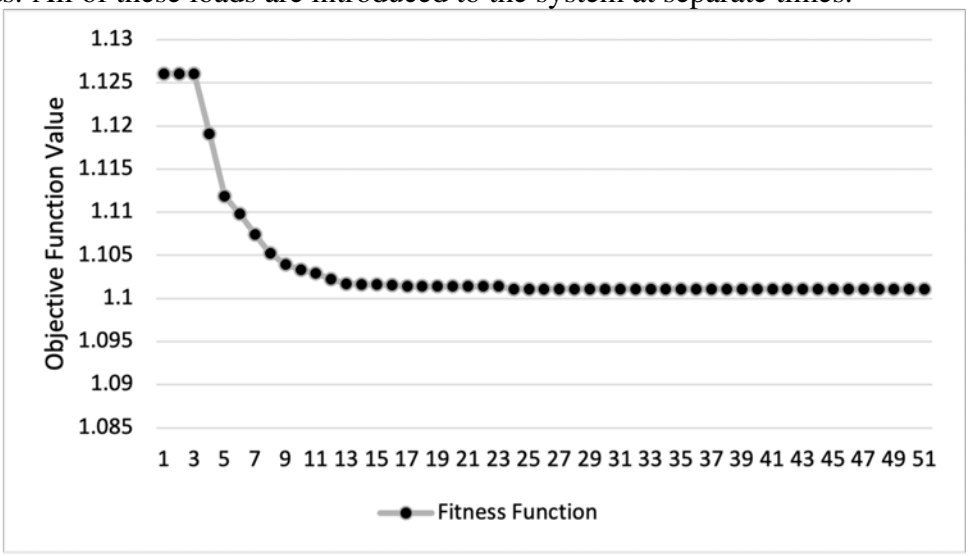

Figure 5.6: Convergence curve for the algorithm

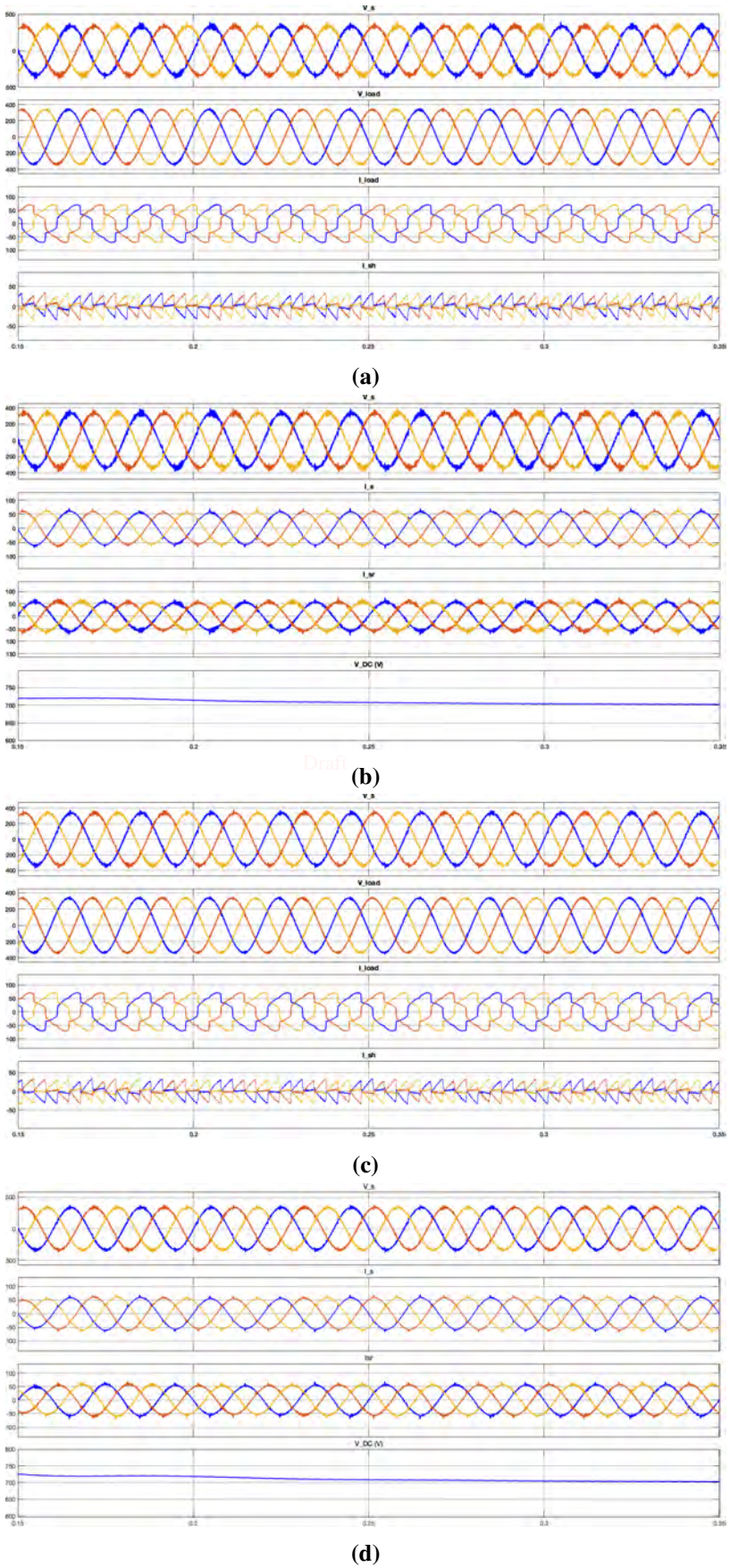

Figure 5.7: Simulation result of base (a and b) and optimized (c and d) UPQC parameters

5.4.1 MATLAB Simulation Result

As explained in section 5.3.1, the developed code of PSO-based optimization of UPQC passive filters is implemented using the MATLAB platform. The conventional UPQC model with the filter parameters is highlighted in Table 5.1. These filter values obtained using conventional approach form the basis for generating initial set particles for PSO based design approach. The initial set of particles is generated randomly within the vicinity of conventionally found parameters. Then the objective function is evaluated for initial set of particles using simulink model of UPQC. The subsequent iterations of PSO are performed as per the procedure mentioned in section 5.3.1 and the minimum value of objective function is found when convergence criteria is met. The duration of whole simulation time depends on the quantity of the particle population. The optimum filter parameters in Table 5.2 are obtained by performing 30 such PSO code runs in which 5 runs with the best objective function are enlisted. The best result in the table is shown in bold letters. The term "base" is considered for the conventionally designed parameters of UPQC and the term "opt." stands for optimized parameters of UPQC. In Table 5.2, opt.4 is preferred as the best optimized solution as it has a minimum objective function. The filter design techniques, in general, are expected to produce lower numerical values of the filters, however, it is observed that the series capacitor and shunt capacitor in opt.4 are higher than those obtained in other cases. In addition, the numerical value of inductor and capacitor are higher than their values obtained in the conventional approach. The reason is that the objective function results from PSO algorithm is minimum as compared to others based on various factor that are involved in customized objective function to enhance the overall performance of UPQC consisting of good power factor, voltage regulation and lower THDs simultaneously, which is practically inconceivable in conventional design approach. The convergence curve for PSO of opt.4 is shown in Fig. 5.6. By analysing the convergence closely, it is found that the objective function value settles at the 44th iteration. Table 5.2 shows that the power loss, voltage regulation and THD of the optimized passive filter is lesser than the conventionally designed filter. Fig. 5.7a & 5.7b shows the performance of UPQC with conventional designed ripple filter. As seen, the DC link is maintained at 700 V. The series APF is compensating the source voltage and maintains load voltage at the rated value by injecting the voltage at a suitable phase. Due to the power angle control approach, the series APF is also engaged in the reactive power compensation

as shown in Fig. 5.7d. The THD values are within the IEEE-519 limit. Furthermore, when compared to Fig. 5.7a, the notches near the peak of load voltage waveform (V_L) are noticeably reduced after implementing the optimised filter. The distortion of the waveform (I_{sr}) is visibly improved in Fig. 5.7d. The significant reduction in power loss can be validated in Table 5.2. So, the result achieved with the approached algorithms are found to be better as compared to the conventional approach.

5.5 Summary

This chapter proposed a method to optimize the ripple filter and interfacing inductor of shunt and series APFs of the UPQC. The optimal values of passive interfacing components of UPQC are found by the Particle Swarm Optimization (PSO) by taking a minimization function that includes key performance measures such as power losses, voltage regulation, harmonics and power factor. A comparative study is conducted between conventional design approach and PSO based design approach proposed in this work. The obtained results indicate that the passive filter designed by PSO approach achieves superior performance in terms of technical viability. The overall power loss in the designed UPQC is 608 W in comparison to the 810 W obtained from conventional UPQC.

Bibliography

[1] D. Li, T. Wang, W. Pan, X. Ding, and J. Gong, "A comprehensive review of improving power quality using active power filters," *Electric Power Systems Research*, vol. 199, p. 107389, 2021.

[2] A.-H. M. Abu-Jalala, T. Cox, C. Gerada, M. Rashed, T. Hamiti, and N. Brown, "Power quality improvement of synchronous generators using an active power filter," *IEEE Transactions on Industry Applications*, vol. 54, no. 5, pp. 4080–4090, 2018.

[3] V. Khadkikar, "Enhancing electric power quality using UPQC: A comprehensive overview," *IEEE Transactions on Power Electronics*, vol. 27, no. 5, pp. 2284–2297, 2012.

[4] N. Patnaik and A. K. Panda, "Performance analysis of a 3 phase 4 wire UPQC system based on PAC based SRF controller with real time digital simulation," *International Journal of Electrical Power & Energy Systems*, vol. 74, pp. 212–221, 2016.

[5] A. K. Panda and N. Patnaik, "Management of reactive power sharing and power quality improvement with SRF-PAC based UPQC under unbalanced source voltage condition," *International Journal of Electrical Power & Energy Systems*, vol. 84, pp. 182–194, 2017.

[6] A. Patel, H. D. Mathur, and S. Bhanot, "Enhancing VA sharing between the shunt and series APFs of UPQC with a modified SRF-PAC method," *IET Power Electronics*, vol. 13, pp. 275–285, 2020.

[7] S. Devassy and B. Singh, "Modified pq-theory-based control of solar-PV-integrated UPQC-S," *IEEE Transactions on Industry Applications*, vol. 53, no. 5, pp. 5031–5040, 2017.

[8] A. Q. Ansari, B. Singh, and M. Hasan, "Algorithm for power angle control to improve power quality in distribution system using unified power quality conditioner," *IET Generation, Transmission & Distribution*, vol. 9, no. 12, pp. 1439–1447, 2015.

[9] A. Lakum and V. Mahajan, "Optimal placement and sizing of multiple active power filters in radial distribution system using grey wolf optimizer in presence of nonlinear distributed generation," *Electric Power Systems Research*, vol. 173, pp. 281–290, 2019.

[10] J. Ye, H. B. Gooi, and F. Wu, "Optimal design and control implementation of UPQC based on variable phase angle control method," *IEEE Transactions on Industrial Informatics*, vol. 14, no. 7, pp. 3109–3123, 2018.

[11] G. S. Kumar, P. H. Vardhana, B. K. Kumar, and M. K. Mishra, "Minimization of VA loading of unified power quality conditioner (UPQC)," in *2009 International Conference on Power Engineering, Energy and Electrical Drives*. IEEE, 2009, pp. 552–557.

[12] B. Singh, A. Chandra, and K. Al-Haddad, *Power quality: problems and mitigation techniques*. John Wiley & Sons, 2014.

[13] V. Khadkikar, P. Agarwal, A. Chandra, A. Barry, and T. Nguyen, "A simple new control technique for unified power quality conditioner (UPQC)," in *Proc. 11th IEEE International Conference on Harmonics and Quality of Power*, 2004, pp. 289–293.

Chapter 6

Comparing Power Losses in Diverse Control Strategies of UPQC

6.1 Preamble

Power Quality problems are the emerging problem in today's world where electricity is only a reliable source of power. Modern technology appliances and sizeable industrial equipments require continuous sinusoidal voltage with constant amplitude and frequency. Present scenario of AC distribution system facing irregularity in power supply, voltage sag, voltage swell, and excessive reactive problems and so on. Poor power quality leads to improper functioning of electrical devices and abnormal behaviour of AC loads. Many electronic equipments generate harmonic current and increased reactive power causing loads to unbalance and voltage fluctuation.

An extensive review of various power quality enhancement devices on distribution level is presented in the literature [1] commonly known as Unified Power Quality Conditioner. This device is the combination shunt APF and series APF with DC link capacitor connected between them (Fig. 6.1). Shunt APF commonly called DSTATCOM provides the current compensation in case of load unbalancing, harmonics reduction and reactive power injection. The series compensation devices called DVR provide interrupted voltage supply to the load in the case of voltage sag/swell, voltage fluctuation etc.

Various researchers have published papers in the category of UPQC based on (i) converter type (ii) topology type (iii) control type and (iv) rating based. A comprehensive review of various category of UPQC is reported in article [1,2]. On all of the major classifications, the rating based UPQC focused on the mitigation of voltage sag/swell on the distribution system.

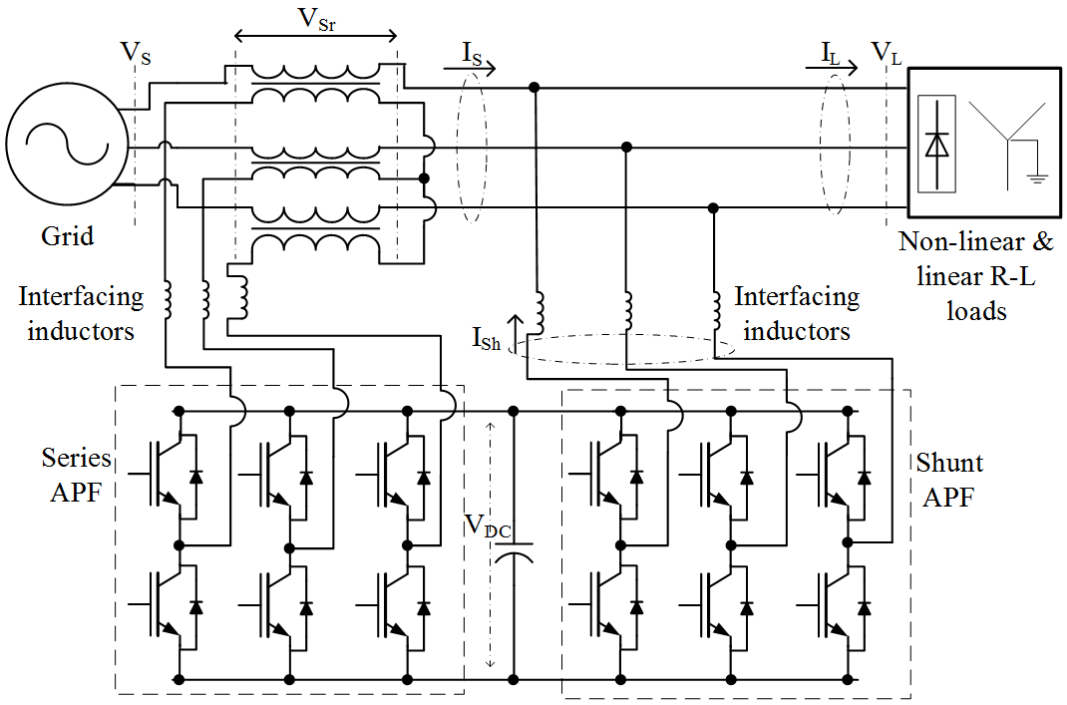

Figure 6.1: Configuration of UPQC system.

The control strategies of UPQC includes: UPQC-P, UPQC-Q, UPQC-S. In UPQC-P, active power control is achieved by injecting voltage in phase with the supply voltage, which is the simple one and yields minimum voltage rating of DVR, but increases VA rating due to exchange of active power. UPQC-Q control aims at minimizing the active power exchange by making DVR inject voltage in quadrature with source voltage. The UPQC-S control aims at overall VA minimization by injecting voltage at an angle with source voltage.

This chapter presents the loss comparison of UPQC-P, UPQC-Q and UPQC-S. Each model have been simulated in MATLAB/Simulink and investigated in detailed manner. The losses are compared and categorized in three modes, such as steady state mode, 30% sag mode, 30% swell mode. The steady state mode is further categorized in two-parts, one with a full load and the another one is with partial load. The full load consists of linear and nonlinear load along with the harmonic load. However, the partial load contains the linear load only.

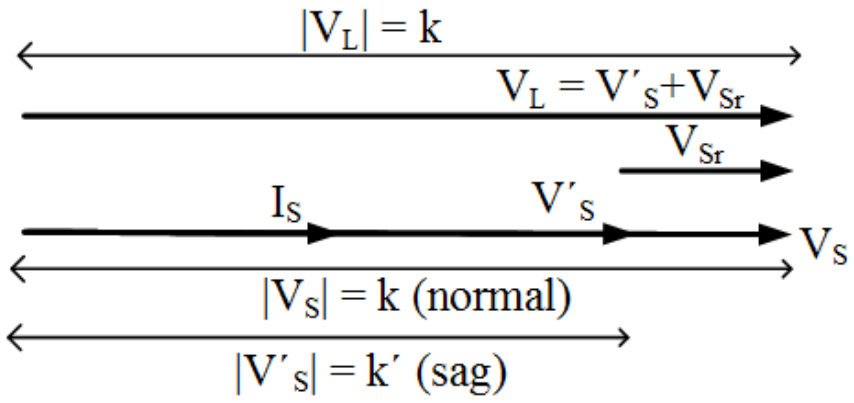

Figure 6.2: Phasor representation of a UPQC-P for voltage sag compensation.

6.2 Control Strategies of UPQC

The system configuration of UPQC shown in Fig. 6.1 is designed for three-phase system.

The system consists of shunt APF connected toward the right side of the circuit (load side) and the series APF connected to the left side of the circuit (source voltage). Series APF interfaced with a grid system with the help of inductor and injection transformer. Similarly, shunt APF is integrated across the load with inductor. Ripple filters are also used to filter out the harmonics generated by the power electronics load.

6.2.1 UPQC-P

In UPQC-P, the DVR is used to maintain the load voltage at the rated value and the injected voltage in phase or out of phase with the supply voltage [3–5]. This control strategy leads to minimum voltage injection by DVR, but it involves considerable active power exchange of UPQC with grid leading to increase in its VA rating. During sag, active power is injected by DVR and during swell, it withdraws power from the grid. In both cases, balanced active power after meeting losses of UPQC, is routed back to the grid by DSTATCOM of UPQC.

From Fig. 6.2, it is evident that UPQC-P can satisfactorily perform the compensation of voltage sag and swell smoothly. The series inverter injects voltage in the same phase with the supply voltage. For doing so, the series APF fed active power

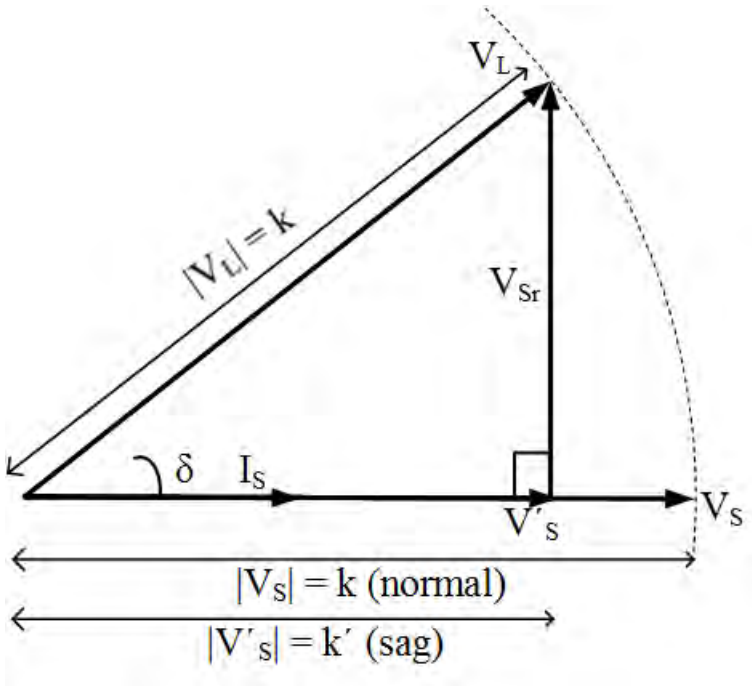

Figure 6.3: Phasor representation of a UPQC-Q for voltage sag compensation.

from shunt APF. The reactive power is compensated by shunt inverter and the rating of series inverter is at minimum value.

6.2.2 UPQC-Q

In this control, DVR injects voltage in quadrature with the supply current. DVR does not consume any active power during the process. Similarly, DSTATCOM performs the current based compensation to fulfil the reactive power demand and to maintain the DC-link voltage constant [6, 7]. The magnitude of the compensated voltage is higher than that of UPQC-P. This configuration is suitable only for sag compensation.

The phasor diagram of UPQC-Q is shown in Fig. 6.3, where DVR is compensating the fundamental voltage by injecting the reactive power into the bus bar at the quadrature angle (90°). With the supply current, Fig. 6.3 shows clearly that the series inverter cannot compensate voltage for voltage swell. However, DSTATCOM achieves the reactive power compensation of the load efficiently. In sag mode, DVR do not supply the active power and VA rating is at minimum value.

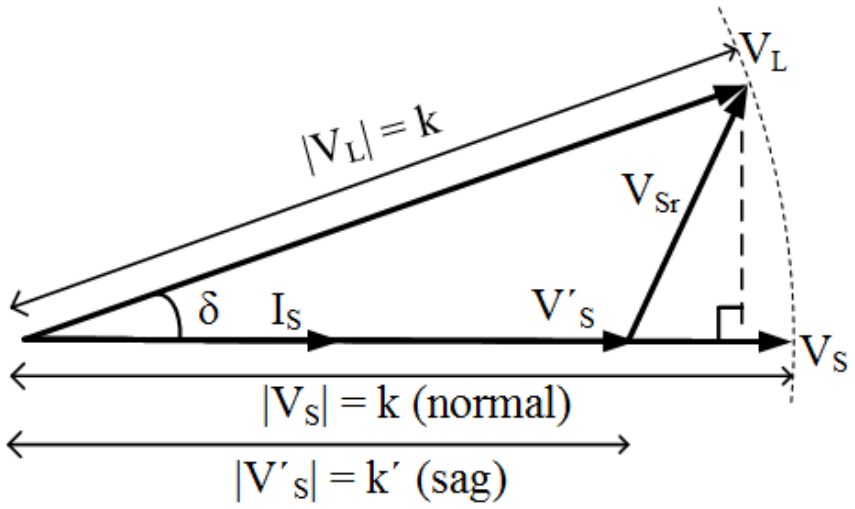

Figure 6.4: Phasor representation of a UPQC-S for voltage sag compensation.

6.2.3 UPQC-S

DVR can compensate both active power and reactive power simultaneously, while DSTATCOM is used for all current based compensation [8]. The rating of DVR and DSTATCOM are relatively minimal as compared to UPQC-P and UPQC-S and can be utilized to full capacity of VA loading.

Unlike the above two control modes, the control strategy of UPQC-S is proved to be best for the compensation of active and reactive power. The DVR can inject voltage for both conditions of voltage sag/swell compensation. The compensation done on a predetermined phase angle with the minimum utilization of VA loading as shown in Fig. 6.4.

6.3 Control of UPQC

Figure 6.5 shows the control block diagram of the UPQC system. For the control of series APF, three phase PLL is used to generates the reference signal for series inverter. The measured voltage source is converted to frequency (Hz) by PLL. Then the output signal is converted to three phase fundamental signal with 120°. Later the signal is multiplied with the peak voltage that we desired to get in the load voltage. The desired reference load voltage can be expressed as

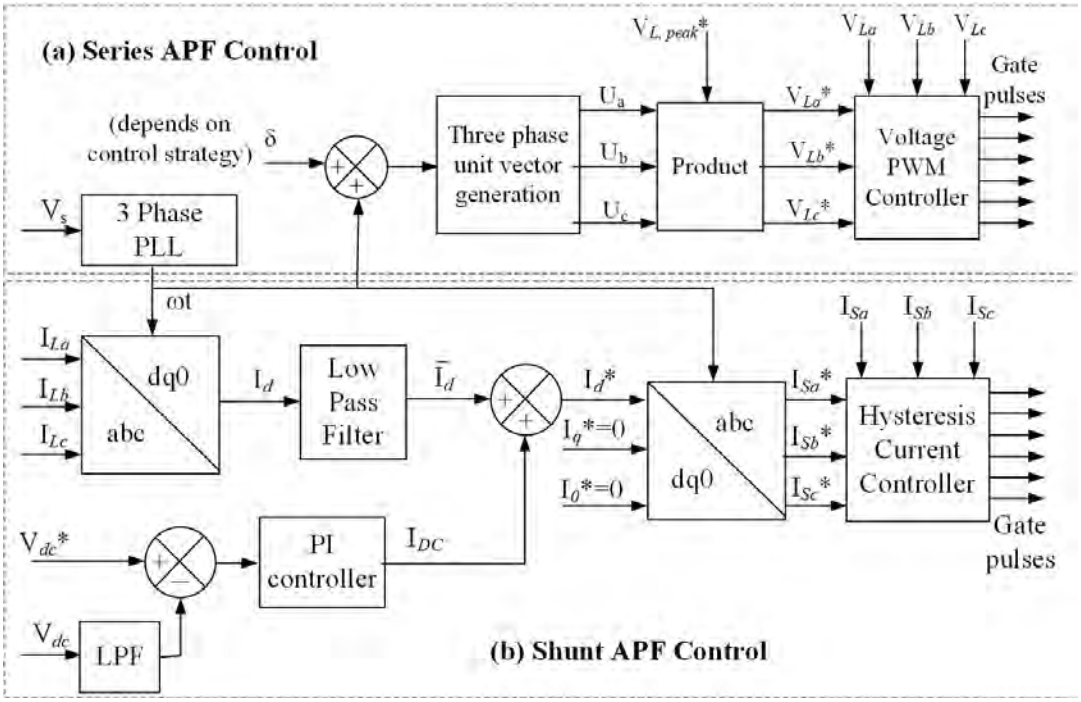

Figure 6.5: Control structure of series APF and shunt APF.

$$\begin{bmatrix} v^*_{La} \\ v^*_{Lb} \\ v^*_{Lc} \end{bmatrix} = \begin{bmatrix} v_{La}(sin\omega t) \\ v_{Lb}(sin\omega t - 120^\circ) \\ v_{Lc}(sin\omega t + 120^\circ) \end{bmatrix} \tag{6.1}$$

Equation (6.1) will be compared with actual load voltage with the help of PWM controller to get required gate pulses for the series inverter. This method is known as UVTG (Unit Vector Template Generation) [9].

The SRF method (Synchronous Reference Frame Theory) [10] will transfer three phase voltage signal in ABC form to synchronously rotating reference frame (DQ-theory) using park's transformation as expressed in Eq. (6.2)

$$\begin{bmatrix} i_{Ld} \\ i_{Lq} \\ i_{Lo} \end{bmatrix} = \frac{2}{3} \begin{bmatrix} cos\theta & -sin\theta & \frac{1}{2} \\ cos(\theta - \frac{2\pi}{3}) & -cos(\theta - \frac{2\pi}{3}) & \frac{1}{2} \\ cos(\theta + \frac{2\pi}{3}) & sin(\theta - \frac{2\pi}{3}) & \frac{1}{2} \end{bmatrix} \begin{bmatrix} i_{La} \\ i_{Lb} \\ i_{Lc} \end{bmatrix} \tag{6.2}$$

The aforementioned current signal is synchronized with source voltage by three phase PLL. These signals are then passed through band pass filter and summed with the desired value of DC link voltage signal. The reference DC link voltage is obtained from the computation of PI controller followed by the comparison of actual DC bus

voltage and its reference value. The resultant d-axis component of the load current is transformed to reference current using inverse park transformation with assuming that q-axis component and zero axis component to be zero. Now, the reference source current is compensated to the actual source current to get the desired gate pulses for the shunt inverter as shown in Fig. 6.5.

Power angle δ is the angle between the source voltage and the series compensated voltage. It is important factor for controlling UPQC with effective utilization of shunt APF and series APF at various condition of voltage disruption. Based on the control strategies, estimated power angle is summed up with ωt to generate three phase balanced unit vectors using Eq. (6.1). The later signal is multiplied with reference load voltage to generate reference load voltage signals with displaced power angle (δ). For UPQC-S, power angle is calculated [11] as follows

$$\delta = sin^{-1}\left(\frac{Q_{Sr}}{P_L}\right) \tag{6.3}$$

where Q_{Sr} reactive power supplied by series APF is taken as 37.5% of Q_L (load reactive power) . Shunt APF supplies rest of Q_L, where as P_L is load active power. For UPQC-Q, the power angle is calculated [12] as follows

$$\delta = cos^{-1}\left(\frac{V_S^{'}}{V_{L,ref}}\right) \tag{6.4}$$

where, $V_s^{'}$ is instantaneous RMS magnitude of source voltage, abs $V_{L,ref}$ is a load reference voltage (the desired value of load voltage). While, For UPQC-P, the δ is taken as zero.

6.4 Simulation Results

All the three models of UPQC have been developed and simulated in MATLAB/ Simulink and their dynamic performances investigated and analyzed in detail. Losses caused by dynamical behavior of the UPQC at different types of load have been evaluated by the simulation and shown in Table 6.2.

System parameters are designed and calculated using the method given in [2]. A three phase source of 400V, 50Hz with source resistance of 0.05Ω and source inductance of 0.5 mH considered for the UPQC system.

Table 6.1: System Parameter

Source	Voltage and Frequency	400 V, 50Hz
	Impedance	R_S = 0.05, L_S = 0.5mH
DC link	Capacitor	C_{DC}=5500μF
	Reference DC link	700 V
Shunt APF	Interfacing Inductor	1.2mH/ph
	Ripple Filter	R = 10Ω/ph, C = 10 μF/ph
Series APF	Interfacing Inductor	3.6 mH/ph
	Ripple Filter	R= 5Ω/ph, C = 50 μF/ph
	Injection Transformer	4.5 kVA

In Fig. 6.6, waveforms for UPQC controlled using UPQC-S strategy are shown. Initially the system is in steady-state and load current harmonics and reactive power are compensated. Using UPQC-S control, series APF supplies a part of reactive power and hence, there will be a phase difference (power angle) between source and load voltages. In steady state, source current is harmonics free at unity power factor. At 0.4 sec, a voltage sag of 30% occurs which is compensated by series APF making load voltage magnitude unaffected. On the occurrence of sag, series voltage injected by series APF changes to accommodate the voltage required for compensating voltage sag.

In Fig. 6.7, key waveforms of UPQC-Q control strategy are shown (current waveform are not shown as they are repetitive and to save space). In steady state, voltage injected by series APF is minimal just to maintain voltage regulation. On the occurrence of sag, voltage is injected by series APF in quadrature with source current/source voltage. Of course, the magnitude of voltage required for the same amount of sag is larger in this control compared to UPQC-S. In this control, power angle has small value in steady state and it goes to maximum value (45°) during sag.

In Fig. 6.8, key waveforms of UPQC-P are shown. In steady-state, series voltage is practically zero. On the occurrence of sag, series voltage is injected in phase with source voltage to maintain the load voltage. Power angle is always zero in this control. Similarly during the occurrence of swell, the power angle is zero in the case of UPQC-P as shown in Fig. 6.9 as well in the control of UPQC-Q.

Table 6.2. illustrates the power losses associated with UPQC-P, UPQC-Q and UPQC-S. The source power and load power are calculated and the total losses of current through shunt and series inverter along with the voltage injection are included in the table. The losses of UPQC-P is found out to be 3.2% and 1.73% in the case

Table 6.2: Losses Associated with a Different Model of UPQC Under Various Load Scenario. (A) UPQC-P. (B) UPQC-Q. (C) UPQC-S. (**Overall** Case: Individual Durations: **Sag**-0.2 sec, **Swell**-0.1 sec, **SS-FL**-2 sec, **SS-PL1**-1.3 sec, **SS-PL2**-0.4 sec)

(A) UPQC-P	**Time (s)**	**P_s (W)**	**P_L (W)**	**P_upqc_loss (W)**	**Delta (°)**
SS-FL	0.4	41830	40932.5	-897.5	0
Sag-30%	0.4	40955	39647.5	-1307.5	0
Swell-30%	0.4	42980	42245	-735	0
SS-PL	0.4	31790	31217.5	-572.5	0
Overall	4	35870.3	35152.3	-718	0
(B) UPQC-Q	**Time (s)**	**P_s (W)**	**P_L (W)**	**P_upqc_loss (W)**	**Delta (°)**
SS-FL	0.4	41572.5	40750	-822.5	8.2
Sag-30%	0.4	35420	34992.5	-427.5	45
Swell-30%	0.4	43040	42310	-730	0
SS-PL	0.4	31697.5	31170	-527.5	6.1
Overall	4	35516.5	34875.8	-640.8	4.0- 45.0
(C) UPQC-S	**Time (s)**	**P_s (W)**	**P_L (W)**	**P_upqc_loss (W)**	**Delta (°)**
SS-FL	0.4	41122.5	40272.5	-850	16.1
Sag-30%	0.4	37437.5	36335	-1102.5	16.5
Swell-30%	0.4	44412.5	43667.5	-745	13.8
SS-PL	0.4	31465	30912.5	-552.5	14.2
Overall	4	35294.3	34603.5	-690.8	10.2-16.5

of voltage sag (30%) and voltage swell (30%). Similarly, in UPQC-S and UPQC-Q, the loss percentages are 3.03% and 1.2% for sag and 1.7% and 1.72% for swell respectively.

The simulation time of each variation of the loads are set to 0.4 sec. In other words, a sag of 30 % is introduced on the system for t = 0.4 s. Then in next phase of, simulation swell of 30% is imposed on the system for t = 0.4 s. Similarly, a time period of 0.4 s is applied to the system with a partial and full load in every control strategy of UPQC's as explained in above section.

In the last row of each table shows the overall simulation done at a single run on a single simulation time of 4 seconds. Initially for t_1= 2 s, the UPQC system was working at steady state condition with full load. After time interval t_1, steady state partial load L_1 is introduced for t_2 = 1.3 s followed by next partial load L_2 for t_3 = 0.4 s. Between t_4 = 3.7 s to t_5 = 3.9 s, sag of 30% is imposed in the system. Further, swell of 30% is introduced for t_6 = 0.1 s. The result of the simulation is outlined as

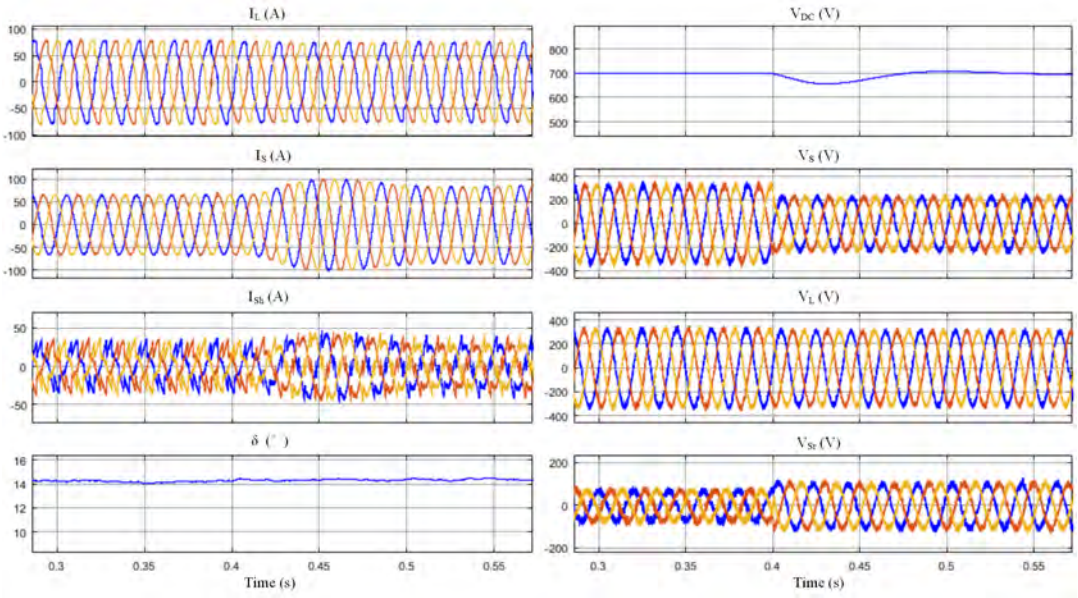

Figure 6.6: Waveforms of UPQC controlled using UPQC-S (30% sag).

follows:

- From Fig. 6.8 and Fig. 6.9, the waveforms shows that shunt APF injects minimum voltage for compensation of voltage sag/swell. The power angle (δ) is zero which implies that DVR only requires active power for voltage injection. The comparisons result also evaluates that UPQC-P consumes maximum power than the other two UPQC's control system in the case of voltage sag/swell.

- From Fig. 6.6, the waveforms of UPQC-S shows that the load voltage is maintained at desired level on the occurrence of voltage sag and with minimum system losses. Referred to the Table 6.2, the power angle (δ) is maintained at 16.1° and 16.5° during voltage sag and steady state respectively. During voltage swell the power angle is maintained at 13.8°. There will be an increase in the reactive power compensation during voltage sag and voltage swell due to increase in the source current.

- In Fig. 6.7, the series inverter injects the voltage in quadrature with the load end. It can be shown that there is an increase in the magnitude of the series injected voltage. In the case of voltage swell as indicated in Table 6.2, the power angle (δ) is zero which concludes that UPQC-Q cannot be used for the compensation of voltage swell.

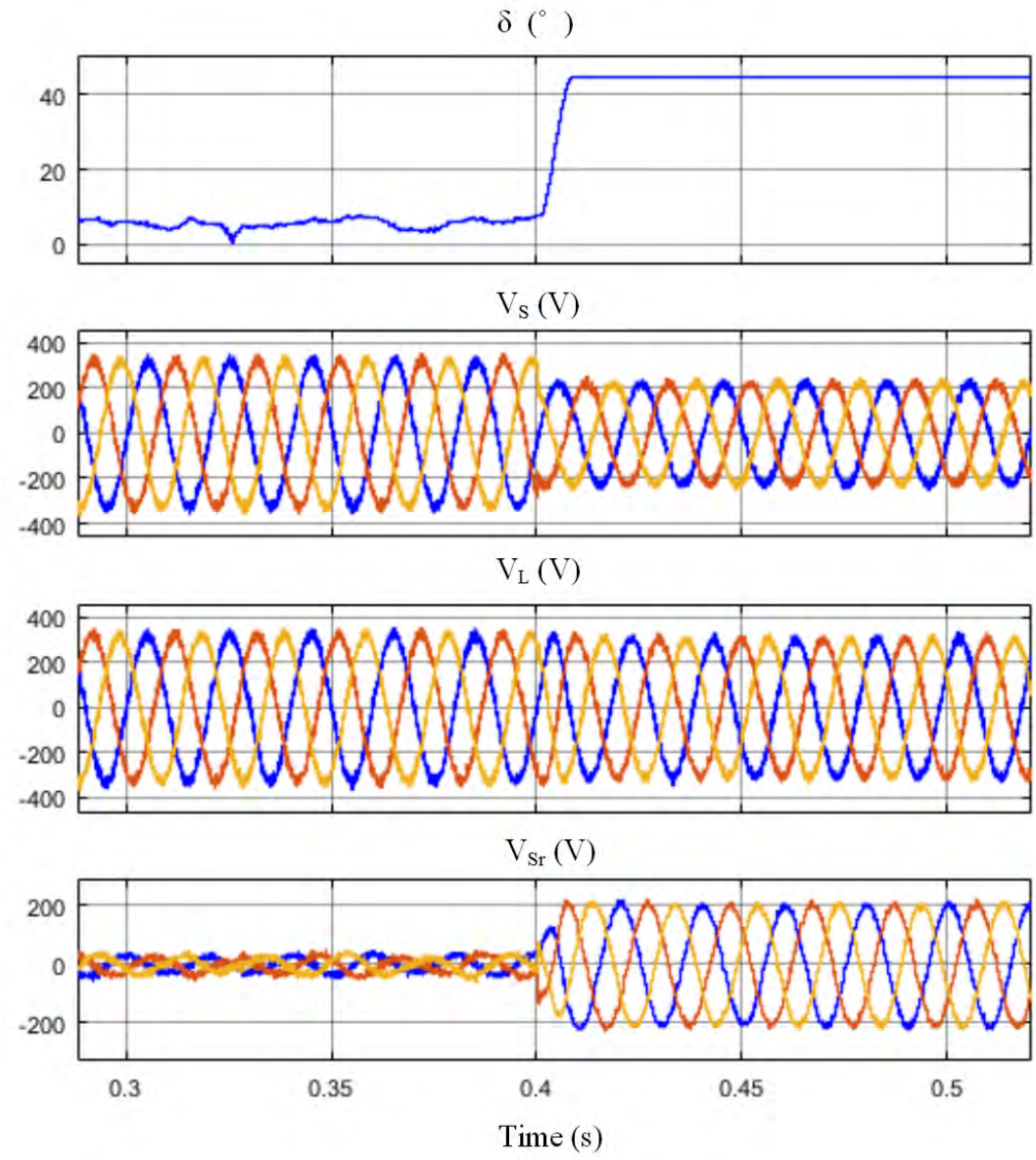

Figure 6.7: Voltage compensation waveforms for UPQC-Q (30% sag).

6.5 Summary

The design and performance of all three different control strategies of three phase UPQC have been analyzed under various operating conditions. The control strategies are mathematically formulated and simulated in the MATLAB/Simulink environment. It is observed that UPQC-Q able to mitigate harmonic components between the source voltage and the load with minimal consumption of power. The

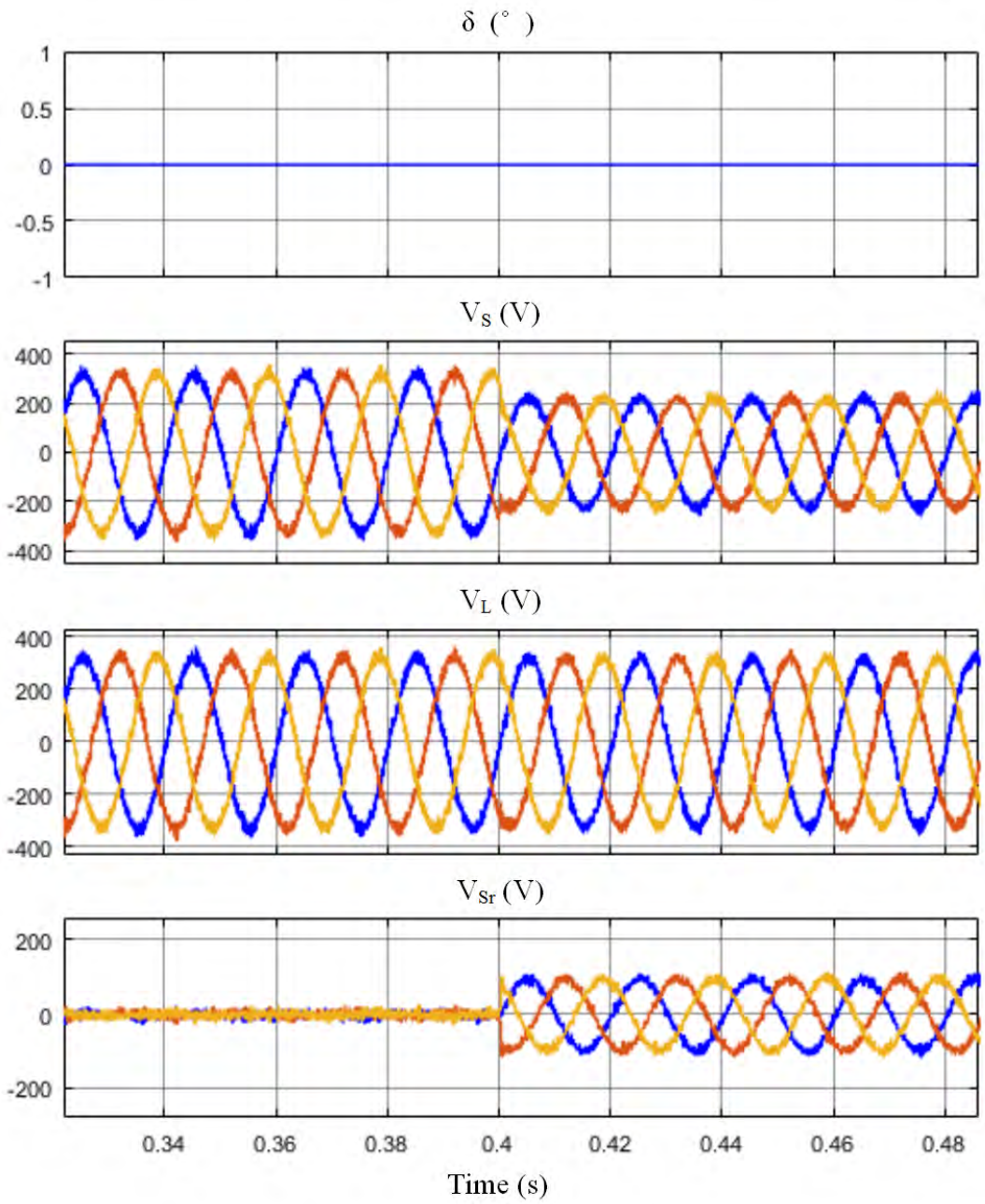

Figure 6.8: Voltage compensation waveforms for UPQC-P (30% sag).

overall losses of combined series inverter and shunt inverter of UPQC-P is found out to be 2.04% which more than UPQC-S (1.90%) and UPQC-Q (1.80%). The minimum losses occurred during overall compensation for various loads confirm the good performance of UPQC-Q with minimal consumption of active power and improved power angle. Nevertheless, the evaluated result also shows the incapability of

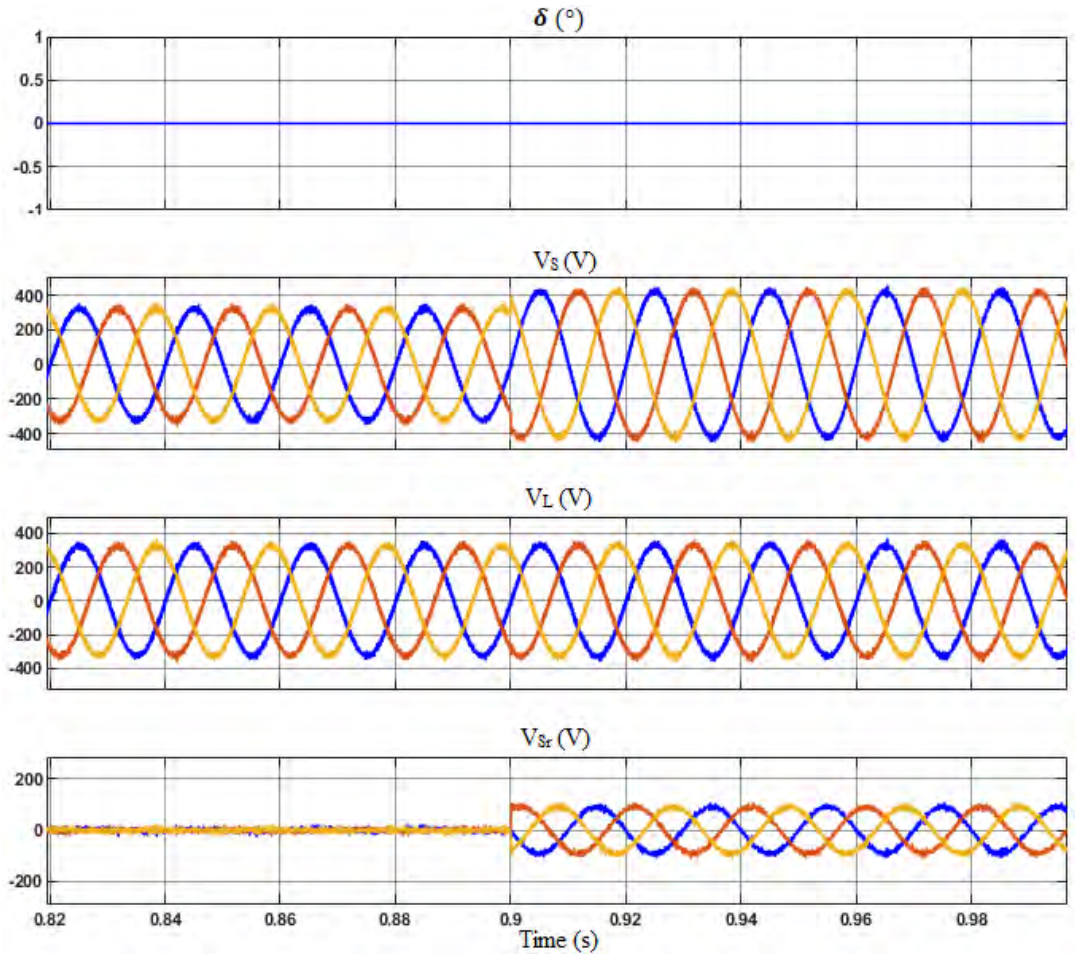

Figure 6.9: Voltage compensation waveforms for UPQC-P (30% swell).

UPQC-Q in case of voltage swell compensation.

Bibliography

[1] V. Khadkikar, "Enhancing electric power quality using UPQC: A comprehensive overview," *IEEE Transactions on Power Electronics*, vol. 27, no. 5, pp. 2284–2297, 2012.

[2] B. Singh, A. Chandra, and K. Al-Haddad, *Power quality: problems and mitigation techniques*. John Wiley & Sons, 2014.

[3] R. Rajasree and S. Premalatha, "Unified power quality conditioner UPQC control using feed forward FF/ feed back FB controller," in *2011 International Conference on Computer, Communication and Electrical Technology (ICCCET)*,

2011, pp. 364–369.

[4] V. Khadkikar, A. Chandra, A. Barry, and T. Nguyen, "Power quality enhancement utilising single-phase unified power quality conditioner: digital signal processor-based experimental validation," *IET Power Electronics*, vol. 4, no. 3, pp. 323–331, 2011.

[5] T. Zhili and Z. Dongjiao, "Design of DC voltage controller for UPQC by using its small signal model," in *2010 International Conference on Electrical and Control Engineering*, 2010, pp. 3572–3575.

[6] W. C. Lee, D. M. Lee, and T. K. Lee, "New control scheme for a unified power-quality compensator-Q with minimum active power injection," *IEEE Transactions on Power Delivery*, vol. 25, no. 2, pp. 1068–1076, 2010.

[7] V. Khadkikar and A. Chandra, "A novel control approach for unified power quality conditioner Q without active power injection for voltage sag compensation," in *2006 IEEE International Conference on Industrial Technology*. IEEE, 2006, pp. 779–784.

[8] A. Patel, H. D. Mathur, and S. Bhanot, "Enhancing VA sharing between the shunt and series APFs of UPQC with a modified SRF-PAC method," *IET Power Electronics*, vol. 13, pp. 275–285, 2020.

[9] V. Khadkikar, P. Agarwal, A. Chandra, A. Barry, and T. Nguyen, "A simple new control technique for unified power quality conditioner (UPQC)," in *Proc. 11th IEEE International Conference on Harmonics and Quality of Power*, 2004, pp. 289–293.

[10] S. Bhattacharya and D. Divan, "Synchronous frame based controller implementation for a hybrid series active filter system," in *IAS'95. Conference Record of the 1995 IEEE Industry Applications Conference Thirtieth IAS Annual Meeting*, vol. 3. IEEE, 1995, pp. 2531–2540.

[11] V. Khadkikar and A. Chandra, "UPQC-S: A novel concept of simultaneous voltage sag/swell and load reactive power compensations utilizing series inverter of UPQC," *IEEE Transactions on Power Electronics*, vol. 26, pp. 2414–2425, 2011.

[12] V. Khadkikar and A. Chandra, "A novel structure for three-phase four-wire distribution system utilizing unified power quality conditioner (UPQC)," *IEEE Transactions on Industry Applications*, vol. 45, no. 5, pp. 1897–1902, 2009.

Chapter 7

Examining the Power Losses of UPQC and UPQC-DG: A Comparative Study

7.1 Preamble

Power quality (PQ) is now becoming fundamental need of modern power distribution network at different level of usages in both industrial and commercial sectors including domestic area. However, due to the rigorous advancement of power electronics devices and increased non-linear loads in recent decades worldwide, power industries are facing a lot of uncommon power quality problems leading to equipment failures and production losses which is further leading towards financial losses to the nation's economy.

In order to mitigate PQ issues such as poor power factor operation due to uncontrolled reactive power, voltage sag, voltage swell, voltage and current harmonics and to further enhance sinusoidal distribution network system, numerous custom devices have been developed, such as static compensators (STATCOMs), dynamic voltage restorers (DVRs) that can minimize the effect of different PQ problems, however UPQC emerges to be a complete solution for the compensation of power quality problem [1].

For any power electronics based devices, a good algorithm design is required for overall system efficacy. To control these above compensating custom devices, various algorithms/control schemes have been developed. Synchronous reference frame theory (SRF) [2], unit vector template generation (UTVG) technique [3], power angle control (PAC) method [4, 5], model predictive control (MPC) [6] and artificial neural network (ANN) [7] are among the popular control strategies that are available in literatures.

The configuration of UPQC allows the compensation of current and voltage by shunt APF and series APF respectively [8]. The shunt APF acts as a current source, reducing current- related issues like unbalanced current, low power factor (reactive current) and voltage regulation problems. Series APF eliminates voltage-related issues like sag and swell. It is used to revive the grid voltage by injecting a suitable voltage of a specified magnitude through an injection transformer. In UPQC-DG configuration, distributed generation (solar, wind etc) is also connected at the DC-link as an alternate source. Because the shunt APF inverter and grid-interactive inverter have comparable configurations, this architecture avoids the solar inverter's added cost [9]. Due to presence of DG, compensation of voltage interruption with UPQC-DG becomes easier. The current injected by DG helps in the voltage regulation of the DC-link [10] and improves the compensation performance of UPQC. UPQC-DG is also helpful in microgrid operation in both grid-connected and islanded modes [11, 12]. The combination of UPQC and DG has the ability to export reactive power support to the grid [13]. In most of the works available, DG has been chosen as a renewable source because of environmental concerns, and solar PV is the most commonly used DG for UPQC-DG configuration. Since PV array output varies due to many environmental factors such as temperature, irradiation, dust etc. which leads to poor efficiency. To overcome the situation, maximum power point tracking (MPPT) is used. Perturb & observe (P&O) method [14], [15] and incremental conductance (IC) methods [16] are the most common types of MPPT methods used now a days. As compared to conventional UPQC, the PV connected UPQC has numerous benefits, such as:

- Improved power quality compensation due to better DC-link regulation.
- Elimination of costly grid-tied inverter required for DG.
- Ability to compensate for supply voltage interruptions.
- Centralized and economical control of series APF, shunt APF and DG converter.
- Encourages clean energy generation.

In spite of above advantages, UPQC-DG suffers from increased power losses and its quantification is required to be evaluated for its overall performance. Power losses of UPQC have been studied for different control techniques in [5] and a preliminary

study on losses of UPQC-DG is presented in [17]. Functionalities and the performance analysis of UPQC & UPQC-DG have been discussed in many literatures, however, quantified evaluation of their power losses including switch modeling and switching losses are missing. It is therefore required for evaluating the utility of UPQC-DG as single solution for compensating power quality issues and integrating distributed generation simultaneously.

The comparison of power losses presented in [17] for UPQC and UPQC-DG configurations are not much appropriate and fair since PV is not considered in UPQC while comparison. To ensure a fair and justified comparison, UPQC with independent DG (UPQC-IDG) is executed in this work for comparison with UPQC-DG. With an insightful review of available literatures at very fundamental level, all the simulations and validations have been performed with updated parameters. The sole difference between UPQC-DG and the newly executed UPQC-IDG configuration in this work is that for UPQC-IDG, DG is not directly connected to the UPQC power circuit via DC-link as in case of UPGC-DG, rather it is connected to the distribution network randomly using a grid-interactive inverter.

In this chapter, an attempt have been made to present the comparison of conventional UPQC, UPQC with distributed generation (UPQC-DG) and UPQC with independent DG (UPQC-IDG) in terms of their respective power losses. The power losses have been found for different operating conditions such as steady-state, voltage sag, swell, change in irradiation and change in load. The loads are considered as a mix of linear and non-linear loads. The losses are also computed for the power angle control technique in the case of UPQC-DG. All the configurations have been simulated in MATLAB/Simulink and real-time simulation separately using Opal-RT and their power loss comparisons have been investigated in a detailed manner and further concluded for selecting the best possible configuration to be used in practical applications based on requirements and economical viability.

The chapters are organized in following subsequent manner: Following the introduction part, circuit architecture, configurations of UPQC, UPQC-DG & UPQC-IDG and control of SRF-PAC are discussed in section 7.2. Section 7.3 illustrates the details of power loss calculations. Power loss comparisons using Matlab/Simulink results discussed in section 7.4. Section 7.5 presents the power loss comparison in real-time simulation using Opal-RT. The chapter is finalized by concluding the discussions and results in section 7.6.

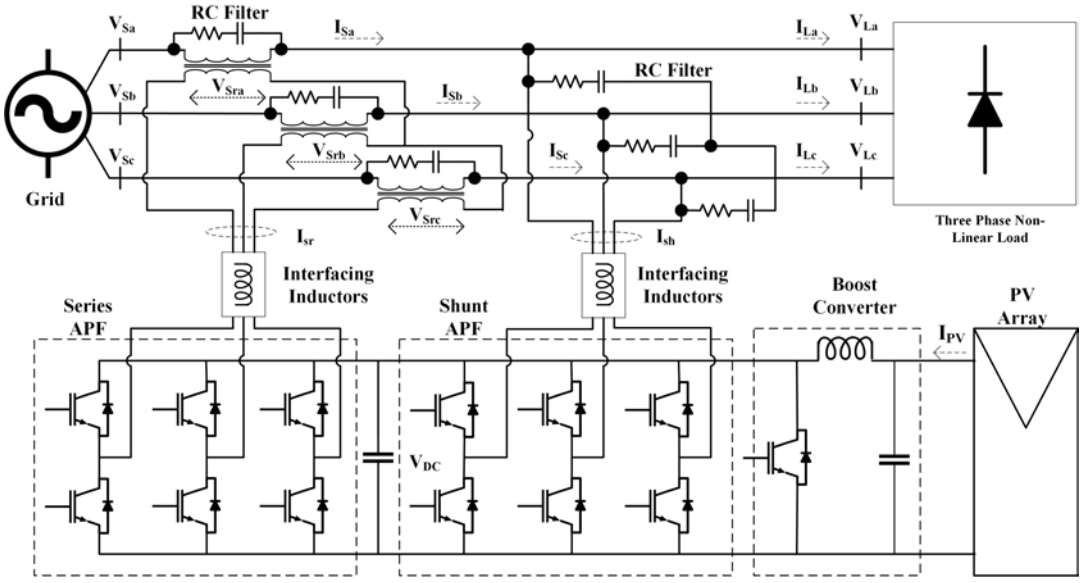

Figure 7.1: Configuration of UPQC-DG with PV array and Boost Converter.

7.2 Configuration and Control

Since majority of AC power is handled using a three-phase system, the three-phase three wire category of UPQC is used for the investigation. The power circuitry of UPQC-DG is shown in Fig. 7.1. The configuration and control schemes of UPQC, UPQC-DG and UPQC-IDG are discussed here below;

7.2.1 UPQC

In this configuration, the shunt APF (DSTATCOM) is connected across the load side to tackle the current associated problems and the series APF (DVR) is connected on the source side to address voltage associated problems. Shunt APF and series APF are three-leg voltage source inverters with six switching devices. A constant voltage across DC-link is required for both APFs to perform their designated tasks. DC-link voltage is selected to be more than twice of the peak AC system voltage [1] in order to have distortion free compensation by shunt compensator. The primary function of shunt APF is to regulate the voltage of the DC-link at a fixed value.

The voltage is injected by DVR using three single-phase transformers to maintain the load voltage at the desired level. It injects the required voltage in series with the supply voltage during the occurrence of sag/swell condition as shown in the phaser

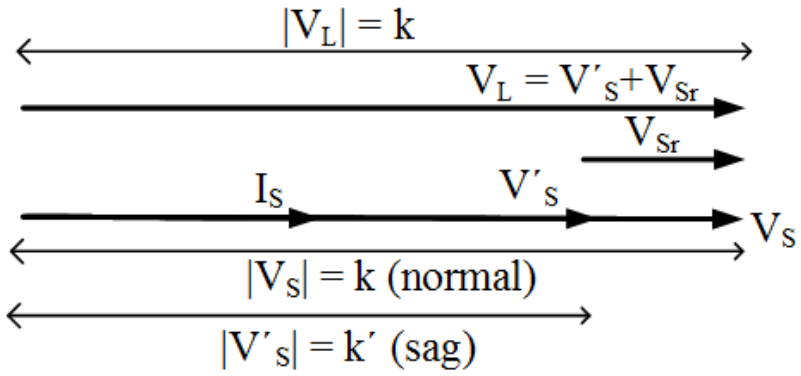

Figure 7.2: Phasor representation of a UPQC during sag.

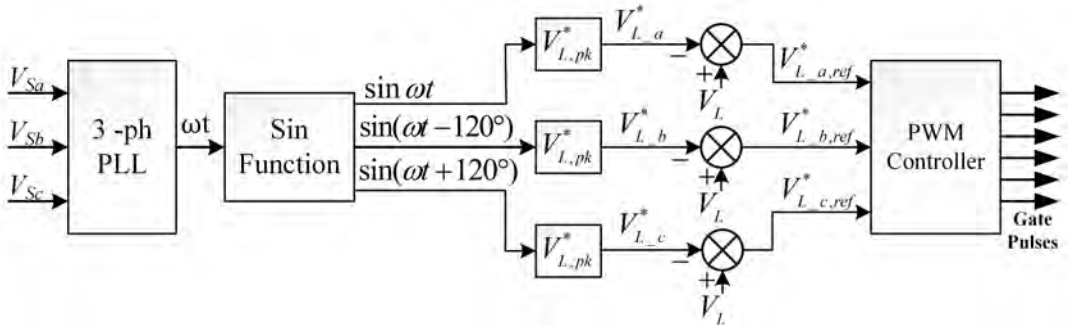

Figure 7.3: Series APF controller.

diagram of UPQC in sag condition (Fig. 7.2). The ripple filter is used in the circuit model to filter out the unwanted component in the injected voltage.

The DVR is controlled using the unit vector template generation technique (UVTG), which is a simple control algorithm that does not need a PI controller to generate the reference signal. In this method, three-phase PLL is used to generate a three-phase unit vector, which is subsequently multiplied with fundamental peak amplitude load voltage ($v^*_{La,pk}, v^*_{Lb,pk}, v^*_{Lc,pk}$) to give an ideal sinusoidal voltage with fixed amplitude [18] can be obtained as:

$$\begin{bmatrix} v^*_{La} \\ v^*_{Lb} \\ v^*_{Lc} \end{bmatrix} = \begin{bmatrix} v^*_{La,pk}(sin\omega t) \\ v^*_{La,pk}(sin(\omega t - 120°)) \\ v^*_{La,pk}(sin(\omega t + 120°)) \end{bmatrix} \tag{7.1}$$

Afterwards, the generated load voltages (Eq. 7.1) are compared with measured load voltage (V_{La}, V_{Lb}, V_{Lc}) to give a reference load voltage signal ($v^*_{La,ref}, v^*_{Lb,ref}, v^*_{Lc,ref}$) for the PWM controller, as shown in Fig. 7.3.

To control shunt APF as depicted in Fig. 7.4, a time-domain control technique called SRF technique is used to determine the reference signals. In this control technique, the instantaneous value of load current is converted to a *DQ* domain using Park's transformation, as shown in Eq. (7.2).

$$\begin{bmatrix} i_{Ld} \\ i_{Lq} \\ i_{Lo} \end{bmatrix} = \frac{2}{3} \begin{bmatrix} sin\theta & sin(\theta - \frac{2\pi}{3}) & sin(\theta + \frac{2\pi}{3}) \\ cos\theta & cos(\theta - \frac{2\pi}{3}) & cos(\theta - \frac{2\pi}{3}) \\ \frac{1}{2} & \frac{1}{2} & \frac{1}{2} \end{bmatrix} \begin{bmatrix} i_{La} \\ i_{Lb} \\ i_{Lc} \end{bmatrix} \tag{7.2}$$

The transformation technique is frequency synchronized with source voltage by using three-phase PLL to get the angular position of the *DQ* rotating reference frame. The average value of $I_{Ld,av}$ is accomplished using LPF to achieve a positive sequence component of load voltage current. A PI controller is used for regulating the DC-link voltage. The output of the DC-link voltage controller (I_{dc}) is summed with the d-axis value of load current ($I_{Ld,av}$) and transformed back to three-phase frame (abc) with the assumption of other components (q-axis component and zero axis component) being zero [18]. It can be noted that I_{Ld} is the load active power component and is in the phase with load voltage (V_L) whereas, I_{Lq} is the load reactive power component which is out of phase with load current (I_L). The resulting reference shunt current ($I^*_{Sha}, I^*_{Shb}, I^*_{Shc}$) is obtained by subtracting load current from their respective positive sequence reference current obtained from inverse park's transformation.

7.2.2 UPQC-DG

In this configuration PV array is interfaced with DC link using DC-DC boost converter as shown in Fig. 7.1. The series APF is connected towards the source and the shunt APF is connected across the load. It is expected to improve the performance of the UPQC because UPQC can compensate for power interruptions using the power supplied by PV array and its DC-link response improves because of feed forward gain. It also reduces the burden on main grid by supplying power from PV without any need for an additional grid-tied converter. So, it mainly consists of three primary functional converters (i) DVR (ii) DSTATCOM and (iii) DC-DC boost converter.

The active power from the PV array is fed to the grid using shunt APF. The only difference between the shunt controller of UPQC and UPQC-DG is that in the case of UPQC-DG, PV current (I_{pv}) is subtracted from net load current ($I_{Ld} + I_{dc}$) [10] as

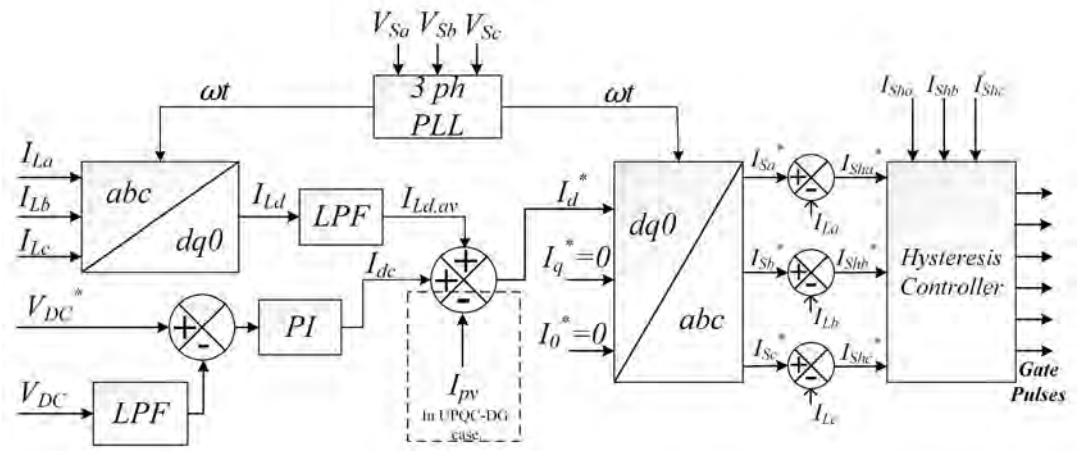

Figure 7.4: Shunt APF controller.

shown in Fig. 7.4. The d-axis component of the load current can be obtained from the Eq. (7.3).

$$I_d^* = I_{Ld} + I_{dc} - I_{pv} \tag{7.3}$$

A similar but enhanced technique called SRF-PAC [19] which aims to effectively utilise series and shunt APF by sharing the load reactive power burden between the two inverters is implemented to demonstrate the applicability and hence compare the losses with non SRF-PAC control approach. In this approach, the load voltage phase differs from source voltage by an angle called power angle. This enables the series APF controller to provide reactive power compensation along with the shunt APF controller [5]. The value of the power angle can be obtained as follows:

$$\delta = sin^{-1}(\frac{Q_{Sr}}{P_L - P_{PV}}) \tag{7.4}$$

where Q_{Sr} is series APF reactive power, P_L is load power and P_{PV} is PV power.

Boost converter acts as an interface between the DC-link and the PV array. It is controlled to extract the maximum power from PV using MPPT technique and to ramp up the voltage at the output terminal of PV as per the DC-link voltage. For the execution of MPPT, a simple method called Incremental conductance with an integral regulator [15] is used, as shown in Eq. (7.5).

$$\frac{dI}{dV} = \frac{-I}{V} \tag{7.5}$$

Boost converter is designed in such a way that output is nearly equal to the reference value of the DC-link controller. So that DC-link voltage and MPP voltage is ensured to be equal. Similarly, shunt APF is also designed in order to withstand the peak power output of the PV array.

7.2.3 UPQC-IDG

In this configuration, DG is connected separately using a grid tie inverter. Fig. 7.5 depicts the power circuit of UPQC-IDG. To step up the voltage at PV array output terminal, DC-DC boost converter is connected between the DC link of the inverter and the PV output. UPQC and the grid tie inverter are independent entities with their separate controls. To compensate current and voltage issues, the techniques of SRF and UVTG have been used. The SRF approach is used to create desirable gate pulses for the grid-tie inverter while controlling the independent DG.

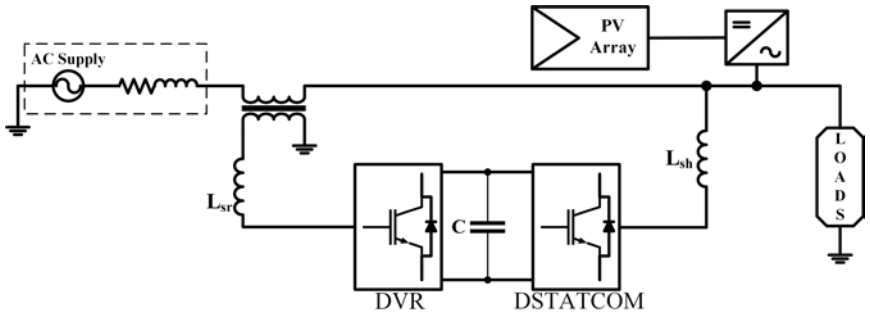

Figure 7.5: Power structure scheme of UPQC with separate PV.

Table 7.1: Switching Losses in DVR and DSTATCOM of UPQC and UPQC-DG/IDG Under Different Scenarios

Topology	Cases	DVR Losses (W)				DSTATCOM Losses (W)				IDG Inverter Losses (W)			
		IGBT		Diode		IGBT		Diode		IGBT		Diode	
		SW_L	FW_V_L	FW_D_L	FW_V_L	SW_L	FW_V_L	FW_D_L	FW_V_L	SW_L	FW_V_L	FW_D_L	FW_V_L
UPQC	**Sag**	241.68	100.04	238.07	150.06	126.58	52.40	172.30	78.60	-	-	-	-
	Swell	175.39	72.60	202.81	108.90	104.40	43.22	156.47	64.82	-	-	-	-
	SS-FL	174.34	72.17	202.21	108.25	96.57	39.97	150.49	59.96	-	-	-	-
	SS-PL	178.00	73.68	204.31	110.52	96.05	96.05	150.08	59.64	-	-	-	-
	Overall	255.78	105.88	244.92	158.82	176.43	73.03	203.41	109.55	-	-	-	-
UPQC -DG	**Sag**	135.20	55.96	178.06	83.95	115.88	47.97	164.85	71.95	-	-	-	-
	Swell	115.36	47.75	164.48	71.63	117.45	48.62	165.96	72.93	-	-	-	-
	CH-IR	138.85	57.48	180.45	86.21	103.35	42.78	155.69	64.17	-	-	-	-
	SS-FL	109.10	45.16	159.95	67.74	109.62	45.38	160.34	68.06	-	-	-	-
	SS-PL	109.62	45.38	160.34	68.06	109.10	45.16	159.95	67.74	-	-	-	-
	Overall	213.49	88.38	223.76	132.56	171.21	70.87	200.38	106.31	-	-	-	-
UPQC- with separate PV	**Sag**	334.07	138.29	279.91	207.43	161.82	66.98	194.81	100.48	146.16	60.50	185.14	90.75
	Swell	186.35	77.14	209.05	115.71	99.70	41.27	152.91	61.91	135.72	56.18	178.41	84.27
	CH-IR	254.21	105.23	244.17	157.84	95	39.33	149.26	58.99	148.25	61.37	186.46	92.05
	SS-FL	318.41	131.81	273.27	197.71	183.74	76.06	207.58	114.09	153.99	63.74	190.03	95.61
	SS-PL	250.56	103.72	242.41	155.57	99.18	41.05	152.51	61.58	146.16	60.50	185.14	90.75
	Overall	373.22	154.49	295.85	231.74	180.09	74.55	205.51	111.82	153.99	63.74	190.03	95.61

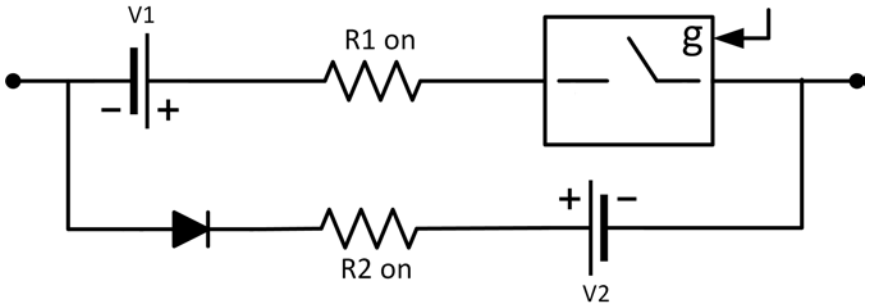

Figure 7.6: IGBT switch model.

7.3 Power Loss Calculation

The three-phase three-wire UPQC consists of two voltage source inverters made up of 12 active switches. In the case of UPQC-DG, one additional active switch of boost converter is included. However, in the special case of UPQC-IDG, three inverters are involved along with one boost converter.

The flow of current through the device and the voltage drop across its terminal generates conduction losses. The on-state resistance of semiconductor switches and the equivalent series resistor (ESR) of passive element are also an important factor contributing the conduction losses. The duty cycle has also a direct relationship with these losses. Apart from conduction losses, switching losses are another significant component of losses. The power loss calculation incorporates the dynamical behaviour of IGBTs and their freewheeling diode and the boost converter diode. The IGBT switch model considered for simulation is shown in Fig. 7.6 including on-state resistance, switch's forward voltage drop and anti-parallel diode. So the total power losses of UPQC and UPQC-DG/IDG are inclusive of;

- Conduction losses of power electronics switches including anti-parallel diodes.
- Switching losses of power electronics switches and anti-parallel diodes.
- On-state power losses of switches caused by forward voltage drop.
- Power losses of RC filtering elements.

Of the above mentioned power losses, except switching losses, all other losses are found using simulations. Switching losses are computed using the empirical approach with the help of voltage and current values obtained from the simulation.

To get the detailed performance analysis, the simulated power model are made more practical by adopting the actual numerical values of forward voltage and forward diode voltage of IGBT from the datasheet of SEMIKRON inverter stack type no. MD B6U 415/560-45F (IGBT V_f = 0.8 V IGBT V_{fd} = 1.2 V). The IGBT module type is SKM 75GB12T4. The formula to measure the switching energy dissipation of IGBT [20] is expressed as follows:

$$E_{sw} = E_{swref} . \left(\frac{I}{I_{ref}}\right)^{Ki} . \left(\frac{V_{cc}}{V_{CCref}}\right)^{Kv} .(1 + TC_{sw}(T_j - T_{jref})) \tag{7.6}$$

where

Ki: Exponent of current dependency

Kv: Exponent of voltage dependency

TC_{sw} : Temperature coefficient of switching losses

However, the switching energy of IGBT (E_{sw}) is dependent upon the turn-on (E_{on}), and turn-off energy dissipation (E_{off}) is given as;

$$E_{sw} = E_{on} + E_{off} \tag{7.7}$$

According to IEC 60747-9 standard, the expression for turn-on energy dissipation can be written as;

$$E_{on} = \int_{t_2}^{t_1} p_v(t)dt = \int_{t_2}^{t_1} v_{CE}(t) * i_c dt \tag{7.8}$$

The upper and lower integral limits are between 10% of $V_G(on)(t_1)$ and 2% of V_{CC} (t_2). The expression for E_{off} with integral limits of 90% of $V_G(on)(t_3)$ and 2% of I_C (t_4) can be defined as;

$$E_{off} = \int_{t_4}^{t_3} p_v(t)dt = \int_{t_4}^{t_3} v_{CE}(t) * i_c dt \tag{7.9}$$

The formula for energy dissipation in freewheeling diode, E_{rr} can be written as;

$$E_{rr} = \int_{t_6}^{t_5} p_v(t)dt = \int_{t_6}^{t_5} v_{CE}(t) * i_c dt \tag{7.10}$$

where t_5 is zero crossing of diode reverse current and t_6 is the 2% of decreasing diode current.

The energy loss dissipation for the combined six switches of DVR and DSTATCOM are highlighted in Table 7.1 for the UPQC and UPQC-DG/IDG. It is observed

Table 7.2: Switching Losses in DC-DC Boost Converter of UPQC-DG/IDG Under Different Scenarios

Topology	Cases	DC-DC Boost Converter Losses (W)					
		IGBT				Diode	
		SW_L	FW_V_L	FW_D_L	FW_V_L	FW_D_L	FW_V_L
UPQC -DG	Sag	149.81	10.34	187.44	15.50	184.48	15.02
	Swell	143.55	9.90	183.48	14.86	180.62	14.40
	CH-IR	143.50	9.90	183.45	14.85	180.11	14.32
	SS-FL	173.82	11.99	201.90	17.99	197.92	17.29
	SS-PL	173.82	11.99	201.90	17.99	197.61	17.23
	Overall	164.95	11.38	196.68	17.07	193.07	16.45
UPQC- with separate PV	Sag	172.26	11.88	200.99	17.83	200.08	17.66
	Swell	164.95	11.38	196.68	17.07	192.91	16.42
	CH-IR	105.44	7.27	157.25	10.91	152.91	10.32
	SS-FL	96.57	6.66	150.49	9.99	148.44	9.72
	SS-PL	96.57	6.66	150.49	9.99	148.44	9.72
	Overall	173.30	11.96	201.60	17.93	197.61	17.23

that the energy loss dissipation is more in DVR inverter switches if compared to DSTATCOM switches. Similarly, switching losses in boost converter of UPQC-DG/IDG is tabulated in Table 7.2. The switching losses are computed from switching energy dissipation by Eq. (7.6):

$$P_{sw} = E_{sw} * f_{sw} \tag{7.11}$$

where, f_{sw} is switching frequency.

7.4 MATLAB Simulation Results and Discussion

The steady-state and dynamical performances of UPQC, UPQC-DG and UPQC-IDG are simulated in MATLAB/Simulink environment. The optimized parameter for the power circuit shown in Fig. 7.1 is designed using the method given in [1] and [11] are detailed in Table 7.3. Basically, three types of loads are considered for the proposed system. Load-1 is a three-phase uncontrolled rectifier, Load-2 & Load-3 are the combinations of resistive and inductive load with specific values. A three-phase source 415 V, 50 Hz is selected with R_s & L_s as source impedance. Two inductors

Table 7.3: System Parameters

Source	Voltage and Frequency	415 V, 50 Hz
	Impedance	R_s =0.05 Ω, L_S = 0.5 mH
DC link	Capacitor	C_{DC} = 5500 μF
	Reference DC Voltage	700 V
Shunt APF	Interfacing Inductor	1.22 mH/ph
	Ripple Filter	R =5.07 Ω/ph
		C =20.7 μF/ph
Series APF	Interfacing Inductor	4.84 mH/ph
	Ripple Filter	R =2.79 Ω/ph
		C =72 μF/ph
	Injection Transformer	2.5 kVA
Solar PV Array	Maximum Power	15.3 kW
	Voltage at MPP	547 V
	Current at MPP	28.8 A

L_{sh} and L_{sr} are used as interfacing inductors for shunt APF & series APF, and the third inductor is used for the boost converter.

7.4.1 Comparison between UPQC and UPQC-DG

The steady-state and various dynamical conditions are imposed on the systems to investigate and analyze the power losses in different conditions. Those conditions are categorized as 25% voltage sag, 25% voltage swell, steady-state mode with a full load, steady-state mode with partial load and change in irradiation up to 40%. The complete summarized value of conduction losses obtained from the two systems subjected to different conditions are compared in Table 7.4. The conduction losses of all the topologies are computed independently using MATLAB simulation, while the switching losses are calculated separately from experimental formula provided in section 7.3. All these losses are summed up and categorized for different cases in Table 7.5.

7.4.1.1 Performance during dynamic situation

The dynamical performance of UPQC–DG during voltage sag is shown in Fig. 7.8. The voltage sag occurs at $t = 0.45s$, and it has been noticed that voltage is injected by DVR (V_sr) to maintain a constant load voltage magnitude. The source current (I_s) is increased to maintain power balance. A similar case can be observed in the UPQC

Table 7.4: Conduction Losses Associated with UPQC-DG and UPQC Under Different Scenarios

Case	Duration	P_L	UPQC-DG			UPQC	
	(s)	(kW)	P_s (W)	P_PV (W)	Losses (W)	P_s (W)	Losses (W)
Sag	0.45	29.53	15827	15196	1491	30689	1183
Swell	0.45	30.53	16724	15196	1393	31333	833
CH-IR	0.45	30.00	19056	12376	1423	-	-
SS-FL	0.45	40.06	11880	15196	1533	41178	1172
SS-PL	0.45	30.02	16256	15196	1422	30956	931
Overall	1.65	33.01	20848	14230	1489	34055	1046

waveform in Fig. 7.7. To compensate for voltage sag, the PI controller maintains a constant DC-link voltage. The DC-link voltage waveform (V_DC) on the other hand shows an abrupt transient change. The load current (I_load) is non-linear and reactive and it is corrected by UPQC-DG shunt APF which results in sinusoidal in-phase source current (I_s).

The performance of UPQC-DG during the change in irradiation is shown in Fig. 7.9. Solar irradiation changes from 1000 W/m^2 to 600 W/m^2, causing a reduction in PV power output (from 15kW to 12.3kW). The amplitude of DC-link voltage (V_DC) and load voltage (V_load) are maintained at the desired level. A total power loss of 9.33% is observed when both inverter (shunt VSI and series VSI) of UPQC-DG and boost converter are in operation.

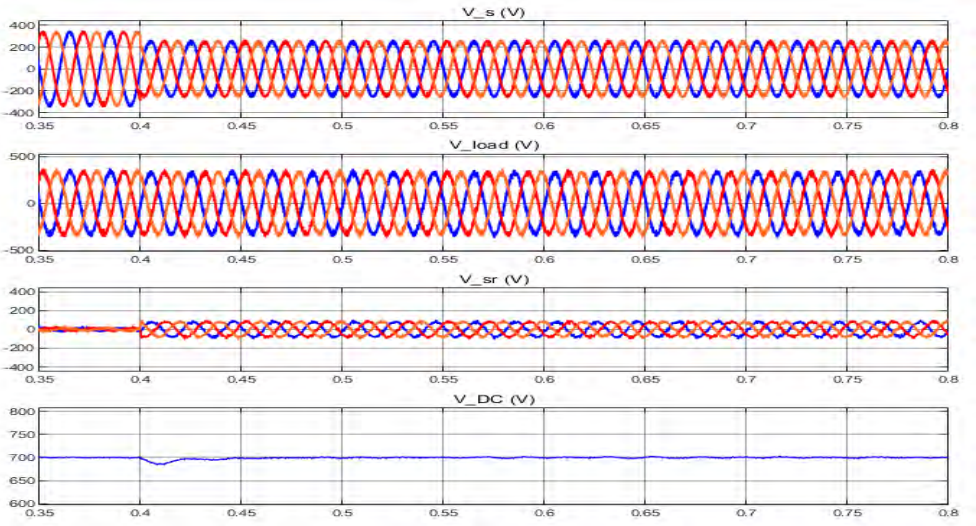

Figure 7.7: Waveform of UPQC during sag (25%).

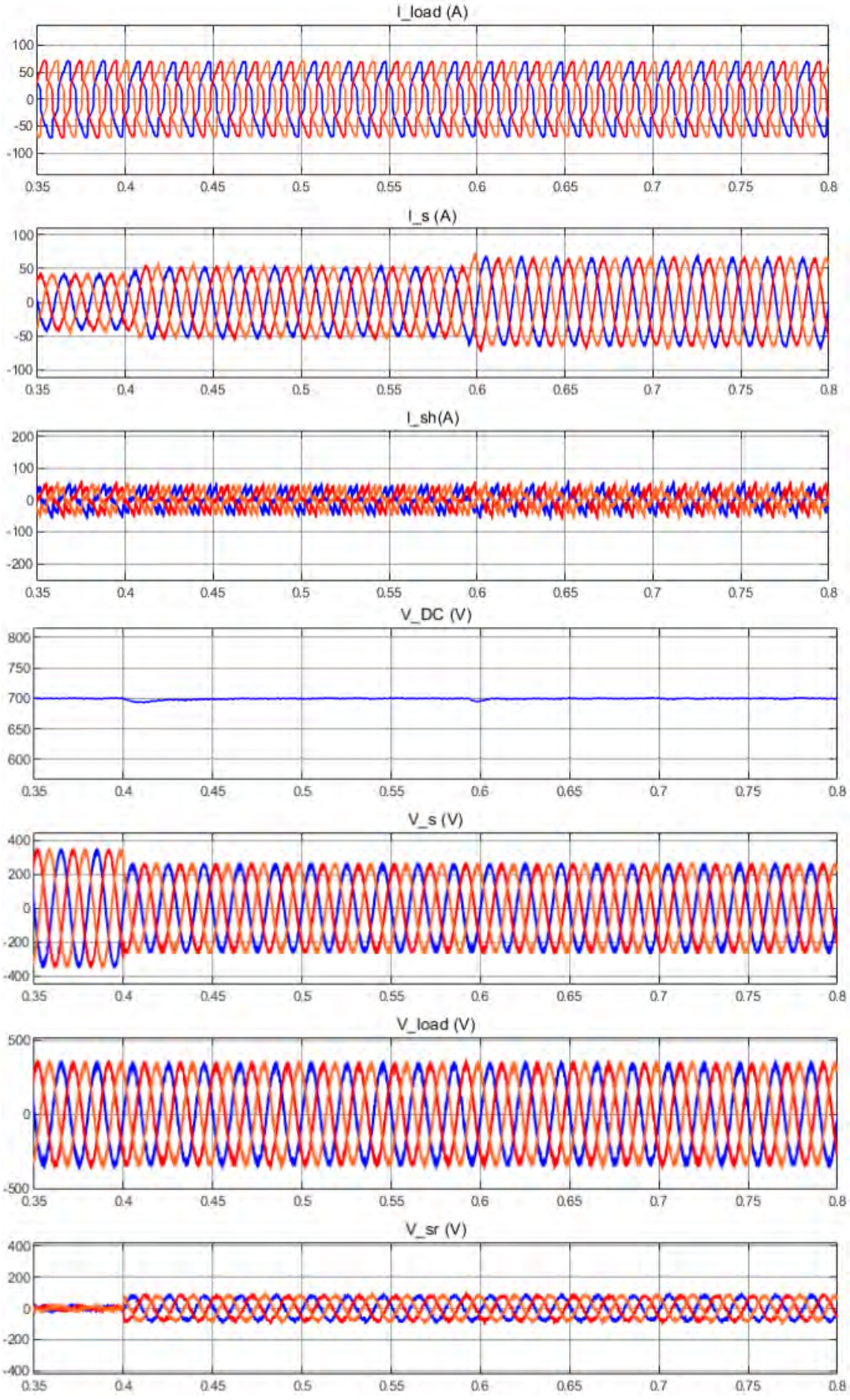

Figure 7.8: Waveform of UPQC-DG during voltage sag (25%).

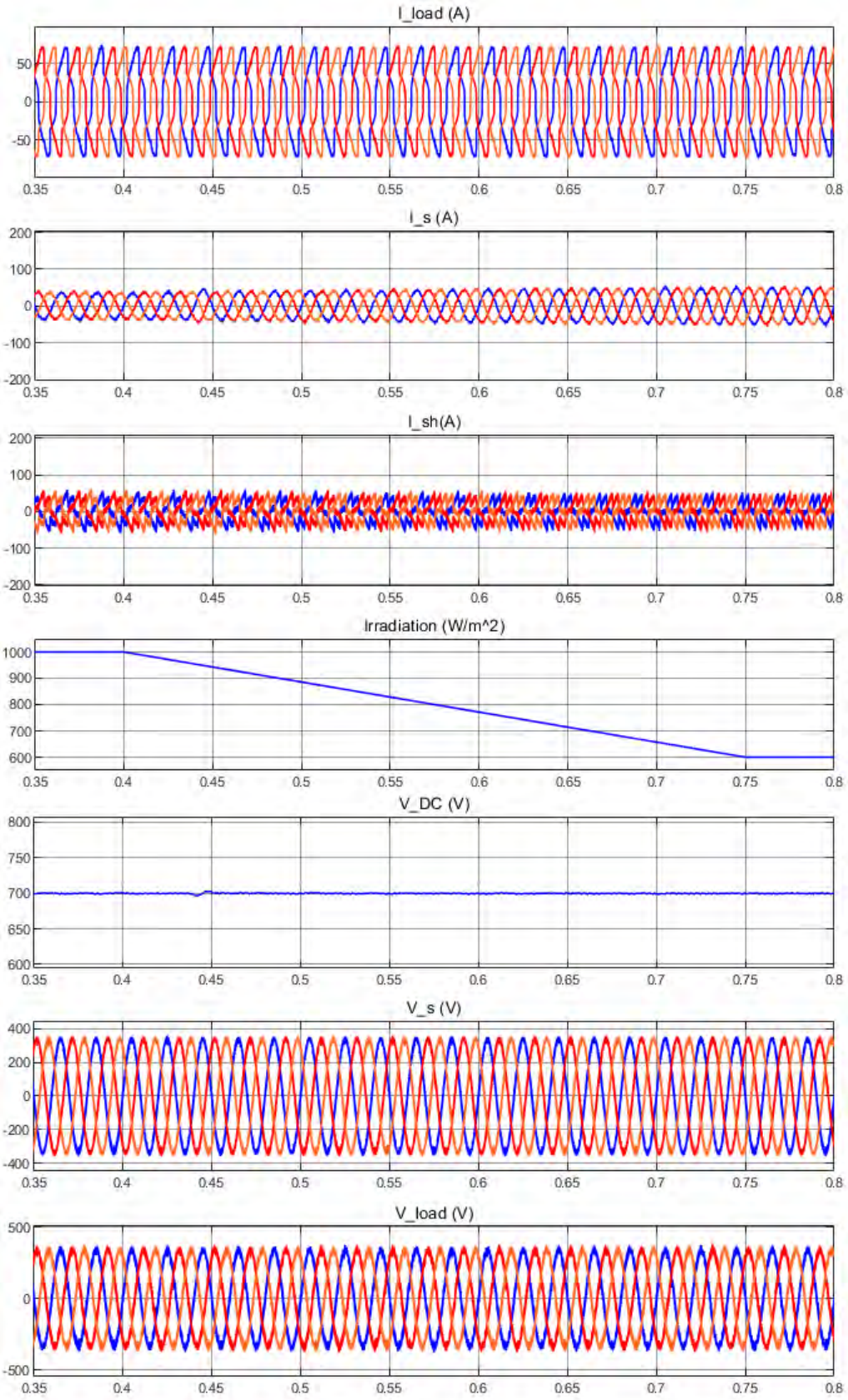

Figure 7.9: Waveform of UPQC-DG during change in PV irradiation (40%).

Table 7.5: Total Power Losses (Conduction Loss + Switching Loss)

Cases	UPQC			UPQC-DG			UPQC-IDG			UPQC	UPQC-DG	UPQC-IDG
	C_L (W)	SW_L (W)}	Total (W)	C_L (W)	SW_L (W)	Total (W)	C_L (W)	SW_L (W)	Total (W)	% Loss	% Loss	% Loss
Sag	1183	1160	2343	1491	1416	2908	2132	2587	4719	7.93	9.84	15.98
Swell	833	929	1762	1393	1351	2744	1963	1998	3961	5.77	8.99	12.97
CH-IR	-	-	-	1423	1375	2744	2027	2036	4063	-	9.33	13.54
SS-FL	1172	904	2076	1533	1386	2919	2324	2428	4752	5.18	7.29	11.86
SS-PL	931	968	1899	1422	1386	2808	2126	2011	4137	6.33	9.35	13.78
Overall	1046	1328	2374	1478	1807	3285	2238	2750	4988	7.19	9.95	15.11

7.4.1.2 Analysis of power losses and comparison

The conduction loss comparison of conventional UPQC and UPQC-DG is illustrated in Table 7.4. As per Table 7.5; Summarized total power (switching and conduction) losses under different cases are detailed as under;

- **Sag**: In the first condition, a sag of 25% is imposed on both the systems. The decreased source voltage (V_s) can be observed in Fig. 7.8. The power losses that occurred during voltage sag are much more significant than the other conditions imposed as the source current magnitude increases, raising the conduction and switching losses. Under this condition, a source power of 15.8 kW and 30.68 kW is observed in UPQC-DG and UPQC respectively. The total power loss obtained during the occurrence of voltage sag in UPQC-DG is 9.84% and in UPQC, it is 7.93%.

- **Swell**: Under this scenario, a voltage swell of 25% is subjected to the systems. As the magnitude of the source current decreases, the source power in UPQC and UPQC-DG rises to 31.33 kW and 16.72 kW respectively. The power loss is comparatively minimal due to reduced rms current in shunt and series inverter. In UPQC-DG, total power losses during voltage swell is 8.99%, while in UPQC, total power loss is 5.77%. In both the conditions, the shunt APF compensates for active/reactive power along with harmonic elimination of load current.

- **CH-IR**: In UPQG-DG, the variation in irradiation of the PV array is introduced. The variation occurred for the duration of 0.45 s. This causes a decrease in the PV power output, which leads to a decrease in the current fed to the grid. In the shunt APF, there is a dramatic drop in current causing a switching loss of 4.58% and conduction loss of 4.74%. A overall power loss of 9.33% is observed in this case.

- **SS-FL**: The performance of the system in steady-state with full load is evaluated for 0.45 s. It is observed that power delivered from the PV is nearly 15 kW. In this state, the system is not exposed to any dynamical constraints during simulation. The load power and source power are 40.06 kW and 11.88 kW respectively. During this condition, the total percentage power loss in UPQC-DG and UPQC are 7.29% and 5.18% respectively.

- **SS-PL**: When the system is subjected to steady state partial load, proportionally higher power losses are detected (UPQC-DG: 9.35% and UPQC: 6.33%) because the load power gets reduced.

- **Overall**: A combination of all the conditions mentioned above is imposed on both the systems. The time duration for this condition is set for 1.65 s with a reduction in irradiation of 40% employed on the system. The individual duration of simulation under overall scenario case considered as SS-FL (0.4 s) + Sag (0.2 s) + Swell (0.1 s) + SS-PL (0.85 s) + CH-IR (0.1 s). In terms of comparison, UPQC-DG has overall losses of 9.95% which is higher than traditional UPQC with having 7.19%, however the difference is considerable.

7.4.2 Comparison between UPQC-DG and UPQC-IDG

Power losses are compared between UPQC-DG and UPQC with PV integrated using an independent DG inverter (UPQC-IDG). Table 7.6 presents the conduction losses in UPQC-IDG for different operating conditions. It can be observed that UPQC-IDG has more conduction losses than UPQC-DG. The involvement of three inverters (shunt VSI, series VSI, and grid-tie inverter for separate PV) and one DC-DC boost converter is the main reason for the increased power dissipation in UPQC with independent PV. Indeed, having more converters results in increased power losses and tends to increase harmonics. On the occurrence of the sag, the rms current in the DVR switch and DSTATCOM switches is 64 A and 31 A respectively, if compared to the DVR and DSTATCOM switch of UPQC-DG having the current of 25.9 A & 22.2 A respectively. Furthermore, a substantial rms current of 71.5 A and 34.5 A in series and shunt inverters respectively caused by changes in sun irradiation. As a result, the switching losses in UPQC-IDG are higher than in UPQC-DG/UPQC (see Table 7.1 & Table 7.2). Another reason for higher power losses with UPQC-IDG is that maintaining the separate DC-link for the DG inverter requires more power, which raises the current. Furthermore, due to the issue of intermittency, the independent PV continuously distorts the grid voltage. Total percentage losses have been summarized in Table 7.5 for different cases discussed.

Table 7.6: Conduction Losses Associated with a UPQC-IDG Under Different Scenarios

Case	Duration	P_L	UPQC with separate PV		
		(kW)	P_s (W)	P_PV (W)	Losses (W)
Sag	0.45	29.48	17513	14107	2132
Swell	0.45	30.57	18436	14107	1963
CH-IR	0.45	30.02	20149	11896	2027
SS-FL	0.45	40.02	28244	14107	2324
SS-PL	0.45	30.04	18062	14107	2126
Overall	1.65	33.02	25000	10261	2238

7.5 Real Time Simulation Results and Discussion

The performances of UPQC-DG and UPQC are validated in real-time simulation in order to verify the power losses obtained in Table 7.5. The system has been implemented on high speed FPGA based computational engine of Opal-RT (OP-4510) (Fig. 7.10) to compare the losses in transient as well as in steady-state conditions with a time step of 15 µs. The parameters of real-time simulation is given in Appendix B. The DSO results are obtained from the analog output of the simulator. Table 7.7 presents the real time simulated power losses data of UPQC and UPQC-DG. The average power losses (W) are determined by taking the difference between load power (P_L) and source power (P_s) for UPQC, while power losses in UPQC-DG are evaluated by subtracting the load power (P_s) from the sum of source power (P_s) and PV power (P_{PV}).

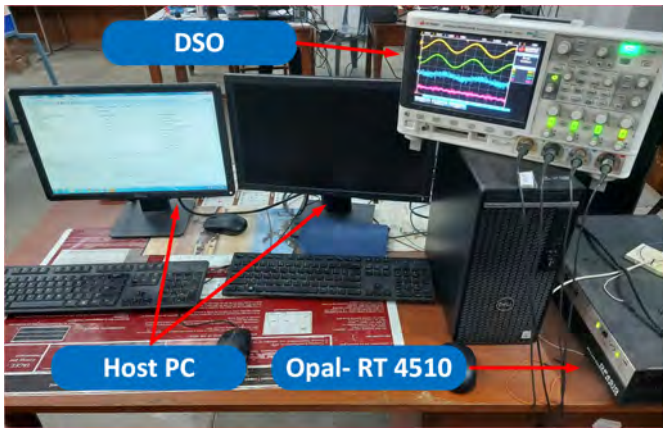

Figure 7.10: Real time simulator for validation.

Table 7.7: Real Time Simulated Power Losses of UPQC-DG and UPQC Under Different Scenarios

Cases	Duration	P_L	UPQC-DG			UPQC		UPQC-DG	UPQC
	(s)	(kW)	P_s (W)	P_PV (W)	Losses (W)	P_s (W)	Losses (W)	% Loss	% Loss
Sag	0.45	34.14	22735	14790	2238	36120	1041	6.79	2.96
Swell	0.45	37.34	24803	14798	2257	37974	632	6.04	1.69
CH-IR	0.45	36.23	26397	11998	2157	-	-	5.95	-
Overall	1.65	38.11	26232	14096	2212	38945	827	5.80	2.17

Four different scenarios are considered for computing the losses which are as follows: (1) 25% sag (2) 25% swell (3) change in irradiation (4) overall scenarios (combination of sag, swell, irradiation change and load change). Waveforms of real-time simulation under sag and swell conditions for UPQC-DG and UPQC are shown in Fig. 7.11. To compare the power loss dissipation with PAC and without PAC method in UPQC-DG (Fig. 7.12), the overall scenario is considered and the corresponding computed losses are recorded in Table 7.8.

7.5.1 Loss comparison between UPQC-DG and UPQC using real time simulation

Waveforms for a voltage sag of 25% for a duration of 0.45 s are shown in Fig. 7.11a & Fig. 7.11c. As observed, the load voltage (V_L) remains undisturbed with an increase in series APF voltage which is in phase with the voltage source (V_s). The DC-link voltage experiences an undershoot for a short duration which restores back in a short time. A power loss of 6.79% occurs in UPQC-DG and 2.96% in UPQC. On the occurrence of voltage swell, the DC-link voltage experiences an overshoot of 15V, as shown in Fig. 7.11b & Fig. 7.11d. The series APF starts compensating the load voltage by providing the opposite phase voltage. In voltage swell condition referring to Table 7.7, UPQC-DG has 6.04% power loss recorded if compared to 1.69% in UPQC. The sag condition generates more losses because of a sudden increase in the rms current of inverter switches.

In the case of varying irradiation, the active power fed to the grid from the PV source is reduced which causes an increase in the source current. Due to this, a power losses of 5.95% are observed in UPQC-DG. In this condition, the source power and power losses of UPQC remained zero as there is no PV connected. As seen in Table 7.7, for an overall scenario, UPQC-DG (5.80%) suffered significantly

more power losses than UPQC (2.17%). The computation confirms that UPQC-DG incurred greater power losses than UPQC.

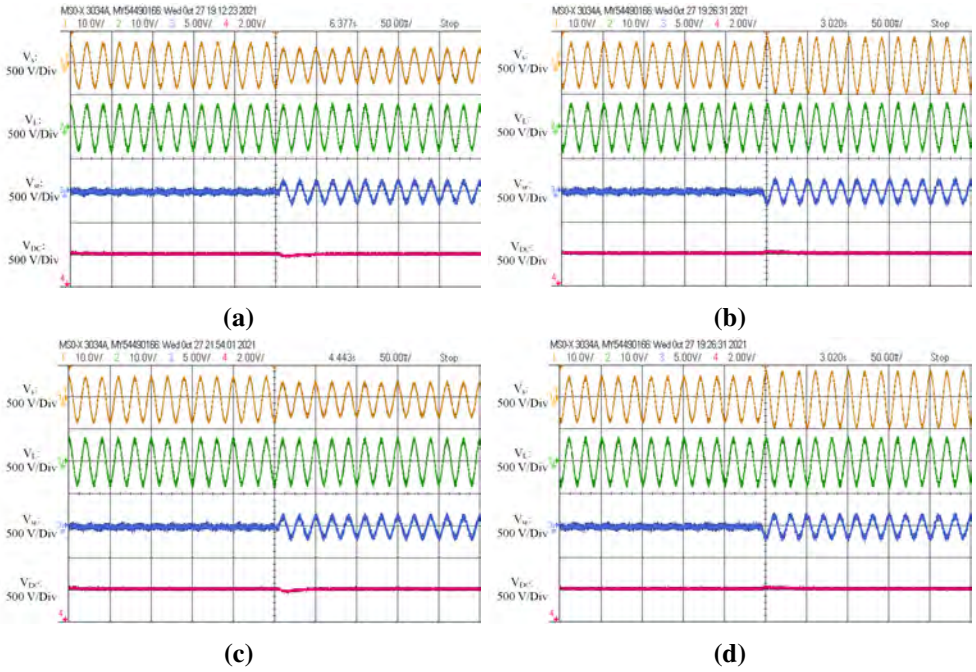

Figure 7.11: Real time simulation result of (a) UPQC-DG during sag of 25%. (b) UPQC-DG during swell of 25%. (c) UPQC during sag of 25%. (d) UPQC during swell of 25%.

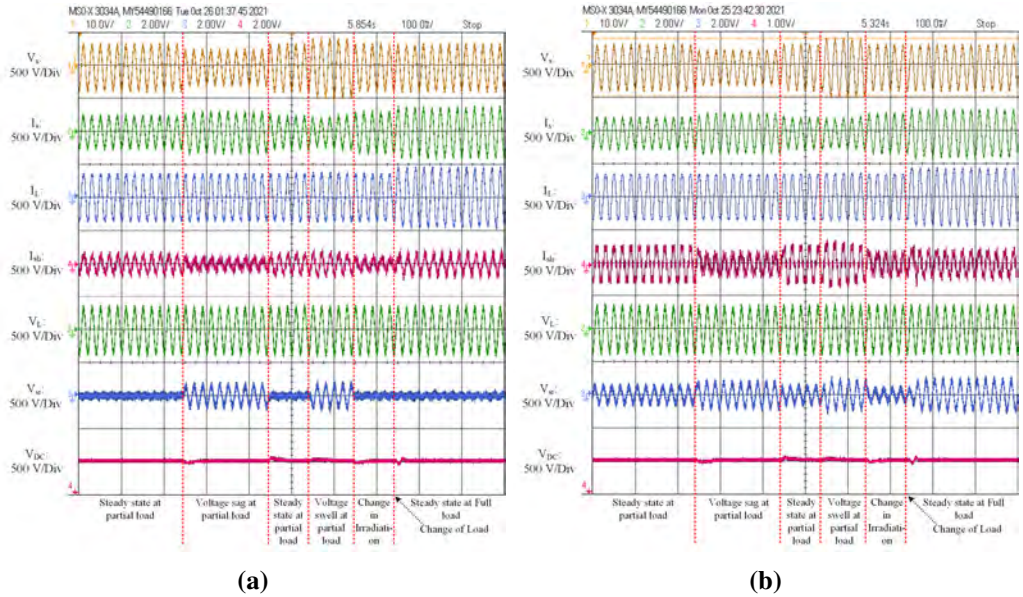

Figure 7.12: Real time simulation result of UPQC-DG (a) without PAC approach. (b) with PAC approach.

Table 7.8: Real Time Simulated Power Losses of UPQC-DG with PAC and without PAC

Controller	Duration (s)	P_L (kW)	UPQC-DG P_s (W)	UPQC-DG P_PV (W)	UPQC-DG Losses (W)	% Loss
UPQC-DG with PAC	1.65	37.60	25714	14091	2207.30	5.87
UPQC-DG without PAC	1.65	38.11	26244	14091	2220	5.82

7.5.2 Loss comparison for UPQC-DG with and without PAC approach using real time simulation

The performance of UPQC-DG under PAC and without PAC approach have been validated in real time simulation in order to compare the power loss dissipation in the system. Losses are computed for the overall case inclusive of sag, swell, change in load with varying irradiation and the corresponding evaluated power losses are listed in Table 7.8. Waveforms shown in the Fig. 7.12a depicts that model initially is operated in steady-state condition with partial load. The series inverter compensates for active power and the shunt inverter supports reactive load power. On the occurrence of sag, the series inverter operates in normal mode to compensate for the required voltage. However, in UPQC-DG with PAC approach, the compensation of reactive power is supported both by shunt and series APF (I_{sh} & V_{sr}) in steady-state as well as in transient conditions as shown in Fig. 7.12b. Similar phenomena emerges when the system is exposed to voltage swell. With the following condition, sun irradiation is varied to observe substantial changes in the system. The source current (I_s) tends to increase due to the decrement in power from PV. On changing from partial load to full load, the source current and load current (I_L) escalates abruptly. An increase in load widens the losses in the shunt APF of UPQC-DG administered by power angle control δ. From Fig. 7.12b, it can be clearly observed that during the case of steady-state with full load, the reactive power demand is shared between series APF and shunt APF (see waveform of V_{sr} and I_{sh}) which intensively increases the rms current in both the inverters. The PAC strategy causes 5.87% power losses in UPQC-DG while the non-PAC approach causes 5.82% power losses. This demonstrates that the UPQC-DG with the PAC approach suffers from somewhat higher losses than the UPQC-DG without PAC approach.

7.6 Summary

The performance of UPQC-DG and UPQC is investigated in various operating conditions under non-linear load for the study of power losses. The applied control algorithms are successfully able to compensate for the current and voltage PQ problems along with the integration of solar PV. The power losses computed are inclusive of conduction losses, switching losses and losses in passive filtering elements. If we look at overall losses of UPQC and UPQC-DG then it is found that the connection of DG at the DC link of UPQC lead to significant additional losses. The overall power loss of UPQC-DG is 5.80% and UPQC is 2.17% in real time simulation. In Matlab simulation the corresponding values are 9.95% and 7.19% respectively. The loss difference is significant in both cases. The PAC approach generates more power losses in UPQC-DG as compared to those without PAC controller. Despite more power losses, the UPQC-DG arrangement is more practicable for real-world distribution systems because the combination of PV and shunt APF reduces the cost of an additional power circuit to a level that is economically viable. PV injects active power into the grid, improving grid power quality and limiting load harmonic current, which is impossible to achieve with UPQC. Moreover, in the configuration of UPQC with separately integrated PV, higher power losses (15.11%) are observed, demonstrating the unsuitability of implementation in practical application in the distribution system.

Bibliography

[1] B. Singh, A. Chandra, and K. Al-Haddad, *Power quality: problems and mitigation techniques*. John Wiley & Sons, 2014.

[2] M. Kesler and E. Ozdemir, "Synchronous-reference-frame-based control method for UPQC under unbalanced and distorted load conditions," *IEEE Transactions on Industrial Electronics*, vol. 58, no. 9, pp. 3967–3975, 2011.

[3] V. Khadkikar, P. Agarwal, A. Chandra, A. Barry, and T. Nguyen, "A simple new control technique for unified power quality conditioner (UPQC)," in *Proc. 11th IEEE International Conference on Harmonics and Quality of Power*, 2004, pp. 289–293.

[4] V. Khadkikar and A. Chandra, "A new control philosophy for a unified power quality conditioner (UPQC) to coordinate load-reactive power demand between shunt and series inverters," *IEEE Transactions on Power Delivery*, vol. 23, no. 4, pp. 2522–2534, 2008.

[5] V. Khadkikar and A. Chandra, "UPQC-S: A novel concept of simultaneous voltage sag/swell and load reactive power compensations utilizing series inverter of UPQC," *IEEE Transactions on Power Electronics*, vol. 26, pp. 2414–2425, 2011.

[6] J. Kotturu, S. Kothuru, and P. Agarwal, "Simplified predictive control of unified power quality conditioner," in *2018 9th IEEE International Symposium on Power Electronics for Distributed Generation Systems (PEDG)*, 2018, pp. 1–6.

[7] S. Vinnakoti and V. R. Kota, "ANN based control scheme for a three-level converter based unified power quality conditioner," *Journal of Electrical Systems and Information Technology*, vol. 5, no. 3, pp. 526–541, 2018.

[8] D. Li, T. Wang, W. Pan, X. Ding, and J. Gong, "A comprehensive review of improving power quality using active power filters," *Electric Power Systems Research*, vol. 199, p. 107389, 2021.

[9] Y. Bouzelata, E. Kurt, N. Altın, and R. Chenni, "Design and simulation of a solar supplied multifunctional active power filter and a comparative study on the current-detection algorithms," *Renewable and Sustainable Energy Reviews*, vol. 43, pp. 1114–1126, 2015.

[10] S. Devassy and B. Singh, "Design and performance analysis of three-phase solar PV integrated UPQC," *IEEE Transactions on Industry Applications*, vol. 54, no. 1, pp. 73–81, 2017.

[11] B. Han, B. Bae, H. Kim, and S. Baek, "Combined operation of unified power-quality conditioner with distributed generation," *IEEE Transactions on Power Delivery*, vol. 21, no. 1, pp. 330–338, 2006.

[12] S. K. Khadem, M. Basu, and M. F. Conlon, "Intelligent islanding and seamless reconnection technique for microgrid with UPQC," *IEEE Journal of Emerging and Selected Topics in Power Electronics*, vol. 3, no. 2, pp. 483–492, 2015.

[13] A. Patel, S. K. Yadav, and H. D. Mathur, "Utilizing UPQC-DG to export reactive power to grid with power angle control method," *Electric Power Systems Research*, vol. 209, p. 107944, 2022.

[14] Y. Bouzelata, E. Kurt, R. Chenni, and N. Altın, "Design and simulation of a unified power quality conditioner fed by solar energy," *International Journal of Hydrogen Energy*, vol. 40, no. 44, pp. 15 267–15 277, 2015.

[15] M. Abdulkadir, A. Samosir, and A. Yatim, "Modelling and simulation of maximum power point tracking of photovoltaic system in Simulink model," in *Proc. IEEE International Conference on Power and Energy*, 2012, pp. 325–330.

[16] F. Liu, S. Duan, F. Liu, B. Liu, and Y. Kang, "A variable step size INC MPPT method for PV systems," *IEEE Transactions on Industrial Electronics*, vol. 55, no. 7, pp. 2622–2628, 2008.

[17] S. K. Yadav, A. Patel, and H. D. Mathur, "Study on comparison of power losses between UPQC and UPQC-DG," in *2020 IEEE 17th India Council International Conference (INDICON)*, 2020, pp. 1–6.

[18] A. Patel, H. D. Mathur, and S. Bhanot, "A new SRF-based power angle control method for UPQC-DG to integrate solar PV into grid," *International Transactions on Electrical Energy Systems*, vol. 29, no. 1, p. e2667, 2019.

[19] A. Patel, H. D. Mathur, and S. Bhanot, "Enhancing VA sharing between the shunt and series APFs of UPQC with a modified SRF-PAC method," *IET Power Electronics*, vol. 13, pp. 275–285, 2020.

[20] U. Nicolai and A. Wintrich, "Determining switching losses of SEMIKRON IGBT modules," *SEMIKRON Application Note, AN*, vol. 1403, 2014.

Chapter 8

Exporting Reactive Power to Grid with using UPQC-DG

8.1 Preamble

Electricity has become an integral part of modern life and thus quality and reliability of electric power are important aspects of the concept of smart grid, designed to cater to the necessities of the modern world. These two goals of smart grid- the power quality and reliability can be met using state of art technologies such as Active Power Filters (APFs) and distribution level grid integration of renewable sources respectively [1–5]. APFs are proven solutions for compensating for power quality issues [6]. Shunt APF primarily compensates for load current related power quality problems such as poor power factor (or compensating reactive power of the load), unbalance, and harmonics. Series APF compensates for source voltage related power quality issues such as voltage sag, swell, unbalance, and harmonics. Unified Power Quality Conditioner (UPQC) is a combination of series and shunt APFs connected in back-to-back configuration and sharing a common DC link [7, 8]. UPQC combines the benefits of both series and shunt APFs and reduces the burden of maintaining two DC links.

UPQC-DG is a further advanced topology of UPQC, which allows DG integration via common DC link [9]. In UPQC-DG topology, the shunt APF feeds the power supplied by DG to the grid and thus this topology avoids the use of additional complex grid-tie inverters [10] for interfacing the DG and saves the overall cost.

Power Angle Control (PAC) method has been devised for UPQC to share VA burden between series and shunt APFs of the UPQC [11–14]. PAC method becomes specifically significant in the case of UPQC-DG because feeding DG power through

shunt APF increases its VA burden. The PAC method also helps in optimizing the overall size and cost of UPQC and UPQC-DG [15, 16].

UPQC and UPQC-DG both have been researched for possible applications in power quality, microgrid, and renewable energy integration [17–22]. Though solar PV has been the most popular renewable source for UPQC-DG due to its simplicity, other sources of distributed generation like wind have also been considered for their combined integration with UPQC [23–25]. All these applications have focused on providing quality voltages to the load and drawing distortion-free, balanced currents from the source at unity power factor.

However, the smart grid scenario expects that customer devices participate in ancillary services like providing reactive power support to the grid whenever required. Incorporation of reactive power support to the grid for purpose of grid-side voltage regulation using the iUPQC approach has been demonstrated in [26], but the reactive power supplied is not controllable but is dependent on the amount of voltage drop. Apart from this, the iUPQC controllers are complex because of using shunt APF in voltage control mode and series APF in current control mode [27–29]. Simple, conventional, and versatile UPQC is based on using shunt APF in current control mode and series APF in voltage control mode for compensating current and voltage based power quality issues respectively.

This chapter focuses on incorporating the feature of reactive power support to the grid in UPQC-DG as part of ancillary services in the modern smart grid scenario. The key features of the proposed method are:

- In addition to compensating load reactive power, the UPQC-DG can supply reactive power to the grid, when required.
- Reactive power is supplied to the grid on demand from grid-operator, so the amount of reactive power exported is flexible as per the requirement from the grid.
- Reactive power can be supplied to the grid under normal operating conditions (even if there is no fault or sag in grid voltage), if the grid requires it as an ancillary service (to take care of reactive power balance or power losses).
- To control and regulate the reactive power to the grid as per the set-point, an additional PI controller is added in the controller.

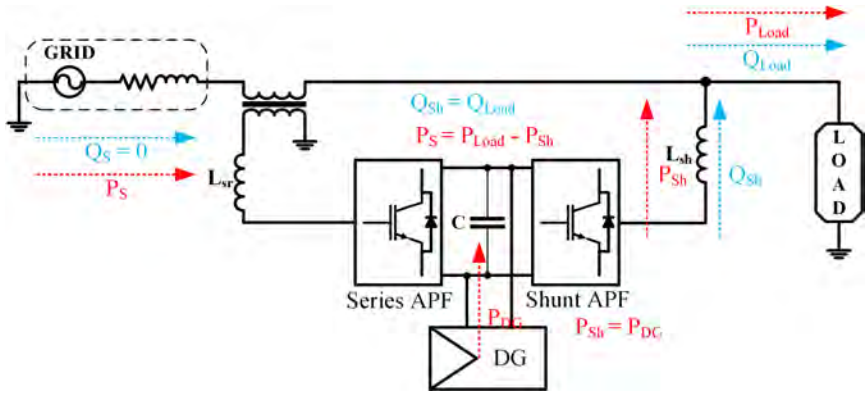

(a) UPQC-DG

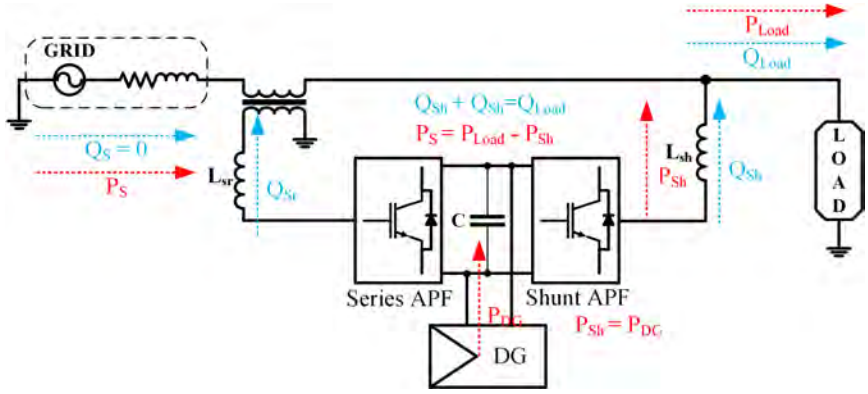

(b) UPQC-DG with PAC

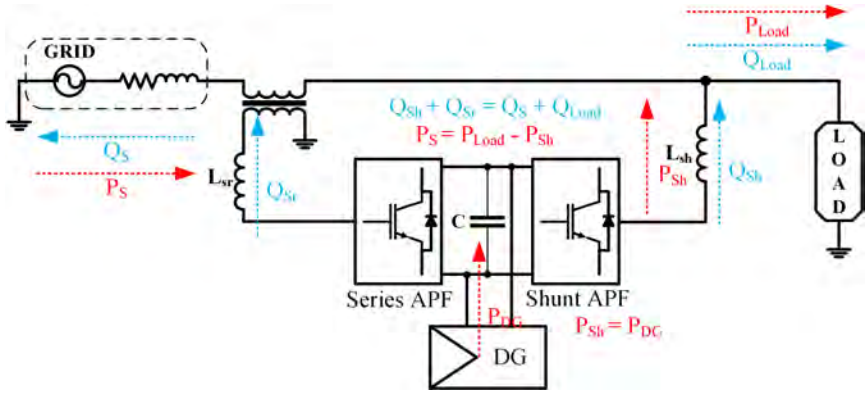

(c) UPQC-DG with reactive power support to grid under PAC

Figure 8.1: Active and reactive power flows under different control paradigms of UPQC-DG

- To take care of additional VA burden due to reactive power supply to the grid, power angle control is adopted, which utilizes series APF of UPQC-DG in generating reactive power.

Figure 8.1 illustrates the specific contribution of the proposed work through the

steady-state flows of active and reactive power in a UPQC-DG based system. In conventional UPQC-DG, active power is taken from the grid and DG the sum equals to load active power demand if losses are neglected. The load reactive power, in conventional UPQC-DG, is fully compensated by shunt APF and no reactive power is drawn from the grid [21] (Fig .8.1a). When UPQC-DG functions under the PAC approach, the series APF participates in reactive power compensation and reactive power exchange with the grid is still zero [18, 20] (Fig. 8.1b). In the proposed work, the reactive power is supplied to the load as well as the grid (when there is a requirement from the grid), and the total reactive power burden is shared by series and shunt APFs of the UPQC-DG (Fig. 8.1c). The reactive power fed to the grid is controllable to meet the variable need of the grid. Since the total reactive power burden is more in the proposed case, the PAC method is employed to share it between series and shunt APFs.

Some of the disadvantages of the proposed method are: the increase in complexity of the control, the increase in the number of PI controllers & difficulty in involved in tuning, and the increase in the value of the angle between source and load voltages to cater to the higher amount of reactive power sharing between two APFs.

The subsequent section of the chapter is organized in the following manner: section 8.2 presents the configuration of a solar PV based UPQC-DG used in the work, section 8.3 explains the proposed control method with its subparts, section 8.4 presents the real time validation results, and section 8.5 concludes the work.

8.2 UPQC-DG configuration

In this work, a Solar PV tied UPQC configuration has been considered (Fig. 8.2). Though, in general, a DG based system includes a mixture of different DG sources, in this work only solar PV is considered, since the work mainly focuses on providing reactive power support to the grid via UPQC-DG system. With suitable modifications, the proposed work can be extended for a more complicated system having more DGs. UPQC-DG configuration is based on three-phase, three-wire supply system. PV is connected to the DC link of the UPQC through a Boost DC-DC converter, which is responsible for tracking maximum power point of PV and matching PV output voltage with DC link voltage of the UPQC-DG. Three power electronic converters of the configuration, shown with yellow-shade, are- series APF, shunt APF and Boost converter. DC link capacitor eliminates the need of output capacitor filter

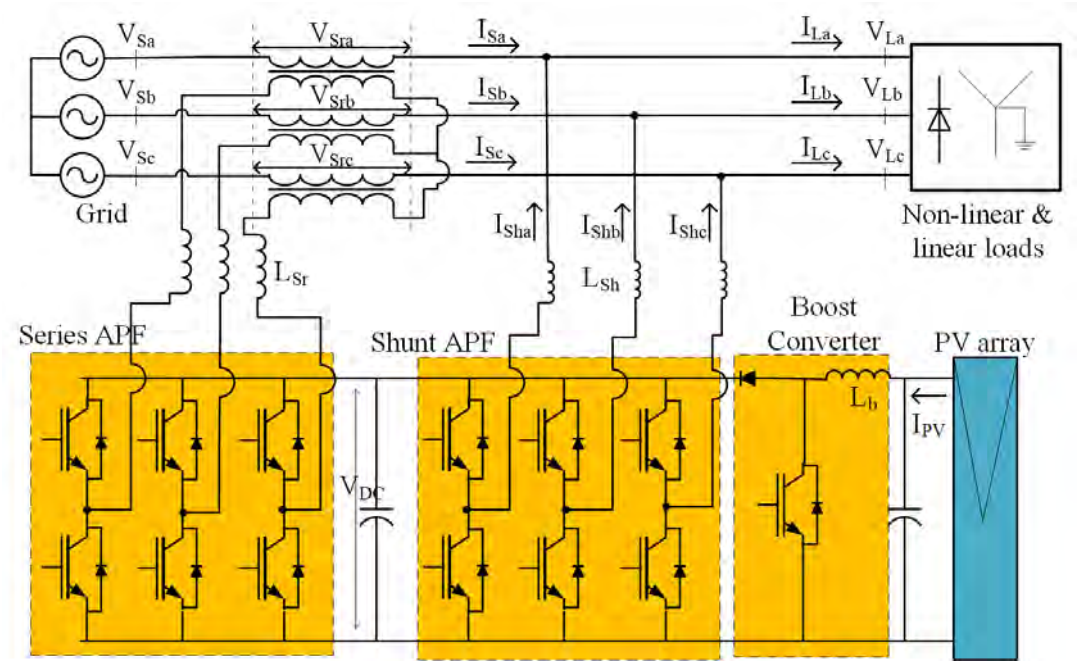

Figure 8.2: Configuration of three-phase, three-wire UPQC-DG with solar PV as a DG

for Boost converter. Control of all these converters, except boost converter is dealt in next section. Boost converter is controlled using conventional Perturb and Observe (P&O) technique to track maximum power point of solar PV array.

8.3 Proposed Control of UPQC-DG with Reactive Power to Grid Option

Control approach proposed in this work incorporates reactive power support to grid option in UPQC-DG. Since, in general, shunt APF of UPQC-DG is responsible for supplying reactive power demand and power generated by DG, proposed method adopts PAC method to share its reactive power burden with series APF. Overall controller block diagram appears in Fig. 8.3, which has been divided in three sub-parts that are explained in detail in following subsections:

8.3.1 Estimation of Power Angle

PAC method facilitates the series converter to inject series voltage in quadrature with source current in order to supply a part of reactive power demand of load. This phenomenon creates a phase difference between supply voltage and load voltage called

power angle. The equation used for computing power angle requires the magnitude of load active power, PV output power and reactive power supplied by series converter as shown in Eq. (8.1) [18].

$$\delta_D = \sin^{-1}\left(\frac{Q_{Sr}}{P_L - P_{DG}}\right) = \sin^{-1}\left(\frac{Q_{Sr}}{P_L - P_{PV}}\right) \tag{8.1}$$

The estimation of reactive power delivered by series converter when it is shared in proportion to VA rating of the converters of UPQC-DG is given by the Eq. (8.2), where Q_L is load reactive power and λ is ratio of series converter rating to the sum of VA ratings of series and shunt converter. Conclusively, the desired power angle is calculated using Eq. (8.3).

$$Q_{Sr} = \frac{Q_L S_{Sr,rated}}{S_{Sr,rated} + S_{Sh,rated}} = \lambda Q_L \tag{8.2}$$

$$\delta_D = \sin^{-1}\left(\frac{\lambda Q_L}{P_L - P_{PV}}\right) \tag{8.3}$$

The maximum allowable power angle is confined by voltage and kVA rating of the series converter (Eq. 8.4). k'_{max} is ratio of rated voltage of the series converter to reference load voltage.

$$\delta_M = \cos^{-1}\left[\frac{1 + k^2 - {k'_{max}}^2}{2k}\right] \tag{8.4}$$

So, the maximum power angle is calculated based on the conditions needed to meet voltage output and VA limits of series APF of UPQC-DG in Eq. (8.5):

$$\delta_M = \cos^{-1}\left[\frac{1 + \left(\frac{V_S}{V_{L,rated}}\right)^2 - \left(\frac{V_{Sr,rated}}{V_{L,rated}}\right)^2}{2\left(\frac{V_S}{V_{L,rated}}\right)}\right] \tag{8.5}$$

The final value of power angle (δ) is found by taking the minimum of the two-the desired power angle (δ_D) and the maximum power angle (δ_M).

8.3.2 Series APF control

A simple control algorithm of Unit vector template generation [30] for series APF is shown in the Fig. 8.3. This techniques is implemented to generate desired PWM

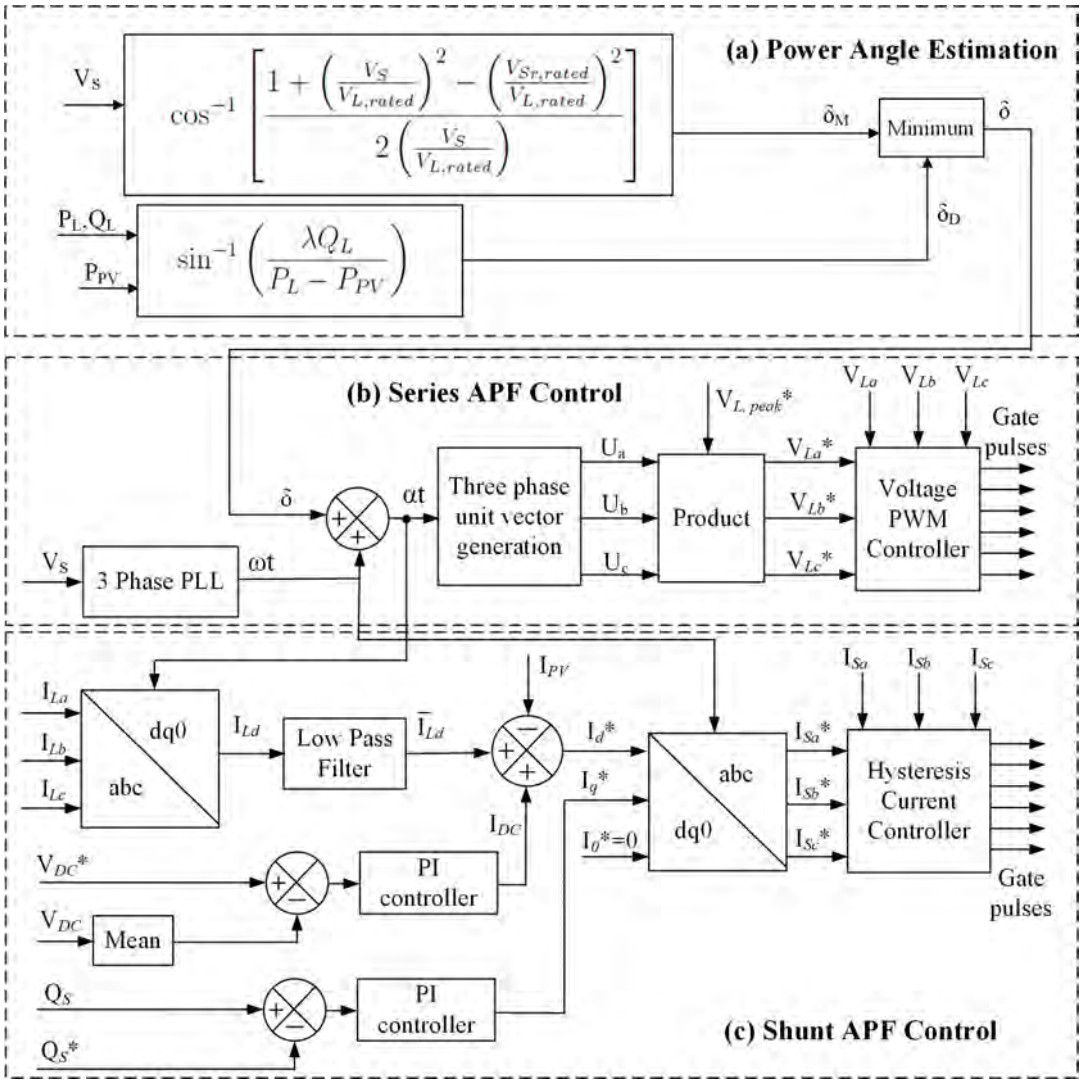

Figure 8.3: Proposed controller of UPQC-DG with provision of reactive power support to grid

pulses to control series APF for eliminating undesired components from the supply. The three-phase unit vector synchronized with PCC voltage by three phase PLL to generate three-phase fundamental signal, which later amplified using the amplitude of load voltage. The required switching gate pulse is generated by PWM controller, which compares the resultant three-phase time varying reference load voltage and its measured counterpart as inputs.

8.3.3 Shunt APF control

The proposed controller uses Synchronous Reference Frame theory (SRF) [31] based control method for shunt APF (Fig. 8.3). In SRF method measured load currents are first converted from abc to dq0 frame for extraction of fundamental and in-phase component in d-axis. The obtained d-axis load current ($\bar{I}_{Ld}$) is algebraically summed with PV current (I_{PV}) and internal DC link current I_{DC} (representing power losses) to produce desired d-axis component, which gives desires source currents after dq0 to abc transformation. The equation for abc to dq0 transformation (commonly known as Park's transformation [32] is shown below:

$$\begin{bmatrix} I_{Ld} \\ I_{Lq} \\ I_{L0} \end{bmatrix} = \frac{2}{3} \begin{bmatrix} sin\alpha t & sin(\alpha t - \frac{2\pi}{3}) & sin(\alpha t + \frac{2\pi}{3}) \\ cos\alpha t & cos(\alpha t - \frac{2\pi}{3}) & cos(\alpha t + \frac{2\pi}{3}) \\ 1/2 & 1/2 & 1/2 \end{bmatrix} \begin{bmatrix} I_{La} \\ I_{Lb} \\ I_{Lc} \end{bmatrix} \tag{8.6}$$

Park's transformation requires ramp signal synchronized with reference sinusoidal waveform, which is load voltage. In control approaches without PAC, the load and source voltages are in phase and thus ωt signal generated by PLL on source voltage is taken for Eq. (8.6) but in PAC approaches this needs to be added by power angle, the phase difference between load and source voltage [33]. Similarly, abc to dq0 transformation (Inverse Park's transformation) is carried out using following equation:

$$\begin{bmatrix} {I_{sa}}^* \\ {I_{sb}}^* \\ {I_{sc}}^* \end{bmatrix} = \begin{bmatrix} coswt & sinwt & 1 \\ cos(wt - \frac{2\pi}{3}) & sin(wt - \frac{2\pi}{3}) & 1 \\ cos(wt + \frac{2\pi}{3}) & sin(wt + \frac{2\pi}{3}) & 1 \end{bmatrix} \begin{bmatrix} {I_d}^* \\ {I_q}^* \\ {I_0}^* \end{bmatrix} \tag{8.7}$$

Shunt APF control incorporates two PI controllers: one responsible for regulating DC link voltage and another for regulating reactive power supplied to source. PI controller for regulating DC link voltage is a conventional one, which is inevitable for functioning of UPQC. Output of this PI controller is a current which represents the power losses in UPQC-DG and is added to the d-axis load current.

PI regulator for source reactive power is additionally added in present work to obtain precise control of reactive power supplied to the grid. This PI controller takes input as the error between measured and reference value of source reactive power and outputs a q-axis reference source current corresponding to the reference reactive power. The q-axis component of the current is responsible for the reactive power and when aiming to keep unity power factor at source this component is kept zero and

Table 8.1: System parameters

System Component	Specifications
1. Source	3-phase, 415 V, 50 Hz
2. Load-1	3-phase R-L load, 12 kW, 10 kVAR
3. Load-2	3-phase R-L load, 6 kW, 6 kVAR
4. Load-3	3-phase diode rectifier, 12.5 kW
5. DC-Link of UPQC-DG	700 V, 5.5 mF
6. Interfacing filters of shunt APF	1.4 mH, 5 Ω, 20 μF
7. Interfacing filters of series APF	3.0 mH, 4 Ω, 80 μF
8. Solar PV array	15.26 kW, Vmpp = 547 V, Impp = 27.9 A

thus no PI controller is required in that case. However, to set a non-zero value of reactive power a corresponding q-axis component of the current is computed by the additional PI controller used in this work. The reference reactive power is a signal received from grid-operator, which varies based on requirement of the grid.

Of course, three-phase reactive power can be expressed in terms of d-q frame voltage and currents using equation: $Q_S = \frac{-3}{2} V_d I_d$, by which q-axis current can be directly be computed based on required reactive power, but the actual value of reactive power supplied will be different due to inherent circuit parameters not taken care of in the computation. So, a PI controller will still be required to adjust the value of q-axis current to bring reactive power to the desired value. Since, PI controller alone is able to effectively adjust the q-axis current, equation based computation, which also requires computation of d-axis voltage, is avoided in this work to reduce burden on the controller. Effectiveness of proposed method is shown using real time simulations presented in next section.

8.4 Real-time Simulation Results

Real-time simulation using Opal-RT validates the proposed reactive power support to gird concept for the UPQC-DG system. A multi-rate validation of the system is performed in Opal-RT, in which the controller executes at 15 μs time step and electrical circuit is simulated at 0.5 μs time step (Fig. 8.4). Controller provides control signals (PWM outputs) to the circuit and it receives measurements from the circuit.

The specifications of system parameters for the case study are shown in Table 8.1. A three phase Unified quality conditioner with AC line voltage source of 415V (rms)

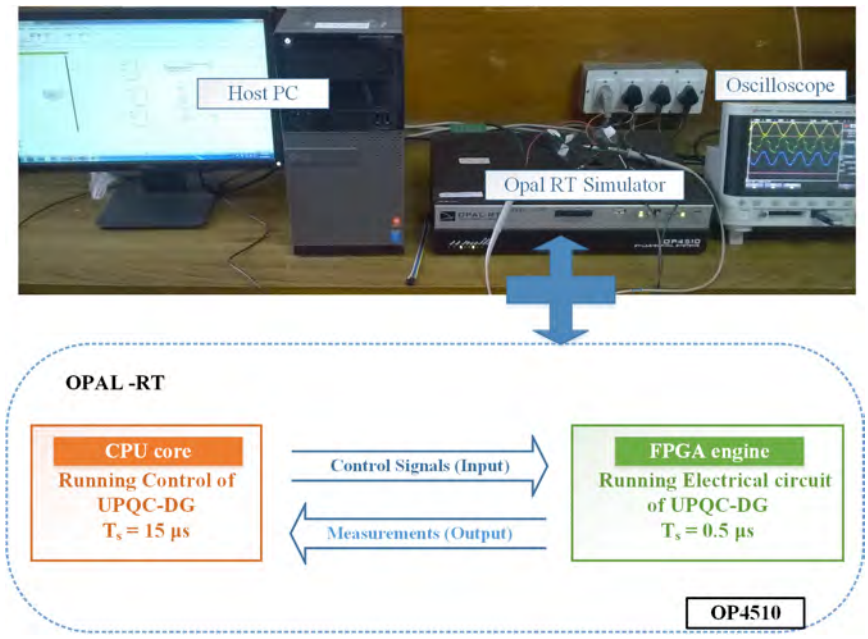

Figure 8.4: Real time simulation set-up

at 50 Hz is designed for the linear load of 12 kW, 10 kVAR and 6 kW, 6 kVAR and for nonlinear load of 12.5 kW. The DC bus capacitor of 5.5 mF of 700 V is adopted to provide support to overall functioning of UPQC-DG. The interfacing filters required for two VSCs, which are working as shunt APF and series APF are highlighted in the Table 8.1. For distributive generation, a solar PV array of 15.26 kW is considered for the research.

8.4.1 Steady-state results

Steady state performance of proposed UPQC-DG system with reactive power support to grid is shown in Fig. 8.5. Steady state comprises of all three loads connected to the system and solar PV array operating at standard operating point (at $1000W/m^2$, $25°C$). In steady state shunt APF compensates for load current harmonics and reactive power and also supplies reactive power to the grid. Part of total reactive power (load and grid) is supplied by the series APF and therefore its output voltage is in quadrature with the source current. Load voltage leads the source voltage by power angle, indicating the use of PAC method in UPQC-DG. The reactive power supplied to the grid is 10 kVAR, and so the source current leads the source voltage. As oppose to active power from the source, the reactive power is negative because it is supplied to the source (grid).

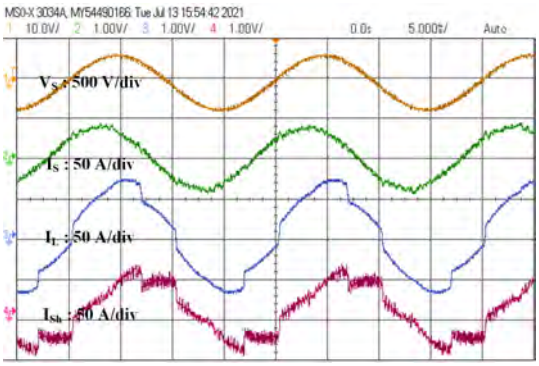

(a) Shunt APF compensates for current related issues.

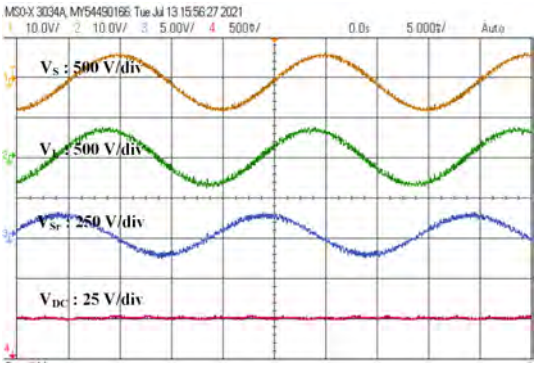

(b) Steady state compensation provided by series APF.

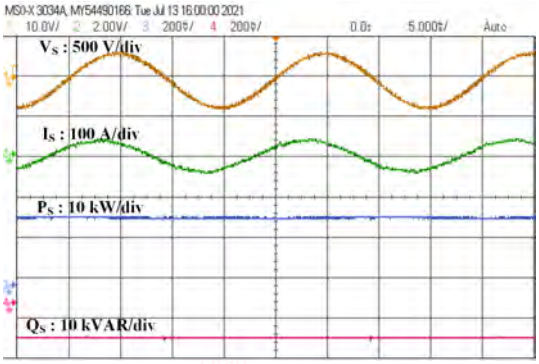

(c) Source active and reactive powers.

Figure 8.5: Steady state compensation performance of UPQC-DG.

8.4.2 Performance of reactive power regulator

When reactive power demand from the grid is altered, the reference reactive power to PI controller changes and accordingly the reactive power to the grid changes. Dynamics of reactive power change following the alterations in the reference is shown in Fig. 8.6. When reactive power reference is changed in step fashion from -10 to -6 kVAR, the actual source reactive power follows the reference after experiencing an undershoot of 1 kVAR and settling within 2 cycles (Fig. 8.6a). Source current experiences a phase shift but settles within 2 cycles. A similar dynamics is observed when reactive power reference is changed from -6 to -10 kVAR (Fig. 8.6b).

8.4.3 Results for other system dynamics

Dynamic performance of proposed system is validated under four commonly occurring disturbances in UPQC-DG system: voltage sag, swell, change in load and

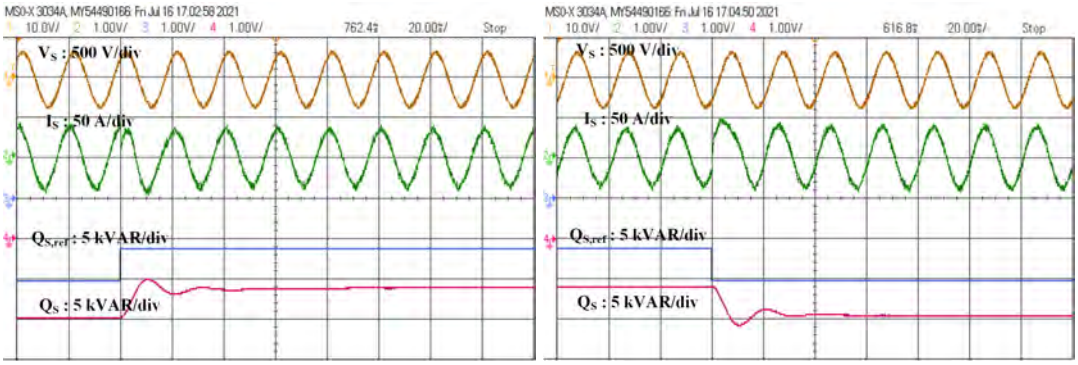

(a) Decrease in reactive power to grid. **(b)** Increase in reactive power to grid.

Figure 8.6: Alterations in reactive power supplied to grid.

change in solar irradiation (Fig. 8.7). When a sag of 25% occurs on the grid side voltage (V_S), the load voltage is maintained constant by series APF's compensation (Fig. 8.7a). Due to voltage sag, output voltage of series APF changes to accommodate the voltage sag compensation, thus reactive power sharing is affected and source reactive power experiences an overshoot of 0.55 kVAR but settles within 1.5 cycles. A similar dynamics is observed for voltage swell condition, except that an undershoot occurs in source reactive power on occurrence voltage swell (Fig. 8.7b). For a 25% voltage swell, an undershoot of 0.45 kVAR is observed which also settles within 1.5 cycles.

For evaluation of performance during change in load, load-2 is introduced while load-1 and load-3 were already connected. Due the increase in load, the load current and the current drawn from the source increase, but the source reactive power remains constant except slight variation (Fig. 8.7c). Similarly, when solar irradiation is reduced from 1000 to 600 W/m^2, the source current increases to compensate for reduction in PV output power, but the source reactive power remains the same (Fig. 8.7d).

Performance of other PI controller, responsible for DC link voltage regulation, is shown in Fig. 8.8, for voltage sag condition. On occurrence of 25% voltage sag, the DC voltage goes through an undershoot of 8 V, but settles to steady state value within one cycle.

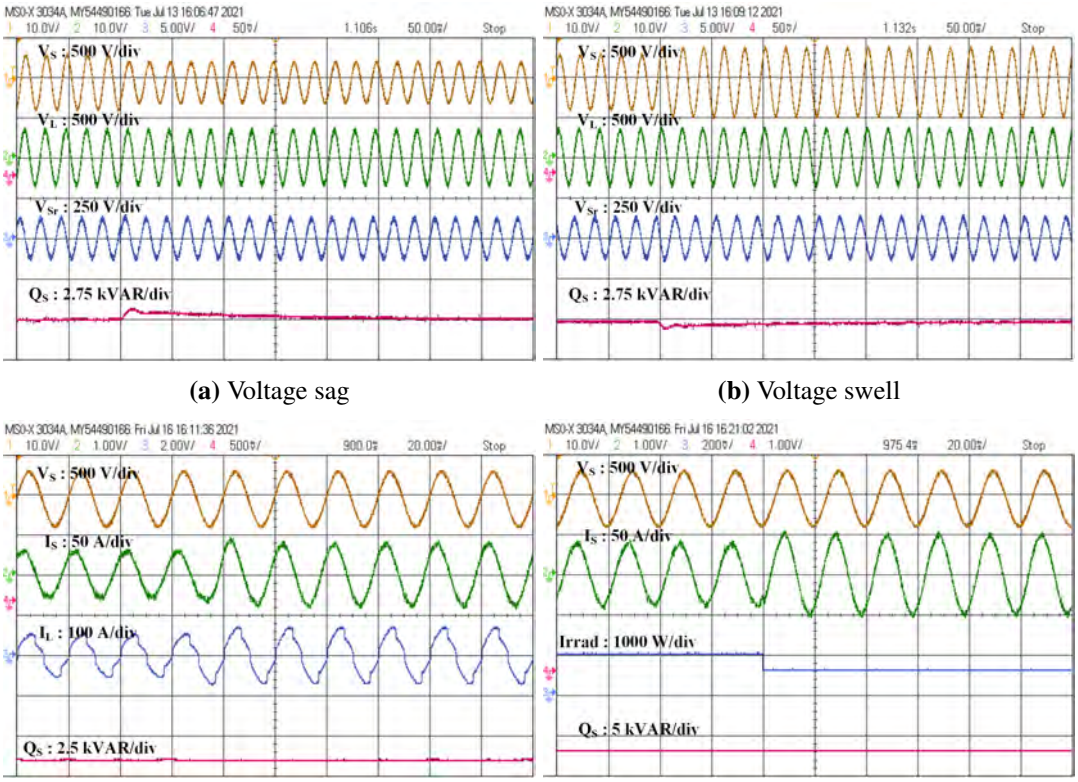

(a) Voltage sag **(b)** Voltage swell

(c) Change in load **(d)** Change in solar irradiation

Figure 8.7: Dynamic performance under various disturbances

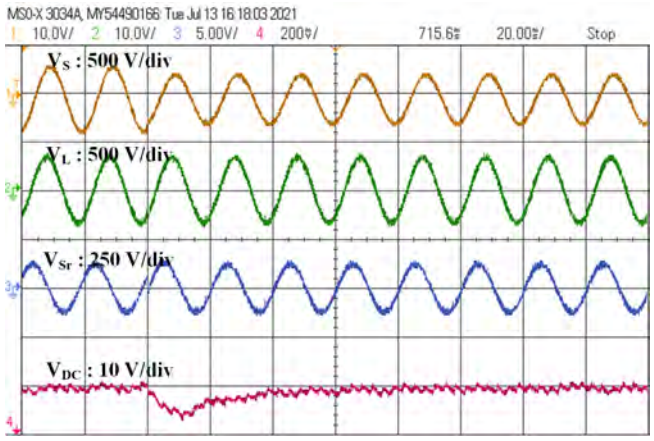

Figure 8.8: DC link voltage regulation of UPQC-DG during voltage sag

8.4.4 Benefit of PAC method

Benefit of using power angle control is found after analyzing the VA loading of series and shunt APFs of UPQC-DG for two cases: when PAC method is used and when it

Table 8.2: VA loading of series and shunt APFs of UPQC-DG under different operating conditions for proposed PAC method and without PAC approach

Operating condition	With proposed PAC		Without PAC	
	S_{Sr} (kVA)	S_{Sh} (kVA)	S_{Sr} (kVA)	S_{Sh} (kVA)
1. Steady state with PV	2.1+j4.8	12.8+j20.2	-0.1+j0.0	15.1+j25.1
2. Steady state without PV	1.2+j5.5	-1.45+j19.9	0.0-j0.2	-0.2+j25.3
3. Voltage sag with PV	7.0+j1.0	7.6+j23.6	4.8-j3.2	9.9+j27.9
4. Voltage sag without PV	11.6+j4.0	-12.1+j20.7	10.0-j3.6	-10.8+j28.4
5. Voltage swell with PV	-2.2+j3.8	17.2+j21.7	-3.2+j2.2	18.1+j23.6
6. Voltage swell without PV	-5.2+j5.3	4.9+j20.0	-6.1+j1.8	5.8+j23.7

is not used. Results of such an analysis for key operating conditions of UPQC-DG is presented in Table 8.2. The steady state includes all three loads, and voltage sag and swell are of 25% of the nominal voltage. Complex VA loading of series and shunt APFs are found for all these cases considering full presence and absence of PV power. The kVA loading magnitudes are shown in Table 8.3 correspondingly. In proposed PAC, maximum VA loading (magnitude) of series APF is 12.27 kVA for the case of voltage sag without PV, and maximum VA loading of shunt APF is 27.69 kVA for voltage swell with PV. Thus, the rating of UPQC-DG for proposed PAC is 39.96 kVA. Without using PAC method, the maximum VA loading of series and shunt APFs are found to be 10.63 kVA and 30.38 kVA, for the case of voltage sag without PV and the rating of UPQC-DG is 41.01 kVA. So, proposed PAC method gives 2.57% reduction in rating of the UPQC-DG. Also, utilization of series APF is found better in proposed PAC method. The improvement obtained in VA ratings might seem insignificant but it is system-specific, specifically when UPQC-DG is utilized for reactive power support to grid. The improvement can be enhanced further by optimizing design and control of the system. PAC methods in other UPQC-DG based works have reduced the VA ratings by 5% [16].

8.5 Summary

In this chapter, a UPQC-DG system with the additional functionality of providing reactive power support to the grid is demonstrated. The proposed UPQC-DG system not only compensates for conventional voltage and current based power quality

Table 8.3: kVA loading (magnitude) of series and shunt APFs of UPQC-DG under different operating conditions for proposed PAC method and without PAC approach

Operating condition	With proposed PAC		Without PAC	
	S_{Sr} (kVA)	S_{Sh} (kVA)	S_{Sr} (kVA)	S_{Sh} (kVA)
1. Steady state with PV	5.24	23.91	0.10	29.29
2. Steady state without PV	5.63	19.95	0.20	25.30
3. Voltage sag with PV	7.07	24.79	5.77	29.60
4. Voltage sag without PV	12.27	23.98	10.63	30.38
5. Voltage swell with PV	4.39	27.69	3.88	29.74
6. Voltage swell without PV	7.42	20.59	6.36	24.40

issues but integrates renewable energy into the distribution system and provides ancillary service of reactive power support to the grid simply and robustly. The amount of reactive power supplied to the grid is controlled and regulated using an additional PI controller in the control loop. The control method of UPQC-DG is based on Synchronous Reference Frame (SRF) theory for shunt APF and Unit Vector template Generation (UVTG) for series APF and also incorporates power angle control to share reactive power burden between series and shunt APFs of the UPQC-DG. Steady-state, as well as the dynamic performance of the proposed UPQC-DG system, have been validated using multi-rate real-time simulations carried out in Opal-RT. In steady-state, the source reactive power precisely follows its set-point, and in dynamic situations such as a change in set-point, voltage-sag, swell, and changes in load or irradiation, the peak overshoot and settling time are kept sufficiently small. Maximum peak overshoot under step change in reference reactive power is determined to 10% and maximum settling time is 2 cycles of power frequency. Also, power angle control proves to be effective in utilizing series APF in reactive power sharing and thus reduces the overall rating of UPQC-DG under study by 2.57%.

Bibliography

[1] B. Singh, A. Chandra, and K. Al-Haddad, *Power quality: problems and mitigation techniques*. John Wiley & Sons, 2014.

[2] T. Adefarati and R. C. Bansal, "Integration of renewable distributed generators into the distribution system: A review," *IET Renewable Power Generation*, vol. 10, no. 7, pp. 873–884, 2016.

[3] L. Gidwani, H. Tiwari, and R. C. Bansal, "Improving power quality of wind energy conversion system with unconventional power electronic interface," *International Journal of Electrical Power & Energy Systems*, vol. 44, no. 1, pp. 445–453, 2013.

[4] M. E. Meral and D. Çelík, "A comprehensive survey on control strategies of distributed generation power systems under normal and abnormal conditions," *Annual Reviews in control*, vol. 47, pp. 112–132, 2019.

[5] D. Çelik and M. E. Meral, "Current control based power management strategy for distributed power generation system," *Control Engineering Practice*, vol. 82, pp. 72–85, 2019.

[6] D. Li, T. Wang, W. Pan, X. Ding, and J. Gong, "A comprehensive review of improving power quality using active power filters," *Electric Power Systems Research*, vol. 199, p. 107389, 2021.

[7] H. Fujita and H. Akagi, "The unified power quality conditioner: The integration of series and shunt-active filters," *IEEE Transactions on Power Electronics*, vol. 13, no. 2, pp. 315–322, 1998.

[8] V. Khadkikar, "Enhancing electric power quality using UPQC: A comprehensive overview," *IEEE Transactions on Power Electronics*, vol. 27, no. 5, pp. 2284–2297, 2012.

[9] A. Patel, H. D. Mathur, and S. Bhanot, "A new SRF-based power angle control method for UPQC-DG to integrate solar PV into grid," *International Transactions on Electrical Energy Systems*, vol. 29, no. 1, p. e2667, 2019.

[10] D. Çelik and M. E. Meral, "Voltage support control strategy of grid-connected inverter system under unbalanced grid faults to meet fault ride through requirements," *IET Generation, Transmission & Distribution*, vol. 14, no. 16, pp. 3198–3210, 2020.

[11] V. Khadkikar and A. Chandra, "UPQC-S: A novel concept of simultaneous voltage sag/swell and load reactive power compensations utilizing series inverter of UPQC," *IEEE Transactions on Power Electronics*, vol. 26, pp. 2414–2425, 2011.

[12] V. Khadkikar, "Fixed and variable power angle control methods for unified power quality conditioner: operation, control and impact assessment on shunt and series inverter kVA loadings," *IET Power Electronics*, vol. 6, no. 7, pp. 1299–1307, 2013.

[13] A. Q. Ansari, B. Singh, and M. Hasan, "Algorithm for power angle control to improve power quality in distribution system using unified power quality conditioner," *IET Generation, Transmission & Distribution*, vol. 9, no. 12, pp. 1439–1447, 2015.

[14] N. Patnaik and A. K. Panda, "Performance analysis of a 3 phase 4 wire UPQC system based on PAC based SRF controller with real time digital simulation," *International Journal of Electrical Power & Energy Systems*, vol. 74, pp. 212–221, 2016.

[15] J. Ye, H. B. Gooi, and F. Wu, "Optimization of the size of UPQC system based on data-driven control design," *IEEE Transactions on Smart Grid*, vol. 9, no. 4, pp. 2999–3008, 2018.

[16] A. Patel, S. K. Yadav, H. D. Mathur, S. Bhanot, and R. C. Bansal, "Optimum sizing of PV based UPQC-DG with improved power angle control," *Electric Power Systems Research*, vol. 182, p. 106259, 2020.

[17] V. Madhaiyan and V. Subramaniam, "Extended reference signal generation scheme for integration of unified power quality conditioner in grid-connected photovoltaic system," *Electric Power Components and Systems*, vol. 43, no. 8-10, pp. 914–927, 2015.

[18] S. Devassy and B. Singh, "Modified pq-theory-based control of solar-PV-integrated UPQC-S," *IEEE Transactions on Industry Applications*, vol. 53, no. 5, pp. 5031–5040, 2017.

[19] P. G. Khorasani, M. Joorabian, and S. G. Seifossadat, "Smart grid realization with introducing unified power quality conditioner integrated with DC micro-grid," *Electric Power Systems Research*, vol. 151, pp. 68–85, 2017.

[20] A. Patel, H. Mathur, and S. Bhanot, "An improved control method for unified power quality conditioner with unbalanced load," *International Journal of Electrical Power & Energy Systems*, vol. 100, pp. 129–138, 2018.

[21] S. Devassy and B. Singh, "Design and performance analysis of three-phase solar PV integrated UPQC," *IEEE Transactions on Industry Applications*, vol. 54, no. 1, pp. 73–81, 2017.

[22] J. Wang, K. Sun, H. Wu, J. Zhu, Y. Xing, and Y. Li, "Hybrid connected unified power quality conditioner integrating distributed generation with reduced power capacity and enhanced conversion efficiency," *IEEE Transactions on Industrial Electronics*, 2020.

[23] J. X. Jin, R. H. Yang, R. T. Zhang, Y. J. Fan, Q. Xie, and X. Y. Chen, "Combined low voltage ride through and power smoothing control for DFIG/PMSG hybrid wind energy conversion system employing a SMES-based AC-DC unified power quality conditioner," *International Journal of Electrical Power & Energy Systems*, vol. 128, p. 106733, 2021.

[24] R. H. Yang and J. X. Jin, "Unified power quality conditioner with advanced dual control for performance improvement of DFIG-based wind farm," *IEEE Transactions on Sustainable Energy*, vol. 12, no. 1, pp. 116–126, 2020.

[25] K. Sarita, S. Kumar, A. S. S. Vardhan, R. M. Elavarasan, R. Saket, G. Shafiullah, and E. Hossain, "Power enhancement with grid stabilization of renewable energy-based generation system using UPQC-FLC-EVA technique," *IEEE Access*, vol. 8, pp. 207 443–207 464, 2020.

[26] B. W. Franca, L. F. da Silva, M. A. Aredes, and M. Aredes, "An improved iUPQC controller to provide additional grid-voltage regulation as a STATCOM," *IEEE Transactions on Industrial Electronics*, vol. 62, no. 3, pp. 1345–1352, 2015.

[27] M. Aredes and R. M. Fernandes, "A dual topology of unified power quality conditioner: The iUPQC," in *2009 13th European Conference on Power Electronics and Applications*. IEEE, 2009, pp. 1–10.

[28] R. A. Modesto, S. A. O. da Silva, A. A. de Oliveira, and V. D. Bacon, "A versatile unified power quality conditioner applied to three-phase four-wire distribution systems using a dual control strategy," *IEEE Transactions on Power Electronics*, vol. 31, no. 8, pp. 5503–5514, 2016.

[29] T. S. Prakash, P. S. Kumar, and R. Chandrasena, "A novel iUPQC for multi-feeder systems using multilevel converters with grid integration of hybrid renewable energy system," *IEEE Access*, vol. 8, pp. 44 903–44 912, 2020.

[30] V. Khadkikar, P. Agarwal, A. Chandra, A. Barry, and T. Nguyen, "A simple new control technique for unified power quality conditioner (UPQC)," in *Proc. 11th IEEE International Conference on Harmonics and Quality of Power*, 2004, pp. 289–293.

[31] S. Bhattacharya and D. Divan, "Synchronous frame based controller implementation for a hybrid series active filter system," in *IAS'95. Conference Record of the 1995 IEEE Industry Applications Conference Thirtieth IAS Annual Meeting*, vol. 3. IEEE, 1995, pp. 2531–2540.

[32] R. H. Park, "Two-reaction theory of synchronous machines generalized method of analysis-part I," *Transactions of the American Institute of Electrical Engineers*, vol. 48, no. 3, pp. 716–727, 1929.

[33] A. Patel, H. D. Mathur, and S. Bhanot, "Enhancing VA sharing between the shunt and series APFs of UPQC with a modified SRF-PAC method," *IET Power Electronics*, vol. 13, pp. 275–285, 2020.

Chapter 9

Hardware Validation

9.1 Preamble

Power quality is a critical aspect of modern electrical systems, directly impacting the efficiency, reliability, and lifespan of both power generation and consumption equipment. With the growing use of renewable energy sources such as solar photovoltaics (PV), ensuring consistent power quality becomes more difficult due to the intermittent nature of these energy sources. In order to tackle these difficulties, it is crucial to use modern power conditioning systems such as Unified Power Quality Conditioners (UPQC) [1, 2] that include Distributed Generation (DG) [3, 4]. This chapter focuses on validating a hardware prototype of a shunt Active Power Filter (APF) [5–7] that is combined with a real PV panel. Additionally, the study focuses on utilizing Particle Swarm Optimization (PSO) [8–10] to fine-tune the proportional-integral (PI) controller of the shunt APF. Another goal optimize the design of the UPQC-DG system by implementing power angle control.

The Synchronous Reference Frame (SRF) method is widely used for controlling shunt APFs due to its effectiveness in extracting the fundamental component of the load current. In the SRF method [11, 12], the load currents are transformed into a rotating reference frame, making it easier to separate the harmonic components from the fundamental frequency components. This approach enhances the shunt APF's ability to compensate for reactive power and harmonic currents, thereby improving overall power quality.

The Unit Vector Template Generation (UVTG) method is another technique employed in series APF control [13]. It involves generating unit vectors synchronized with the supply voltage to accurately detect and compensate for voltage disturbances

such as sags, swells, and harmonics. By using the UVTG method, the series APF can effectively maintain a stable and distortion-free voltage at the load terminals, ensuring consistent power delivery.

The Synchronous Reference Frame-Power Angle Control (SRF-PAC) method is a novel approach that combines the advantages of the SRF method with power angle control to optimize the performance of the UPQC-DG system [14, 15]. This method adjusts the power angle to control the active and reactive power flow, thereby enhancing the stability and efficiency of the integrated system. The SRF-PAC method is particularly beneficial in managing the power quality issues arising from the integration of renewable energy sources.

The selection of the PV panel for this study is based on its compatibility with the shunt APF and its ability to provide a stable DC link voltage under varying environmental conditions. The PV panel's characteristics, such as its voltage-current (V-I) curve and maximum power point (MPP), are considered to ensure optimal performance when integrated with the shunt APF.

The load selection is crucial for validating the hardware prototype. A representative load that exhibits typical power quality issues, such as harmonics and reactive power demand, is chosen to evaluate the effectiveness of the shunt APF and the PSO-based PI tuning [16]. This load includes nonlinear components that introduce harmonics, thereby providing a comprehensive test scenario for the UPQC-DG system.

Designing the hardware implementation involves careful consideration of various parameters, including the ratings of power electronic components, control algorithms, and the overall system architecture. The hardware prototype is designed to be scalable and adaptable to different load conditions and renewable energy sources. The benefits of hardware implementation include real-world validation of theoretical models, performance assessment under actual operating conditions, and the ability to identify and address practical challenges that may not be evident in simulation studies.

The PSO-based PI tuning approach is employed to dynamically optimize the PI controller parameters of the shunt APF. PSO is a robust optimization technique that mimics the social behavior of birds flocking or fish schooling to find the optimal solution in a search space [17]. By continuously adjusting the PI parameters, the PSO algorithm ensures optimal control performance, resulting in improved power quality and system stability. The use of PSO in this study highlights its advantages

over traditional tuning methods, such as faster convergence, lower computational complexity, and better global search capability.

In summary, this study aims to validate a hardware prototype of a shunt APF integrated with a PV panel in section. To demonstrate the effectiveness of the PSO-based PI tuning approach for the optmial PI parameters using power angle control (PAC). The technical insights gained from this validation will contribute to the development of more efficient and reliable power conditioning systems, ultimately enhancing the power quality and stability of electrical grids with high penetration of renewable energy sources.

9.2 Hardware Validation of PV fed Shunt APF

The configuration of a shunt APF integrated with a photovoltaic (PV) system is designed to enhance the overall power quality and efficiency of electrical systems. In this configuration, the PV system is connected to the DC link of the shunt APF. The single diagram of the system is shown in the Fig. 9.1. The output voltage of the PV is arranged in such as way that it matches with the voltage of DC voltage link so it eliminated the need of DC-DC boost converter. This setup simplifies the configuration but requires careful selection and sizing of PV array to ensure stability and efficient power quality management. The DC link acts as a common node where the PV system and the shunt APF interface. To prevent reverse power flow into the PV array, a diode is added in between the PV and DC link.

In this hardware model, the DC link voltage varies according to a variable reference value, which depends on the MPP of the PV array. The specification of the WAARRI SS 335 PV module is shown in Table 9.1. Three PV modules are connected in series to form a string to develop a complete PV array of 1.1 kW with an output voltage of 100 V under standard irradiation and temperature conditions.

This configuration can reduce complexity and cost while maintaining effective power quality improvement and maximizing the utilization of renewable energy. However, the success of this integration heavily relies on inverter control techniques to ensure stability and efficient operation. The shunt APF is connected to the point of common coupling (PCC) where it can inject compensating currents to cancel out harmonics and reactive power caused by nonlinear loads.

The main purpose of the hardware prototype are as follows:

- To validate hardware setup of PV fed shunt APF.

- To compensates for current harmonics by injecting anti-phase harmonics into the grid, thereby canceling out distortions caused by nonlinear loads.
- To compensate reactive power to improve power factor and reduce the burden on the grid.
- It balance imbalanced currents in the system, ensuring that the current flowing through all phases is equal.

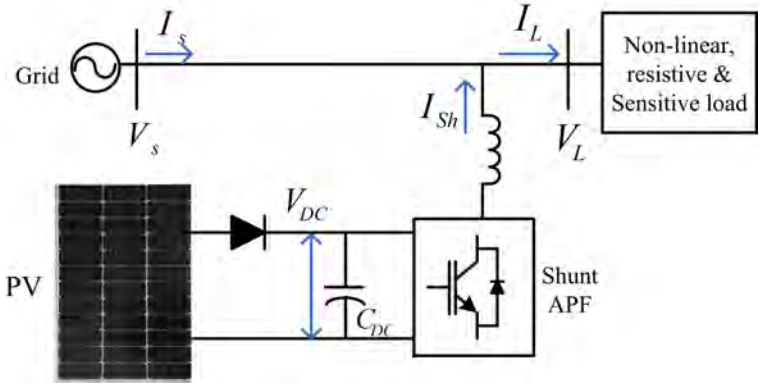

Figure 9.1: The configuration of the shunt APF integrated with PV

Table 9.1: Specifications of solar PV module

Maximum power (P_{max})	335 W
Open circuit voltage (V_{oc})	46.80 V
Short circuit current	9.30 A
Maximum Power Voltage (V_{MPP})	38.10 V
Maximum Power Current (I_{MPP})	8.80 A
Maximum System Voltage Weight	1500 VDC

9.2.1 Shunt APF control

The shunt APF is often controlled using the Synchronous Reference Frame (SRF) approach, as seen in Fig. 3. The SRF approach employs Park (Eq. 9.1) and inverse park transformations (Eq. 9.2) to convert the load currents into a rotating reference frame. This transformation enables the isolation of harmonic components and the fundamental frequency component. By extracting the direct and quadrature components

of the current, the APF can generate shunt APF reference currents that are injected back into the grid to counteract the unwanted harmonics and maintain a sinusoidal waveform. The specific details of the SRF approach are elucidated in Chapter 3.

$$\begin{bmatrix} I_{Ld} \\ I_{Lq} \\ I_{L0} \end{bmatrix} = \frac{2}{3} \begin{bmatrix} sin\alpha t & sin(\alpha t - \frac{2\pi}{3}) & sin(\alpha t + \frac{2\pi}{3}) \\ cos\alpha t & cos(\alpha t - \frac{2\pi}{3}) & cos(\alpha t + \frac{2\pi}{3}) \\ 1/2 & 1/2 & 1/2 \end{bmatrix} \begin{bmatrix} I_{La} \\ I_{Lb} \\ I_{Lc} \end{bmatrix} \tag{9.1}$$

$$\begin{bmatrix} {I_{sa}}^* \\ {I_{sb}}^* \\ {I_{sc}}^* \end{bmatrix} = \begin{bmatrix} coswt & sinwt & 1 \\ cos(wt - \frac{2\pi}{3}) & sin(wt - \frac{2\pi}{3}) & 1 \\ cos(wt + \frac{2\pi}{3}) & sin(wt + \frac{2\pi}{3}) & 1 \end{bmatrix} \begin{bmatrix} {I_d}^* \\ {I_q}^* \\ {I_0}^* \end{bmatrix} \tag{9.2}$$

9.2.2 Result Discussion

The validation of a shunt APF integrated into a photovoltaic (PV) system is performed using hardware setup as shown in the Fig. 9.2. It involves several critical steps to ensure effective operation and performance. The SRF control technique has been implemented using Opal-RT 4510. The sample time for the control is taken as 16 μs. Measurement are taken from the N4L PPA500 Power Analyzser and oscilloscope. The gate pulse are provided to the shunt converter by digital output of the FPGA based controller. Key performance indicators, such as harmonic distortion, reactive power compensation, and voltage stability, are measured and analyzed. The design of interface inductors and RC filters, used at the output of converters, has been performed according to the methodology outlined in [2].

The setup has been connected to the rectifier load and RC load to verify the performance. Key performance metrics, such as harmonic distortion, reactive power compensation, and voltage stability, are tracked and assessed in real time operation. Voltage and current are measured using LV-25P and LA-25P sensors that are connected across load, source and converter outputs.

As illustrated in Fig. 9.3, the steady-state results demonstrate that the integrated shunt APF with PV system effectively mitigates power quality issues by compensating for harmonics and reactive power while maintaining a stable DC link voltage. The system actively filters out harmonic currents and compensates for reactive power in the source current by injecting currents that are equal in magnitude but opposite in phase to the harmonic currents drawn by the load, thereby canceling them out. As a result, the source current waveform becomes nearly sinusoidal, closely aligning with

Figure 9.2: Hardware setup of PV fed shunt APF

the voltage waveform (Fig. 9.3a). However, the source current waveform remains out of phase with the source voltage, indicating that the PV system is actively providing power to the grid. This is further evidenced by Fig. 9.4b which shows that the source power is -296.83 W, while the power provided by the solar PV system is 506 W (calculated value).

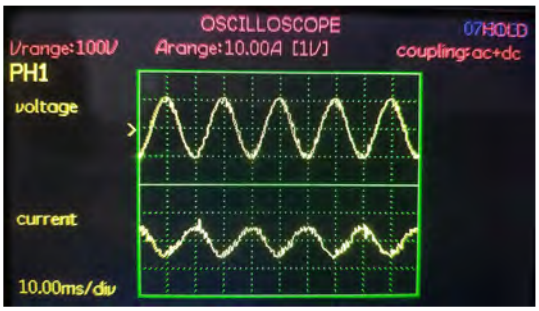

(a) Waveform of source voltage and source current

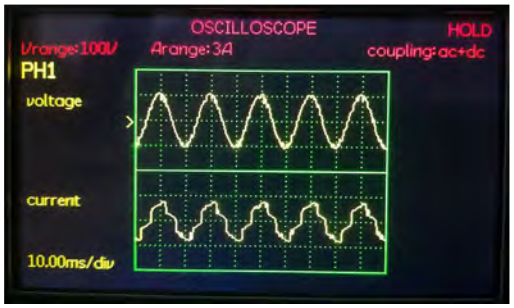

(b) Waveform of load voltage and load current

Figure 9.3: Output waveforms of hardware setup

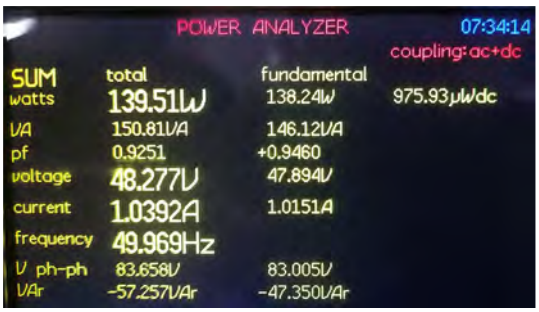

(a) Measured result of load power

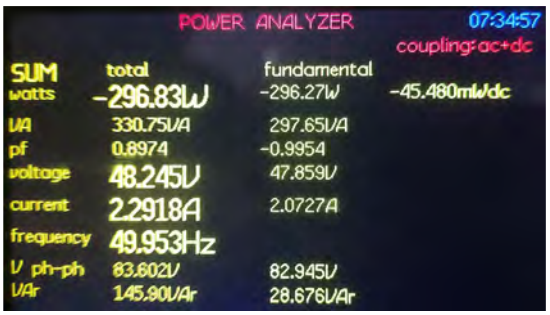

(b) Measured result of source power

Figure 9.4: Output measurement of hardware setup

The load voltage maintains a constant voltage profile (Fig. 9.3a), achieved through the compensation of reactive power and mitigation of harmonics. Nevertheless, the load current exhibits considerable harmonic distortions due to the presence of non-linear loads (Fig. 9.3b). The fundamental load power factor is 0.94, and the fundamental source power factor is -0.99, as depicted in Fig. 9.4. The load power is 139.51 W, with total system losses amounting to 70 W.

9.3 Hardware Validation of PSO based PI controller for Shunt APF integrated with PV

The proposed method of tuning the PSO-based PI controller (from Chapter 4) for shunt APF integrated with PI has been validated using hardware setup (Fig. 9.5). The hardware setup configurations are shown in Table 9.5. The method's validation remains unaffected by a fairly low system voltage that was chosen in the hardware configuration for safety reasons. In the hardware configuration, the Opal-RT system

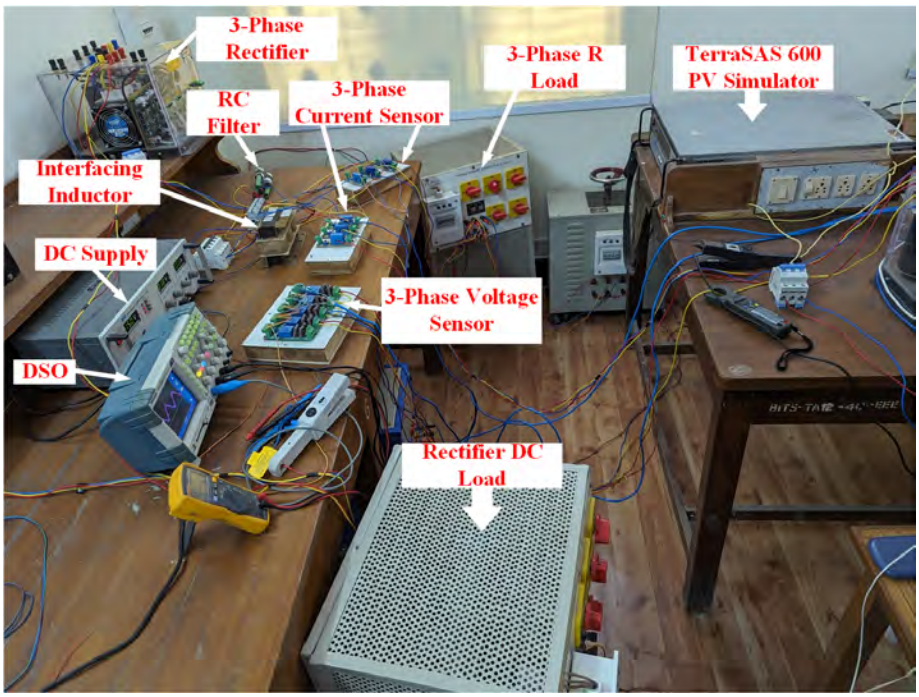

(a) Part-1 of Hardware setup

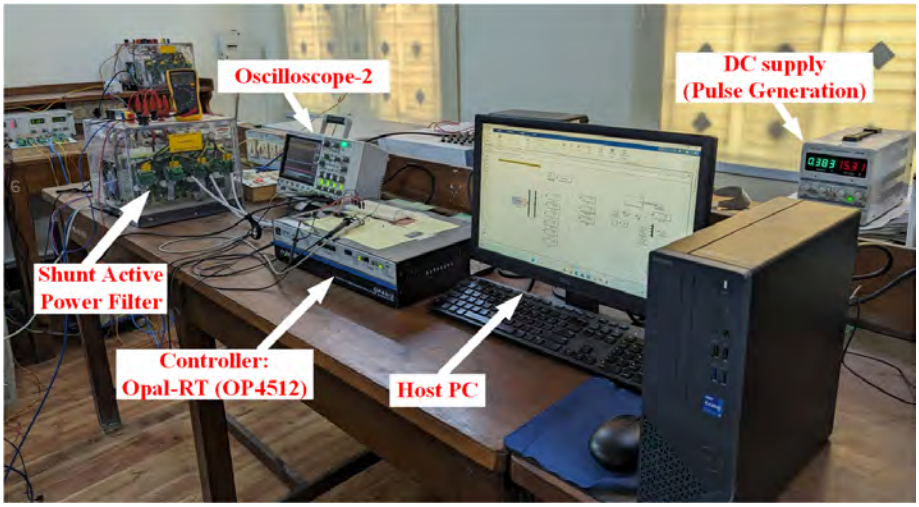

(b) Part-2 of Hardware setup

Figure 9.5: Shunt APF hardware setup

functions as the controller, generating switching pulses for the shunt APF. This is achieved through a control strategy based on real-time measurements of the DC link voltage, source voltages, three-phase load currents, and shunt APF currents. Two loads are used - one is a three-phase RL-load, while the other is a three-phase uncontrolled diode rectifier with a resistance on the DC side. The output of the solar PV

Table 9.2: System parameters of hardware-setup

Parameter	Specifications
1. Grid	3-phase, 100 V, 50 Hz
2. Load-1 (3-phase R-load)	67.5 Ω
3. Load-2 (3-phase diode rectifier)	R_{dc} = 94.2 Ω
4. DC-Link of shunt APF	190 V, 2.35 mF
5. Interfacing filters of shunt APF	9.0 mH, 10 Ω, 10 μF
6. Solar PV array	V_{oc} = 250V, I_{sc} = 1.50 A, FF = 80%

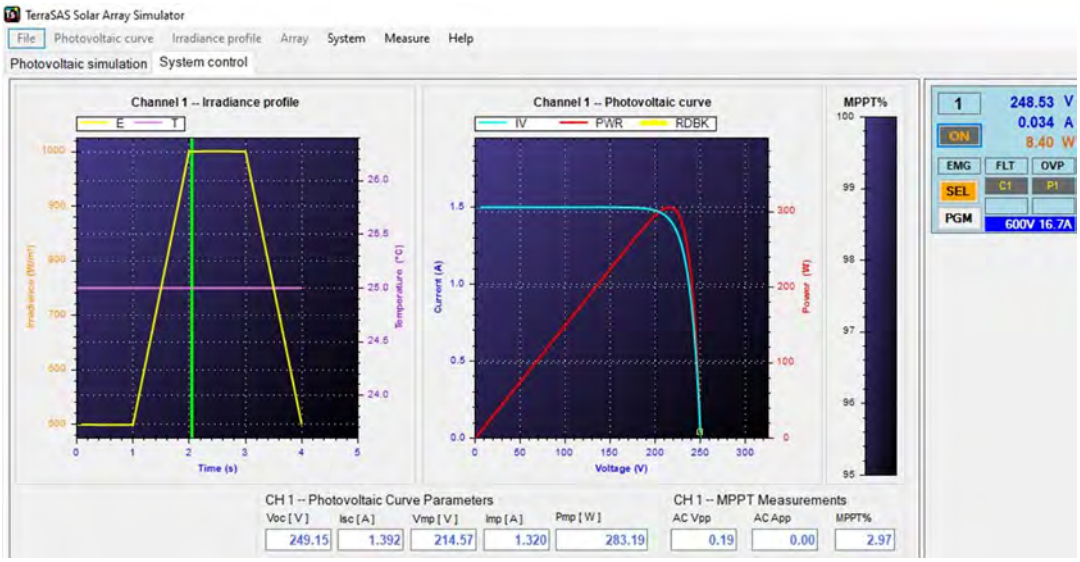

Figure 9.6: PV output power at varying irradiation

simulator is linked to the DC link of the shunt APF in order to provide power generated from solar emulator TerraSAS 600. The varying irradiation profile is shown in the Fig. 9.6.

The structure of the controller and the method of adjusting the PI controller in the hardware configuration is identical to what was addressed in Chapter 4. However, in this case, it has been applied to the shunt APF with PV rather than UPQC-DG. Naturally, to guarantee hardware setup safety, certain filters and currents limits are also established in the controller. It is important to observe that the output of the PI controller must always remain within a specified limit, even throughout the tuning process, in order to guarantee safety. Fig. 9.7a displays the waveforms obtained during the Zeigler-Nichols technique of tuning the PI controller. This approach results in sustained oscillations in the DC link voltage at the ultimate gain.The oscillations have a peak-to-peak amplitude of about 3.2% of the steady-state value, which is 190

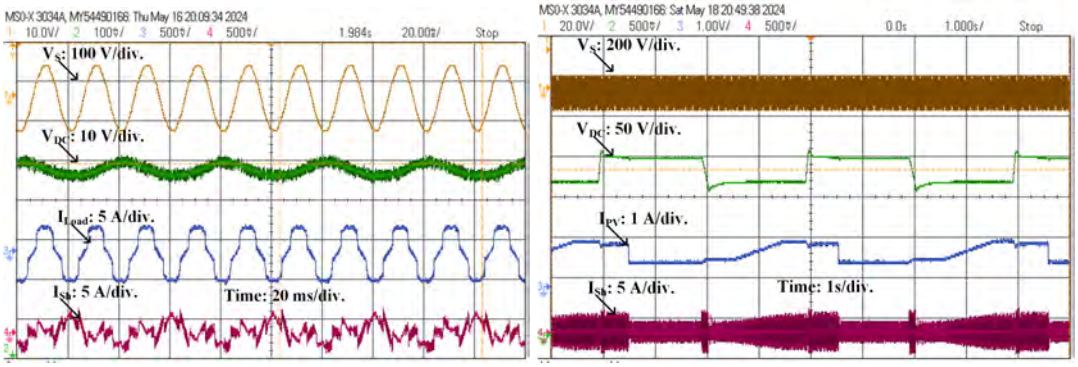

(a) Waveform during the tuning of PI controller using ZN method in hardware setup

(b) Waveform during the tuning of PI controller using proposed PSO method in hardware setup

Figure 9.7: Waveforms during PI controller tuning in the hardware setup

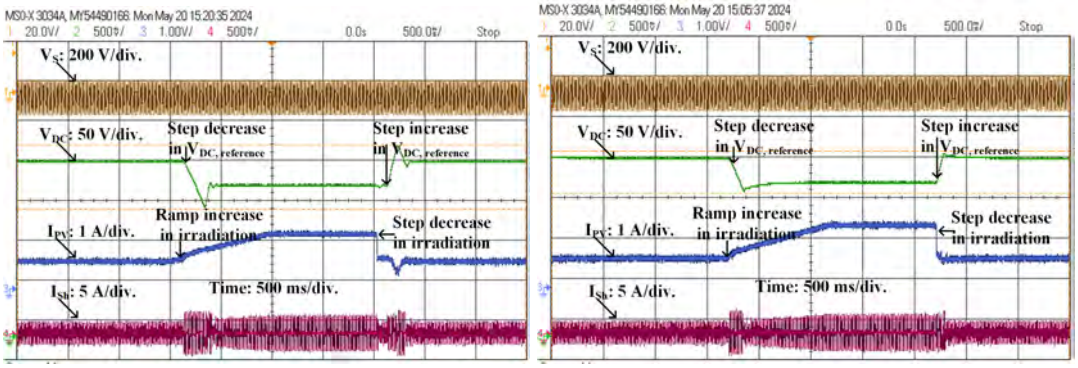

(a) Test waveform of ZN tuned PI controller in hardware setup

(b) Test waveform of PSO tuned PI controller in hardware setup

Figure 9.8: Test waveforms of the ZN and proposed tuning methods of the converter.

V. The values of K_p and K_i are determined to be 0.54 and 16.20, respectively, based on the ultimate gain and ultimate time period.

The waveforms depicting the tuning process utilizing the suggested approach based on PSO are shown in Fig. 9.7b. In this tuning method, disturbances are systematically generated for various controller gain settings, which are then optimized using PSO to achieve the best ITAE performance. This contrasts with ZN tuning, which produces sustained oscillations via time step change. The duration of one iteration of PSO, which includes the evaluation and updating of one particle, is set to 4 seconds in the hardware configuration. During this time frame, the reference voltage for the DC link is raised by 30 V, while the solar irradiation varies in a pattern of ramp and step changes. The 30^{th} iteration utilizing 9 particles yielded the optimal values of K_p and K_i as 0.733 and 4.149, respectively.

Table 9.3: Comparing the hardware results of the two methods of tuning

Method	Tuned Controller gains	Controller Performance Indices ITAE, Mp (peak overshoot)
Z-N	$K_p = 0.54$, $K_i = 16.2$	ITAE = 8.682, $M_p = 11.05\%$
PSO	$K_p = 0.733$, $K_i = 4.149$	ITAE = 8.103, $M_p = 4.21\%$

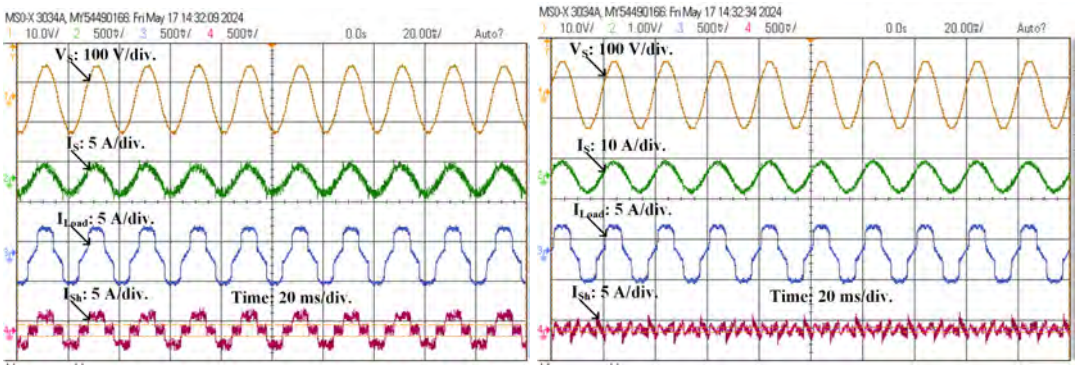

(a) Steady-state waveforms of the shunt APF hardware in the presence of PV power

(b) Steady-state waveforms of the shunt APF hardware in the absence of PV power

Figure 9.9: Steady-state waveforms of the shunt APF hardware

As a result, the ZN is used to tune the controller, and the ITAE is calculated after testing the suggested PSO-based approach in the hardware configuration with comparable periodic disturbances (Fig. 9.8). The results of the hardware testing are shown in Table 9.3. The findings demonstrate that the suggested tuning strategy, based on PSO, achieves superior performance by lowering the ITAE by 6.66% and peak overshoot by 61.90%. The proposed technique exhibits superior dynamic performance compared to the Z-N method, as it achieves a higher reduction in peak overshoot. This improvement attributed to the Z-N method's inability to effectively tune the PI controller owing to output limitations.

The steady waveforms of the shunt APF hardware integrated with PV are shown in Fig. 9.9. The shunt APF injects a current that adjusts for the harmonics produced by the load and feeds the PV power. In the absence of PV power, the shunt current only injects the compensatory harmonic components. In both circumstances, the source current is free of harmonics.

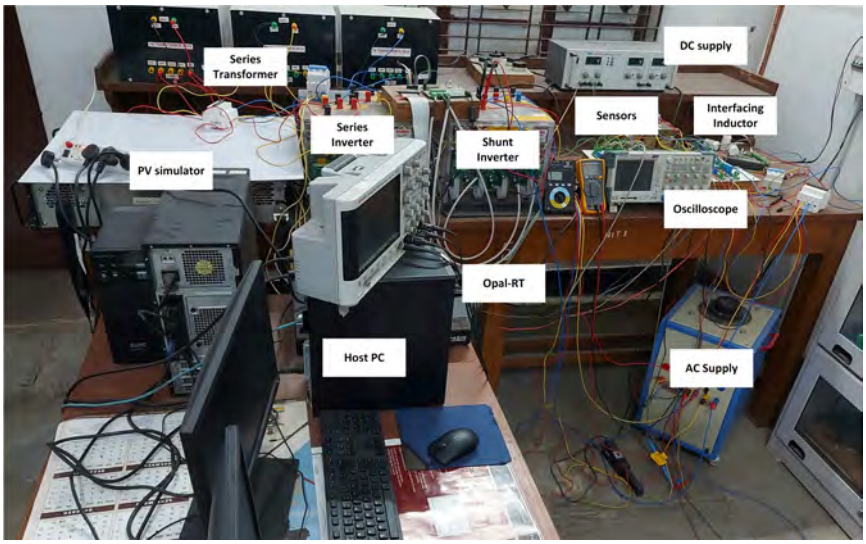

Figure 9.10: Hardware setup of UPQC-DG

9.4 Hardware Validation of UPQC-DG

The hardware validation of the UPQC-DG system controlled by SRF-PAC involves a comprehensive assessment to ensure that the system performs optimally under various conditions. It include both series and shunt APFs to compensate for voltage sags/swells and harmonics, respectively. Parameters of the setup is given in the Table 9.4 The solar emulator (Terra SAS 600) is connected to the DC link vai DC-DC boost converter. To implement the controller algorithms in real time, FPGA based Opal-RT 4510 is used. The digital output generate desired gate pulse based on the feedback signal from the sensor. The hardware prototype of UPQC-DG is depicted in Fig. 9.10. A suitable load is considered for the experiment which consists a rectifier load and RL load. For validation of the Hardware setup, three operating parameters are considered namely voltage sag, voltage swell and change in irradiation.

During the 30% of voltage sag condition (in Fig. 9.11), the source voltage waveform displayed a temporary reduction in magnitude. The UPQC-DG system responded by injecting compensatory voltage (V_{Sr}) through the series APF to maintain a stable (5%) load voltage (V_L). This compensation is verified from the load voltage waveform (in Fig. 9.11a) remained relatively unaffected, maintaining a consistent voltage profile despite the sag in the source voltage. The source current waveform (I_s) also showed simusoidal waveform, indicating effective compensation of harmonics and reactive power during this disturbance. The DC link voltage (V_{DC}) remains

Table 9.4: Specifications of UPQC-DG prototype

Grid	80 V, 3-phase, 50 Hz
Load-1	3-phase uncontrolled rectifier (R_{DC} = 100 Ω)
Load-2	R_Y = 15.5 Ω/ph, L_Y = 70 mH/ph
PV array	P_{MPP} = 102 W, V_{MPP} = 150 V, V_{OC} = 175 V, I_{SC} = 0.72 A
DC link	V_{DC} = 150 V, C_{DC} = 1500 μF
Shunt APF	$S_{Sh,rated}$ = 220 VA, L_{Sh} = 5.0 mH
Series APF	$S_{Sr,rated}$ = 200 VA, L_{Sr} = 5.0 mH
Series Transformer	n_T = 2 (100/50 V), $S_{T,rated}$ = 200.0 VA

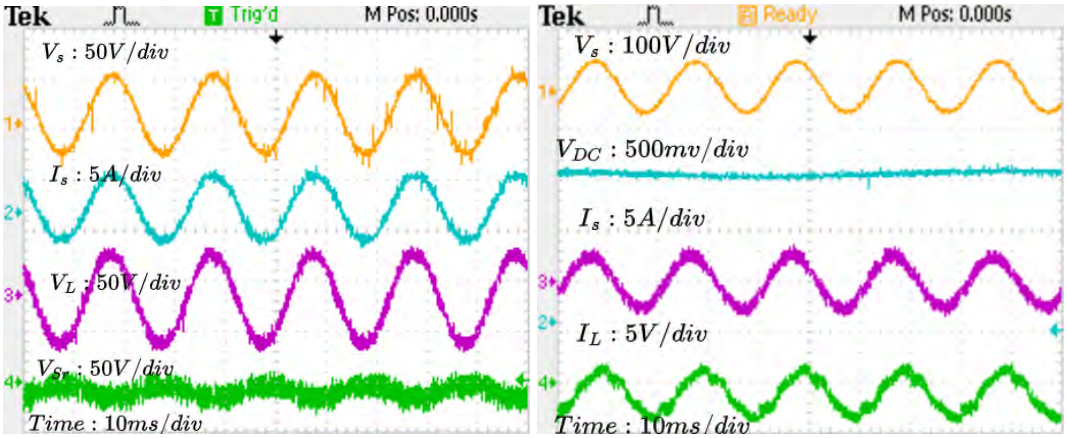

(a) Performance during voltage sag **(b)** Performance of DC link during voltage sag

Figure 9.11: Performance of UPQC-DG during voltage sag

relatively stable in this mode, showing minimal fluctuation in Fig. 9.11b. This stability is crucial as it ensures that the energy storage and power conversion processes are operating efficiently and that the system can respond rapidly to any sudden changes in load or generation.

In the event of a voltage swell (from Fig. 9.12), the source voltage waveform experienced a temporary increase in magnitude. Similar to the sag condition, the UPQC-DG system, through the series APF, injected a counteracting voltage (V_{Sr}) to stabilize the load voltage (V_L). As a result, the load voltage waveform (V_L) remained stable, demonstrating the system's ability to protect sensitive loads from overvoltage conditions. The source current waveform (I_s) continued to display a nearly sinusoidal shape, highlighting the system's effectiveness in maintaining power quality.

In the case of varying irradiation condition (from $1000w/m^2$ to $600w/m^2$), the DC link voltage may experience slight variations as the power output from the PV system changes with irradiation levels (Fig. 9.13). However, the UPQC-DG system

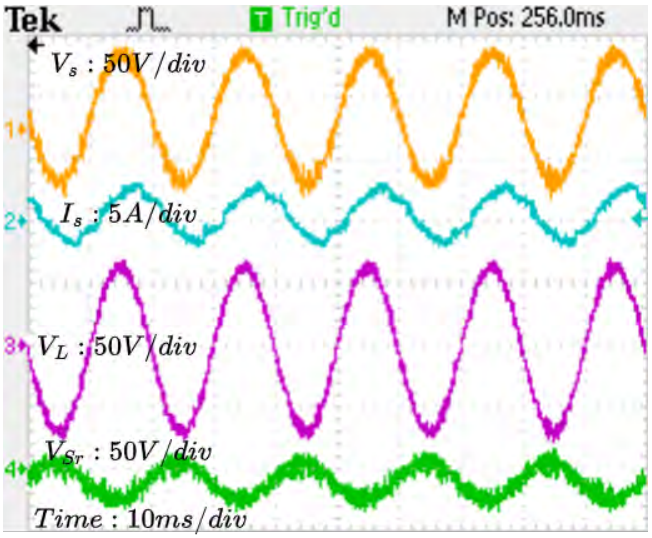

Figure 9.12: Transient waveforms of the UPQC-DG during voltage swell

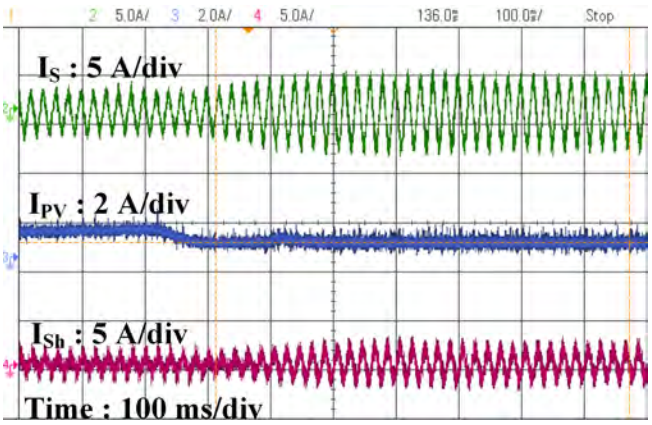

Figure 9.13: Performance during change in solar irradiation.

quickly compensates to stabilize the DC link voltage. The source current shows a exhibit slight increase in magnitude due to the reduction in power supplied by the DG source. The system ensures that these changes do not introduce significant harmonics or distortions. The PV current (I_{PV}) also get reduced due to variation in PV power. The shunt APF current (I_{Sh}) rises to take power directly from the PV to keep the DC link voltage stable and compensate for power losses. Despite the variations in irradiation, the load voltage is kept stable, highlighting the system's ability to maintain power quality. The load current may vary depending on the actual load demand and the power available from the DG source.

9.5 Summary

In conclusion, the hardware validation of the PV-fed shunt APF, alongside the proposed PSO-based PI tuning method for the PV-fed shunt APF and UPQC-DG using the UVTG-SRF based technique, demonstrated significant improvements in power quality and system performance. The integration of PV with the shunt APF effectively mitigated harmonics and maintained a stable DC link voltage, proving the system's capability to enhance power quality. The PSO-based PI tuning method showed superior control over the DC link voltage compared to traditional methods, ensuring more efficient and reliable operation under varying conditions. The hardware result shows the reduction in ITAE and peak overshoot by 6.66% and 23.60% respectively. The SRF-PAC technique in the UPQC-DG system successfully balanced load currents and provided stable voltage profiles, validating its effectiveness in practical applications. Overall, these advancements contribute to the development of robust and efficient power quality management systems, ensuring stable and reliable power supply from distributed generation sources.

Bibliography

[1] V. Khadkikar, "Enhancing electric power quality using UPQC: A comprehensive overview," *IEEE Transactions on Power Electronics*, vol. 27, no. 5, pp. 2284–2297, 2012.

[2] B. Singh, A. Chandra, and K. Al-Haddad, *Power quality: problems and mitigation techniques*. John Wiley & Sons, 2014.

[3] S. Devassy and B. Singh, "Modified pq-theory-based control of solar-PV-integrated UPQC-S," *IEEE Transactions on Industry Applications*, vol. 53, no. 5, pp. 5031–5040, 2017.

[4] S. Devassy and B. Singh, "Enhancement of power quality using solar PV integrated UPQC," in *2015 39th National Systems Conference (NSC)*. IEEE, 2015, pp. 1–6.

[5] R. Noroozian and G. B. Gharehpetian, "An investigation on combined operation of active power filter with photovoltaic arrays," *International Journal of Electrical Power & Energy Systems*, vol. 46, no. 1, pp. 392 – 399, 2013.

[6] V. Khadkikar and A. Chandra, "UPQC-S: A novel concept of simultaneous voltage sag/swell and load reactive power compensations utilizing series inverter of UPQC," *IEEE Transactions on Power Electronics*, vol. 26, pp. 2414–2425, 2011.

[7] L. Limongi, D. Roiu, R. Bojoi, and A. Tenconi, "Analysis of active power filters operating with unbalanced loads," in *Proc. IEEE Energy Conversion Congress and Exposition*. IEEE, 2009, pp. 584–591.

[8] M. Clerc, *Particle Swarm Optimization*. John Wiley and Sons, Ltd, 2006.

[9] W. Al-Saedi, S. W. Lachowicz, and D. Habibi, "An optimal current control strategy for a three-phase grid-connected photovoltaic system using particle swarm optimization," in *2011 IEEE Power Engineering and Automation Conference*, vol. 1, 2011, pp. 286–290.

[10] G. S. Kumar, B. K. Kumar, and M. K. Mishra, "Mitigation of voltage sags with phase jumps by upqc with PSO-based ANFIS," *IEEE Transactions on Power Delivery*, vol. 26, no. 4, pp. 2761–2773, 2011.

[11] A. Patel, H. D. Mathur, and S. Bhanot, "A new SRF-based power angle control method for UPQC-DG to integrate solar PV into grid," *International Transactions on Electrical Energy Systems*, vol. 29, no. 1, p. e2667, 2019.

[12] A. Patel, H. Mathur, and S. Bhanot, "An improved control method for unified power quality conditioner with unbalanced load," *International Journal of Electrical Power & Energy Systems*, vol. 100, pp. 129–138, 2018.

[13] S. K. Yadav, A. Patel, and H. D. Mathur, "Study on comparison of power losses between UPQC and UPQC-DG," in *2020 IEEE 17th India Council International Conference (INDICON)*, 2020, pp. 1–6.

[14] A. Patel, H. D. Mathur, and S. Bhanot, "Enhancing VA sharing between the shunt and series APFs of UPQC with a modified SRF-PAC method," *IET Power Electronics*, vol. 13, pp. 275–285, 2020.

[15] A. Patel, S. K. Yadav, H. D. Mathur, S. Bhanot, and R. C. Bansal, "Optimum sizing of PV based UPQC-DG with improved power angle control," *Electric Power Systems Research*, vol. 182, p. 106259, 2020.

[16] A. Patel, S. K. Yadav, and H. Datt Mathur, "Particle swarm optimization based tuning method of PI regulator for PV fed shunt active power filter," in *2022 IEEE IAS Global Conference on Emerging Technologies (GlobConET)*, 2022, pp. 822–827.

[17] J. Kennedy and R. Eberhart, "Particle swarm optimization," in *Proceedings of ICNN'95 - International Conference on Neural Networks*, vol. 4, 1995, pp. 1942–1948 vol.4.

Chapter 10

Closure

10.1 Conclusions

The UPQC is a highly developed power electronic device that was developed with the purpose of enhancing the power quality of electrical systems [1,2]. In the UPQC-DG system, the benefits of UPQC are paired with a focus on distributed generation [3–5]. This intervention has three outcomes: improving power quality, increasing energy efficiency, and contributing to a more sustainable and robust power system. Enhanced control and cost-effective design for UPQC are complicated because currently available research does not thoroughly analyse the power losses that occur in UPQC under a range of different operating scenarios. On the other hand, a significant amount of research has to be investigated to determine whether UPQC, in conjunction with PV, can supply reactive power to the grid in a controlled manner in smart grid distribution network. The thesis aims to enhance the controller performance, optimal design, and practical applicability of the UPQC. By integrating renewable energy resource (PV), the research demonstrates notable improvements in power quality and overall system efficiency, thereby maintaining a reliable and high-quality power supply.

The purpose of this thesis is to conduct an exhaustive investigation of the performance and design of UPQC under different operating condition. The study includes an analysis of the various control mechanisms used by the UPQC, the optimization of critical parameters that have an impact on its operation, the incorporation of a PV source into the system, and an evaluation of the system's ability to provide reactive power to the grid. Through an in-depth validation of the proposed method using real-time simulation on Opal-RT, this research provides details into the applications and performance enhancements of the UPQC.

10.2 Specific Contributions

The thesis makes the following specific contributions:

1. Design and development of UPQC using SRF and UVTG control demonstrated efficient power quality improvement in various operating situation, with rapid response to grid voltage and load disturbances. The hardware implementation of UPQC-DG validated the system's ability to balance load currents and maintain stable load voltage profiles.

2. The PSO-based PI tuning approach in the UPQC-DG system successfully identified optimal PI parameters of k_p = 1.19 and k_i = 16, resulting in a significant reduction in the ITAE from 4.82% to 2.38%. This method effectively decreased the overshoot voltage from 190 V to 40 V and minimized oscillations in the DC link voltage response. Consequently, it ensures a more stable and responsive control system under varying operational conditions. The proposed approach has been validated through implementation in a hardware prototype which proves the reduction in ITAE and peak overshoot by 6.66% and 23.60% respectively.

3. Using the PSO method, the optimal ripple filter and interfacing inductor are designed to reduce the THD, overall power losses and improve the power factor. The results show that PSO-based passive filters achieve a reduced power loss of 608 W compared to a conventional designed method that causes 810 W of power losses.

4. A study on power losses investigates three control mechanisms for UPQC under various operating conditions. The result demonstrates that UPQC-Q effectively reduces harmonic components while causing a modest power loss of 1.80%. UPQC-P exhibits more losses (2.04%) compared to UPQC-S and UPQC-Q. However, UPQC-Q struggles with voltage swell compensation, highlighting its limitations in this aspect.

5. Investigation of the performance of UPQC-DG/IDG and UPQC under various conditions is conducted. UPQC-DG has significant additional losses (5.80%) due to the connection of DG at the DC link. Despite these losses, UPQC-DG is more practical for real-world distribution systems due to the cost-effectiveness

of PV and shunt APF. Nevertheless, the UPQC with independently integrated PV (UPQC-IDG) exhibits significant power losses of 15.11%, which suggests that it is not suitable practical implementation.

6. UPQC-DG system provides provides reactive power support to the grid which uses the synchronous reference frame (SRF) theory to shunt APF and unit vector template generation (UVTG) for series APF. It also incorporates power angle control to share reactive power burdens between series and shunt APFs. The system's steady-state and dynamic performances are validated using Opal-RT simulations. The proposed system reduces overall rating of APFs by 2.57%.

10.3 Future Scope

In spite of improvements provided by proposed control techniques, there are inherent limitations and rooms for improvements leaving scope for future research, which are as follows:

1. The developed UPQC-DG has been implemented in Opal-RT with a balanced source and fixed non-linear load. However, in practical scenarios, it should be able to regulate power in the presence of dynamically varying load demands with unbalanced grid voltage.

2. It is required to do research on methods for multi-objective optimisation that take into consideration objective functions such as cost, performance, and environmental effect in order to find the best potential UPQC solutions.

3. Investigate the idea of employing UPQC as a grid-interactive device by examining its function in smart grids, demand response programs, and grid support services such as frequency matching and voltage regulation.

4. To ensure UPQC systems are secure from cyber attacks, it is required to address cybersecurity concerns in the smart grid. This is essential since power systems are becoming increasingly interconnected and dependent on digital control.

Bibliography

[1] V. Khadkikar, "Enhancing electric power quality using UPQC: A comprehensive overview," *IEEE Transactions on Power Electronics*, vol. 27, no. 5, pp. 2284–2297, 2012.

[2] B. Singh, A. Chandra, and K. Al-Haddad, *Power quality: problems and mitigation techniques*. John Wiley & Sons, 2014.

[3] B. Han, B. Bae, H. Kim, and S. Baek, "Combined operation of unified power-quality conditioner with distributed generation," *IEEE Transactions on Power Delivery*, vol. 21, no. 1, pp. 330–338, 2006.

[4] A. R. Reisi, M. H. Moradi, and H. Showkati, "Combined photovoltaic and unified power quality controller to improve power quality," *Solar Energy*, vol. 88, pp. 154–162, 2013.

[5] B. Rahmani, W. Li, and G. Liu, "An advanced universal power quality conditioning system and MPPT method for grid integration of photovoltaic systems," *International Journal of Electrical Power & Energy Systems*, vol. 69, pp. 76–84, 2015.

Appendix A

Appendix-I (Specific parameters considered in simulation and hardware)

The important parameters considered for the simulation of UPQC and UPQC-DGs (Chapter-3) are as follows:

Simulation sample time T_s = 10 μs, Solver type = Fixed Step, Solver = ode4 (Dormant Prince), Series Injection Transformer parameters: Nominal power = 2500 VA, frequency = 50 Hz, winding 1 & 2 nominal voltage= 100 V_{rms}, winding resistance (R_1 & R_2) = 0.002 pu, winding inductance (L_1 & L_2) = 0.008 pu, magnetization resistance = 500 pu, magnetization inductance = 500 pu.

The important parameters considered for the real-time simulation of PSO based PI controller (Chapter-4) are as follows:

No. of iteration = 30, population size = 9, No. of variables = 2, reference DC-link voltage = 730V, c_1 = 1.05; c_2 = 1.05; w_{max} = 1.0; w_{min} = 0.4; V_s frequency = 50 Hz; voltage sag = 20%, voltage swell = 30%, winding 1 & 2 nominal voltage= 150 V_{rms}, winding resistance (R_1 & R_2) = 0.002 pu, winding inductance (L_1 & L_2) = 0.04 pu, magnetization resistance = 500 pu, Magnetization inductance = 500 pu, Hysteresis bandwidth = 1e-3 Ω, IGBT R_{on} = 1e-3 Ω, IGBT R_s = 1e5 Ω, IGBT C_s = inf, IGBT V_f = 0, IGBT V_{fd} = 0, IGBT T_f = 1e-6, IGBT T_t = 2e-6, DIODE R_{on} = 1e-3 Ω; DIODE R_s = 1e5 Ω, DIODE C_s = inf, DIODE L_{on} = 0, DIODE V_f = 0.

The important IGBT parameters considered (Chapter-7) for the calculation of losses are as follows:

E_{on}:Energy dissipation during turn-on time = 26 mJ, E_{off}: Energy dissipation during turn-off time = 39 mJ, E_{swref}: Reference value of energy dissipation during switching process = 65 mJ, I_{ref}:Reference value of IGBT or FWD current = 300 A, V_{ccref}:Reference value of supply voltage = 600 V, TC_{sw}:Temperature coefficient

of switching losses = 0.003, T_{jref}:Reference value of chip temperature = 150°C, K_i:Exponent of current dependency for switching loss calculation = 1, K_v:Exponent of voltage dependency for switching loss calculation = 1.3, V_{cc}:Supply voltage = 700 V, T_j:Chip temperature = 60, f_{sw}:Switching frequency = 10 kHz.

The important diode parameters (Chapter-7) considered for the calculation of losses are as follows:

E_{on}:Energy dissipation during turn-on time = 4.7 mJ, E_{swref}:Reference value of energy dissipation during switching process = 4.7 mJ, I_{ref}:Reference value of IGBT or FWD current = 75 A, V_{ccref}:Reference value of supply voltage = 600 V, TC_{sw} : Temperature coefficient of switching losses = 0.003, T_{jref}:Reference value of chip temperature = 150°C, K_i:Exponent of current dependency for switching loss calculation = 0.5, K_v:Exponent of voltage dependency for switching loss calculation = 0.6, V_{cc}:Supply voltage = 700 V, T_j:Chip temperature = 60, f_{sw}:Switching frequency = 10 kHz.

The parameters considered for real time simulation (Chapter-7) are as follows:

Three phase supply Source = 415 V, Frequency = 50 Hz, Source impedance = 0.01 Ω and 0.25mH, Load 1 : Bridge Rectifier with RL load 15.69 Ω, 0.1 mH & linear load with RL = 5.3 Ω & 25.3mH, Load 2 : linear load with RL = 5.3 Ω & 25.3 mH, DC Link Capacitor = 5500 μF, interfacing inductor for series APF = 4.84 mH, interfacing inductor for shunt APF = 4.84 mH, Shunt inverter RC filter = 5.07 Ω, 2.07E-05 μF, series inverter RC filter = 2.79 Ω, 0.7μF. PV array data: P_{PV} = 15 kW, V_{oc} = 64.2 V, I_{sc} = 5.96 A, V_{mpp} = 700 V, I_{mpp} = 25 A.

The parameters specifications for hardware prototype (Chapter-9) are as follows:

Shunt APF & series APF Inverter Type: Semikron Inverter Type- B6U415/560-45F, LV25-P Voltage sensor, LA25-P current sensor, TerraSAS ETS 600/17 PV Simulator, Injection Transformer, 3 phase Autotransformer = 20 A, 415 V, star connected, Power resistor (5 Ω), Capacitor (10 μF, 400 V, 50 Hz, 5% tolerance), 3 phase inductive load (415 V, 5 A, 3.5 kVAR, star-connected, continuous variation), 3 phase resistive load (415 V, 3.25 kW, 4.5 A, 3.5 kVAR, star-connected 4 equal step-change), Oscilloscope used (Keysight InfiniVision MSOX 3034A, Tektronix TPS 2024B), Multimeter devices (Fluke 115), N4 Power Analyzer PPA500. Opal-RT Assumptions: CPU sample time = 16 μs, Solver type = Fixed Step, Solver = ode45 (Dormant Prince).

Appendix B

Appendix-II (Model parameters considered in MATLAB and Opal-RT)

Model assumption for IGBT switch in Opal-RT and MATLAB Simulation. Theoretical and simulation model assumption:

Parameters	**Opal-RT**	**MATLAB Simulation**
Internal resistance R_{on} **(Ω)**	15e-3	1e-3
Snubber resistance R_s **(Ω)**	1e5	1e5
Snubber capacitance C_s **(F)**	0.8	inf
Forward voltage (V)	0.8	1
Diode Forward Voltage (V)	1.2	0.8
Diode R_{on} **(Ω)**	14e-3	1e-3
Diode R_s **(Ω)**	1e5	500
Diode C_s **(F)**	inf	250e-9
Diode L_{on}	0	0

Model assumption for Injection Transformer in Opal-RT and MATLAB Simulation:

Parameters	**Opal-RT**	**MATLAB Simulation**
Nominal power (VA) and Frequency (Hz)	2.5e3, 50	2.5e3, 50
Winding 1: Nominal voltage (V),	100	100
Resistance (Ω), Inductance (H)	0.002, 0.008	0.002, 0.008
Winding 2: Nominal voltage (V),	100	100
Resistance (Ω), Inductance (H)	0.002, 0.008	0.002, 0.008
Magnetization resistance (Ω) & Inductance (H)	500, 500	500, 500

Measurement Errors: Noise, inaccuracies, or limitations in sensors and measurement equipment.

- **Source Voltage Sensor gain**: V_{sa} = 115.34, V_{sb} = 115.54, V_{sc} = 114.89
- **DC link voltage sensor**: V_{dc} = 114.27
- **Load current sensor**: I_{La} = 2.2776, I_{Lb} = 2.353, I_{Lc} = 1.319
- **Shunt APF current sensor**: I_{sha} = 1.085, I_{shb} = 1.055, I_{shc} = 1.102

FPGA based real time simulator specifications: Timing and Synchronization Issues: Differences in real-time processing, delays, or timing mismatches, particularly relevant in real-time digital simulations.

- **FPGA**: Xilinx® Kintex®-7 410T
- **Computer**: Intel Xeon E3-1240 V6 4 cores, 3.7 GHz, 8 GB RAM, 250 GB SSD
- **Operating system**: Opal-RT Linux 3.5.4
- **MotherBoard**: X11SSM-F-O Supermicro Server Motherboard, Intel socket H4 LGA-1155 μATX
- **AC input**: 100-240 V, 60-50 Hz
- **Minimum Sample Time**: 6 μs

Comparison of assumption taken for Opal-RT and MATLAB simulation: Timing and synchronization issues, along with differences in real-time processing, can cause delays and timing mismatches, which are particularly relevant in real-time digital simulations

Parameters	**Opal-RT**		**MATLAB Simulation**
	CPU model	**FPGA Model**	**Simulink Model**
Sample Time (s)	15e-6	1e-6	5e-6
Solver Type	eHS (by Pejovic method)	Discrete Backward Euler	ode45 (dormand prince)

List of Publications

Journal Publications

The following papers, which are included in this thesis, have been published in the journals that are listed below:

1. S. K. Yadav, A. Patel & H. D. Mathur, "Study on Comparison of Power Losses Between UPQC and UPQC-DG," in *IEEE Transactions on Industry Applications*, vol. 58, no. 6, pp. 7384-7395, Nov.-Dec. 2022, DOI: https://doi.org/10.1109/TIA.2022.3191985 (I.F.- 4.4)

2. A. Patel, Yadav, S. K. Yadav, & H. D. Mathur, "Utilizing UPQC-DG to export reactive power to grid with power angle control method." *Electric Power Systems Research*, 209, (2022): 107944. DOI: https://doi.org/10.1016/j.epsr.2022.107944 (I.F.- 3.414)

3. S. K. Yadav, A. Patel and H. D. Mathur, "PSO-based Online PI Tuning of UPQC-DG in Real-Time." in *IEEE Open Journal of Power Electronics*, vol. 5, pp. 1419-1431, 2024, DOI: https://doi.org/10.1109/OJPEL.2024.3445719 (I.F.- 5)

4. S. K. Yadav, A. Patel and H. D. Mathur, "Enhanced Performance of UPQC through PSO based Passive Filter Design" in *IEEE Transactions on Industry Applications* (under review)

5. S. K. Yadav, A. Patel and H. D. Mathur, "A Novel Particle Swarm Optimization based Plant-in-Loop Tuning Method for PI Controller of Integrated Power Converters," in *IEEE Journal of Emerging and Selected Topics in Power Electronics* (communicated)

Conferences

The following papers, which are included in this thesis, have been published in the conferences that are listed below:

1. A. Patel, S. K. Yadav, S. Tiwary and H. D. Mathur, "Digital Twin of a Single-Phase Home Converter System Integrating Distributed Energy Resources," *2023 IEEE International Conference on Energy Technologies for Future Grids (ETFG)*, Wollongong, Australia, 2023, pp. 1-6, DOI: https://doi.org/10.1109/ETFG55873.2023.10408449

2. S. K. Yadav, A. Patel and H. D. Mathur, "PSO based Optimum Design of Passive Interfacing Elements of UPQC," *2023 IEEE International Conference on Energy Technologies for Future Grids (ETFG)*, Wollongong, Australia, 2023, pp. 1-6, DOI: https://doi.org/10.1109/ETFG55873.2023.10407275

3. A. Patel, S. K. Yadav and H. D. Mathur, "A Single-Phase Grid-Tied Converter System Integrating Solar PV, Battery and Compensating Power Quality," *2023 IEEE IAS Global Conference on Renewable Energy and Hydrogen Technologies (GlobConHT)*, Male, Maldives, 2023, pp. 1-6, DOI: https://doi.org/10.1109/GlobConHT56829.2023.10087733

4. A. Patel, S. K. Yadav and H. Datt Mathur, "Particle Swarm Optimization based Tuning Method of PI Regulator for PV fed Shunt Active Power Filter," *2022 IEEE IAS Global Conference on Emerging Technologies (GlobConET)*, Arad, Romania, 2022, pp. 822-827, DOI: https://doi.org/10.1109/GlobConET53749.2022.9872475

5. S. K. Yadav, A. Patel and H. D. Mathur, "Study on Comparison of Power Losses between UPQC and UPQC-DG," *2020 IEEE 17th India Council International Conference (INDICON)*, 2020, pp. 1-6, DOI: https://doi.org/10.1109/INDICON49873.2020.9342284

6. S. K. Yadav, A. Patel and H. D. Mathur, "Comparison of Power Losses for Different Control Strategies of UPQC," *2020 IEEE 9th Power India International Conference (PIICON)*, 2020, pp. 1-6, DOI: https://doi.org/10.1109/PIICON49524.2020.9113005

Brief Biography of the Candidate

Sisir Kumar Yadav (Student Member, IEEE) received his B.Tech. degree in Electrical Engineering from Veer Bahadur Singh Purvanchal University, Jaunpur, Uttar Pradesh, India, in 2015, and his M.E. degree with a specialization in Power Electronics from the Birla Institute of Technology (BIT), Mesra, Ranchi, Jharkhand, India, in 2019. He is currently working toward the Ph.D. degree in Electrical Engineering with the Birla Institute of Technology and Science (BITS), Pilani, Rajasthan, India.

In 2019, he was appointed as a Junior Research Fellow (JRF) through an R&D project vacancy for CPRI research project under Research Scheme on Power (RSoP), Birla Institute of Technology and Science, Pilani, Rajasthan, India, in 2019, where he has been a full time Research Fellow. His research interests includes power electronics, converter design and its applications for custom power devices including power quality monitoring and mitigation issues.

Brief Biography of the Supervisor

Prof. Hitesh Datt Mathur (Senior Member, IEEE) received the B.E. degree in Electrical Engineering from Nagpur University, Nagpur, Maharashtra, India, in 1998, the M.E. degree in Power Systems specialization from the Malviya National Institute of Technology, Jaipur, Rajasthan, India, in 2000, and the Ph.D. degree in Electrical Engineering from Birla Institute of Technology & Science (BITS), Pilani, Rajasthan, India, in 2007.

He was Postdoctoral Research Fellow with the Department of Automatic Control, École supérieure d'électricité, Supélec, France in 2013. He is currently a Professor in the Department of Electrical and Electronics Engineering, Birla Institute of Technology & Science, Pilani, Rajasthan, India. His research interests includes smart grid, Internet of Things-based energy management, grid integration issues of renewable energy sources, e-mobility challenges, power quality analysis, power system stability, and control.

Brief Biography of the Co-supervisor

Prof. Ashish Patel (Member, IEEE) received the B.Tech. degree in Electrical Engineering from Indian Institute of Technology (IIT)-BHU, Varanasi, Uttar Pradesh, India, in 2011, the M.Tech degree in Energy System Engineering from IIT Bombay, Mumbai, Maharashtra, India, in 2015, and the Ph.D. degree in Electrical Engineering from Birla Institute of Technology & Science (BITS), Pilani, Rajasthan, India, in 2020.

He is currently an Assistant Professor with the Department of Electrical and Electronics Engineering, Birla Institute of Technology & Science, Pilani, Rajasthan, India. His research interests include power electronics for renewable energy, power quality, microgrids, multiagent application to smart grids, and FACTS devices. He is co-principal investigator of a research project entitled, "Development of Improved Design and Control Strategies for UPQC-DG" funded by Central Power Research Institute, Bangalore under RSoP scheme.